CHEMICAL REVIEWS

REVIEW

pubs.acs.org/CR

Templated Techniques for the Synthesis and Assembly of Plasmonic Nanostructures

Matthew R. Jones,[†,§] Kyle D. Osberg,[†,§] Robert J. Macfarlane,[‡,§] Mark R. Langille,[‡,§] and Chad A. Mirkin*[,†,‡,§]

[†]Department of Materials Science and Engineering, [‡]Department of Chemistry, and [§]International Institute for Nanotechnology, Northwestern University, 2145 Sheridan Road, Evanston, Illinois 60208-3113, United States

CONTENTS

Special Issue: 2011 Plasmonics

Received: December 21, 2010
Published: June 08, 2011

1. INTRODUCTION

The field of plasmonics has become one of the most interesting and active research areas in nanotechnology, enabling numerous fundamental studies and applications in a variety of scientific disciplines.[1,2] A plasmon oscillation can be described as the collective motion of conduction band electrons relative to fixed positive ions (i.e., atoms) in a metal that is driven by the electric field component of incident light.[2,3] When excited in subwavelength structures, these oscillations allow for extraordinary confinement and manipulation of light at nanometer length scales.[4] In addition, coupling between neighboring nanostructures, particularly when arranged in a periodic lattice, can lead to unique emergent properties that have motivated an understanding of the assembly of these materials.[2] Such phenomena have already led to applications as diverse as ultrasensitive detection schemes[1,5,6] and waveguides and lenses,[7,8] as well as advances in the fields of light harvesting[9,10] and metamaterials.[11] While relatively simple, generally isotropic, and homogeneous nanostructures have demonstrated some of these effects and have been crucial for understanding the fundamental phenomena underlying this field, building structures with increased complexity and hierarchy will be necessary to realize the most useful and scientifically fruitful nanoscale architectures. Many recent advances by chemists and materials scientists to overcome the barriers for achieving these requisite levels of intricacy can be traced to a simple and generalizable synthetic strategy—the use of a nanoscale template that serves to influence the growth or assembly of nanostructures with rationally designed dimensions, morphologies, phases, and/or supercrystal symmetries.

Although complex plasmonic nanostructures can be categorized by other synthesis methods, such as seed-mediated growth, nanoscale lithographies, and thin-film techniques, we have chosen to focus solely on templated approaches to nanoscale fabrication. For this reason, we have excluded general discussions of topics such as simple colloidal nucleation and growth,[12−14] anisotropic nanoparticle synthesis,[15−17] and lithographically generated structures[18−21] that do not make explicit use of a template and have been covered in excellent review papers elsewhere. Here, we define a templated nanoscale architecture as one whose final structure mimics the symmetry of the molecular or nanoscale species used to direct its fabrication (Figure 1). This guiding principle of preserving the symmetry of an extant material's shape, crystallographic arrangement, or potential energy distribution can be exploited for the formation of plasmonic materials through two primary methods: synthesis and assembly.

Templated synthesis refers to the use of a prefabricated, nanostructured material to influence and/or order the placement of building blocks (typically atomic or molecular species) in specific locations during the growth of the material (Figure 1a,b). Synthetic templates typically achieve this either through physically restricting metal deposition to occur in a specific geometry (e.g., growth of a metal in a rod-shaped pore) or through chemically directing growth to occur at a specific location or in a specific direction (i.e., growth of a metal at certain crystallographic sites on a nanoparticle). Templated assembly, on the other hand, utilizes a prefabricated structure to collect multiple, discrete nano-objects into a larger, well-defined, ordered architecture (Figure 1a,c). In some cases, nanostructures can be assembled into small clusters or even large superlattices through driving forces imposed by molecular or supramolecular species (i.e., metal particles assembled by proteins or oligonucleotides), while in others, nanomaterials adsorb to and adopt the physical geometry of a solid template (i.e., ordering of particles in a porous membrane). Frequently, synthesis and assembly

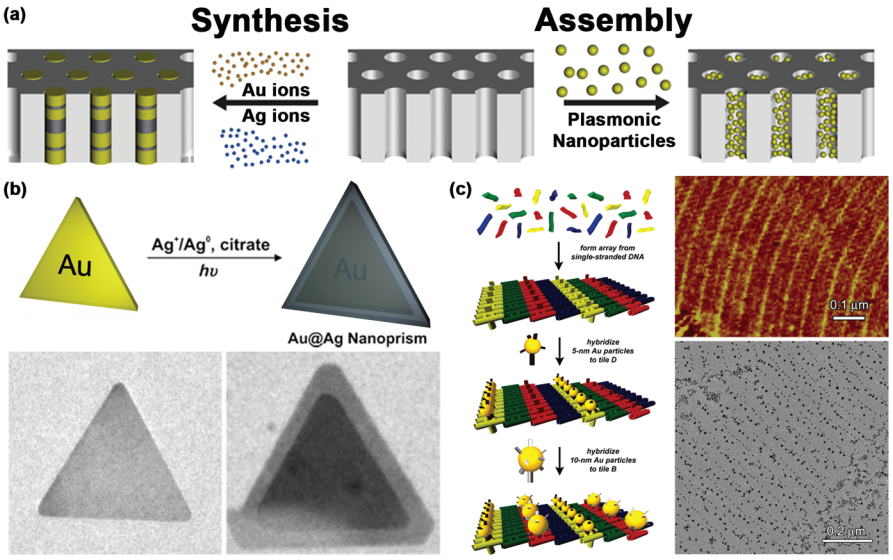

Figure 1. Templated synthesis and assembly: (a) Schematic illustration of the distinction between templated synthesis (left) and assembly (right) of plasmonic materials. In the former, nanostructures are synthesized directly on or in the template; in the latter, nanostructures are first synthesized and then placed on or in the template structure. In each case, the size and shape of the final structure are dictated by the geometry of the template. (b) Example of templated synthesis, where silver ions are reduced onto a gold nanoprism and the shape of the prism dictates the shape of the final synthesized structure (see section 3.1.2). (c) Example of templated assembly, where the positions of different oligonucleotide sequences on a DNA scaffold determine the 2-D ordered arrangement of gold nanoparticles (see section 6.1.3). (b) Adapted with permission from ref 135. Copyright 2007 Wiley-VCH Verlag GmbH & Co. KGaA. (c) Adapted with permission from ref 953. Copyright 2005 American Chemical Society.

methodologies can be combined, wherein both occur simultaneously on a single nanoscale template that has been designed to have an ordered arrangement of nucleation sites.

This diversity of strategies, unified by their common use of a guiding template, represents a central theme of nanoscale chemistry that provides ways to synthesize otherwise unobtainable nanostructures that are poised to provide fundamental insights into how light interacts with matter at the nanoscale. It is one of the most common currently used approaches, along with anisotropic nanoparticle synthesis and lithographic methods, for generating extremely complex nanostructures with tailorable geometries that exhibit a diverse set of plasmonic properties. Despite these advantages and the ubiquity of templated methodologies, few review papers have covered these topics in depth, especially in the context of plasmonic nanostructures. Several reports have considered various aspects of the methods that will be addressed here, but nearly without exception, they have focused on a specific type of template structure (e.g., porous membranes, carbon nanotubes, colloidal nanoparticles, peptides), while including many different material compositions. Conversely, we will cover a broad range of templates, while remaining specific to nanostructures only with plasmonic properties.

Here, we intend to show that an enormous number of seemingly disparate approaches to nanoscale synthesis and assembly can be unified under a simple tenet—that templates act to direct the growth or organization of nanostructures under conditions that preserve the template's shape or symmetry. We begin with a brief discussion of the basic physical concepts underlying plasmonics, with an overview of some of the unique effects that will be referenced throughout the document, as they commonly arise from templated nanostructures. From this starting point, the majority of the review will constitute discussions of templated synthesis (sections 3−5) and templated assembly (sections 6−8) techniques. Templated synthesis has been divided into several categories on the basis of whether reactions occur in solution (section 3), inside porous membranes (section 4), or on substrates being masked by a secondary nanostructure (section 5). Templated assembly techniques will follow, being broadly separated into organizational processes that manipulate naturally occurring biological materials (section 6), take advantage of synthetic organic materials (section 7), or make use of a physical substrate (section 8). In most cases, historical or earliest known examples are given first, followed by a gradual increase in the complexity of structures and methods that fall within the particular category being addressed. This allows for a comprehensive coverage of the topic, while also establishing well-known techniques at the beginning that are usually improved upon to arrive at more intricate morphologies. In addition, we have intentionally allowed for the inclusion of reports that do not make any explicit measurement of plasmonic properties but nonetheless demonstrate nanostructures capable of plasmon excitation so that the interested reader can take advantage of unique strategies that may not have yet been applied to plasmonic systems. Where possible, we have included references to review publications that partially address concepts covered in a portion of the document at the beginning of the relevant section. To end, a topical overview of several novel properties and applications of these plasmonic nanostructures will be briefly provided, where the focus has been given to templated nanostructures already covered in the synthesis or assembly sections. Finally, we will give our opinions on the future outlook of this burgeoning field and what directions are likely to spur the most innovation and scientific progress.

2. FUNDAMENTALS OF PLASMONICS

Scientists have long been interested in the interaction of light with matter. Of particular interest has been the condition where the size of a material is reduced to less than or equal to the wavelength of incident light. In the 1800s, Michael Faraday was responsible for the first scientific investigations into particles of gold that met this criterion. He found that a solution of nanometer-sized gold particles was red in color, unlike the yellow color of bulk gold, and that varying the size of the particles could change the color of the colloid.[22] The explanation for this observation could be found in Maxwell's equations; however, it would not be extracted until 1908 when Gustav Mie provided an analytical solution to the equations for a sphere of arbitrary size.[23] Mie was able to calculate the extinction spectra (summation of absorption and scattering spectra) for metal colloids containing spherical particles of any size. In doing so, he was able to explain many of the experimental observations of his day, including the red color of Faraday's gold colloid. Since its beginnings, the field encompassing the understanding of how light interacts with metals on the nanometer length scale has exploded and evolved into an interdisciplinary field known as *plasmonics*. At the core of this growing field is the phenomenon of *surface plasmon resonance*: a coherent oscillation of conduction band electrons driven by incident electromagnetic radiation.

For a qualitative understanding of a surface plasmon, the analogy to a mechanical oscillator can be made. When a simple harmonic oscillator is displaced from its equilibrium position, it experiences a restoring force that brings the oscillator back to its initial position or configuration. A simple oscillator, once perturbed from equilibrium, will undergo a continuous sinusoidal-type motion until damping forces bring the system to rest. The effects of damping can be overcome if an additional (external) force is applied to the oscillator. In the case of a sinusoidal applied external force, there exists at least one frequency at which the force applied will result in the oscillator achieving maximum amplitude. This particular frequency is called the resonant frequency: a frequency either above or below the resonant frequency yields lower amplitudes of oscillation. This phenomenon arises when the external force is applied "in phase" with the natural frequency of the oscillator, resulting in the oscillator absorbing a maximum amount of energy from the driving force. At such conditions, a small amount of applied force can induce large amplitudes of oscillation due to the effective transfer of energy from the driving force to the oscillator. Resonance is a widespread physical phenomenon that occurs at all length scales and for many types of forces; therefore, it is not surprising to find that such behavior exists when light interacts with the conduction band electrons of a metal.

The delocalized electrons of a metal are often described as being a free electron "gas" (or cloud) around positively charged nuclei. When the oscillating electric field from incident light interacts with the delocalized electrons of a metal, the electron cloud can be perturbed in such a way that it is physically displaced from the metal framework. This charge polarization is short-lived, because the Coulombic attraction from the positively charged nuclei of the metal will pull the electron cloud back to its initial position. Due to the large difference in mass, it is typically assumed that the heavy nuclei remain in a fixed position while the lighter electrons experience motion. With the electric field component of incident light acting as a sinusoidal driving force and Coulombic attraction acting as a restoring force, all of the components of a harmonic oscillator are present. Consequently, resonant conditions can be achieved when light is coupled in phase to the natural frequency of the plasmon oscillation. At these resonant conditions, the metal structures absorb the maximum amount of incident electromagnetic radiation, causing the greatest amount of charge displacement.

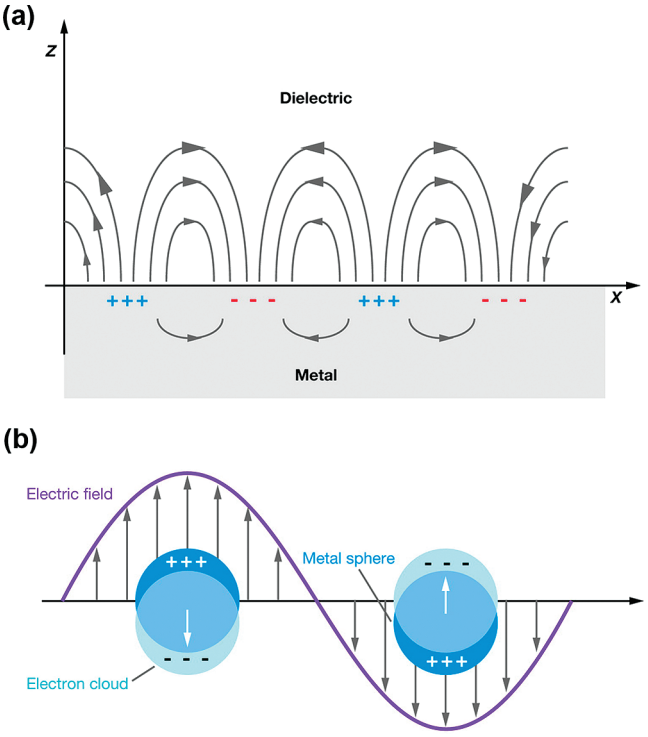

Figure 2. Schematic diagrams illustrating (a) a surface plasmon polariton and (b) localized surface plasmon resonance. Adapted with permission from ref 72. Copyright 2007 Annual Reviews.

It should be noted that the term *plasma oscillation* is applicable to any system where there is coherent motion of electrons or ions in a conductive medium and refers to the bulk oscillation of such a system. The topics of this review are concerned with *surface plasmons* (SPs), a specific type of plasma oscillation occurring at lower energies than the bulk plasmon, which happens when light is coupled to the coherent oscillation of free electrons at the surface of a conductor. The term *surface plasmon resonance* (SPR) is used to describe this type of oscillation when at resonant conditions. SPs are unique from bulk plasma oscillations in that surface topography is an important parameter that can greatly affect how light interacts with the conductor. For simplicity, this review will only qualitatively describe the factors that influence the properties of a surface plasmon; however, quantitative and more mathematically rigorous explanations can be found in many of the references cited herein.

There are two types of SPRs that can be generated: one that originates from propagating waves along a metal surface, called *surface plasmon polaritons* (SPPs),[24,25] and another that is localized to a volume with dimensions smaller than the wavelength of incident light, called *localized surface plasmon resonance* (LSPR).[25−28] Often the term SPR is applied to both cases to denote the general phenomenon of confined plasma oscillations. Similar to how Mie made some of the first significant contributions to describing how light interacts with small particles, R. H. Ritchie was responsible for introducing the concept of

dx.doi.org/10.1021/cr1004452 |*Chem. Rev.* 2011, 111, 3736–3827

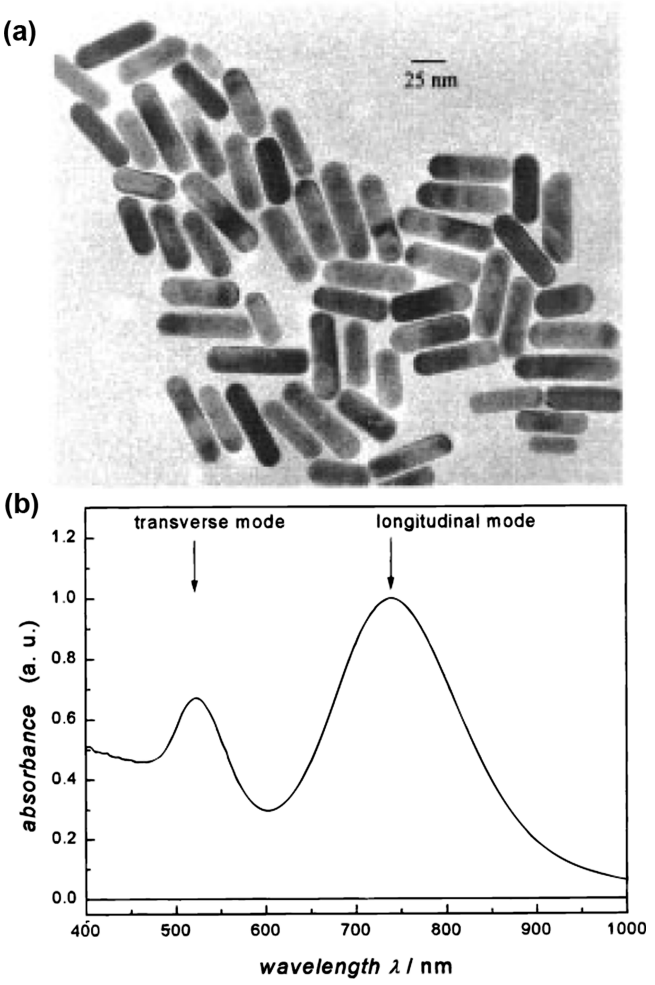

Figure 3. (a) TEM image of Au nanorods and (b) corresponding extinction spectrum. Due to the anisotropy of the particles, the dipole plasmon resonance is split into a transverse plasmon absorption at 525 nm and a longitudinal plasmon absorption at 740 nm. Adapted with permission from ref 48. Copyright 1999 American Chemical Society.

propagating surface plasmons on thin metal films in the 1950s.[29] SPPs are generated when light becomes trapped at a metal–dielectric interface (Figure 2a). Incoming electromagnetic radiation can be coupled into the free conduction electrons at the surface of a metal through use of a prism, waveguide, or grating coupler.[24] Typically, thin films of Cu, Ag, or Au are used as metal substrates, although any material with a dielectric constant consisting of a large negative real component and a small positive imaginary component can support surface plasmons.[24] Once coupled, the resulting charge density waves propagate along all directions in the plane of the interface (x- and y-directions), reaching distances on the order of micrometers. The electromagnetic radiation also extends in the direction normal to the interface (z-direction), with the field decaying exponentially away from the surface, reaching roughly 200 nm into the dielectric environment.[30−33] In addition to the type of metal and refractive index (dielectric) of the environment, surface topography will greatly influence the propagation and behavior of an SPP. For example, roughened or textured surfaces are commonly used to tune the electric field enhancements resulting from plasmon excitations on metal surfaces.[34,35] SPPs can also be generated on smaller nanostructures, such as metal nanowires, with propagation occurring along the long axis of the wire.[36−38] When light is coupled into an appropriate metal–dielectric interface, it will continue to propagate until either the interface is interrupted or the propagation distance becomes too great and the SPP decays away.

Light will also interact with metal particles smaller than the wavelength of incident light to generate a localized surface plasmon resonance when the dimensions of the particle are too small to support a propagating wave (Figure 2b). The confinement of a surface plasmon to a small volume results in an oscillating electromagnetic field that resides very close to the particle surface, extending only nanometers into the dielectric environment.[27] Consequently, LSPR can generate much higher local field enhancements (100−10000 times the incident field) as compared to those of an SPP (10−100 times the incident field).[39] Many factors will affect the resonance frequency of a particle, including the material composition, size, shape, and dielectric environment.[3,40−45] While a variety of metals have been used to generate LSPRs, much of the literature is dominated by particles of gold and silver due to their stability at small sizes and strong LSPR absorption bands in the visible region of the spectrum.[27] Small spherical particles have a single, sharp absorption band due to the excitation of what is called a dipole plasmon resonance, where the entire charge distribution of the particle oscillates at the frequency of the incident electric field as illustrated in Figure 2b. Larger spherical particles, however, have multiple absorption bands due to the generation of quadrupole and other higher ordered resonances where, for example, half of the electron cloud moves parallel to the incident field and half moves antiparallel. Other LSPR modes can arise if anisotropic, or nonspherical, particles are considered. Nanorods are the quintessential demonstration of how optical properties are dependent on the dimensions (or shape) of a particle. The dipole plasmon resonance of a solution of nanorods is typically split between transverse and longitudinal dipole resonances due to the different dimensions along the width and length of the particles (Figure 3).[46−48] The positions of the two bands depend on both the aspect ratio and the absolute dimensions of the particles.[49−51] The resonance at the longer wavelength (the longitudinal plasmon resonance) is associated with oscillations along the length of the nanorod, while the resonance at the shorter wavelength (the transverse plasmon resonance) is associated with oscillations along the width of the nanorods. Although higher ordered resonances are lower in intensity than dipole plasmon resonances, certain anisotropic particles can have extinction spectra that are greatly influenced by higher ordered resonances as evidenced by the in-plane and out-of-plane quadrupolar resonances observed for samples of triangular nanoprisms of silver or gold.[52−54] Extrinsic factors can also affect peak positions, with small changes to the dielectric constant of the environment causing visible changes to the color of a colloid.[42] The localization of a plasmon resonance can also be achieved when the propagation of an SPP is interrupted by nanoscale holes in a metal film.[55−58] The optical properties of such cavities are similar to the properties of solid particles of identical dimensions.[59]

One of the exciting features of surface plasmons is that they can be coupled. When two or more discrete plasmonic materials are in close proximity to one another (on the order of nanometers), their oscillating electric fields can interact to yield new resonances.[60,61] This is visibly apparent when gold

nanoparticles aggregate and the color of the solution changes from red to purple.[62] When interparticle coupling is effectively controlled, extremely high local electric fields can be generated which would otherwise not be possible with single particles. These areas of intense electromagnetic radiation are often referred to as "hot spots".[63] Sharp features will also produce intense electromagnetic radiation due to a "lightning rod" effect from the crowding of electric field lines.[64] The generation of hot spots and areas of concentrated electric field is advantageous for many surface-enhanced spectroscopic methods.[39] Raman, infrared, and fluorescence are just a few examples of techniques that can have orders of magnitude increases in signal due to the concentrated electromagnetic fields produced by surface plasmons at metal−dielectric interfaces.[65−67] By rationally designing electric field-enhancing nanostructures, the spectroscopic signal can be improved by several orders of magnitude so that single-molecule detection is possible.[68−71]

Essentially, surface plasmon resonance provides a means to control the intensity and location of electromagnetic radiation with subwavelength precision. As would be expected, this has led to the development of a variety of SPR-based technologies. The biosensing community has benefited greatly from the high sensitivity of surface plasmons to their dielectric environment. When small molecules or biologically relevant species bind to a plasmonic substrate (usually made from Au or Ag), the SPR of that substrate will be affected due to a change in dielectric constant induced by the local concentration of target molecules. Target binding is assessed in real time by monitoring changes to the properties of an SPP if the substrate is a thin film or to LSPR if the substrate is a particle array. Many excellent reviews have been written discussing both types of detection schemes and can be found in refs 5, 6, and 72−74. Another class of SPR-based sensors is the colorimetric detection systems that rely on the controlled aggregation of particles in the presence of specific targets. As mentioned previously, when particles aggregate, they undergo a change in their optical properties due to the coupling of their resonances. When appropriately functionalized, Au nanoparticles can be programmed to aggregate upon target binding, causing a red-shift in their absorbance, with the colloid visibly changing color from red to purple.[1,75]

The physical properties of SPs have also made them of interest for subwavelength optical and electromagnetic applications. When incident light is coupled into an SPP, the light essentially becomes trapped at the metal surface. The ability of the propagating wave to follow the interface even if it changes dimensions or directions makes possible the production of SP-based waveguides. Combined with the ability to localize and concentrate electromagnetic radiation, such devices are able to control the behavior of light with a spatial precision well below the diffraction limit.[4,7,76−80] Incident electromagnetic radiation can also be manipulated by substrates with regular nanoscale features, called plasmonic crystals.[81−83] Merging the properties of propagating plasmons on a metal film with localized plasmons produced from nanoscale holes or features can yield exciting new metamaterial properties such as negative index of refraction and optical cloaking.[84−86]

Only a few applications of plasmonic materials have been mentioned so far, yet all of them rely on the ability to generate nanoscale objects from plasmonic materials. When the dimensions of a material are reduced to the nanoscale, its size and shape have profound effects on its properties. The ability to control the morphology of nanoscale features or particles directly correlates to the ability to tune the properties of a surface plasmon. Advances in chemical colloidal synthesis[15,17,87,88] and lithographic techniques[19,20] have allowed many of the exciting properties of SPs to be observed and utilized. However, if progress in the field of plasmonics is to continue, then it will be of pressing importance that synthetic techniques are able to meet the demand for generating highly controlled and well-formed nanostructures. Consequently, the majority of this review will focus on how one class of methods, templated techniques, has been used to successfully synthesize and assemble plasmonic materials to generate a wide range of desired properties.

3. SYNTHESIS WITH SOLUTION-PHASE TEMPLATES

Solution-phase nanomaterials are one of the most diverse sets of nanostructures, constituting oxide, metal, and semiconductor colloids, proteins, DNA, supramolecular architectures, and others that are often available in extremely high yield due to their thermodynamically controlled synthesis (e.g., nucleation and growth) or large-scale commercial availability (e.g., amino acids, lipids). Although some structures function by physically restricting nanostructure growth in a particular direction or geometry,[89,90] because reactions occur in solution, such templates usually serve as a scaffold to which the growing plasmonic material conforms.[91−93] In addition, templates are often elegantly designed to make use of thermodynamic differences in spatially distributed nucleation sites to construct complex nanoscale architectures.[94−96] Finally, nanomaterials synthesized from this class of template also tend to be relatively small in all dimensions and are thus incapable of supporting long-range propagating plasmon oscillations (SPPs) and almost exclusively exhibit LSPR behavior.

3.1. Metallic Core Templates

One of the most straightforward examples of a nanoscale template that acts to guide the growth of a plasmonic nanostructure is a metal nanoparticle. Although gold and silver colloids have been studied since the days of Michael Faraday, only recently have chemical methods become available to coat these structures in a continuous shell of a different material. This, of course, significantly modifies the electronic structure and optical properties of such materials as the new interface defines an abrupt change in the dielectric constant and can allow sharing of electrons across the boundary. These effects and others allow the shell material to chemically communicate with and "feel" the core material and vice versa. More recently, shape-controlled syntheses of metal nanostructures that can likewise be modified to act as supports for the deposition of a second element have been demonstrated, introducing the concept of shape as an additional variable that can impact the properties of the compound structure. Here, we will cover metal nanoparticles that act as templates for the growth of a second material that results in modified plasmonic properties for the composite. In the case of shaped nanoparticles that behave as templates, we will not cover the features that lead to anisotropic growth as they can be found in excellent review papers elsewhere.[15−17] However, we will discuss at length the chemical methods used to modify pre-synthesized anisotropic nanostructures so that they facilitate the growth of shells of different materials. Here we will use the common notation of the "@" symbol to denote the core−shell morphology, where X@Y signifies a core nanoparticle of X surrounded by a continuous shell of Y.

One can envision two primary mechanisms by which a continuous shell of a dissimilar material around a metal template could yield interesting plasmonic behavior from the composite structure. First, the shell material is itself metallic. This morphology arises often, particularly in the case of the noble metals Au, Ag, and Pd as they can readily form epitaxial interfaces. For example, Au and Ag particles of a particular shape are often used as templates for the reduction of a secondary plasmonic metal layer, resulting in a structure that has optical properties arising from both components. The second mechanism that can affect plasmonic behavior is the case where a conformal dielectric shell surrounds a plasmonic metal template. While examples of these materials with altered optical properties or anisotropic cores are fewer, several seminal examples have shown their utility in constructing materials with complex optical features.

3.1.1. Spherical Particles with Metallic Shells. Pioneering work on understanding the properties of spherical metal nanoparticles (NPs) coated in metal shells was carried out by Henglein et al. using AuNP or AgNP templates. In these early experiments, effort was focused on understanding the electrochemical properties of reactions involving the deposition of metals such as Cd, Pb, and Tl onto Au or Ag nanoparticles.[97] Dramatic shifts to the plasmon resonance of the final structures could be interpreted by donation of electrons to the template metal or Fermi-level equilibration between the two species over time.[98,99] These investigations aided in elucidating some of the fundamental chemical principles of metal nanostructures and paved the way for others to synthesize more exotic structures.[100] Following this initial work, many researchers sought to differentiate the optical features of core−shell and alloy particles composed of the more strongly plasmonic metals (Au and Ag) through Mie theory calculations and experimental verification.[101,102] For example, Henglein and co-workers used a radiolytic technique to reduce $Au(CN)_2^-$ onto preformed AgNP templates.[102] Monitoring the absorption spectra during the reaction, only one peak was observed at all times, whereas Mie theory predicted the presence of two peaks centered at approximately 380 and 520 nm if continuous Au shells were present around the AgNPs. The authors concluded that immediate alloy formation between reduced Au atoms and the parent AgNPs prevented observation of the expected plasmonic properties. Extending this work, Hartland and co-workers later showed the use of a similar γ-irradiation process using 15 nm AgNP or 20 nm AuNP templates to synthesize both Ag@Au and Au@Ag nanoparticles.[103] In both cases, two absorption peaks were observed, corresponding to the predicted plasmon resonances of core−shell particles, with their intensities being consistent with the relative abundance of each element in the composite structure. Interestingly, the authors then used picosecond-laser-irradiation-induced heating to alloy these two components and confirm the subsequent recovery of a single plasmon peak at ~450 nm. These radiolytic reduction methods were later applied to other noble-metal systems to generate more diverse core−shell nanostructures of Au@Pt,[104] Pd@Au,[105] and Pd@Au@Ag.[105]

Although early examples utilized radiolytic reduction of metal precursors, chemical reduction reactions are more common and have been used extensively to generate core−shell nanostructures. Gemperlová and co-workers first showed the chemical synthesis of Ag@Au nanoparticles by reducing $HAuCl_4$ in the presence of AgNP templates using hydroxylamine.[106] These same particles were later used by Moskovits to further elucidate and compare the optical properties of Ag@Au and AuAg alloy nanoparticles.[107] Importantly, further characterization of the Ag@Au nanoparticles prepared using this method by Hasslett and co-workers showed that while the core was indeed Ag, the shell most likely consisted of a AuAg alloy, rather than a pure Au shell as was previously thought.[108] Several other conflicting accounts on the structure and optical properties of the particles produced from this synthesis have been reported.[109] This morphology is particularly difficult to synthesize as aqueous Au^{3+} can readily undergo a redox replacement reaction with Ag^0, making observation of a truly phase-separated Ag@Au morphology challenging. More common is the inverse Au@Ag morphology, which avoids this issue and can be synthesized easily by chemical reduction of $AgNO_3$ in the presence of AuNP templates.[110]

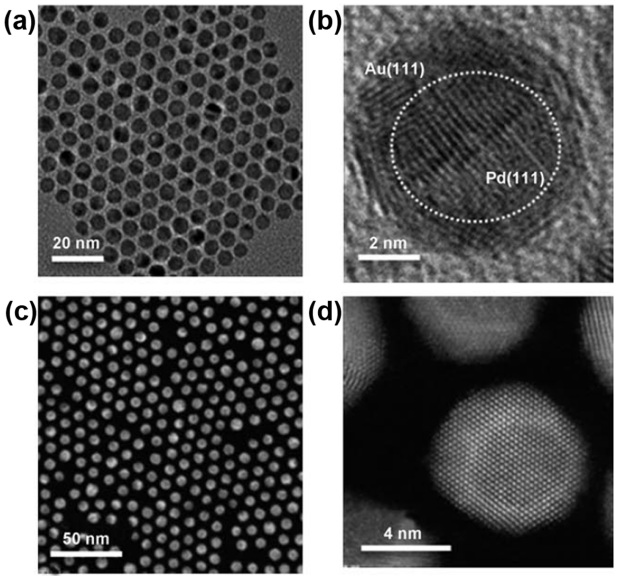

Figure 4. Representative electron microscopy images of Pd@Au nanoparticles: (a) TEM, (b) HR-TEM, (c) scanning transmission electron microscopy, (d) high-resolution high-angle annular dark-field scanning transmission electron microscopy. Adapted with permission from ref 91. Copyright 2010 Wiley-VCH Verlag GmbH & Co. KGaA.

Contemporary syntheses for core−shell particles have advanced considerably from these first examples and have now achieved an exquisite level of control over the materials and dimensions of the final structures. Ying and co-workers, for example, have developed a general phase-transfer method for preparing metal-complex precursors of over 20 different elements which can be used in numerous combinations to generate heterometallic nanocrystals.[111] In this case, dodecylamine acts as the phase-transfer agent, and upon reduction with $NaBH_4$, hexadecanediol, or tetrabutylammonium borohydride in nonpolar solvents (e.g., toluene or hexane), alloy particles of AuAg, PdPt, PtRh, and PtRu are formed by simultaneous reduction of both precursors and core−shell particles of Au@Ag, Pt@Ag, Ag@Au, and Ag@Pt by a sequential reduction process. In all cases, the bimetallic particles are less than ~15 nm in total diameter. In addition, Sun and co-workers are particularly adept at organic solvent-based syntheses of particles with extremely thin and tunable shells (Figure 4).[91,112,113] For example, they have shown growth of 1.5−2 nm thick Au shells around ~5 nm PdNP templates using oleylamine in 1-octadecene at elevated

dx.doi.org/10.1021/cr1004452 |Chem. Rev. 2011, 111, 3736–3827

temperatures.[91] Recently, several other complex core−shell structures have been demonstrated having intricate morphologies, such as Au@Pd@Pt,[114] and showing the incorporation of dissimilar materials, such as Au@Co[115] and Au@$FePt_3$.[116]

3.1.2. Plasmon-Mediated Syntheses of Bimetallic Structures. Heterometallic core−shell nanostructures can also be prepared through a photomediated method that utilizes Au core particles as plasmonic seeds to template the growth of Ag shells. Plasmon-mediated reactions have proven to be one of the most controllable synthetic methods for the preparation of Ag nanostructures. This class of reactions takes advantage of the intense electromagnetic field enhancement of Au and Ag nanocrystals to facilitate the reduction of Ag^+. These reactions are often high yielding and provide outstanding shape control in the context of prisms,[52,117,118] bipyramids,[119,120] decahedra,[121,122] and tetrahedra.[123] The first plasmon-mediated synthesis was introduced by Mirkin and co-workers, who described a photoinduced method to convert silver spherical nanoparticles to triangular nanoprisms.[52] In this protocol, an aqueous solution of 8 nm Ag spherical nanoparticles, trisodium citrate, and bis(*p*-sulfonatophenyl)phenylphosphine dipotassium salt (BSPP) was irradiated with fluorescent light for 70 h to yield a nearly complete (>99%) conversion of the spherical particles into ∼100 nm edge length triangular nanoprisms. The authors later demonstrated the utility of this photomediated synthetic method by showing that the excitation wavelength (λ_{ex}) could be used to exquisitely control the edge length of the nanoprisms, with the prisms growing until their plasmon resonances were slightly red-shifted from λ_{ex}.[117] These results, first confirmed by Brus and co-workers[124] and Callegari and co-workers,[125] demonstrated that light can be used to finely tune the architectural parameters of Ag nanostructures.

Mechanistic studies aimed at understanding the photomediated chemistry occurring in these reactions have been conducted by both Mirkin and co-workers[126] and Brus and co-workers.[127] It was found that the light-induced transformation from Ag spheres to nanoprisms occurs by a series of redox reactions: one being the plasmon-mediated reduction of Ag^+ at the surface of citrate-protected Ag nanoparticles and the other being the oxidative dissolution of small nanoparticles by O_2 which is facilitated by BSPP, a water-soluble triarylphosphine that forms coordination complexes with Ag^+. While BSPP is not essential for the reaction to occur, it functions to increase the total Ag^+ concentration in solution and, consequently, improves the monodispersity of the product.[120,126] The chemical reduction of Ag^+ is controlled by two half-reactions: (1) the oxidation of citrate to 1,3-acetonedicarboxylate and carbon dioxide and (2) the reduction of Ag^+ to Ag^0. The reduction of Ag^+ does not occur in the dark or in the absence of plasmonic seed particles, indicating that the seeds serve as photocatalysts for the reaction. Brus and co-workers have proposed that these reactions occur by a charge transfer from adsorbed citrate to "hot" holes generated from plasmon decay.[128−130] Consistent with this claim, a negative photovoltage has been measured for citrate-protected Ag colloids deposited onto indium tin oxide substrates[131] or Formvar/carbon transmission electron microscopy (TEM) grids,[132] indicating that adsorbed citrate is being irreversibly photooxidized when the colloids are exposed to light. This process results in an accumulation of electrons on the nanoparticles. If Ag^+ is present in solution, the shifted potential of the seeds can thermally reduce Ag^+ to Ag^0, leading to particle growth. Similar results have also been obtained from studies conducted on citrate-protected Au nanoparticles.[133,134]

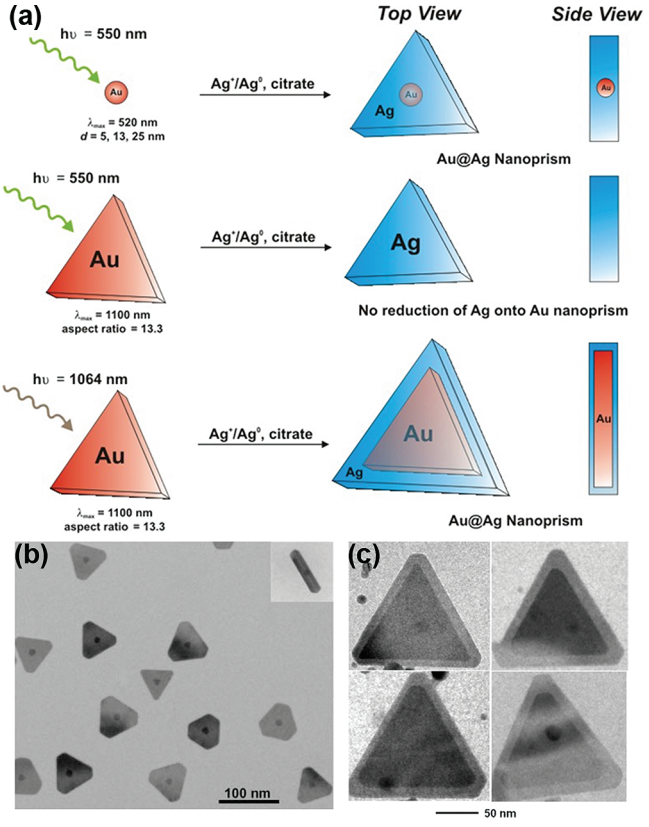

Figure 5. Illustration of the growth pathways for the Au core−Ag shell nanostructures: (a) The plasmon-mediated reduction of Ag^+ onto either spherical (top, TEM image in (b)) or prismatic (bottom, TEM image in (c)) Au cores yields heterometallic particles with Ag prismatic shells if the excitation wavelength is equal to the SPR of the seed particles. If the excitation wavelength is far from the SPR of the seed particles (middle), monometallic Ag triangular nanoprisms form without Au cores. Adapted with permission from ref 135. Copyright 2007 Wiley-VCH Verlag GmbH & Co. KGaA.

By combining a templated synthetic strategy with plasmon-mediated methods, unique Au core−Ag shell morphologies can be generated by the epitaxial deposition of Ag onto Au plasmonic seeds. Mirkin and co-workers demonstrated that Ag nanoprism shells can be epitaxially grown from either spherical or prismatic Au seeds.[135] Consistent with the proposed mechanism, the surface plasmon resonance of the seed particles has to be excited for the growth of heterometallic nanostructures to be observed (Figure 5). For instance, Ag is only deposited onto prismatic Au seeds, with a surface plasmon resonance in the near-IR, when a longer excitation wavelength (1064 nm) is used. In contrast, a shorter excitation wavelength (550 nm) results in the generation of monometallic Ag nanoprisms with no growth observed on the Au seed particles. More recently, Mirkin and colleagues have demonstrated that templated plasmon-mediated techniques are not limited to producing heterometallic structures with prismatic Ag shells.[136] By using Au decahedral seed particles, heterometallic nanorods and icosahedra can be selectively prepared. In these reactions, pH controls the reduction rate of Ag^+ and, consequently, the growth habit of Ag onto the Au decahedra. The faster reaction at pH 11 results in the epitaxial growth of {100}-faceted pentagonal nanorods, while the slower reaction at pH 7 results in the asymmetric growth of {111}-faceted icosahedra.

dx.doi.org/10.1021/cr1004452 |*Chem. Rev.* 2011, 111, 3736–3827

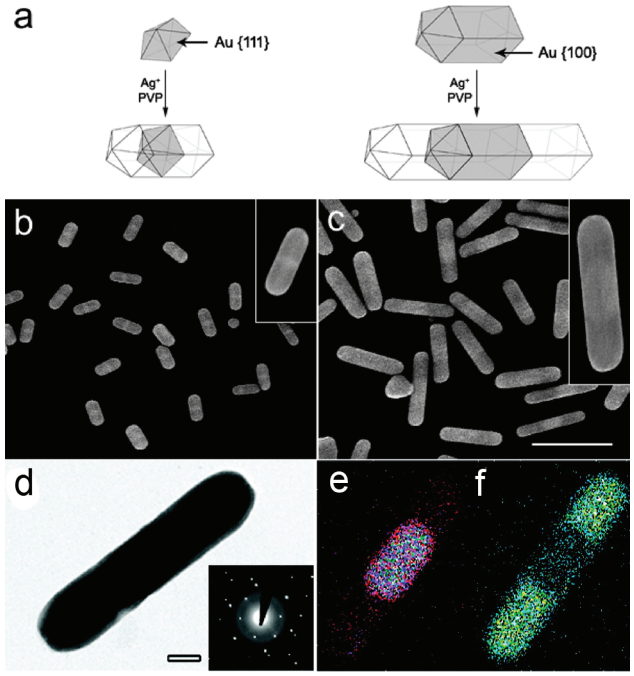

Figure 6. Directional growth of anisotropic Ag nanorods from a Au nanostructure template: (a) synthetic scheme describing the selective deposition of Ag onto the {111} faces of 5-fold-twinned Au decahedra or Au nanorods, (b, c) SEM images of the Au-decahedra-templated (b) and Au-nanorod-templated (c) bimetallic nanostructures; (d) TEM image and (e, f) corresponding EDX map of a composite nanorod with a core of Au (e) and symmetric segments of Ag (f). Adapted with permission from ref 144. Copyright 2008 American Chemical Society.

3.1.3. Anisotropic Particles with Metallic Shells. While in some cases plasmon-mediated syntheses offer a unique pathway to achieve bimetallic core−shell nanostructures that incorporate anisotropy, nanoparticles with well-defined shapes are often used as templates for the chemical reduction of secondary materials. Because gold nanorods were the first anisotropic metal nanostructures that could be reproducibly synthesized in high yield, they were the first used as scaffolds for the reduction of secondary metals. Jang and co-workers first demonstrated that surfactant-stabilized Au nanorods could function as templates by coating them in Ag through the reduction of $AgCl_4^{3-}$ ions with hydroxylamine.[137] This resulted in dramatic blue-shifts to both the transverse and longitudinal plasmon resonances, which could be reversed by the addition of HCl to selectively etch the Ag shell. Following this initial report, several groups demonstrated the reduction of $AgNO_3$ using ascorbic acid at basic pH to generate Ag shells around Au nanorods.[138−140] In all cases, it was observed that although for thin coatings Ag formed a conformal shell, additional reduction of Ag occurred selectively at the nanorod ends, resulting in the formation of nanorods with sharp, diamond-shaped tips. It was hypothesized that the surfactant stabilizing the original Au nanorod templates could not pack as densely on the {111} facets composing the nanorod tips as on the higher index {100} or {110} facets along the sides, leading to preferential Ag deposition. Importantly, this Ag coating strategy led to extremely tunable longitudinal plasmon resonances throughout the visible spectrum as a function of the Ag shell thickness.[139,140] This synthesis strategy has been investigated by numerous others, and the selective Ag deposition effect has been used to produce nanorod morphologies with a variety of asymmetric Ag coatings.[141,142] Surprisingly, with the addition of a well-known AuNP stabilizing polymer, poly(vinylpyrrolidone) (PVP), Xia and co-workers showed that with reactants otherwise identical to those of the prior examples, Au nanorods could template the growth of Ag octahedral shells.[143]

In an interesting alternative approach, Song and co-workers have demonstrated the colloidal synthesis of segmented metallic nanorods from various pentatwinned Au nanoparticle templates (Figure 6).[144−146] Starting with Au decahedra that exhibit a 5-fold symmetric twinning structure, the authors demonstrated that the reduction of $AgNO_3$ with PVP in a heated diethylene glycol solution resulted in the epitaxial growth of two symmetric Ag segments from the Au templates along the direction of the shared twin axis [110].[144] Equivalently, 5-fold-twinned Au nanorods could be used as the templates with similar results. Selective removal of the Ag by etching with HNO_3 resulted in the recovery of the original Au templates with little to no evidence of alloying. Additional work with this system elucidated a more fundamental understanding of the growth mechanism and demonstrated that changing the size of the Au decahedral templates correspondingly changed the diameter of the final nanorod structures.[145,146]

Although the high-yielding and relatively simple syntheses for Au nanorods facilitated initial investigations that used these structures as templates, several other anisotropic nanoparticles have been successfully coated with various metals to modify their optical properties. For example, Mirkin and co-workers used Ag triangular nanoprisms as templates for the deposition of Au using a slow reducing agent (ascorbic acid) in the presence of the stabilizing surfactant cetyltrimethylammonium bromide (CTAB).[147] For a relatively low ratio of Au to Ag in the reaction, they observed the growth of a Au shell surrounding the Ag prism core, with evidence for preferential deposition of Au at the tips or edges. Aherne et al. later showed that these thin Au coatings could be used to protect the Ag prisms from etching under conditions that would ordinarily attack and truncate the prism tips.[148] In both cases, corresponding red-shifts in the plasmon resonances were observed with thicker Au shells. Later, Mirkin and co-workers showed that the inverse morphology occurs when Ag is reduced onto the surfaces of Au triangular prisms.[149] In this case, Ag was found to selectively coat the triangular {111} faces, resulting in a truncated morphology and a final shape known as a bifrustrum. Remarkably, this thin Ag coating resulted in a blue-shift of the dipole plasmon resonance from 1230 nm for the discrete Au nanoprisms to below 800 nm, demonstrating a high degree of tunability in the optical properties of the bimetallic particle.

More recently, several varieties of polyhedral particles, including cubes and octahedra, have been used as templates. Starting with Au octahedra templates, Tian and co-workers showed that reduction of Pd using ascorbic acid in a CTAB solution resulted in the growth of a Pd cube surrounding the Au octahedra.[150] Interestingly, replacing Pd with Ag resulted in the same $octahedra_{Au}@cube_{Ag}$ morphology, suggesting the possibility of a similar crystal-facet-selective growth mechanism across all epitaxially deposited metals. Transitions between cubic and octahedral nanostructures have been observed in several other systems as the two shapes share the feature of being bound entirely by a single, low index crystal facet and are often related through either facet-selective deposition or facet-selective etching.[151] Instead of the growth of a cube, Han and co-workers observed conformal

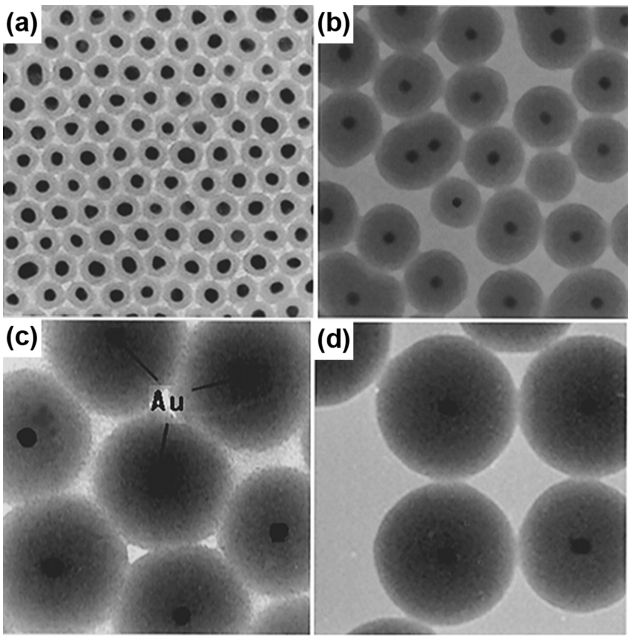

Figure 7. TEM images of silica shells grown around Au nanoparticle templates. The shells have thicknesses of (a) 10 nm, (b) 23 nm, (c) 58 nm, and (d) 83 nm. Adapted with permission from ref 92. Copyright 1996 American Chemical Society.

Pd shells surrounding Au octahedra when they used CTAC as the surfactant and reducing agent.[152] The authors proposed that the weaker binding of chloride anions compared to bromide may have played a role in the difference in morphology. Xia and co-workers similarly showed differences in the morphology of Pd@Au or Au@Ag particles simply by changing the reducing agent or surfactant species, respectively.[153,154] More recently, Huang and colleagues have shown sophisticated Pd tetrahexahedral and concave octahedral shells surrounding Au cube templates through a unique oxidative etching mechanism that also depends on the specific counterion present during the reaction.[155] These examples highlight that although there are still many unknowns, crystal-facet-selective reactions are emerging as a powerful means to modify the optical and chemical properties of anisotropic nanostructures.

3.1.4. Structures with Oxide Shells. All of the examples thus far have used metallic particles as scaffolds for introducing new plasmonic metals. However, an alternative strategy is to manipulate the innate plasmonic properties of the metallic template itself through deposition of a dielectric material that can modulate the optical response.[156,157] This simple strategy has recently produced nanostructures that can function as versatile surface-enhanced Raman spectroscopy (SERS) substrates[158] and have been shown to exhibit remarkable new physical properties such as surface-plasmon-based lasing[159] and light-controlled manipulation of spin[160] (see section 9.3). The first example of this morphology and much of the subsequent fundamental work was demonstrated by Mulvaney and co-workers through the growth of silica shells around AuNPs or AgNPs (Figure 7).[92,161] At the time, the major difficulty in synthesizing such a structure was that most nanoparticle colloids were negatively charged, creating an electrostatic barrier for reactions involving any anionic silicate precursors.[157] To circumvent this issue, Mulvaney rendered AuNPs vitreophilic or "glass-loving" by functionalizing with (3-aminopropyl)trimethoxysilane (APTMS) wherein the amine groups could coordinate to the Au surface, presenting silanol groups to solution. Addition of sodium silicate at the appropriate pH resulted in a slow polymerization reaction yielding a 2−4 nm thick, relatively homogeneous layer of silica surrounding the Au particles. This coating could be further grown to thicknesses as large as ∼80 nm through the base-catalyzed hydrolysis and condensation of tetraethoxysilane (TEOS) using ammonia in a water/ethanol mixture, which is also known as the Stöber method.[162] The effect on the optical response was a red-shift and increase in intensity of the plasmon band for moderate SiO_2 shell thicknesses. Further work demonstrated that the shell was mesoporous by monitoring various chemical reactions, such as the transformation of Ag to AgI and Ag to Ag_2S, and the alloying of Ag and Au as a function of the diffusion of chemical species through variable-thickness silica shells.[163,164] Later improvements to the synthesis came from Xia and co-workers, who demonstrated with iron oxide[165] and AuNPs[166] that the TEOS hydrolysis and condensation reaction could take place directly on the nanoparticle surface without the need for modification with APTMS precursors. Several others have extended these principles to generate conformal silica shells surrounding anisotropic nanostructures such as rods,[167] wires,[168] triangular prisms,[169,170] and cubes.[171]

Silica coatings of nanomaterials have often been used as nanoscale "spacer" layers that provide tunable separation between the core material and a surface-bound component. For example, several investigations have shown selective etching of the silica shell using HF after coating with a polymer layer to produce nanostructures with hollow interiors containing freely moving AuNPs.[172,173] Other groups have utilized this spacer strategy for studying interesting optical effects. For example, initial work demonstrated that several fluorophores bearing thioisocyanide groups could be conjugated to (3-aminopropyl)-triethoxysilane (APTES) and incorporated into the silica shell during the condensation reaction.[165] To accomplish the same goal, Natan and collaborators showed the functionalization of AuNPs with a Raman chromophore, followed by silica encapsulation to embed the molecule in the shell.[174] These examples are important as they demonstrate that the optical activity of chemically sensitive molecular species can be preserved after silica encapsulation. This feature has been used in many investigations to probe the distance dependence of various coupling effects that occur between plasmonic particles and other optically active materials.[175−177]

While silica has been the most popular and thoroughly investigated, a number of other oxide materials have also been grown from metal nanoparticle templates. Liz-Marzán and co-workers were among the first to demonstrate a titania coating around plasmonic nanostructures using a reaction similar to that in the case of silica.[178] Although occurring in a one-pot *N*,*N*-dimethylformamide (DMF)/ethanol mixture, $AgNO_3$ is first reduced by DMF, followed by the slow hydrolysis and condensation of $Ti(OC_4H_9)_4$ in the presence of acetylacetone acting as a chelating agent. The result is a population of ∼20 nm particles that consist of a AgNP core surrounded by a several nanometer thick TiO_2 shell. This thin coating of TiO_2 is able to red-shift the plasmon resonance of the AgNPs from 400 to 435 nm simply on the basis of the altered dielectric environment. Using a different approach, Zeng and collaborators synthesized Au@TiO_2 nanoparticles simply by heating a solution of 50−150 nm citrate-capped AuNPs with TiF_4 in water at 180 °C.[179] The resulting

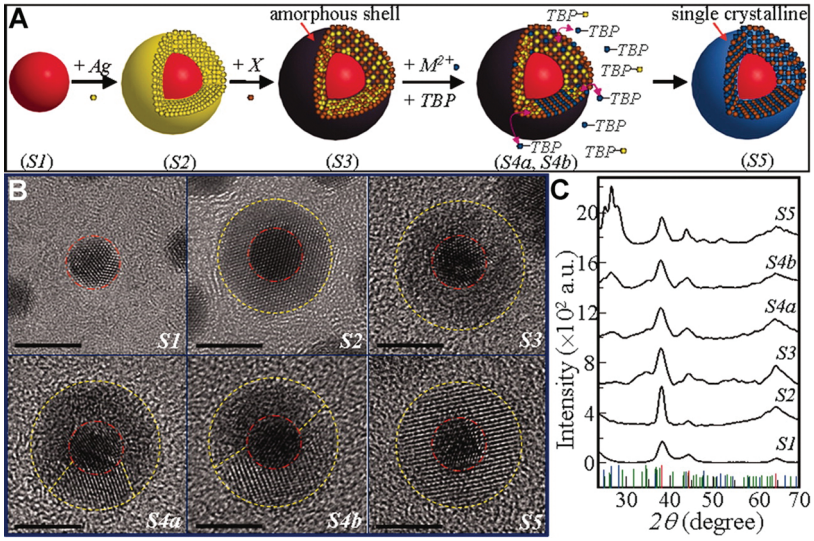

Figure 8. Growth of semiconductor shells around Au nanoparticle templates: (A) scheme illustrating the steps in the synthesis pathway, including growth of a Ag shell (S2), conversion to an amorphous Ag_2X shell (where X = chalcogenides, As, P) (S3), and exchange of Ag with a desired metal (Cd, Pb, Zn) (S4), to yield a variety of single-crystalline shell materials (e.g., CdS, CdSe, CdTe, PbS, ZnS) (S5), (B) HR-TEM images showing the evolution of a Au nanoparticle (S1) to a Au@CdS nanoparticle (S5) following the steps outlined in (A) (scale bars equal to 5 nm), (C) corresponding XRD patterns of the stages illustrated in (B). Adapted with permission from ref 192 Copyright 2010 American Association for the Advancement of Science.

particles consisted of polycrystalline flower-like shells of anatase TiO_2 that were porous enough to allow for a variety of chemical modifications. A similar approach showed that layer-by-layer electrostatic self-assembly could be used to localize a Ti precursor (titanium(IV) bis(ammonium lactato) dihydroxide) around a AuNP surface that could later be hydrolyzed and precipitated at high temperature in the form of a conformal TiO_2 shell.[180] Along the same lines, Mulvaney and co-workers have shown that heating a solution of sodium stannate at pH 10.5 in the presence of 15 nm AuNP templates resulted in the formation of Au@SnO_2 nanoparticles.[181] Although this oxide coating resulted in a red-shifting of the plasmon resonance to 542 nm, the authors showed this could be reversibly blue-shifted by injection and storage of radiolytically generated electrons in the Au core. This type of photocatalytic effect is common with large band gap oxide-coated metal nanostructures and has been a topic of investigation in particles composed of Au@TiO_2, Ag@TiO_2, Au@ZrO_2, and Ag@ZrO_2 as well.[182−185]

3.1.5. Structures with Semiconductor Shells. Semiconductor materials represent another important class of dielectric materials that can be grown on metal nanoparticle templates. Several examples of exotic physical properties that arise from exciton−plasmon coupling, for example, help to motivate the synthesis of these structures.[160] While early examples were able to demonstrate the nucleation of small semiconductor domains on plasmonic nanoparticles,[186] the formation of continuous shells remains a challenge. Hou and co-workers took an interesting approach to solving this problem by first synthesizing ~5 nm AuCd alloy nanoparticles and then reacting them at high temperature with a Se precursor.[187] The resulting particles exhibited a Au@CdSe morphology, although the final shapes were irregular and the cores were frequently offset. Alternatively, AuNPs could be mixed with a cysteine−Cd^{2+} complex which decomposes into a rough but continuous CdS shell after 6 h at 130 °C.[188] Talapin and co-workers have shown the synthesis of Au@PbS nanoparticles through a high-temperature synthesis involving the reaction of dodecanethiol-capped AuNPs with Pb and S precursors.[189] Interestingly, depending on the reaction temperature, the PbS shells could be tailored to be either spherical or cubic, with the composite particles exhibiting extremely red-shifted resonances of ~620 nm due to the high dielectric constant of PbS. Anisotropy can also be imparted to semiconductor shells by using shaped AuNP templates such as rods, plates, or octahedra.[190]

Several groups have developed more general synthetic conditions that can be applied to a variety of material combinations. For example, Wang and co-workers synthesized Au nanoparticles having either a Ag_2S or a CuS shell which could then undergo a cation exchange reaction with several other metal ions (Cd, Zn, Ni) to generate heterostructures with a variety of metal sulfide coatings.[191] Although also observed for Au@CdS nanoparticles, ZnS coatings allowed for particularly tunable plasmon resonances from 550 to 760 nm as a function of the shell thickness. Using the same principle of a sacrificial layer to mediate shell growth, Ouyang and collaborators have shown a particularly elegant approach that deposits an amorphous Ag_2X layer (where X = chalcogenides, As, P) onto AuNP templates, which can be exchanged with a variety of metals to form crystalline shells that are continuous and exhibit no evidence of lattice strain (Figure 8).[192] More specifically, the addition of tributylphosphine (TBP) facilitates the replacement reaction between the desired metal ion and Ag in the starting Au@Ag_2X nanoparticles. For example, Au@CdS nanoparticles could be synthesized by adding Cd^{2+} and TBP to a solution of Au@Ag_2S nanoparticle templates. In addition, if only 1/2 equiv of metal ions is added with respect to Ag, a phase-separated hemispherical shell is formed. This allows one to start, for example, with Au@Ag_2S nanoparticles and replace one hemisphere of the Ag_2S shell with Cd and the other hemisphere of the Ag_2S shell with Pb, resulting in Au@CdS|PbS nanostructures (where the "|" symbol denotes a phase-separated morphology; see section 3.3). This procedure is extremely powerful as it combines significant materials generality

dx.doi.org/10.1021/cr1004452 |*Chem. Rev.* 2011, 111, 3736–3827

with remarkable precision over the size and morphology of nanoscale features.

3.2. Dielectric Core Templates

One of the simplest template-based approaches to fabricating nanostructures with complex plasmonic behavior utilizes a colloidal dielectric material as a substrate for the deposition of a metal. Because both the nature of the dielectric substrate and the detailed morphology of the metal shell affect the optical response, a surprisingly large parameter space exists for modulating the properties of this seemingly simple structure. The most interesting examples of this morphology have continuous metal shells surrounding the dielectric core which support highly tunable plasmon resonances as a function of the core size and shell thickness. Because of the spherical symmetry, the optical properties of these structures can be modeled accurately by Mie theory and were theoretically investigated as early as 1951 by Aden and Kerker[193] with subsequent extensions by several others.[194,195] Although reproducible experimental confirmation of these results followed long after their initial publication,[93,196] the rich history of understanding nanostructures having this metal shell morphology has led to a number of important fundamental advances in the understanding of plasmonic nanoparticles.[197,198] This has also facilitated numerous applications of these structures as powerful multifunctional photothermal cancer therapeutics,[199−205] imaging contrast agents,[206,207] and local field enhancers of Raman scattering,[208−214] infrared absorption,[215−218] or fluorescence emission.[219−221]

Because most dielectric templates differ considerably in their surface characteristics from noble metals, they typically require a sensitization process to make them amenable to metal deposition and growth. In the case of nucleating discrete, usually spherical, nanoparticles on polymer or oxide spheres, coordinating ligands or electrostatics have been used to localize metal ions before a reduction step. For the growth of a continuous metal shell, small ∼2 nm nanoparticles are usually chemically or electrostatically attached to the template material to act as "seed" nucleation sites for the reduction of additional metal. These methods are extremely general and have been used to generate metal structures on a variety of dielectric templates. In rare cases, the chemical or crystallographic conditions of the template are appropriate for reduction of a plasmonic material directly onto the dielectric surface, making the seeding strategy unnecessary. Although there are fewer instances where this alternative strategy has been used, the final structures are usually smaller than those seeded with nanoparticles, and they may therefore have specialized applications for which they are optimum.

3.2.1. Substrates with Discrete Nanoparticle Coatings. The most straightforward morphology that utilizes a dielectric colloid simply involves the nucleation and growth of discrete plasmonic particles on the surface of the template. Early work in this field took the approach of using surface-bound ligands on spherical polymer particles to coordinate metal ions followed by the addition of a reducing agent to generate metal nanostructures.[222−225] Using this strategy, Wannemacher and co-workers explored several combinations of surface functionalization, reducing agent, and Ag precursor to optimize AgNP nucleation onto polystyrene latex spheres.[226] Most of these methods resulted in 20−50 nm AgNPs that, depending on the surface density, showed optical resonances at wavelengths as long as ∼550 nm, indicating strong coupling between closely spaced AgNPs. In an alternative electrostatic approach, Liz-Marzán and co-workers modified silica particles with Sn^{2+} ions, which, when exposed to $Ag(NH_3)_2^+$, undergo a redox reaction that results in the oxidation of Sn^{2+} to Sn^{4+} and the reduction of Ag^+ to Ag^0.[227] This process could be repeated several times and resulted in the formation of a dense layer of AgNPs on the template surface. It was later shown that this reaction also could be used to prepare AuNPs on silica spheres.[228] Electrostatic adsorption of precursor ions is a particularly versatile method for preparing these materials and has been used to deposit metals such as Au[229−233] and Ag[234−237] onto templates of Fe_3O_4,[238] TiO_2,[239−241] and SnO_2.[242] Other common techniques that produce plasmonic structures with this morphology include photoinduced reduction of metals onto semiconductor particles,[243,244] in situ metal reduction during the polymerization or condensation reactions used to generate the templates,[245−248] and ultrasonic/sonochemical reduction of metals onto colloidal dielectric or polymeric spheres.[249−252]

3.2.2. Continuous Metallic Nanoshells. While these particle-on-sphere structures represent important first steps in the construction of complex plasmonic structures, their optical properties are not particularly intricate, because the nanoparticle surface densities are typically too low to observe any collective behavior due to strong interparticle coupling. The presence of a continuous metal shell surrounding a dielectric substrate, however, can support far more complex and interesting plasmonic properties. Although investigated theoretically much earlier,[193−195] one of the first experimental examples of such a nanostructure was reported by Wokaun and co-workers in 1989.[253] Starting with either 44 nm polystyrene or 35 nm poly(methyl methacrylate) (PMMA) spheres, the authors showed that ultrasonication in the presence of a Au or Ag metal salt with a reducing agent resulted in 10−30 nm thick shells around the polymer template. These exhibited plasmon resonances from ∼550 to 600 nm for Ag shells and from ∼615 to 690 nm for Au shells, consistent with corresponding Mie theory calculations of the same geometry. Despite the agreement with theory, only between 7% and 17% of the polymer particles were coated with metal, making the synthesis particularly low yielding and difficult to study in more depth.

A high-yield synthesis of metal nanoshells was subsequently demonstrated by Zhou et al., allowing for some of the first detailed experimental characterizations of these structures.[196] Using a two-step procedure, the authors first synthesized Au_2S dielectric particles through the addition of $HAuCl_4$ to Na_2S in water. Next, by adding additional Na_2S, they observed the appearance of ∼5 nm spherical particles and ∼25 nm Au_2S particles coated with a thin Au shell. These results were manifested in extinction spectra that contained a peak at ∼530 nm, corresponding to the spherical particles, and a red-shifted peak between 700 and 800 nm, corresponding to the core−shell particles. The details of the optical properties and the growth mechanism for this Au nanoshell structure were later determined by Halas and co-workers by using a single-step reaction involving the mixing of aqueous solutions of $HAuCl_4$ and Na_2S.[254] Here, they observed the linear growth of the Au_2S core to a size of ∼30 nm, followed by the linear growth of the Au shell from a thickness of ∼1 nm to a thickness of 5 nm. This two-phase growth model was confirmed by extinction spectra which showed the appearance of a peak at ∼700 nm that red-shifts in time to a maximum value of ∼900 nm before blue-shifting back to ∼700 nm. The explanation for this behavior is that the SPR of a metal nanoshell depends on the ratio of its inner and outer

dx.doi.org/10.1021/cr1004452 |Chem. Rev. 2011, 111, 3736–3827

diameters. When the dielectric core is the largest (30 nm) and the metal shell is the thinnest (1 nm), the most red-shifted peak will be observed. The onset of the second growth stage results in a thickening of the shell and a corresponding blue-shift in the resonance. Mie theory simulations of the nanoshells at each of the growth stages matched well with the experimental data and revealed additional details of the optical response. Several subsequent investigations explored the optical properties[255] and ultrafast electron dynamics[256−258] of these particles in more detail, and they have been used to photothermally trigger the release of encapsulated fluorophores from polymer capsules[259] and as LSPR sensors of molecular binding events.[260]

Interestingly, van Buuren and co-workers have claimed that the existence of the Au_2S core−Au shell morphology lacks sufficient experimental evidence, and the red-shifted peaks observed in the optical spectra are better explained by aggregation of the spherical particles that form concomitantly.[261,262] However, the authors do not address the observed blue-shift of the nanoshell resonance as the Au shell thickens, and single-particle scattering data gathered by Raschke et al. demonstrate polarization-independent spectra with extremely narrow line widths from isolated nanoshells.[260,263] Both of these are indicators of a lack of particle aggregation and suggest that some detail of the synthetic procedure is responsible for the lack of reproducibility. This controversy, however, highlights the importance of obtaining a synthesis that is both high yielding and also free from impurity particles, as the absence of spheres would have allowed a more conclusive determination of the products of the synthesis.

Halas and co-workers were the first to overcome these challenges with a high-yielding, morphologically pure synthesis of Au nanoshells by a seeded growth method (Figure 9).[93] First, silica nanoparticles of a desired size were synthesized via the Stöber method[162] and functionalized using APTES. The silane groups of APTES interact strongly with the SiO_2 surface, presenting terminal amines to an aqueous solution. This amine functionality was used to adsorb small ∼2 nm AuNPs onto the particle surface, effectively "seeding" it for additional growth.[264] Using an aged solution of $HAuCl_4$ and K_2CO_3 (often referred to as K-gold) as the metal source and $NaBH_4$ or formaldehyde as the reducing agent, metal deposition was driven to occur selectively on the existing AuNPs bound to the dielectric surface. This resulted in the enlargement and ultimate fusion of the growing Au domains to form a polycrystalline, continuous shell surrounding the dielectric core. In addition to being morphologically pure, this approach also allows for a degree of structural tunability unavailable to many other methods. Because both the dielectric core size and shell thickness are controlled in separate synthetic steps, the geometric parameters and resulting optical properties can be finely tuned (Figure 9b). Using SiO_2 templates of either 120 or 340 nm with shell thicknesses between 20 and 50 nm, the authors observed dipole plasmon resonances that range from 650 to 950 nm with additional higher order modes that are well described by Mie theory calculations. Subsequent work investigated how the resonance mode order (dipole vs quadrupole) influenced both the SERS response and the angular dependence of scattered light from the nanoshells.[208,265] This work was one of the first demonstrations of a high degree of SPR tunability due to rational structural control of a nanoparticle. In addition, it could be completed in high yield and free from impurity particles of undesired shapes. As a result, it spurred numerous additional avenues of research and remains an actively investigated and utilized nanostructure.

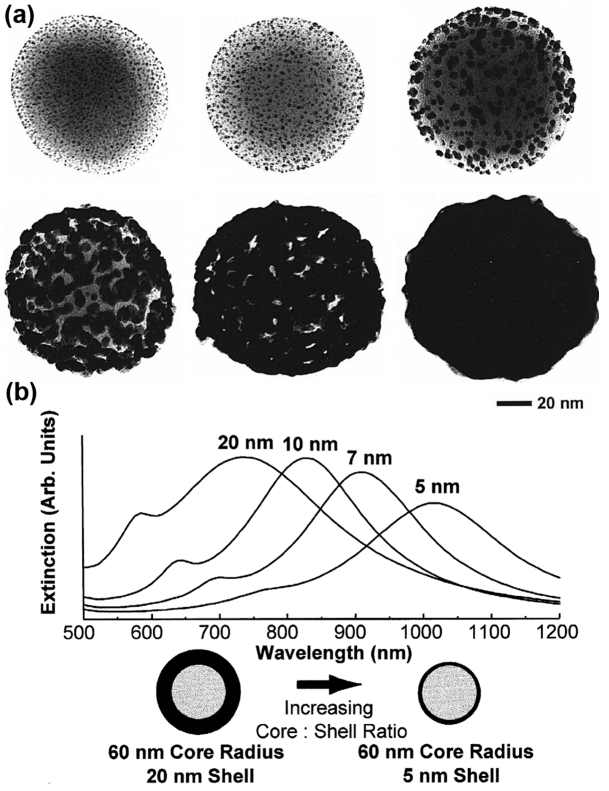

Figure 9. Growth of conformal Au shells surrounding silica dielectric templates: (a) evolution of the seeded growth of ∼2 nm AuNPs on the silica particle surface by electroless deposition to form a continuous Au shell, (b) theoretically calculated extinction spectra of Au nanoshells with differing core:shell ratios. The shell thickness is labeled above the respective peak. Adapted with permission from ref 93. Copyright 1998 Elsevier Science B.V.

After the initial demonstration of the seeding approach to produce high-quality Au nanoshells, efforts to expand the synthetic tunability and measure their optical properties followed. The first modifications to the synthesis involved relatively straightforward changes that nonetheless demonstrated greater control over the properties of the nanoshells. For example, Halas and collaborators showed that by using silica templates as small as 55 nm and Au shell layers as thin as 6 nm, dipole plasmon resonances could be made to cover a much larger range of wavelengths, from 800 to 2200 nm.[266] Interestingly, for larger structures with 210 nm dielectric cores, they could observe the appearance of quadrupole and octupole modes as a function of the shell thickness, demonstrating impressive control over both the position and order of the surface plasmon resonance. Graf et al. showed several modifications to these structures by simple postsynthetic treatment of the seeded Au nanoshells.[267] In one method, after the growth of an additional continuous silica layer around the nanoshells, the particles could be dried in ordered arrays that produced brilliant colors due to Bragg reflections from superlattice planes. In a second approach, hydrofluoric acid was used to etch away the silica core, generating a hollow nanostructure that exhibited modifications to the extinction spectra as a consequence of the change in substrate dielectric constant. Prasad and co-workers extended the principles of the seeded shell growth methodology to templates consisting of polystyrene latex spheres rather than SiO_2 cores.[268]

In this case, carboxyl-functionalized polystyrene spheres were modified with 2-aminoethanethiol hydrochloride via 1-ethyl-3-[3-(dimethylamino)propyl]carbodiimide (EDC) coupling to present thiol moieties on their surfaces. Following treatment with ~2 nm AuNPs that bound these thiol groups, hydroxylamine could be used to reduce additional Au salt in the form of a continuous metal shell surrounding the polymer template. These nanoshells exhibited optical properties analogous to those synthesized by Halas with tunable resonances as a function of the shell thickness. Finally, an improved seed-based synthesis for Au shells on silica templates was provided by Halas and co-workers that allows for the formation of more uniform metal layers without compromising their continuity.[269] After functionalization of silica spheres with APTES and attachment of ~2 nm AuNPs, carbon monoxide gas was introduced to reduce additional metal from a K-gold plating solution to form a continuous shell. This simple change in reducing agent from a common chemical species to CO gas allowed the authors to synthesize thinner Au shells while maintaining their homogeneity, allowing for more tunable plasmonic resonances. These synthetic advances, along with the inherent optical properties of the nanoshell, have facilitated numerous biomedical investigations[270−272] for the development of cancer imaging and therapies,[199−207] immunoassays,[273] optomechanical transducers,[274−276] and light-mediated oligonucleotide release.[277,278] Furthermore, their plasmonic properties have been used for various surface-enhanced effects (e.g., SERS)[208−221] and dielectric sensing[279] and have recently been shown to support exotic magnetic and Fano resonances when assembled into symmetric trimer and heptamer geometries, respectively.[280]

It is important to note that the development of the Au nanoshell synthesis has facilitated a number of theoretical advances in the understanding of complex plasmonic structures.[198] Early modeling of these structures made use of Mie theory, which gave insights into the spectral tunability of multipolar resonances and several effects such as phase retardation and electron-interface scattering.[281−283] Finite difference time domain (FDTD)[284] and time-dependent local density approximation (TDLDA)[285,286] methods helped to reveal the effects of external mechanisms for modulating the plasmon resonance, such as the presence of a dielectric embedding medium[287,288] or a nearby substrate composed of dielectric[289,290] or metallic[291] materials. A fundamentally different way of thinking about and simulating plasmonic effects was introduced by Nordlander and co-workers and was initially applied to understanding the resonances of the Au nanoshell.[197] Known as the plasmon hybridization model, the formalism attempts to first deconstruct a complex structure into several more primitive shapes and then allow the plasmonic modes of these elementary geometries to mix and hybridize, in striking analogy to molecular orbital theory. The result is a more intuitive physical picture of the optical response wherein symmetric or antisymmetric coupling between constituent modes may result in bonding or antibonding plasmon resonances that manifest themselves in different ways depending on their character. This approach has been applied to many systems with complex structural configurations and has become a common method for understanding the optical response of nanoparticles and, in particular, nanoshells and nanoshell-related structures.[198,292−294]

While Au has proven to have chemical properties that are amenable to seeded shell growth, other plasmonic materials are more challenging. However, by making use of many of the same synthetic strategies, additional metals can be grown onto dielectric templates, providing another handle for modulating the physical properties of these nanostructures. Silver is a particularly important plasmonic material as its interband transitions and SPR are significantly separated in energy, which mitigates damping of the plasmon oscillation, resulting in more intense absorption and higher local fields. An initial step toward the synthesis of Ag nanoshells utilized AuNP seeds chemically attached to silica templates by APTMS.[295] In this study, the authors explored several different reduction methods and Ag ion precursors to optimize the nucleation and growth of continuous Ag shells from the AuNP seeds. Although many of the structures exhibited rough or discontinuous morphologies, the reduction of $AgNO_3$ by a combination of formaldehyde and NH_4OH resulted in smooth 15−20 nm thick Ag nanoshells with resonances tunable into the near-infrared. Later approaches to produce Ag nanoshells utilized AgNP seeds synthesized directly onto silica[296] or polystyrene[297] templates followed by reduction of $AgNO_3$ by sodium citrate[296] or formaldehyde.[297] Because these procedures avoid the requisite seeding of the surface with AuNPs, they are able to generate shells composed of the pure metal.[298−301] In an impressive example of the materials generality of this process, Halas and co-workers demonstrated the formation of Cu nanoshells on silica templates with unique optical resonances.[302] Plasmon oscillations in Cu are often strongly damped by interband transitions that occur at similar energies, thus making it a much less often studied material in nanoscale systems. However, by generating 30−50 nm thick Cu shells around 63 nm silica templates, the plasmon resonance can be sufficiently red-shifted away from the interband transitions so as to be easily observable. Interestingly, when the dipole or quadrupole plasmon resonance is chosen to be coincident with the threshold of the interband transitions, a feature with a double-peaked line shape occurs due to spectral overlap of these two excitations.

Straightforward extensions of many of these principles have led to bimetallic systems consisting of Pt or Pd shells[303] or AuAg alloy shells surrounding silica templates.[304] Several reports have sought to incorporate magnetic nanoparticles into the nanoshell structure to afford an added functionality for magnetic manipulation. A common approach is to use a layering strategy of the dissimilar materials wherein templates are modified with one material (Fe_3O_4 or Au nanoshell), coated in a layer of silica, and then modified with the second material (Au nanoshell or Fe_3O_4), producing radially separated components.[305,306] Similarly, an iron oxide nanoparticle can be coated in a layer of silica, followed by AuNP deposition and growth of a Au shell.[307−310] In an alternative approach, Mirkin and co-workers adsorbed both Fe_3O_4 and Au nanoparticles to a silica template and subsequently used the AuNPs as seeds for the growth of a Au nanoshell by formaldehyde reduction of $HAuCl_4$.[311] This resulted in a continuous Au shell embedded with magnetic domains that may be interesting for combined mid-infrared imaging and photothermal therapy applications.[306,312]

3.2.3. Concentric and/or Asymmetric Nanoshell Structures. The optical properties of metal shells with dielectric cores become more complex when one introduces systematic deviations in the simple shell morphology. It is often the case that one can provide a greater degree of tunability in the total optical response of the structure either by embedding plasmonic materials within the dielectric core or by breaking the spherical symmetry of the shell to introduce additional plasmon resonances. Initial attempts at introducing these shape variations

revolved around postsynthetic destruction or modification of spherical Au nanoshells. Reshaping effects using femtosecond pulsed laser irradiation,[313,314] controlled etching using 2-aminoethanethiol,[315] or electron beam-induced ablation[316] revealed that subtle changes in the nanoshell morphology produced striking shifts in the plasmon resonance.[317] By including a spherical Au or Ag nanoparticle embedded in the center of the dielectric core before formation of a metal shell, Liz-Marzán and co-workers demonstrated controlled coupling between the core nanoparticle and shell material as a function of the dielectric spacer thickness (Figure 10a).[318] This structure can be used to investigate the interactions between dissimilar core and shell materials and has garnered theoretical interest because of the strong coupling between the closely spaced components.[319,320] Indeed, this structure has recently been shown to individually support Fano resonances because of the unique mixing between subradiant and superradiant states that arise due to the particle geometry.[321] Additionally, Nordlander and colleages demonstrated the synthesis of a nested structure in which Au nanoshells are coated with a silica layer, followed by the deposition of a second Au shell (Figure 10b).[197] The optical spectra of these structures become increasingly complex with thinner silica spacer layers due to greater coupling between concentric Au nanoshells. Subsequent investigations with this structure have provided a more thorough picture of the optical response and demonstrated a finer degree of structural control with concentric nanoshells as small as 84 nm in total diameter.[322,323] An alternative approach involves a destruction of the spherical symmetry of the nanoshell, which results in the lifting of degenerate plasmon resonances, revealing a more intricate optical response. These strategies typically rely on surface masking techniques to generate variations in the thickness of the Au shell surrounding the dielectric core. This has the effect of essentially displacing the spherical template with respect to the shell. In one example, a substrate is used to mask the adsorption of small AuNPs onto APTMS-functionalized SiO_2 spheres.[324] The absence of seeds during the shell growth step results in the asymmetric deposition of metal. A similar surface-based masking approach was utilized by Halas and co-workers to chemically reduce additional Au onto preformed Au nanoshells that had been deposited on a glass substrate, resulting in offset dielectric cores (Figure 10c).[325] Single-particle dark-field microscopy and plasmon hybridization modeling revealed that the asymmetry of this structure lifted the previous restriction that only primitive plasmon modes of the same order could hybridize. The result of mixing between elementary plasmon resonances of any multipolar index is the emergence of extremely complex optical spectra and high local fields, which may make these structures candidates for surface-enhanced phenomena.

3.2.4. Nanoshells with Exotic Dielectric Cores. The examples given thus far have relied on spherical polystyrene or SiO_2 cores for the growth of a metal shell. However, additional design parameters that can be manipulated to control the optical properties of nanoshells are the composition and/or shape of the underlying template. The composition of the colloidal substrate provides a means to change its dielectric constant, and the shape of the template will dictate the shape of the metallic nanoshell. Both of these parameters cause important modifications to the plasmon resonance. For example, Halas and co-workers reported the growth of Au nanoshells around prolate spheroid (rice-shaped) templates composed of α-Fe_2O_3 using the familiar method of seeding the surface with small AuNPs using APTMS as a bifunctional linker (Figure 10d).[326] The emphasis here was on the rod-like shape, which afforded the nanoshell both transverse and longitudinal plasmon resonances, higher local field enhancement, and better sensitivity to refractive index changes. Several others have obtained spherical Au shells around Fe_3O_4 templates using charged polyelectrolytes,[327−329] dopamine,[330] or thiol groups[331] to adsorb the seed AuNPs. In a particularly interesting report, Levin et al. showed the growth of Au shells on mixed-valency iron oxide templates composed of cores of wüstite (FeO) and edges/corners of magnetite (Fe_3O_4).[332] While the authors separately investigated substrate particles that were either pseudospherical or tetracubic, the Au shells grown by the seeded growth method primarily adopted a spherical shape, limiting the appearance of additional bands due to shell anisotropy. However, the authors point out that because wüstite is a metastable phase and can adopt mixed and spatially varied oxidation states depending on the environmental conditions, its dielectric permittivity is difficult to measure. By comparing the obtained optical spectra to those modeled with different core dielectric properties, it was determined that the dielectric permittivity of the wüstite particles ($\varepsilon \approx 12$) was significantly higher than that of silica ($\varepsilon \approx 2$). In a similar study, a semiconducting particle composed of Cu_2O ($\varepsilon \approx 7$) was used as the core for the growth of a Au nanoshell.[333] These structures exhibit tunable plasmon resonances into the near-infrared (NIR) and further highlight how the dielectric properties of the template can be used to modulate the near- and far-field response of the supported nanoshell. This approach to tailoring the optical properties of nanoshells is very recent, with other notable examples being the growth of Ag shells over AgCl nanocubes[334] and the growth of Au shells over $NaYF_4$:Yb/Tm hexagonal nanoplates[335] for photocatalysis and plasmon-enhanced fluorescence upconversion applications, respectively.

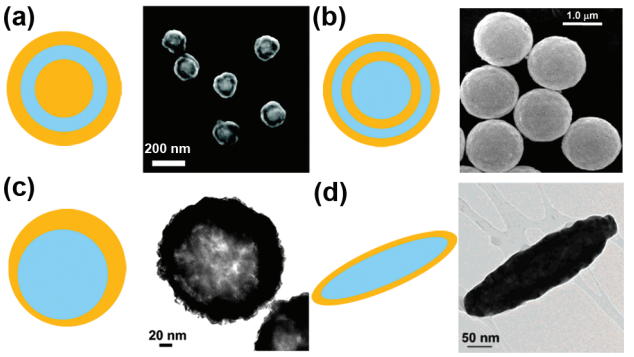

Figure 10. Summary of advanced Au nanoshell morphologies with cross-sectional (left) and electron microscopy (right) images: (a) a spherical AuNP embedded within a nanoshell separated by a silica layer, (b) nested, concentric nanoshells separated by a silica layer, (c) an asymmetric nanoshell, (d) an anisotropic α-Fe_2O_3 rice-shaped dielectric core with a Au shell. (a) Adapted with permission from ref 323. Copyright 2009 American Chemical Society. (b) Adapted with permission from ref 197. Copyright 2003 American Association for the Advancement of Science. (c) Adapted with permission from ref 325. Copyright 2006 The National Academy of Sciences of the USA. (d) Adapted with permission from ref 326. Copyright 2006 American Chemical Society.

3.2.5. Structures with Magnetic Cores. Several "unseeded" methods to directly nucleate continuous shells of plasmonic metals around dielectric templates have also been developed. However, these approaches impart strict synthetic

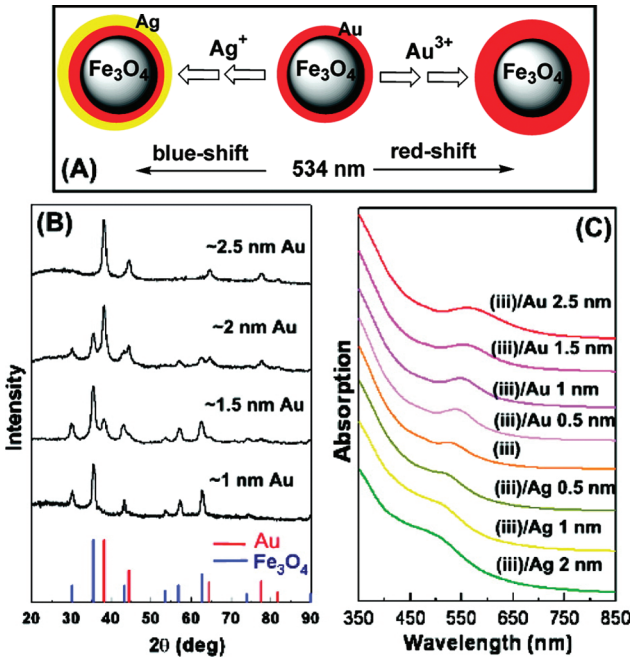

Figure 11. Growth of size-controlled conformal Au or Ag shells around dielectric Fe_3O_4 template materials: (A) scheme illustrating that, by starting with Fe_3O_4@Au nanoparticles, deposition of additional Au or Ag results in continuous shell formation that modifies the optical properties, (B) XRD patterns with increasing Au shell thickness, (C) extinction spectra as a function of the shell thickness and composition. Adapted with permission from ref 112. Copyright 2007 American Chemical Society.

requirements on the chemical nature of the dielectric material, and most combinations result in phase-separated morphologies, rather than uniform shells.[111] Despite the large library of possible template materials, iron oxide is the only dielectric that has been shown to be widely amenable to the growth of either Au or Ag shells. This preference is likely due to the frequent observation of epitaxy between Au and iron oxide domains, which some have explained by noting that the lattice constants of Fe_3O_4 (8.397 Å) and γ-Fe_2O_3 (8.339 Å) are roughly double that of Au (4.080 Å).[336] In addition, considerable effort has been applied toward reproducible syntheses of this morphology, because advantages such as more facile bioconjugation and applications as multifunctional nanostructures for imaging, magnetic separation, and photothermal therapy are highly sought after.[337−342]

One of the first examples of this core−shell morphology using a direct reduction approach was reported by Williams and co-workers using ~9 nm γ-Fe_2O_3 nanoparticle templates.[343] Following the addition of sodium citrate and $HAuCl_4$ to an aqueous solution of these particles with tetramethylammonium hydroxide, hydroxylamine was added in an iterative fashion to gradually reduce the excess Au salt and grow a conformal Au shell. Instead of observing Au shell thickening, with each addition of hydroxylamine, the authors observed a decrease in the polydispersity of the final particles while their average size remained relatively constant around 60 nm. Interestingly, they found that this method was unable to nucleate Au onto Fe_3O_4 nanoparticles unless they had been partially or fully oxidized to γ-Fe_2O_3. Subsequently, Zhong and co-workers demonstrated that the use of both γ-Fe_2O_3 and Fe_3O_4 templates in a high-temperature organic phase synthesis involving the reduction of $Au(OOCCH_3)_3$ in the presence of oleic acid and oleylamine resulted in the formation of extremely thin (0.5−1 nm) Au shells surrounding the dielectric cores.[344,345] Other common reducing agents such as citrate[346] and glucose[347] have been successfully used in aqueous syntheses to generate several nanometer or thinner metal shells around iron oxide nanoparticles. Using a distinct approach, Park et al. have produced several nanometer thick Au shells surrounding ~5 nm Fe_3O_4 or γ-Fe_2O_3 particles by thermally induced fusion of small AuNPs.[348] After mixing oleic acid/oleylamine-capped iron oxide nanoparticles with ~2 nm AuNPs in a toluene solution containing tetraoctylammonium bromide, heating to 149 °C for 1 h resulted in the controlled coalescence of AuNPs in the form of a continuous shell around the dielectric core. By controlling the relative concentrations of iron oxide, Au nanoparticles, and the ligand, the final size and, to some extent, the morphology of the structure could be tailored from 30 to 100 nm, with some of the larger structures containing multiple magnetic cores.

More advanced morphologies that utilize iron oxide core templates include those with bimetallic or anisotropic shells. While early attempts at Ag shells on iron oxide particles showed promising results,[347] Sun and co-workers reported an impressive synthesis of monodisperse metal-coated particles using a room temperature approach (Figure 11).[112] By separating the metal shell formation into a two-stage process involving initial Au shell formation followed by a second shell growth step, a much greater level of structural control was afforded. First, oleic acid/oleylamine-capped ~10 nm Fe_3O_4 particles were reacted with $HAuCl_4$ at room temperature in chloroform to produce a 1 nm thick Au shell, which results in the appearance of a plasmon band at ~534 nm. After these particles were dried and resuspended in an aqueous solution containing sodium citrate and cetyltrimethylammonium bromide, additional Au or Ag could be deposited by the reduction of $HAuCl_4$ or $AgNO_3$ with ascorbic acid. Deposition of Au resulted in a red-shifting of the resonance from 534 to 561 nm, and deposition of a layer of Ag resulted in a blue-shifting of the resonance from 534 to 501 nm (Figure 11C). Using a similar two-step synthesis strategy, Wei and co-workers have shown that Au-coated Fe_3O_4 particles can be used as seeds in the formation of more complex, anisotropic nanostructures.[349] After adding the particles described by Zhong and co-workers (vida supra) to a solution of CTAB, $HAuCl_4$, $AgNO_3$, and ascorbic acid, they observed the growth of highly anisotropic Au nanostructures that consist of an iron oxide core and several sharp spikes or corrugations of Au. Although these specific reaction conditions will be familiar to those who have studied anisotropic nanoparticle syntheses, the clever use of a Fe_3O_4@Au particle seed imparts the final structure with added functionality, including transverse and longitudinal plasmon resonances around 650 and 850 nm, respectively. These unique particles have been utilized in imaging techniques that take advantage of the ability to monitor polarization-dependent NIR light scattering while rotating the structure with a magnetic field.[349,350]

3.3. Colloidal Templates for Phase-Separated Heterogeneous Morphologies

The noncentrosymmetric coupling of two or more nanoscale domains of dissimilar materials into a single nanostructure can lead to structures with minimal perturbation in the properties of each component and, in certain cases, results in multifunctional nanomaterials with combined optical, magnetic, and plasmonic properties. This dual functionality present in a single

dx.doi.org/10.1021/cr1004452 |Chem. Rev. 2011, 111, 3736–3827

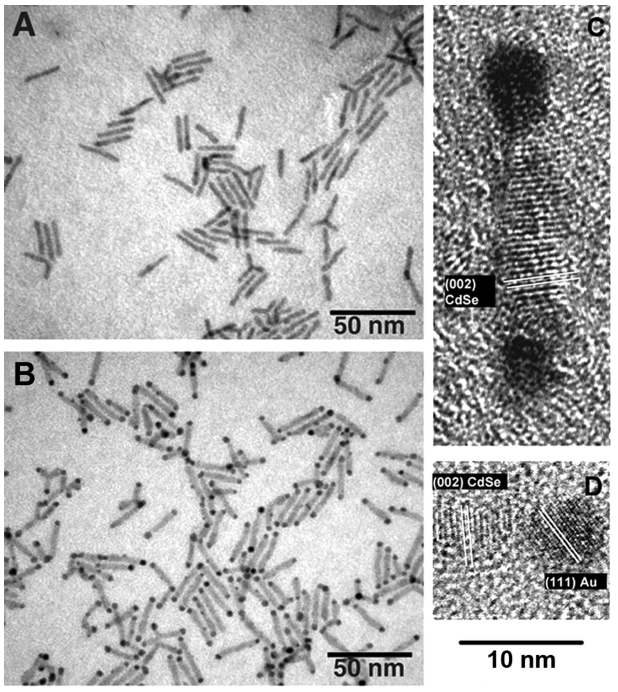

Figure 12. Synthesis of Au-tipped CdSe semiconductor nanorods: (A) starting CdSe nanorods, (B) CdSe nanorods after the reduction of $AuCl_3$, resulting in selective deposition at the rod tips, (C, D) HR-TEM images of the composite nanorods showing lattice fringes on the CdSe (C) and on the Au (D). Adapted with permission from ref 355. Copyright 2004 American Association for the Advancement of Science.

nanoconstruct has been exploited for biological imaging techniques[351,352] and targeted drug delivery applications.[353] Additionally, in many cases synergistic effects arise from the complex interactions between adjacent domains through interfacial electron injection and modifications to the electronic density of states. Such cooperative effects have been observed ranging from enhanced magneto-optical response[354] to modified optical resonances[355] and to improved photogenerated charge separation.[356] Nanoparticles with this general morphology have been discussed and reviewed under several different names, such as janus particles,[357] heterodimers,[358] nanodumbbells,[359] hybrid nanocrystals,[360,361] or multicomponent nanostructures.[362] We will focus on the synthesis of phase-separated nanostructures wherein the plasmonic component may serve either directly as the template or as the nascent, nucleating domain. Here, we introduce the notation of the "|" symbol between the components to denote the phase-separated nature of these structures (e.g., Au|Fe_3O_4 heterodimer).

The primary thermodynamic driving force for the templated synthesis of hybrid nanostructures is heterogeneous nucleation. By utilizing a prefabricated nanoparticle template to lower the activation energy barrier to nucleation, secondary or tertiary domains can be driven to nucleate and grow onto existing nanoscale surfaces rather than forming homogeneously in solution. However, a number of interesting structural and chemical factors govern the appearance of a phase-separated, rather than a core−shell, morphology. For example, the formation of well-defined crystallographic facets on the surfaces of nanomaterials can provide spatially varied reactivity toward secondary nucleation and growth. Interestingly, a high degree of crystallographic epitaxy between attached domains seems to be a common, but not necessary, requirement for a heterogeneous morphology. Furthermore, template nanostructures having regions with a high radius of curvature are more amenable to nucleation, in accordance with the Gibbs−Thompson effect,[363] and therefore favor a phase-separated configuration. Many of these effects are acutely interdependent, making the rational synthesis of these structures a complex challenge for nanoscale chemists.

3.3.1. Tip-Selective Growth on Nanorods. Initial work in the field of heteronanostructures typically took advantage of semiconductor or oxide nanorods as templates for the selective deposition of a plasmonic material. The inherent anisotropy of the template particle naturally lends itself to a heterogeneous morphology, typically through nucleation only on the tips or sides, and thus makes characterization more straightforward. The first prominent example of such a morphology was demonstrated by Weller and co-workers and involved the photoexcitation of ZnO nanorods with UV light to selectively reduce silver domains at one tip.[364] After ZnO nanorods were mixed with $AgNO_3$ in an ethylene glycol/water mixture, photoexcited conduction band electrons reduced the Ag^+ in solution while valence band holes were scavenged by the ethylene glycol. The resulting Ag|ZnO nanorod composite particle consisted of a single silver domain on the tip of a ZnO rod and showed increased plasmon absorption (440 nm) and a quenched fluorescence from the ZnO with increasing silver deposition. Several possible mechanisms were proposed for the origin of the site specificity, including a small lattice mismatch between the two domains, selective Ag^+ adsorption at the tips, or charge separation facilitated by an intrinsic dipole moment along the *c*-axis (long axis) of the rod, resulting in an increased concentration of electrons at one end for the reduction of Ag^+. The latter mechanism was also proposed by Sönnichsen and co-workers in an analogous reaction resulting in the generation of single Au domains at the tips of CdS nanorods under UV irradiation.[365]

In addition to photochemical reactions, Banin and colleagues demonstrated a Au|CdSe nanorod dumbbell morphology using only chemical reducing agents (Figure 12).[355] In this reaction, CdSe nanorods, CdSe@ZnS nanorods, or CdSe tetrapods in toluene served as the nucleation sites, and upon addition of $AuCl_3$, dodecyldimethylammonium bromide, and dodecylamine, they observed selective reduction of Au on both ends of the rods or at all four tips of the tetrapods. The Au domains could be tuned between 2 and 4 nm in diameter by controlling the initial reactant concentrations and demonstrated significant alterations to the absorption and photoluminescence spectra. The growth mechanism for this morphology was later determined by Banin and co-workers through observation of an Ostwald ripening process between the two Au domains.[366,367] In this work, under nearly identical reaction conditions, the dumbbell morphology was observed as a precursor to a CdSe rod with only a single Au domain at one tip. The authors demonstrate that Au first selectively deposits on the two polar facets along the *c*-axis of the wurtzite crystal structure (CdSe). After simultaneous growth of both domains, a critical size is reached in which small fluctuations in Au deposition result in one side being larger than the other. Due to the negative shift in the reduction potential for small particles, the smaller domain is preferentially oxidized. The remaining electrons are able to hop between surface states through the CdSe rod and reduce the released Au ions at the opposite tip. This reaction ceases to continue when the smaller Au domain is completely consumed since electrons are unable to

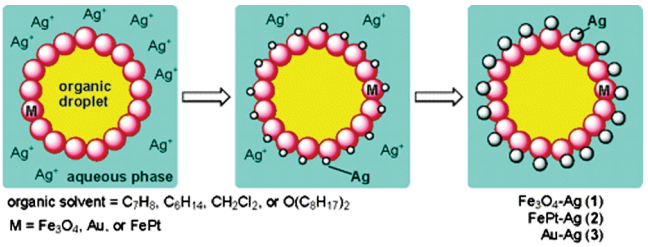

Figure 13. Scheme illustrating the emulsion-based synthesis of Ag|Fe_3O_4 heterodimers. Template particles are assembled at a liquid–liquid interface to break the spherical symmetry and facilitate nucleation on only one side. Adapted with permission from ref 358. Copyright 2004 American Chemical Society.

transfer from rod to rod in solution. By initially using low Au^{3+}:rod ratios, the density fluctuations are kept small and the dumbbell morphology is exclusively observed since the size differences between domains is minimized. With increasing Au^{3+}:rod ratios, these fluctuations become large, which favors the ripening process and the one-sided Au|CdSe morphology. This hybrid nanostructure is one of the most well understood and has been observed in several other forms, such as Au|CdS nanorods,[368] Au|CdSe@CdS nanorods,[369] and Au|CdSe multipods,[370] and has been studied in the contexts of electronic structure,[371] photocatalysis,[372] and charge separation.[356]

Another route to rod-like heterogeneous nanostructures involves the use of a metallic nanorod template. Chaudret and co-workers demonstrated the selective reduction of Au onto the tips of Co nanorods by judicious choice of organometallic precursor.[373] In their system, Co nanorods, hexadecylamine, and lauric acid in toluene are subjected to one of two Au precursors—$AuCl(PPh_3)$ or AuCl(tht) (tht = tetrahydrothiophene). It was found that the weakly bound tht group in the AuCl(tht) precursor allowed for a galvanic replacement reaction between the Au and the Co, resulting in the destruction of the Co nanorod template. However, if the more strongly associated $AuCl(PPh_3)$ complex was used, Au deposition could selectively occur on the tips of the Co rods without oxidation or shortening of the template. By changing the temperature and ligand concentration, the authors show modification of the entire surface of the Co nanorod with Au particles and propose that selective ligand adsorption on the sides of the rods (leaving the tips exposed) and fast exchange of these ligands explains the spatial selectivity of nucleation events. These hybrid nanocrystals show absorption peaks at 550 and 720 nm likely due to discrete and coupled plasmon resonances, respectively.

3.3.2. Heterodimers. Although early work in the field of heterogeneous nanostructures focused on the use of anisotropic templates, spherical nanoparticle-based structures represent the majority of research conducted on hybrid nanomaterials. Initial strategies aimed at achieving a spherical heterodimer morphology took advantage of the tendency for nanoparticles to assemble at liquid–liquid interfaces formed in emulsions (Figure 13).[358] In this case, Gu et al. started with a mixture of 8 nm Fe_3O_4 spherical nanoparticles in an organic solvent and $AgNO_3$ in the aqueous phase. After ultrasonic emulsification to create a large amount of interfacial area, they observed the nucleation of Ag domains on the Fe_3O_4 templates. Through partial exposure of the Fe_3O_4 surface to the aqueous phase, a few of the Fe^{2+} sites on the particle act as catalytic centers for the nucleation of Ag. Further reduction of Ag^+ occurs selectively on the existing Ag domain, resulting in a

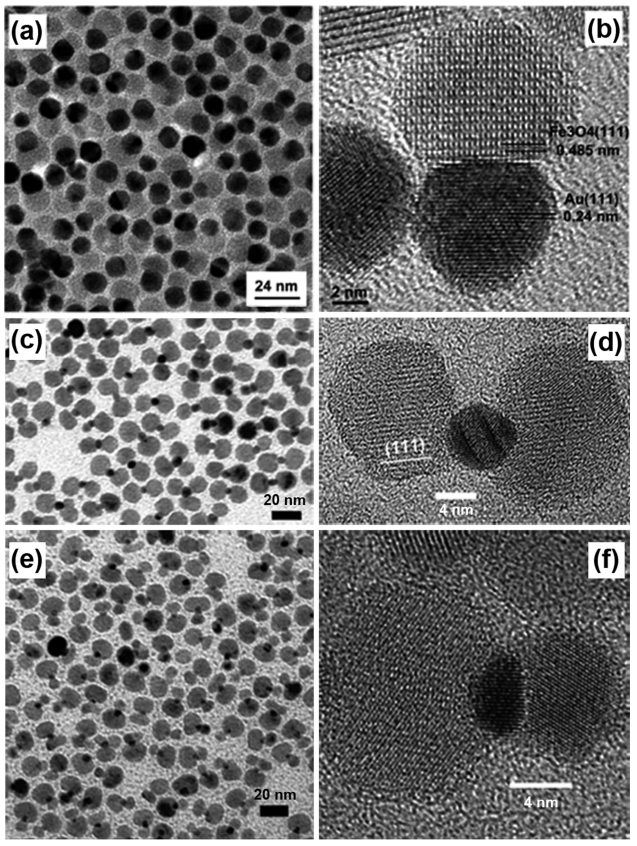

Figure 14. Summary of several two- and three-component phase-separated morphologies: (a, b) TEM and HR-TEM of Au|Fe_3O_4 heterodimers, (c, d) TEM and HR-TEM of Fe_3O_4|Au|Fe_3O_4 heterotrimers, (e, f) TEM and HR-TEM of PbS|Au|Fe_3O_4 heterotrimers. (a, b) Adapted with permission from ref 336. Copyright 2005 American Chemical Society. (c–f) Adapted with permission from ref 378. Copyright 2006 American Chemical Society.

single Ag particle for every Fe_3O_4 particle. This interfacial reaction was shown to be general for a variety of materials and has produced heterodimers of Ag|FePt, Ag|Au, and Au|Fe_3O_4.

Another common strategy to obtain heterodimer plasmonic nanostructures exploits the favorable thermodynamics for heterogeneous nucleation to promote growth of one domain on the other. Sun and co-workers demonstrated this approach in the synthesis of Au|Fe_3O_4 nanostructures by decomposition of $Fe(CO)_5$ onto Au nanoparticle templates in 1-octadecene in the presence of oleic acid and oleylamine (Figure 14a,b).[336] This synthesis allowed for control of the Au domain size from 2 to 8 nm through selection of the appropriate template precursor and control of the Fe_3O_4 domain size from 4 to 20 nm by adjusting the reaction conditions. Interestingly, the interface between the Au and Fe_3O_4 domains shows evidence of an epitaxial relationship, with the lattice spacing of Fe_3O_4 being approximately double that of Au. In addition, conduction electron deficiency in the Au domain due to the presence of the Fe_3O_4 particle results in a red-shifting of the plasmon resonance from 520 nm for discrete particles to 538 nm for heterodimers. Sun and co-workers have used a similar approach to synthesize Ag|$CoFe_2O_4$ heterodimers[354] and have shown the utility of this nanoscale morphology in applications such as biological imaging,[374] catalysis,[375] and drug delivery.[353]

dx.doi.org/10.1021/cr1004452 |*Chem. Rev.* 2011, 111, 3736–3827

This strategy for heterostructured nanomaterials is quite common and has been used successfully for a variety of nanoparticle combinations. For example, Pellegrino et al. demonstrated the epitaxial growth of Au domains on the {111}, {110}, or {100} facets of $CoPt_3$ nanoparticle templates.[376] Here, independent control of both domains was demonstrated by varying the size of the initial $CoPt_3$ particle or by modifying the Au:$CoPt_3$ ratio and reaction temperature. In addition, Cheon and co-workers showed the synthesis of Au|FePt particles by reacting $AuCl(PPh_3)$ with 6 nm FePt nanoparticles in 1,2-dichlorobenzene with hexadecylamine and bubbling of a H_2/Ar mixture.[352] Importantly, the authors point out that, in the absence of FePt templates, the reduction of Au requires reaction temperatures of ~150 °C whereas, in the presence of the FePt particles, this value is reduced to ~70 °C. This demonstrates that the FePt surface lowers the barrier to nucleation, suggesting a heterogeneous mechanism for dimer formation. This effect also has been observed in the context of heterodimer formation by Xia and co-workers, who showed that a Au^+ organometallic precursor could not be reduced by ethylene glycol at room temperature except in the presence of a secondary nanoparticle template.[377]

A number of groups have used a heterogeneous nucleation-based synthesis strategy to show a general method for producing hybrid nanocrystals with arbitrary geometries and materials. Ying and colleagues have complexed metal salts in a water/ethanol mixture with dodecylamine and transferred them to toluene to produce a vast array of heterogeneous nanocrystals, including Au|Ag_2S and Ag|Fe_3O_4 heterodimers.[111] However, the majority of particles synthesized using this approach are core−shell, alloy, or multidomain morphologies. Prasad and co-workers have demonstrated a number of heterodimers from Au nanoparticle templates through appropriate combination of precursors in high boiling point solvents.[378] For example, decomposition reactions in the presence of oleic acid and oleylamine resulted in Au|Fe_3O_4, Au|$MnFe_2O_4$, and Au|$CoFe_2O_4$ nanoparticles with coherent interfaces between the two domains. In addition, Au nanoparticle templates mixed with PbO, oleic acid, and a sulfur or selenium precursor resulted in Au|PbSe and Au|PbS heterodimer particles, but with less well-defined epitaxy between adjacent nanocrystals. In these products the Au domains were typically 3−5 nm, the oxide domains 10−15 nm, and the semiconductor domains 6−8 nm. Plasmon resonances for these structures were typically red-shifted 10−20 nm compared to those of discrete Au nanoparticles due to the altered dielectric environment as a consequence of the secondary domain.

3.3.3. Heterotrimers. While generic methods for synthesizing hybrid nanostructures with arbitrary domain sizes and materials have led to impressive results, most examples of ternary heterostructures require specialized conditions due to the complexity and number of interactions present in these systems. Prasad and co-workers have shown the synthesis of several two-component nanostructures with three phase-separated domains.[378] For example, Fe_3O_4|Au|Fe_3O_4 nanoparticles were prepared by heating a solution of Au|Fe_3O_4 heterodimers in the presence of sulfur, which promoted the fusion of two Au domains into a single nanostructure (Figure 14c,d). A similar mechanism is thought to result in PbS|Au|PbS nanostructures synthesized using the correct concentration of Au template nanoparticles in the presence of Pb and S precursors.[378] Interestingly, the plasmon resonance of PbS|Au|PbS heterostructures showed a large red-shift of ~90 nm to a wavelength of 615 nm due to the high dielectric constant of PbS. This fusion approach to generating heterostructures has also been demonstrated with molecular iodine to control the coalescence of Au domains in various Au|CdS morphologies.[379] Instead of chemical species, Pang et al. used a bidentate ligand, ethylenediamine, to facilitate the union of two Ag domains in Ag|hollow Ag_2S nanostructures synthesized through a coupled galvanic replacement−heterogeneous nucleation mechanism.[380] An alternative strategy of using prefabricated Au|Fe_3O_4 heterodimers as templates to nucleate an additional domain of Au was recently used to investigate size-dependent interfacial stress accumulation in Au|Au|Fe_3O_4 particles.[381] This heterodimer seeding strategy also has been applied to the synthesis of three-component ternary heterostructures such as PbS|Au|Fe_3O_4 or PbSe|Au|Fe_3O_4 from Au|Fe_3O_4 templates[378] and Au|FePt|CdS from FePt|CdS templates (Figure 14e,f).[377]

In addition to ternary heterostructures with approximately spherical domains, the growth of anisotropic domains from heterodimer templates has allowed for an additional level of control over the plasmonic properties of hybrid nanomaterials. For example, Chen et al. have used the phase separation of 4-mercaptophenylacetic acid and poly(acrylic acid) on the surface of 44 nm Au nanoparticles to coat one hemisphere with silica and then use these as templates for the nucleation of Ag spheres or Ag nanorods from the exposed surface of the Au domains.[382] Both products showed unique optical spectra resulting from transverse Au and Ag excitations as well as longitudinal coupling between domains. Prasad and colleagues have also demonstrated anisotropic growth of PbSe nanorods from the Au domains of Au|Fe_3O_4 heterodimer seeds.[383] By changing the concentration of Au|Fe_3O_4 particles added to Pb and Se precursors, the PbSe domain could adopt several other morphologies, such as spherical, multiple-rod, and branched structures. Finally, by using phase-transferred $CoPt_3$ nanoparticles as templates in standard aqueous seed-mediated anisotropic nanoparticle syntheses, Giersig and co-workers have generated heterogeneous $CoPt_3$|Au cube and $CoPt_3$|Au rod nanostructures.[384]

3.3.4. Nanostructures with Multiple Symmetric Domains. Rather than regard nucleation broadly as either homogeneous or heterogeneous, some groups have utilized energetic differences between spatially distributed nucleation sites on a single nanoparticle as a result of crystallographic or geometric effects to control the growth of multiple domains. One of the first examples of this was the nucleation of one, two, or three separate domains of Se (50 nm) onto 100 nm Ag nanoparticle templates by reducing different concentrations of Na_2SeO_3 with ascorbic acid.[385] Interestingly, the Se domains were typically coplanar and oriented 120° apart, suggesting a strict geometric restriction to the nucleation process. Further elucidation of this method was provided by Yang et al., who demonstrated the nucleation of multiple Au domains on single PbS nanoparticles by injecting a toluene solution of $HAuCl_4$, tetraoctylamine bromide, and dodecylamine into a solution of 12 nm PbS quantum dots (Figure 15).[94] Although a low gold concentration resulted in PbS particles with a single Au domain, intermediate gold concentrations resulted in four Au domains (3 nm) in a tetrahedral arrangement on the surface of the PbS template. The authors hypothesized that the differences in polarities between the {111} and $\{\bar{1}\bar{1}\bar{1}\}$ planes explain the selective nucleation and tetrahedral orientation of the Au domains. These multidomain Au|PbS nanostructures represent an extraordinary degree of control over the spatial preference for nucleation and were also shown to have

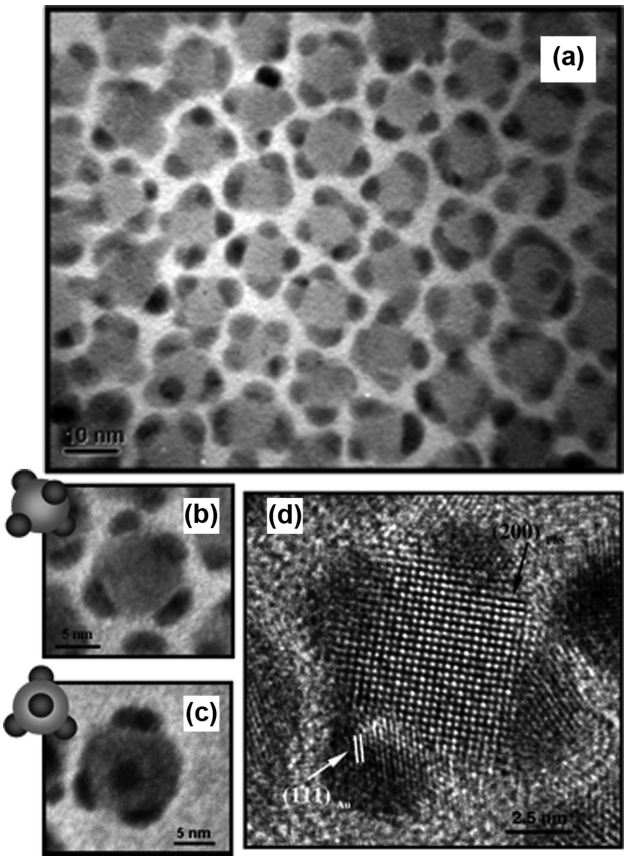

Figure 15. Synthesis of PbS nanoparticles with multiple Au domains in a tetrahedral arrangement: (a) TEM image showing large-area uniformity, (b, c) TEM images demonstrating the tetrahedral organization of Au domains on the surface of the PbS template, (d) HR-TEM image. Adapted with permission from ref 94. Copyright 2006 American Chemical Society.

unique optical properties and could assemble into a hexagonal array upon drying (Figure 15a).

A similar level of spatially controlled nucleation was demonstrated by Sun and co-workers in the growth of one to four domains of Au onto the {111} facets of Pt nanoparticle templates.[207] Unlike previous examples, an increase in the size of the Pt seed particle and a decrease in the solvent polarity were both shown to increase the number of Au domains in the final nanostructure. This was explained through Monte Carlo simulations, which reveal an intricate thermodynamic competition between factors such as the overall particle surface energy, the Au coherence energy, and the Pt−Au interfacial energy. Interestingly, Grzybowski and collaborators specifically showed that the controlled nucleation of one to four domains of Fe_3O_4 onto Au nanoparticle templates depends only on the molar ratio of Fe to Au and is independent of the solvent polarity.[386] In this case, the multiply twinned structure of the Au nanoparticle seeds is thought to play an important role, with each monocrystalline section of the particle being responsible for a discrete nucleation event. The red-shift, broadening, and decrease in intensity of the surface plasmon bands of these structures with increasing Fe_3O_4 deposition was explained by the altered dielectric environment surrounding the particles as well as the tunneling of conduction band electrons into the projected density of states of the Fe_3O_4 domains.

In addition to site-specific nucleation controlled by nanoparticle crystallography, the geometry or shape of the template also has been shown to influence heterogeneous growth. For example, Xia and co-workers have suggested that sites with a high radius of curvature are more reactive to nucleation events by a secondary metal.[377] To confirm this, they have shown the selective nucleation of AuAg alloy domains on all the corners of Cu_2O nanocubes. In this case, the low coordination environment for atoms at the cube tips make them more reactive to new nucleation events and provide the driving force for the phase-separated morphology. Talapin et al. have observed the same effect in the reduction of Au onto PbSe nanowires of various geometries.[387] Small Au domains (∼5 nm) were found to nucleate at the regions of highest curvature, i.e., at the corners of zigzag nanowires and at the corners and tips of branched nanowires, providing further evidence that the local morphology dictates the energetics of heterogeneous nucleation. These geometric factors, although related to crystallographic effects, demonstrate the large parameter space that has yet to be explored for spatial and elemental control over the nucleation and growth of metals onto nanoscale templates.

3.4. Sacrificial Templates

A particularly widespread and versatile approach to generating complex plasmonic architectures has been the use of a sacrificial template. Here, we define a sacrificial template as one that undergoes a destructive chemical transformation resulting in the formation of a new nanostructure while maintaining the symmetry of the starting material. This is in contrast to core−shell morphologies in which the template remains relatively unchanged during the course of the reaction. Just as methods for anisotropic nanoparticle synthesis can promote the growth of particular crystallographic facets, resulting in an impressive array of shapes,[15,16] destructive etching or replacement reactions can also occur in a face-dependent manner, resulting in an equally diverse assortment of unique templated structures.[95,388] By controlling the degree of chemical transformation of the template, the morphology of these structures can be easily tuned and often results in porous or hollow nanostructures which exhibit unique plasmonic properties.[389−391] These properties have led to numerous applications in SERS,[389,392−395] dielectric sensing,[396,397] and particularly as agents in biological settings[398−401] for photothermal therapy,[402−404] drug delivery,[405] and imaging contrast.[406−408]

The vast majority of sacrificial template-mediated nanostructures are synthesized through a redox reaction wherein partial or complete dissolution of the template occurs simultaneously with deposition of a plasmonic material (usually Au or Ag). Typically, this reaction results in the reduction of one species (**B**) at the expense of the oxidation of the other (**A**) and can be written generally as

$$m\mathbf{A}_s + n\mathbf{B}^{m+}{}_{aq} \rightarrow n\mathbf{B}_s + m\mathbf{A}^{n+}{}_{aq}$$

which is commonly known as a galvanic replacement reaction if **A** and **B** are both metals. A number of interesting chemical insights can be gained from a brief analysis of the details of this reaction. First, the standard reduction potential of the B^{m+}/B pair must be higher than that of the A^{n+}/A pair. This ensures the flow of electrons from the less noble to the more noble species and imposes restrictions on the choice of the template material. Second, although not necessarily the case, it is often true that $m \neq n$, meaning that, to satisfy charge and mass balance, several atoms of the template are required to reduce a single atom of the ionic species. This has important consequences as the reaction

dx.doi.org/10.1021/cr1004452 |*Chem. Rev.* 2011, 111, 3736–3827

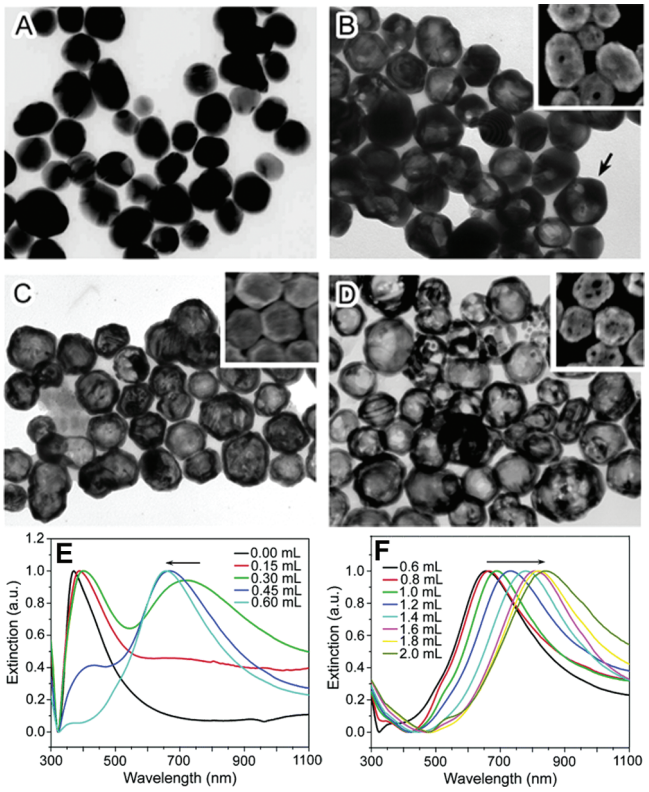

Figure 16. Hollow spherical nanostructures synthesized by galvanic replacement: (A−D) progression of morphologies starting with AgNPs (A) during reaction with $HAuCl_4$ to yield hollow, porous AuAg shells (D), (E, F) extinction spectra as a function of the degree of replacement showing the appearance and red-shift of additional plasmon bands due to the hollow cavity. Adapted with permission from ref 415. Copyright 2004 American Chemical Society.

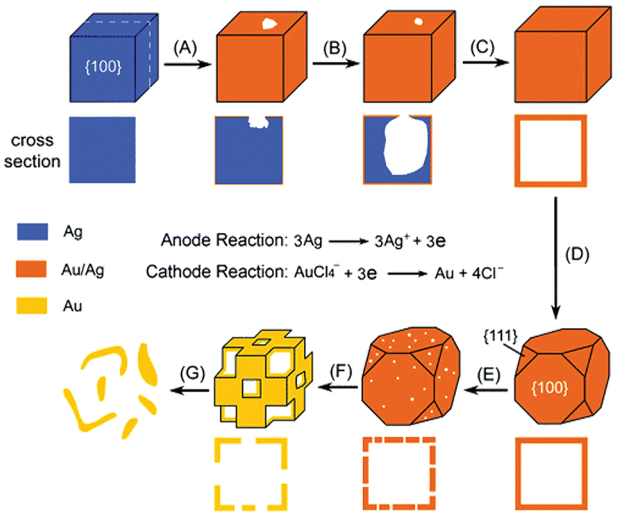

Figure 17. Schematic illustration of the steps involved in the galvanic replacement reaction between $HAuCl_4$ and Ag nanostructures. The replacement reaction initially forms a uniform AuAg alloy shell around the structure (A) and through a pitting process allows for the formation of a cavity (B). The pore is later covered over (C), forming a hollow shell which can be further dealloyed (D, E), resulting in a porous structure composed entirely of Au (F) that eventually fragments (G). Adapted with permission from ref 415. Copyright 2004 American Chemical Society.

proceeds as vacancies are formed in the template which can coalesce into small pores or singular voids, depending on the conditions. Finally, by ensuring the more noble ionic species (**B**) is the limiting reagent, the extent of reaction can be precisely controlled to yield structures with intermediate morphologies and compositions that can be a homogeneous alloy between the two components.

3.4.1. Nonmetallic Redox-Active Templates. One of the first examples using this methodology was by Yang and co-workers using $LiMo_3Se_3$ molecular chains which self-assemble into 10−100 nm nanowire bundles as sacrificial templates.[409] After preparation of these nanowires in DMSO, a solution of gold salt was added, resulting in the nucleation of small Au clusters on the surface of the nanowires which eventually grew to consume the template as additional Au^{3+} was reduced. The final morphology was found to be polycrystalline, continuous Au nanowires with approximately the same dimensions as the $LiMo_3Se_3$ structures, suggesting complete oxidation of the starting materials. It was proposed that any metal with a sufficiently high reduction potential would therefore be capable of oxidizing the initial template, forming metallic nanowires. Indeed, this process was shown to be generalizable to Ag, Pd, and Pt, demonstrating the versatility of such an approach. Several other examples of using nanoscale semiconductor templates such as CdS, CdSe, CdTe, or PbSe to produce segmented[410] or branched[411] nanorods and hybrid spherical structures[412] have provided further evidence that the redox properties of a host of materials can be exploited in plasmonic nanoparticle synthesis.

3.4.2. Spherical Galvanic Replacement-Based Structures. By extending these ideas to metallic nanostructure templates, Xia has pioneered and perfected the use of galvanic replacement reactions to generate novel plasmonic materials. Seminal work published in 2002 demonstrated the use of Ag nanoparticles to generate hollow Au nanostructures with tunable optical properties based on the template size and shape.[413] This approach was termed the "template-engaged replacement reaction" and has since found widespread use as a versatile and relatively simple synthetic method. In this initial example, spherical 50 nm Ag nanoparticles were reacted with $HAuCl_4$ in water at 100 °C to yield hollow, pinhole-free shells with a diameter of 50 nm and a wall thickness of ~6.5 nm (Figure 16). A more thorough mechanistic investigation later revealed the detailed steps resulting in the formation of hollow shells from the exchange process between Au and Ag (see also Figure 17).[414,415] During the initial stages of the reaction, Au^{3+} reacts with the surface Ag atoms and forms an alloy shell around the template particle. Typically, a single pinhole can be seen in this shell through which additional Ag from the template can be oxidized and removed. Because three Ag atoms are oxidized for every Au atom reduced, as more Au is deposited, the core of the template becomes hollow and, once exhausted of all Ag, the pinhole is covered over, forming a continuous, homogeneous alloy shell. The high temperatures used in this reaction are important in facilitating the diffusion of Ag out of the core and in the Ostwald ripening and surface reorganization processes responsible for "filling in" the pinhole and forming a single-crystalline shell. These diffusional effects are accelerated if a particle rich in twin boundaries is used instead, as grain boundaries allow for faster outward diffusion of Ag, preventing the formation of a continuous alloy shell around the template.[416] Interestingly, the Ag in the AuAg alloy shell is thermodynamically

dx.doi.org/10.1021/cr1004452 |*Chem. Rev.* 2011, 111, 3736–3827

more stable than the elemental Ag and therefore more difficult to oxidize.[417] However, with Au^{3+} in sufficient excess, a dealloying[418] of the Ag can occur, resulting in the formation of pores in the nanoshells with the composition approaching that of pure Au.

Importantly, the optical properties of the resulting hollow shells were shown to be highly dependent on their size and wall thickness and could be tailored by the reaction conditions (Figure 16E,F).[413] The surface plasmon resonance of the Ag template particles was shown to red-shift with increasing replacement by Au from 400 to 720 nm as a result of the formation of a hollow cavity and the concomitant increase in the particle aspect ratio (outer diameter:inner diameter).[396] It is thought that such highly anisotropic nanostructures are more optically sensitive to local changes in their chemical environment, making them promising candidates as sensors for probing binding events on the nanoscale. This effect was studied by Xia and co-workers by monitoring shifts in the SPR band of the Au nanoshells after immobilization on APTMS-coated glass sides and immersion in solvents with different refractive indices.[396] Hollow Au nanoshells were found to be as much as 7-fold more responsive to changes in the refractive index than similarly sized spherical Au nanoparticles. In addition, Schatz and colleagues found using DDA calculations that the presence of one or two pinholes in the surface of a Au nanoshell has little effect on the extinction spectrum of the particle but can magnify the electromagnetic field enhancement by as much as a factor of 10 compared to pinhole-free shells.[389] Since the formation of small pores can be controlled by the dealloying of the shell, these structures may be relevant to SERS measurements for which the presence of electromagnetic "hot spots" are crucial. This level of understanding in both the particles' properties and synthesis mechanism remains a challenge for most nanoscale chemical reactions but has, in this case, played a significant role in its adaptation to numerous alternative systems.

Starting with Ag nanoparticle sacrificial templates, a number of alternative methods have led to interesting modifications to the original Au nanoshell synthesis.[419] Several practical improvements were focused on mitigating the precipitation of insoluble AgCl species which were detrimental to achieving a shell morphology. By preparing AgNP templates and $HAuCl_4$ on opposite sides of a dialysis membrane impermeable to nanoparticles, the reaction kinetics could be controlled and Ag^+ could diffuse away from the nanoshells, preventing contamination by AgCl.[420] In addition, Sastry and co-workers found that when the redox reaction was carried out in an organic solvent, replacement between AgNP templates and Au^{3+} could be completed at room temperature and did not result in AgCl precipitates.[421] Chemical changes to the synthesis were achieved by introducing hydroxylamine into the replacement reaction, resulting in the formation of sharp corrugations protruding from the hollow Au nanoshells.[422] The added hydroxylamine acts as a reducing agent for the Ag^+ oxidized from the center of the particle, allowing it to be redeposited on the shell surface in the form of sharp features. This approach has also been applied to the addition of H_2PtCl_6 to AgNP templates, resulting in the simultaneous exchange between Ag and Pt^{4+} and reduction of liberated Ag^+ by hydroxylamine to create AgPt hollow alloy shells.[423] These particles also had tunable surface plasmon resonances from 430 to 750 nm despite the presence of Pt, which ordinarily does not have optical features in the visible. A full generalization of this procedure was demonstrated by replacing hydroxylamine with ascorbic acid as the reducing agent, resulting in the transformation of AgNP templates to Pt, Pd, PdPt, AuPd, and AuPt nanoshells simply by changing the metal salt added to the reaction.[424]

Rather than use Ag nanoparticles as sacrificial templates, a number of groups have investigated the use of small Co nanoparticles as they can often produce a more monodisperse Au nanoshell product.[425] Liang et al. were among the first to show Co as a redox-active template by adding a mixed solution of H_2PtCl_6 and $HAuCl_4$ to CoNPs to generate hollow AuPt alloy shells approximately 24 nm in diameter.[426] Interestingly, they found that if the concentration of the capping ligand (citric acid) was sufficiently low, the spontaneous 1-D ferromagnetic ordering of the Co templates resulted in a continuous chain of hollow shells one particle thick and as many as several micrometers in length. Increasing the citric acid concentration increased the steric repulsion between particles, preventing the ordering of the templates and resulting in discrete AuPt shells. CoNP-templated synthesis was later applied to the formation of hollow Au shells by Jiang and co-workers[427] and was ultimately perfected by Zhang and colleagues.[425] In these cases, the reactions were carried out at room temperature and the synthesized hollow Au shells had a polycrystalline structure. Because of the monodispersity of the starting CoNP templates (~10%), the resulting Au shells are highly uniform and have well-defined, tunable SPRs from 530 to 800 nm.[425] A number of groups have utilized these advantages to synthesize Au nanoshells for SERS[428] and catalysis applications.[429]

3.4.3. Anisotropic Galvanic Replacement-Based Structures. Although the use of spherical nanoparticle templates has generated a better understanding of the replacement mechanism and the basic optical properties of hollow structures, anisotropic templates can be used to synthesize more complex plasmonic structures.[430] A particularly influential example of this was first provided by Xia and co-workers in the transformation of Ag cubes into hollow Au boxes.[431,432] After synthesis of Ag nanocubes by reducing $AgNO_3$ with ethylene glycol and PVP, $HAuCl_4$ was added to initiate galvanic exchange between the two metals.[433] Although the starting Ag cubes were single crystalline and bound by six {100} facets, the final products were found to be hollow Au polyhedra with six {100} facets and eight {111} facets. This change in shape was presumably due to truncation of the Ag cube tips during the reaction and suggested that the oxidation process might have some crystallographic preference. The dissolution mechanism for this hollow anisotropic structure was found to be analogous to that for spherical particles (vida supra) and followed the same basic sequential stages, including initial Au deposition on the surface, oxidation of the Ag from the center of the structure through a small pinhole, filling in of the pinhole, creating a hollow AuAg alloy box, and formation of pores if additional Ag is removed through dealloying (Figure 17).[415] The first optical spectra of these structures demonstrated that the tunability in the surface plasmon resonance was even greater than for spheres, with SPR bands red shifting from 495 to 1180 nm for the transformation from solid Ag cubes to hollow, porous Au shells.[415] In a later report, it was shown that Na_2PdCl_4 or Na_2PtCl_4 could be substituted for $HAuCl_4$ in the above reaction, generating AgPd or AgPt alloy cubic nanoboxes.[434] Although Pd was able to form a more homogeneous alloy with Ag due to better lattice epitaxy, both AgPd and AgPt hollow shells showed tunable optical properties from 440 to 730 nm, which matched well with companion DDA calculations.

dx.doi.org/10.1021/cr1004452 |*Chem. Rev.* 2011, 111, 3736–3827

Despite these impressive examples regarding the tunability of the properties of plasmonic nanostructures, two important advances in the sacrificial template-mediated synthesis of hollow cubes have facilitated an additional degree of morphological control. First, by annealing the Ag nanocube templates at 160 °C in ethylene glycol with the appropriate concentration of PVP and HCl, slight truncation of their corners could be induced, thus exposing {111} facets on the Ag template.[95] With the addition of $HAuCl_4$, instead of a pinhole or etch pit forming randomly on one of the {100} facets as before, it selectively formed on all eight of the nascent {111} truncated corners (Figure 18). This allowed for Au to deposit only on the {100} facets and for the oxidation of Ag to occur through the pores on the {111} facets. As alluded to previously, the crystal facets of the template clearly play an important role during the replacement reaction and allow for the synthesis of an extremely uniform population of AuAg alloy hollow particles with pores on each corner, which the authors have termed "nanocages" to differentiate them from the previous structures known as "nanoboxes". The second advance was the use of $Fe(NO_3)_3$ as a selective etchant for Ag, allowing one to decouple the Au reduction and Ag dealloying steps that usually occur simultaneously.[435] After the replacement reaction was stopped at the nanobox stage, cubic hollow AuAg alloy shells were formed and subsequently treated with $Fe(NO_3)_3$ to selectively oxidize the Ag and precisely tune the wall thickness of the final structure. If additional etchant was added, pinholes formed selectively in the middle of the {100} facets, resulting in a hollow cubic structure with holes in each face known as a "nanoframe". This method for controlling the morphology allows for the SPR to be continuously tuned from 590 nm for the nanobox to 1210 nm for the most porous nanoframe. Interestingly, El-Sayed and co-workers have found that this unique hollow morphology supports electromagnetic coupling between the fields generated by the interior and exterior surfaces,[436] making them extremely sensitive to dielectric shifts[397] and promising candidates for SERS.[391] Taken together, the degree of synthetic control over these structures and their resultant plasmonic properties is impressive and has spawned interest in using them in photothermal therapy[402−404] and as imaging contrast agents.[406−408]

A number of other anisotropic nanoparticle templates have been used in galvanic replacement reactions to generate interesting plasmonic nanostructures, including triangular Ag nanoprisms and Ag nanorods/nanowires. For example, Xia and colleagues demonstrated that photochemically generated Ag triangular nanoprisms could be reacted with $HAuCl_4$ to generate AuAg alloy triangular rings.[437] Unlike the case of hollow cube-based nanostructures, the surface plasmon resonance of these triangular ring particles was considerably damped and relatively featureless. Mirkin and co-workers confirmed this observation and introduced the concept of "backfilling" the pore created by the galvanic replacement reaction to better control the morphology of the final structure.[438] By adding ascorbic acid to the solution of triangular AuAg rings, remaining ions or added $HAuCl_4$ could be redeposited onto the structure, filling the hole in a controllable manner and allowing for pores as small as 4 nm and a recovery of the plasmonic properties. The selective deposition of Au on the side {110} facets and preferential etching of the top {111} facets of the Ag nanoprism template are consistent with the results of Xia and have been studied in more depth for the triangular prism structure.[439] These features have led others to use this reaction to plate thin coatings of Au on the Ag prism sides to protect them from other known Ag etchants such as Cl^-.[148] Interestingly, if thicker Ag nanoprisms are used and hydroxylamine and NaOH are introduced during the redox reaction, the familiar hollow morphology is retained with a triangular prism alloy shell.[440]

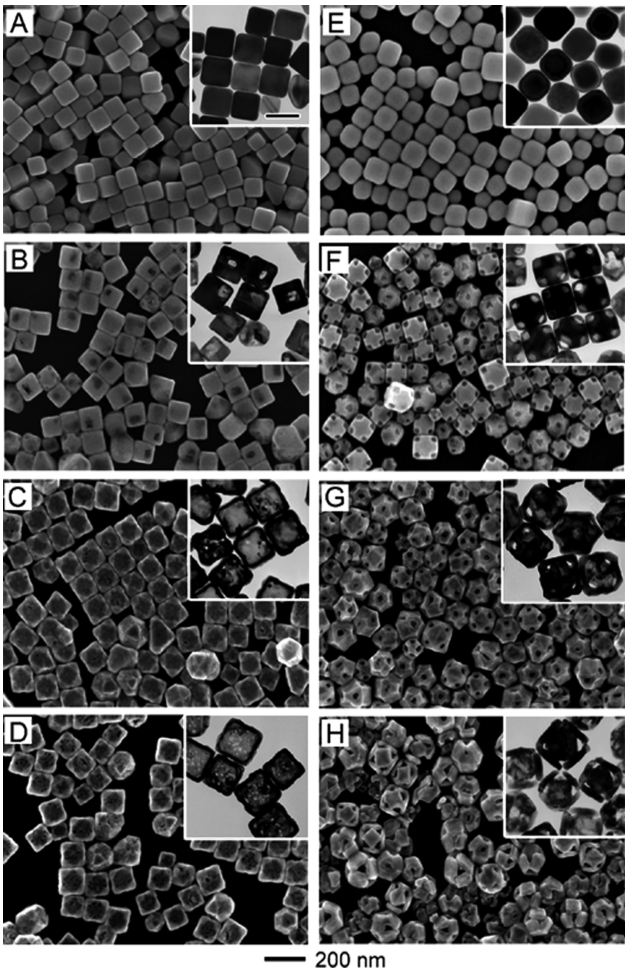

Figure 18. TEM images comparing the nonspecific (A−D) and the preferential (E−H) galvanic replacement reaction between Ag cubes and $HAuCl_4$. By heating the cubes beforehand, their {111} facets can be exposed, which are attacked selectively by the oxidation process, resulting in structures with pores only at their tips (E−H). This is not the case if pristine cubes are used instead (A−D). Adapted with permission from ref 95. Copyright 2006 American Chemical Society.

Ag nanowire templates have also been used to generate hollow Au and AuAg alloy plasmonic structures. Xia and co-workers have applied the same techniques for the hollow cubic structures (vida supra) to polyol-synthesized Ag nanowires and confirmed that the same basic mechanism and crystal-facet selectivity are at play.[413,415] Starting with a unique structure consisting of pentagonally twinned Ag rods grown off both ends of a decahedral Au core (Ag rod|Au|Ag rod), Seo et al. have shown that, for low concentrations of $HAuCl_4$, only one of the two Ag domains will react by galvanic replacement.[441] It is only after the first domain has been completely replaced and made a hollow AuAg shell that the other Ag rod component will follow. The authors propose that Au initially deposits uniformly over the entire exposed Ag surface until a single etch pit forms on one side. Since the Ag atoms can be liberated more readily on the side with this defect,

the reaction goes to completion there before continuing on the opposite side. Other groups have used Ag nanowire templates in redox reactions to synthesize alloy AuAg nanowires which are then typically exposed to either ammonium hydroxide[393,442] or nitric acid[443] to selectively etch the Ag, allowing for fine control over porosity and Au content and, therefore, optical response. This approach is also a popular postsynthetic modification strategy with nanowires synthesized electrochemically using porous membranes (see section 4.1) to achieve polycrystalline rods of varied morphologies.[444−448]

3.4.4. Alloy Nanoparticles. While the majority of examples given thus far have relied on nearly complete galvanic replacement between metals to generate porous or hollow nanostructures, partial exchange under the appropriate synthetic conditions can lead to metal core−alloy shell or compositionally controlled solid alloy materials with tunable properties. Several preliminary examples of a core−shell morphology derived from redox-mediated replacement utilized Ag or Co nanoparticle templates to generate Au shells.[449,450] The relatively low reaction temperatures and use of organic solvent in these cases are likely responsible for the lack of void formation during the synthesis. Boothroyd and co-workers later perfected this procedure using 18 nm AgNPs reacted with $HAuCl_4$ in toluene at 95 °C.[451] Under these conditions, the alloy composition of a AuAg shell surrounding a solid AgNP core could be tuned by controlling the concentration of Au^{3+} added to the reaction mixture. A complex sequence of crystal facet-selective deposition and oxidation of the template followed by Ostwald ripening of the alloy shell was used to explain this morphology.

In addition to core−shell structures, several different homogeneous alloy nanoparticle compositions generated by sacrificial template reactions have been reported by Murray and co-workers.[452,453] By starting with dodecanethiolate monolayer-protected clusters in toluene followed by addition of metal thiolate compounds, galvanic exchange could occur, resulting in alloy nanostructures.[452] Specifically, the use of Au^{+} thiolate and Pd^{2+} thiolate compounds in conjunction with Ag, Pd, and Cu nanoparticles resulted in templated alloy structures of AuAg, AuPd, AuCu, and PdAg, all with plasmonic properties indicative of their homogeneous alloy compositions. A similar approach has been applied to dendrimer-encapsulated nanoparticles with equivalent results (see section 3.5.7).[454,455] Further confirmation of this effect was provided by demonstration of a continuous shift from the plasmonic and luminescence spectra of tiopronin-coated Ag nanoparticles to those of tiopronin-coated Au nanoparticles during a galvanic replacement reaction.[453] This work was later extended[456] and ultimately perfected[457] by Zhang et al. to yield a procedure capable of an impressive degree of control over the size, composition, and morphology of plasmonic alloy nanoparticles. First, the authors developed a sequence of steps including nucleation and growth, digestive ripening, and seed-mediated growth to allow for the size-controlled synthesis of either single-crystalline truncated octahedral Ag nanoparticles or multiply twinned icosahedral Ag nanoparticles.[457] With these particles as templates, galvanic replacement reactions with Au^{3+} in toluene under reflux conditions resulted in homogeneous alloy nanoparticles. Although the final nanoparticles decreased in size with the degree of Au alloying due to the reaction stoichiometry, the authors were able to adjust the starting template size such that a series of alloy nanoparticle solutions could be prepared to have exactly the same diameter (6.1 nm) but with tunable alloy compositions of 0%, 25%, 50%, 75%, and 100% Au. Alternatively, the reaction conditions could be adjusted to prepare a series of nanoparticle solutions of the same alloy composition (50% Au) but with tunable particle sizes of 5.6, 6.6, 7.7, and 8.8 nm. This process could be applied equally well to both twinned icosahedral and single-crystal truncated octahedral AgNP templates and represents an extraordinary level of control over the chemical properties of a nanosystem.

3.4.5. Nested or Recursive Structures. By taking advantage of the selective metal oxidation afforded by galvanic replacement reactions coupled with clever experimental designs, particularly complex nanostructures that are difficult to synthesize by other methods can be produced. Typically referred to as "nanorattles" or "nanoparticles in shells", the final morphology of these structures consists of a partially reacted template nanostructure inside a hollow cavity defined by one or more alloy shells. Here, we will refer to these particles as "recursive" or "nested" to reflect their self-similar but ultimately terminating series of shells. The first example of such a nanostructure was demonstrated by Xia and co-workers and was generated in two parts. First, $AgNO_3$ was reduced with ascorbic acid in the presence of AuAg alloy nanoparticle templates to generate a pure Ag shell over the alloy core.[458] Second, a well-controlled galvanic replacement reaction between Au^{3+} and this Ag coating resulted in the formation of an alloy shell with a freely moving nanoparticle inside. Extinction spectra and Mie theory modeling showed two SPRs corresponding to separate resonances of the core and shell and suggests that both species will be excited only if the separation between the two components is small. By starting with pure AuNP templates coated with Ag, this process has produced structures with AuNPs inside Au shells[459] and AuNPs inside PtAg alloy shells.[460] This procedure has been further generalized to synthesize a host of recursive nanostructures consisting of nanoshells within nanoshells,[458] nanoboxes within nanoboxes,[458] two and three nested layers of alloy nanotubes,[458,461] Au nanorods within AuAg alloy nanoshells,[462] and Au nanorods within AuAg, PdAg, or PtAg hollow octahedra.[143] Each of these unique recursive nanostructures exhibits pronounced shifts in their collective plasmon resonances, and some have been shown to exhibit emergent nonlinear optical properties,[462] resulting in their application toward photothermal therapy and multiphoton imaging.[462]

3.4.6. Nanostructures by Destructive Etching. Although the majority of sacrificial template-based synthesis methods are grounded in the galvanic replacement reaction, several elegant examples highlight the use of selective chemical etchants in redox reactions to produce novel plasmonic nanoparticles. For example, Xia and colleagues demonstrated that significant shape control could be afforded through a destructive corrosion process between Pd nanocubes and O_2.[463] By synthesizing the template particles in a mixture of ethylene glycol and water, dissolved oxygen in the aqueous component could etch the Pd, resulting in the formation of hollow Pd nanoboxes and nanocages. This reaction is analogous to the oxidation of Ag nanocubes by Au^{3+} but results in no change in the template size since no additional material is being deposited. Interestingly, these unique hollow structures show tunable SPRs from 410 to 520 nm, consistent with DDA calculations.[463] In a separate example, Yang and co-workers have utilized a crystal-facet-selective etchant to show a remarkable series of morphological transformations from Ag octahedra to Ag octopods (Figure 19).[388] Using a 9:1 mixture of concentrated ammonium hydroxide and 30% hydrogen peroxide, they were able to achieve

dx.doi.org/10.1021/cr1004452 |*Chem. Rev.* 2011, 111, 3736–3827

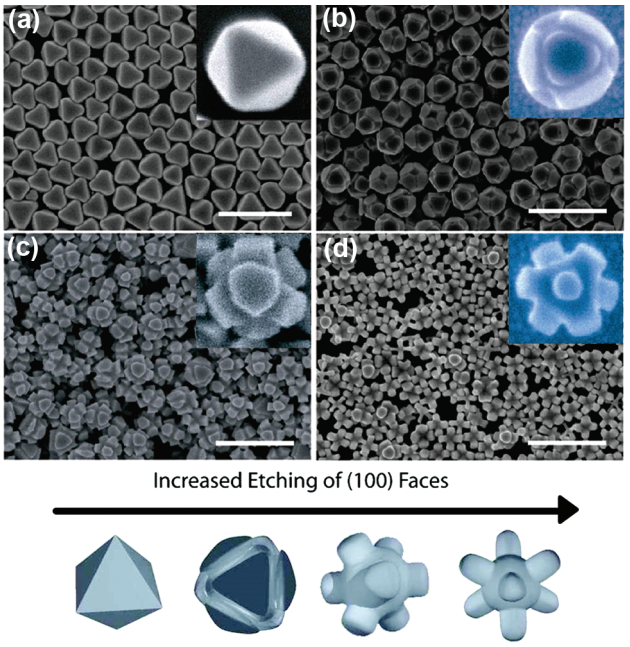

Figure 19. Site-specific oxidation of Ag octahedra leads to Ag octopods. Using a crystal-facet-selective etchant, Ag octahedra (a) can be etched along their edges and tips, resulting in recessed grooves (b) that eventually lead to an eight-armed octopod structure (c, d). Scale bars equal 1 μm. Adapted with permission from ref 388. Copyright 2009 American Chemical Society.

a 20-fold higher preference for the oxidation of {111} crystal faces over {100}. By keeping the etchant the limiting reagent while controlling its concentration, Ag octahedra could be selectively etched at their tips and edges. This process initially resulted in the appearance of recessed grooves at the edges of the octahedral templates, which eventually grew, leaving behind eight arms corresponding to the middle of the eight original triangular {111} facets. These changes result in dramatic shifts in the plasmon resonance, with the octopod structure having absorption bands in the near-infrared. Because of the sharp, closely spaced features on each particle, they were shown to exhibit intraparticle coupling effects that were exploited for measuring single-particle SERS spectra. By virtue of the materials versatility and ease of implementation, redox-active sacrificial templating of nanostructures is one of the most useful methods for generating nanomaterials with tunable plasmonic properties that extend beyond what is possible with their solid counterparts.

3.5. Biological and Organic Templates

Nature has evolved a variety of clever ways to create nanoscale entities with remarkable complexity. An enormous library of biological species exist that can be characterized as having extremely well-defined shapes and chemical activity as a result of the specific placement of relevant functional groups. Likewise, organic and organometallic chemists are extremely skilled at constructing molecules and supramolecular architectures that have impressive structural complexity, in some cases rivaling that of natural proteins. These features have motivated many researchers in the nanoscience community to take advantage of the complexity already present in these materials and manipulate them to function as templates for the formation of intricate nanostructures.[75,464−476] Importantly, the chemical interactions that give rise to the diversity found in these biological and supramolecular species are those that are most often co-opted for the assembly of ordered materials because of their specificity and programmable nature. However, in this section we will cover only those biological or organic templates that aid in the nucleation and growth of plasmonic nanostructures, while those that facilitate the organization of presynthesized materials are summarized in depth in sections 6 and 7.

Because these template structures are all largely carbon based, they make use of many of the same chemical strategies to direct the synthesis of nanomaterials. In addition, because they all share the feature of being entirely organic, they lack the structural rigidity found in many of the colloidal inorganic templates. As a result, discrete molecules or subunits are typically allowed to self-assemble into larger supramolecular structures that are then able to function as efficient templates, although this is not always the case. The template is then exposed to metal ions which associate to the structure according to the location of functional groups that facilitate a specific hydrophilic, electrostatic, or coordination environment favorable to the metal salt. Frequently, the metal nanostructure is then generated by the addition of a reducing agent which can be followed by additional "development" steps to reduce more metal onto the existing structure. Alternatively, certain peptides and proteins are able to both localize and reduce the metal salt in situ without the aid of chemical reducing agents. Given the simplicity of these methods along with the ubiquity of many of these molecules, it is unsurprising that nanostructures synthesized using these templates are prolific and have been studied for some time. However, they tend to suffer from having less well-defined and uniform shapes because they lack mechanical strength, being composed entirely of organic materials, often held together by weak, noncovalent interactions. Despite this fact, significant progress has been made in meeting this challenge, yielding a number of interesting plasmonic materials.

3.5.1. DNA. Some of the first examples of metallic nanostructures templated from biological molecules took advantage of the electrostatic and assembly properties of DNA. As early as 1998, Ben-Yoseph and co-workers showed the formation of 1-D Ag nanowires from long duplexed DNA assembled between two electrodes using complementary oligonucleotides.[477,478] By replacing the Na^+ ions present to facilitate hybridization between the strands with Ag^+, followed by several sequential reduction steps with hydroquinone, the authors generated extremely high aspect ratio nanowires as long as 12 μm with diameters of approximately 100 nm. This initial example sparked numerous further investigations into the "metallization" of DNA templates.[479,480] In follow-up work, several strategies were implemented to mask or mark certain segments of the linear DNA template to either block or encourage metallization at sequence-specific locations to create segmented nanowires. Initially, this methodology was accomplished through the binding of a RecA nucleoprotein filament, a protein responsible for homologous recombination in bacteria, to a specific region of the double-stranded DNA template (Figure 20).[481,482] Since the template DNA had previously been aldehyde modified to allow it to in situ reduce and nucleate metal ions, the RecA nucleoprotein filament acted as a mask, preventing metallization at the regions it had bound. After further development of the reduced metal with Au, this resulted in a nanowire structure with gaps of defined length and placement along the original DNA scaffold. The inverse of the process, the delivery of aldehyde-modified bases to DNA templates via sequence-specific binding of RecA nucleoprotein filaments, was also shown to provide a means to generate segmented

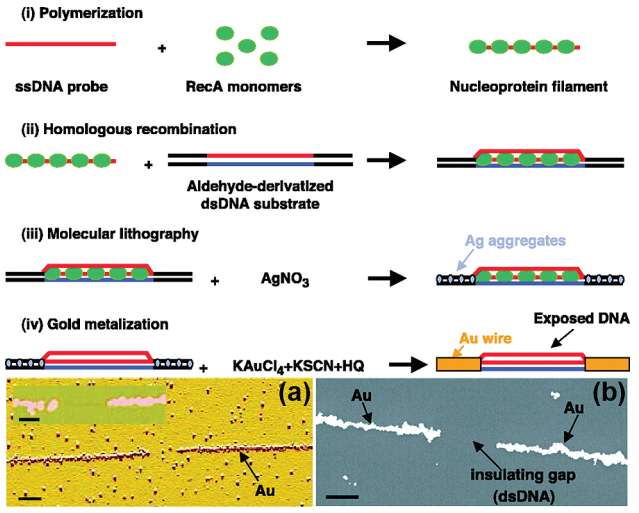

Figure 20. Sequence-specific masking of DNA templates to generate segmented metal nanowires: (a) AFM and (b) SEM image of metallized DNA that had a RecA nucleoprotein filament hybridized to it to block the reduction of Ag by the remaining aldehyde-modified bases. Adapted with permission from ref 481. Copyright 2002 American Association for the Advancement of Science.

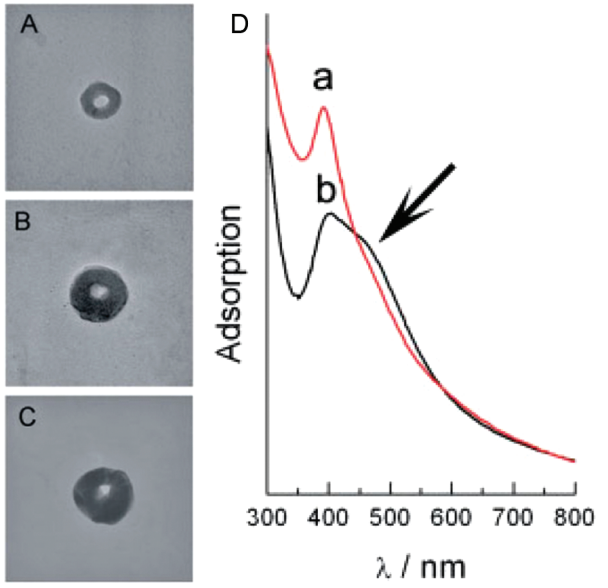

Figure 21. Ring-shaped Ag nanostructures formed from toroidal DNA templates: (A−C) TEM images of Ag nanorings, (D) extinction spectrum showing the appearance of an additional plasmon band as a consequence of the unique morphology (arrow, trace b). Adapted with permission from ref 497. Copyright 2005 Wiley-VCH Verlag GmbH & Co. KGaA.

nanowires.[483] Modifications to this procedure have also led to the formation of branched nanowire structures which may be important for various electrical measurements.[481,484] Further work with the growth of metal nanostructures on linear DNA templates has demonstrated improved size control of the synthesized nanowires,[485,486] typically through alternative synthesis methods such as the immobilization of metal nanoparticle seeds to facilitate metal deposition,[487,488] as well as electrochemical[489] and photochemical reduction strategies.[490]

In addition to linear DNA scaffolds, the extraordinary recognition and assembly properties of DNA have also been used to generate more complex morphologies that can act as templates for the synthesis of plasmonic nanostructures. An early example of this was the construction of elongated ribbons from DNA building blocks consisting of a four-armed branched motif known as a 4 × 4 tile.[491,492] Reduction of $AgNO_3$ by glutaraldehyde-treated DNA ribbons, followed by additional metal deposition, resulted in Ag nanostructures several micrometers in length with heights and widths ∼40 nm or less. Using several other DNA motifs such as triple-crossover tiles[493] and three-helix bundle tiles,[494] LaBean and collaborators have shown the assembly of nanotubes[493] and nanowires,[494] respectively, consisting entirely of DNA that were subsequently metallized to produce 1-D Ag nanomaterials. Using a relatively simple approach of hybridizing three appropriately designed oligonucleotides, Woolley and co-workers constructed a branched DNA nanostructure consisting of three coplanar arms separated by 120°.[495] Specific reduction of Ag or Cu using this structure as a template resulted in similarly branched nanostructures that would be difficult to synthesize by other methods. Rather than metallize the entire template, Chaput and co-workers recently synthesized a linear six-helix DNA bundle modified with equally spaced Au mineralizing peptides along its length that could nucleate AuNPs from a solution of $HAuCl_4$.[496] This resulted in 1-D arrays of nanoparticles with spacings defined by the placement of peptides in the original template design.

As an alternative to assembly of DNA into discrete shapes by programmed hybridization, DNA can adopt several different compacted or extended conformations based on external conditions that can be used to template nanostructures with unique shapes. One such morphological conformation adopted by DNA in the presence of tetracations such as spermine is that of a toroid. Baigl and collaborators have shown that toroidal DNA templates generated in this way can be subsequently metallized through the addition of $AgNO_3$ followed by reduction with $NaBH_4$ (Figure 21).[497] The result is a population of well-defined, solution-phase Ag rings with average inner and outer diameters of 22 and 93 nm, respectively. Interestingly, these structures exhibit two distinct plasmon resonances which are likely caused by transverse modes that occur out of the plane of the ring (∼400 nm) and more strongly coupled modes that arise from interactions between segments in the plane of the ring (∼470 nm). This approach has also been applied to the synthesis of Au ring structures with analogous optical resonances at 520 and 720 nm.[498] In addition, several others have shown that toroidal DNA templates can also be used to synthesize Au disk-shaped structures that lack a hole in their center.[499,500]

It is important to note that, in some cases, the chirality of the template can have a significant influence on the optical properties of the plasmonic nanostructures derived from it. Although only a few examples exist, several authors have shown that the growth of Au or Ag nanoparticles on chiral templates such as DNA or peptide nanotubes (vide supra) can result in a chiral-optical response at the surface plasmon resonance, as evidenced by circular dichroism (CD) measurements.[501−503] This effect has been seen by Kotlyar and co-workers by nucleating AgNPs on double-stranded helical DNA templates.[501,502] If AgNPs are synthesized separately and adsorbed to the chiral template, no peak in the CD spectrum is observed. The origin of this effect is still not well understood and is a phenomenon that is currently under investigation.[504] Importantly, such effects are unlikely to be observed using inorganic templates, as they lack the requisite

dx.doi.org/10.1021/cr1004452 |*Chem. Rev.* 2011, 111, 3736–3827

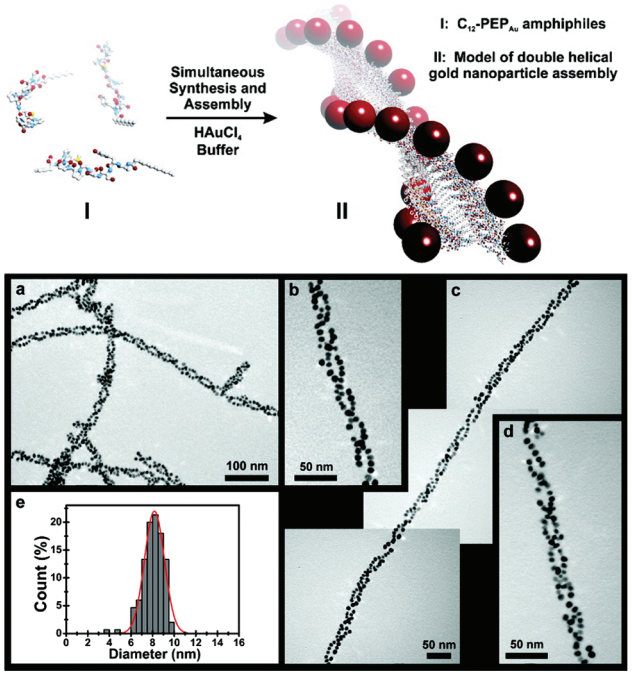

Figure 22. Schematic illustration of the formation of helical peptide supramolecular architectures that template the formation of ordered AuNPs: (a−d) TEM images showing the helical morphology of AuNPs nucleated onto the peptide scaffold, (e) histogram of AuNP sizes. Adapted with permission from ref 96. Copyright 2008 American Chemical Society.

chirality that many biological molecules naturally possess. This suggests that the investigation of plasmonic nanoparticle syntheses that rely on such templates will be a crucial area of understanding in future studies.

3.5.2. Peptides and Peptide Assemblies. While the unparalleled specificity of DNA hybridization interactions can be used to construct intricate nanoscale templates, nucleation of plasmonic materials is achieved through relatively nonspecific chemical deposition techniques. Peptides and peptide assembles, on the other hand, exhibit a wider range of chemical functional groups and, depending on their amino acid sequence, can be used to both nucleate and stabilize metal nanostructures. When assembled into supramolecular architectures, this feature often allows for more localized and precise deposition of metal onto the parent nanostructure dictated by the design of the template. Numerous reports have investigated the ability of particular peptides to reduce metal salts, frequently using phage display selection technologies to identify the optimum peptide sequence.[505−519] While most of these have demonstrated an ability to facilitate the synthesis of spherical particles, some have shown a preference for anisotropic nanostructures such as nanoplates or nanoprisms.[520−522] However, genuine templated nanostructures composed of these materials usually take the form of self-assembled supramolecular structures consisting of many short amphiphilic peptides. The earliest examples of these self-assembled structures come from bolaamphiphile peptides, which are molecules that have hydrophilic terminal ends separated by a covalently attached middle hydrophobic region; these types of peptides often form tube-like or helical ribbon assembled structures, depending on the experimental conditions.[523,524]

Although these supramolecular assemblies have garnered significant interest on their own,[523−526] Matsui and co-workers first demonstrated their utility as templates by using them to synthesize Au nanostructures.[527] The authors first adsorbed a histidine-rich peptide to self-assembled nanotubes constructed from glycine-based bolaamphiphiles. Incubation of this structure with a gold salt solution followed by reduction via $NaBH_4$ resulted in a dense coverage of many ∼6 nm AuNPs over the surface of the template. It was later shown that modification of the pH could provide a handle for modulating the particle density,[528] while changing the sequence of the adsorbed peptide could change the shape of the nucleated particles.[529] Although these peptide tube assemblies can be relatively large (0.5−500 nm in diameter),[530] Matsui and collaborators developed a separation method by using a size exclusion column that allowed them access to peptide nanotubes with diameters around 10 nm.[531] Using these smaller nanotubes as templates for the nucleation of AuNPs resulted in impressive linear arrays of nanoparticles that were only one particle wide. Finally, although bolaamphiphilic peptides have been largely used to synthesize nanowire-like structures, both spherical Au particles[532] and coaxial multiwalled Ag tubes[533] have been made using these unique building blocks.

In addition to bolaamphiphile peptides, Rosi and co-workers have shown that amphiphilic peptides can assemble into several supramolecular architectures while simultaneously templating the formation of unique plasmonic nanostructures. They first demonstrated this approach by conjugating a hydrophilic Au mineralizing peptide to a hydrophobic aliphatic carbon chain that was shown to form 1-D twisted helical ribbon assemblies in an *N*-(2-hydroxyethyl)piperazine-*N*′-ethanesulfonic acid buffer solution (Figure 22).[96] The presence of peptides capable of facilitating the reduction of Au allowed this template to nucleate ∼8 nm AuNPs along its length in an amazing double-helix arrangement. Later work showed control over the helix pitch as well as the particle size and density along these scaffolds by varying conditions such as the reaction time and the presence of various chemical additives.[534] Relatively straightforward modifications to the peptide amphiphile, such as the addition of specific amino acid residues or changes to the hydrophobic component, have allowed for the construction of AuNP-composite wire[535] and sphere[536] morphologies, demonstrating the tailorability of such a system.

Instead of using chemically modified amphiphilic peptides, Gazit and co-workers have shown the synthesis of metallic nanostructures from natural peptide-based supramolecular structures.[89] Using a dipeptide of phenylalanine dissolved in a combination of 1,1,1,3,3,3-hexafluoro-2-propanol and water, they observed the formation of hollow nanotubes in high yield with an average total diameter of ∼100 nm. Addition of these structures to a boiling solution of Ag salt and sodium citrate resulted in the nucleation and growth of Ag nanowires within the hollow cavity of the nanotube. The remaining assembled peptide template could be removed by a proteinase enzyme to yield free nanowires which had a final diameter of ∼20 nm and a length on the order of several micrometers. In an impressive extension of this work, Gazit later showed the synthesis of coaxial nanowires using the same basic peptide templates.[537] After coating the surface of the diphenylalanine nanotubes with a layer of Au by a seeded growth method, the authors used their prior procedure of metallic Ag formation to generate a recursive nanostructure containing a Ag nanowire radially separated from a Au shell by a layer of self-assembled peptides. More recently, these same diphenylalanine nanotubes have been used to nucleate spherical

AuNPs on their surface which exhibit a chiral plasmonic optical response.[503] Interestingly, adsorption of polyethylene glycol (PEG)-coated AuNP seeds to peptide tubes constructed from either D- or L-isomers of diphenylalanine resulted in no peaks in the visible region of the CD spectrum. However, photochemical reduction of $HAuCl_4$ onto these seeded templates resulted in larger AuNP clusters that exhibited CD signals at the SPR of the AuNPs, depending on the chirality of the template. It was proposed that the chirality of the peptide tube was able to impart a structural chirality to the arrangement of Au clusters on the template surface that responded specifically to light of the correct polarization. This work highlights the important role that template chirality might play in future plasmonic nanostructures.

3.5.3. Proteins. Many of the same basic strategies applied to peptide-mediated synthesis of nanostructures can be extended to proteins, as they contain many of the same basic functional groups derived from their amino acid building blocks. As in the case of peptides, and for the same reasons, many proteins have shown the ability to reduce and/or stabilize various noble metals under very mild conditions.[522,538−545] Despite the wide variety of structures to choose from, cage-like proteins represent one of the most obvious starting points for investigating a class of proteins to use as synthetic templates.[471,546] Most common among these are ferritins, which are ubiquitous iron storage proteins that have a 3-D structure that consists of a small ∼8 nm cavity in their center that, under normal physiological conditions, is used to sequester Fe^{3+} atoms, which have a number of crucial functions in nearly all living things.[547] The vacant central cavity in the iron-free version of this protein, known as apoferritin, can be used to constrain the growth of nanoparticles to well-defined sizes. Naik and co-workers were among the first to use this strategy for the formation of plasmonic nanostructures.[548] In an impressive example of template engineering, the authors showed that through careful genetic modification they could append one of the ferritin subunits with a known Ag mineralization peptide such that it was exposed to the inner cavity volume. Addition of $AgNO_3$ to these modified structures resulted in the generation of relatively monodisperse AgNPs in the confined template cages. Elevating the complexity of this methodology, Dmochowski and collaborators have used a computational method to aid in the redesign of the ferritin subunits so as to impart the core with metal coordination capabilities (mainly through cysteine residues) without disturbing the native protein structure.[549] Synthesized versions of these modified proteins indeed maintained their structure and were able to template the formation of Au and Ag nanoparticles between 2 and 4 nm. Others have extended these concepts and demonstrated nanoparticle size control[550] and formation of homogeneous AuAg alloy NPs[551] and have investigated in more depth the binding of metal ions to functional groups located at the core.[549,552]

Perhaps even more common than cage-like protein templates are those that form fibrous, 1-D scaffolds. These structures are usually those that make up components of the cytoskeleton and have been commonly utilized to synthesize linear plasmonic materials. For example, tubulin subunits have been polymerized and fixed using glutaraldehyde into extended microtubule templates that facilitate the formation of 1-D metallic nanostructures.[553] Depending on the reduction method, Unger and co-workers have shown that either Ag nanowires or structures consisting of an array of densely packed AgNPs or AuNPs could be formed from these microtubule templates.[554,555] Interestingly, tubulin can also be coaxed into forming ring-like assembles which can be metallized to generate Ag nanostructures.[556,557] Another cytoskeletal protein that has been used to synthesize metal nanowires is actin. Willner and colleagues have shown the attachment of ∼1.4 nm AuNPs to actin monomers (G-actin) followed by polymerization into the filamentous form of actin (F-actin) using adenosine triphosphate (ATP).[558] By constructing actin templates consisting of regions of AuNP-labeled and unlabeled F-actin, the authors showed the formation of segmented nanowires after a metallization step. As a proof that these nanowires still retain some of their original biological function, the authors also showed the biochemical transport of these structures across a substrate of myosin motor proteins fueled by ATP. Finally, a number of other linear proteins or protein assemblies have been used in the formation of plasmonic nanowire structures, including amyloid fibers,[559,560] bacterial flagella,[561] collagen,[562] and insulin fibrils.[563]

Although 1-D protein assemblies might be the most ubiquitous, several important examples of 2-D and 3-D systems have made possible the formation of ordered planar arrays of plasmonic nanostructures. The earliest examples of this morphology stem from bacterial cell surface layer (S-layer) proteins which can naturally form 2-D lattices of positive and negative features possessing oblique, square, or hexagonal symmetry, with spacings anywhere between 2.5 and 35 nm.[564] Although their biological and technological applications have been studied extensively and covered elsewhere,[564−567] Sleytr and co-workers were the first to use them as synthetic templates to generate metallic nanoparticles.[568] After crystallization of isolated S-layer proteins into a square lattice, the authors treated these substrates with iminothiolane to convert the primary amine groups on the proteins to thiols. Following treatment with $HAuCl_4$ for several days, they observed the formation of a square superlattice of 4−5 nm AuNPs as a result of exposure to the electron beam of a transmission electron microscope. These particles deviated only slightly (±0.5 nm) from the expected spacing of 12.8 nm based on the S-layer template. Rather than use S-layer proteins, Mann and co-workers have shown that lysozyme proteins crystallized into a tetragonal lattice could act as a template for the synthesis of Au and Ag nanostructures.[569] Interestingly, this crystal polymorph contains small 1−2.5 nm solvent channels that run parallel to the *c*-axis of the protein lattice. After glutaraldehyde cross-linking of this protein assembly, these pores could be metallized with Au or Ag using chemical reduction or photoreduction methods. This resulted in an extremely well-ordered array of plasmonic nanorods within the lysozyme templates that exhibited both transversal (Ag, 412 nm; Au, 583 nm) and longitudinal (Ag, 505 nm; Au, 684 nm) plasmon resonances revealed by diffuse reflectance spectroscopy.

3.5.4. Viruses and Microorganisms. Although many of the previous examples highlight man-made approaches to the assembly of proteins or their constituents into useful template materials, nature has also generated well-ordered arrangements of proteins in viruses and microorganisms that can act as templates. Although there are numerous examples of living cells or cell extracts mediating the formation of nanoparticles,[570−577] here we will focus on those cases where the shape of the microorganism itself (or its protein remains) can dictate the symmetry of a nanostructure. Despite being used extensively with semiconductor and oxide materials,[578] one of the first examples of this strategy being applied toward metal structures entails the use of an extremely common viral protein coat known as tobacco mosaic virus (TMV). TMV is a rod-shaped

supramolecular viral protein assembly approximately 300 nm long and 18 nm wide with a hollow ~4 nm inner channel.[579] Kern and co-workers first generated a plasmonic nanostructure using this template through simple reduction of $AgNO_3$ with formaldehyde, forming AgNPs along its length.[580] In an impressive extension of this initial work, Mann and co-workers showed spatially selective deposition of AuNPs or AgNPs on TMV scaffolds based on the solution pH (Figure 23).[579] For example, at pH 3, $AuCl_4^-$ ions associated primarily on the positively charged template surface and formed a dense coating of AuNPs after reduction with hydrazine. On the other hand, at alkaline or neutral pH, the surface charge was mitigated and Ag^+ ions associated with the negatively charged inner channel, forming well-defined linear nanoparticle arrays after photoreduction.

Under the right experimental conditions, Au has also been found to nucleate in a virus's inner cavity.[581] Other groups have observed spatially selective binding of AuNPs to the ends of the viral templates, mediated by the viral RNA.[582] These particles could be grown to larger sizes via electroless metal deposition, forming dumbbell-shaped nanostrucutres. Instead of TMV, Belcher and co-workers have worked extensively with a filamentous bacteriophage virus known as M13 that can also be metallized to template the formation of Au nanostructures.[533] Unlike many of the prior examples, they have also shown the formation of single-crystalline Ag nanowires that possess extremely well-defined shapes and even have a 5-fold twinning structure, like many solution-phase grown nanorods.[583] For most of these templates, including TMV, M13, and cowpea chlorotic mottle virus, extensive effort has gone into genetic modification of the viral proteins to insert specific peptide sequences to afford Au or Ag nucleation capabilities.[533,583−586]

Although 1-D viral or microorganism-based templates are common, several important examples highlight the structural diversity available from these scaffolds. For example, Ward and co-workers have used Chilo iridescent virus (CIV), which possesses a spherical morphology with a diameter of ~140 nm, for the formation of Au nanoshells.[587] By adsorbing small ~2 nm AuNPs onto the viral scaffolds to act as seeds in the reduction of $HAuCl_4$, they show the formation of 22 nm thick Au shells surrounding the CIV template. Similar to nanoshells formed on spherical dielectric cores (see section 3.2), these structures exhibit a dipole plasmon resonance around 800 nm and even support a quadrupole resonance at ~550 nm. Increasing the complexity of these structures, Mirkin and co-workers have created Ag nanostructures with an elaborate pattern of holes and features from microorganism templates known as diatoms.[588] These organisms are an interesting form of unicellular algae that have intricate cell walls consisting of fused or aggregated silica nanoparticles. Using acid to remove the organic components, these silica shells can act as templates for evaporated Ag metal, forming large micrometer-sized structures with nanoscale pores and grooves that can facilitate SERS.

3.5.5. Lipid Assemblies and Other Synthetic Supramolecular Structures. While biomolecules and their precisely assembled scaffolds have yielded several seminal examples of templated nanostructures, other organic small molecules have also been designed to organize into complex architectures for the purposes of nanoscale synthesis. A number of researchers are interested in the more fundamental self-organization processes for amphiphilic systems,[589,590] but here we are concerned with their propensity to create nanostructures once assembled.[473]

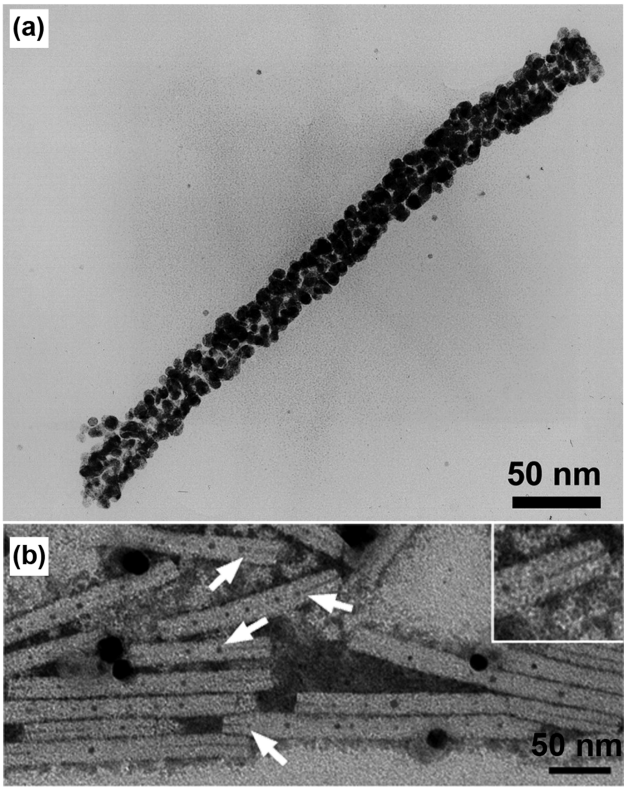

Figure 23. Selective deposition of metal on the outside surface or inner channel of tobacco mosaic virus templates: (a) TEM image of $AuCl_4^-$ ions reduced at low pH where they have associated primarily with the positively charged outer coat, (b) TEM image of Ag^+ ions photoreduced at high pH where they have migrated into the internal cavity. Adapted with permission from ref 579. Copyright 2003 American Chemical Society.

Although lipids are indeed ubiquitous in biological systems, synthetic lipid molecules are often those used to generate interesting plasmonic materials. Mann and co-workers first used this approach with the lipid diacetylenic phosphatidylcholine, which self-assembles into helical tubes.[591] Addition of $HAuCl_4$ to this structure resulted in the nucleation of AuNPs following the helical edges of the template. Importantly, addition of $HAuCl_4$ before the template was fully assembled or addition of preformed AuNPs to the assembled template did not result in the helical arrangement of nanoparticles. Shimizu and co-workers have extended these ideas significantly using a glycolipid (*N*-(11-*cis*-octadecenoyl)-β-D-glucopyranosylamine) that can self-assemble into a hollow nanotube morphology.[592,593] By first lyophilizing the structure, capillary forces could be used to draw a solution of $HAuCl_4$ into the interior that could subsequently be reduced by photoirrdiation. The result was a dense packing of 3−10 nm AuNPs inside the structures, forming well-defined composite metal nanowires.

In addition to lipids or glycolipids, several other amphiphilic molecules have been used to generate self-assembled templates to construct nanoscale materials. For example, Liu and co-workers used a racemic mixture of twisted helical ribbons self-assembled from 2-acryloylamidododecane-1-sulfonic acid to generate right- and left-handed Ag helices.[594] Reduction of $AgNO_3$ by $NaBH_4$ in the presence of these structures resulted in 20−300 nm long nanowires that mimicked the mixed chirality

of the templates. More recently, Kotov and co-workers have studied an assembly of amphiphilic polyurethane that adopts a globule conformation in solution and can template an interesting Au nanostructure with small tentacle-like projections.[595] Although the structure was 50−100 nm in total diameter, it was composed of many small 3−5 nm thick Au "fingers" that were very closely spaced and could facilitate strong intraparticle plasmon coupling for SERS. In another interesting example, Rabe and co-workers have used as a template an amphiphilic cyanine dye that self-assembles into a 13 nm diameter tubular J-aggregate morphology in a water/methanol mixture (Figure 24).[596] Incubating these structures for several hours with $AgNO_3$, followed by photoirradiation, they observed the formation of extremely well-defined polycrystalline Ag nanowires inside the hollow interior of the template. Interestingly, they found that the growth mechanism involved reduction of Ag^+ ions by photoexcited electrons in the cyanine dyes, demonstrating the possibility of constructing chemical templates that actively participate in the synthesis process. Other examples of this methodology include hollow alloy shells made of large spherical vesicles assembled from surfactants[597] and nanowires grown from self-assembled polymer microfibrils.[598]

3.5.6. Micelles and Emulsions. The construction of small, self-assembled micelle scaffolds to direct the synthesis of plasmonic nanostructures represents one of the original templated strategies using organic or "soft" materials. When this strategy was first developed, many groups were focused on improving the monodispersity of their colloidal nanoparticle syntheses and it was thought that preparing a well-defined nanoscale water volume inside a reverse micelle (i.e., an emulsion) would enable greater control over the particle size distribution.[599−601] This was typically accomplished by dissolving a small amount of water, solubilized by a surfactant, in a nonpolar solvent. While this basic concept has appeared in a number of disparate nanoscale systems,[472] one of the first examples using an emulsion demonstrated as early as 1983 that it could facilitate the growth of colloidal nanoparticles.[599] Here, Fendler and co-workers used pentaethylene glycol dodecyl ether to solubilize small volumes of water with $HAuCl_4$ dissolved inside, with *n*-hexane acting as the parent phase. Radiolytically generated electrons could then be used to reduce the metal salt to nanoparticles inside the reverse micelle templates. Barnickel and Wokaun later showed that chemical and photochemical reduction methods could be used to generate both Au and Ag nanoparticles using emulsion-based systems.[600] This group also demonstrated that, by controlling the size of the water volume in the reverse micelle (modulated by changing the ratio of water to surfactant), they could control the particle size.[601]

While some of the initial work synthesizing plasmonic nanostructures was explored by these groups, Pileni and co-workers actively worked to extend and perfect these techniques using a different surfactant system known as sodium bis(2-ethylhexyl) sulfosuccinate (AOT).[602−604] By replacing the Na^+ with Ag^+, reverse micelles of this surfactant could be functionalized to localize the metal ions in the water component using isooctane as the nonpolar phase.[605] They then added to these a separate solution of similarly prepared reverse micelles containing dissolved $NaBH_4$. Dynamic exchange between these two species allowed for the chemical reduction necessary to generate AgNPs.[606] Despite many improvements in understanding this synthesis, the polydispersity of plasmonic particles generated using this technique generally remain high.[607] Monodisperse

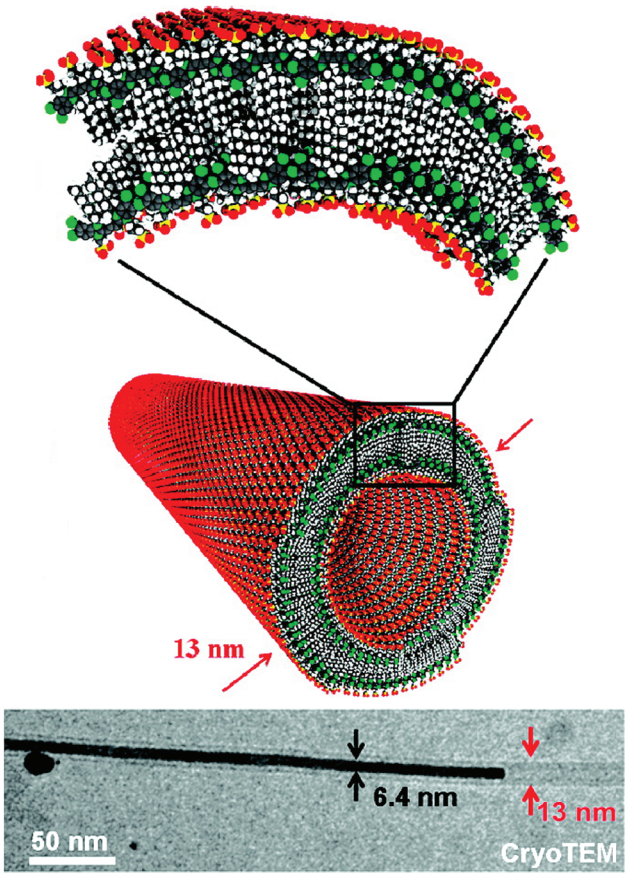

Figure 24. Amphiphilic cyanine dyes self-assembled into a tube morphology can act as a template for the formation of Ag nanowires. Adapted with permission from ref 596. Copyright 2010 American Chemical Society.

syntheses for other materials, on the other hand, such as Cu and certain semiconductors, have been more successful.[604] Others have attempted to improve the monodispersity of reverse-micelle-generated AgNPs using supercritical solvents with some success.[608,609] Using a similar emulsion-based approach, Wu and co-workers have used natural beeswax suspended in water as a template for the formation of Ag nanostructures.[610] Using CTAB as a stabilizing agent, the beeswax was melted and sonicated in an aqueous solution containing KBr to generate an emulsion with suspended droplets approximately 160 nm in diameter. Addition of $AgNO_3$ generated small AgBr seeds on the beeswax surface which were reduced to metallic Ag and further developed to yield well-defined continuous Ag shells.

It should be noted that this reverse micelle approach has also been applied toward the synthesis of anisotropic nanostructures. Using the same AOT surfactant system, Pileni and collaborators mixed together Ag^+ and hydrazine-filled reverse micelles, followed by brief ultrasonication, and observed Ag disk- or prism-shaped particles.[611] In addition, by controlling the hydrazine content, control over the nanodisk size could be achieved.[612] Adair and co-workers have seen similar results using a two-component system of octylamine and amylamine which forms a bilayer assembly with water confined into a roughly 2-D volume.[613] Reduction of $AgNO_3$ by hydrazine in the presence of this bilayer structure resulted in the appearance of Ag disk-shaped particles whose dimensions approximately matched those of the bilayer. Importantly, although this hypothesis was

dx.doi.org/10.1021/cr1004452 |*Chem. Rev.* 2011, 111, 3736–3827

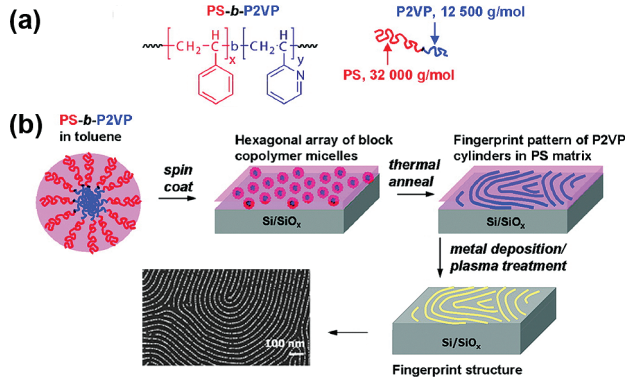

Figure 25. Block copolymer micelles that coordinate metal ions can template the synthesis of fingerprint-like nanowire patterns. PS-*b*-P2VP micelles (a) can be thermally annealed to form lamellar microdomains which, when exposed to $HAuCl_4$ and plasma, form extended nanowire structures (b). Adapted with permission from ref 631. Copyright 2008 American Chemical Society.

proposed initially, it is not clear that the self-assembled surfactant is, in fact, acting as a template in these cases. Despite this reasonable conclusion, significant work by Pileni has shown that, while the surfactant component is important and necessary, it does not likely play the dominant role in determining the final shape of the nanostructure.[614,615] Other factors such as the stability of particular crystallographic facets or the presence of various ionic additives are now known to play a more important role than previously thought.[616−618] Interestingly, a similar progression in understanding has also occurred in the seed-mediated synthesis of Au nanorods. In this case, Murphy and co-workers initially proposed a cylindrical micelle surfactant template mechanism to explain the 1-D growth.[619−621] However, additional pieces of evidence disputed this claim, and several more likely alternatives have now been proposed.[622−624]

Block copolymers represent another class of amphiphilic molecules which can readily self-assemble into micellar reaction vessels for nanoparticle synthesis. Block copolymers are used in an enormous number of nanoscale fabrication strategies due, in part, to the extremely intricate structures that can be created through variations in the polymer sequence and monomer identity.[625,626] One of the simplest and most versatile block copolymer morphologies used for nanoparticle synthesis is the micelle. Seregina and co-workers were among the first to utilize these structures for nanoparticle synthesis by coordinating Au precursor ions to the cores of polystyrene-*b*-poly(4-vinylpyridine) (PS-*b*-P4VP) micelles assembled in THF or toluene.[627] Interestingly, if a powerful reducing agent was used ($NaBH_4$), nucleation occurred quickly and many small AuNPs formed per micelle, whereas if a weak reducing agent was used (N_2H_4), nucleation was slow, resulting in one larger AuNP per micelle template. Using the same system, it was later shown that localization of several different metals inside the PS-*b*-P4VP micelle before reduction could yield alloy nanoparticles such as PdAu.[628] Further efforts have utilized more advanced triblock copolymer designs to provide another means to control the size or morphology of the assembled micelles to affect the templated nanoparticles.[629]

A more common use for copolymer micelles in the synthesis of plasmonic structures is a process known as block copolymer micelle nanolithography.[630] Although we will not cover it in depth here (see sections 5.3.3 and 7.4.2 for more on block copolymers), the basic premise of this procedure is to deposit metal-ion-loaded block copolymer micelles onto a substrate and allow them to self-assemble into an ordered pattern whose structure is dictated by various chemical and physical forces.[630] Standard lithographic prepatterning of the substrate before the micelle deposition process can restrict the micelles to specific areas with well-defined shapes.[630,631] In some cases, a semiconductor substrate can act as the reducing agent for a metal salt embedded within the micelle through a standard redox reaction, allowing for specific metal patterning on nanometer length scales.[632−634] Buriak and co-workers showed that a thermal annealing step could be applied to allow organization of PS-*b*-P2VP micelles into a fingerprint-like pattern of phase-separated microdomains (Figure 25).[631] Addition of Au salt into these structures, followed by oxygen-plasma reduction, resulted in similarly patterned elongated metal nanowires as thin as ~10 nm. More recently, Schütz and co-workers have shown the formation of hexagonally packed, Au-coated FeCo nanoparticles synthesized in a single step using PS-*b*-P2VP micelles loaded with all three materials.[635] Minimization of surface energies between different phases drives the nanoparticles to adopt this morphology, highlighting the complexity available from seemingly simple block copolymer-based systems.

3.5.7. Dendrimers. Although many of the examples thus far have relied on weak, noncovalent interactions between monomeric units to build complex scaffolds, several important examples highlight the ability of chemists to create covalently linked, intricate molecular templates that can direct the growth of nanostructures. First proposed by Tomalia and co-workers to function as nanoscale templates, dendrimers are one such class of molecules that have found popularity because of their monodispersity and chemical tailorability.[474,636,637] Nearly all dendrimer templates that are used for plasmonic nanoparticle synthesis consist of poly(amidoamine) (PAMAM) because the numerous tertiary amine groups that compose their core allow for coordination of metal precursor ions. Interestingly, early work in this field found that, when present during the sodium borohydride reduction of $HAuCl_4$ or $AgNO_3$, PAMAM dendrimers served only as nanoparticle capping ligands and not as templates.[638−640] An initial strategy to circumvent this limitation, demonstrated by Crooks and co-workers, utilized a galvanic replacement reaction between CuNPs synthesized within the dendrimer template and more noble-metal ions such as Au^{3+} or Ag^{+} (see section 3.4).[454] Because CuNPs could be more easily formed within dendrimer templates due to the favorable coordination of Cu^{2+}, this approach allowed for well-defined 1−3 nm AuNPs and AgNPs to be synthesized within the structures. Simultaneous addition of both Au and Pt salts to dendrimer-encapsulated CuNPs was later shown to result in the formation of AuPt alloy nanoparticles by the same mechanism.[455] Amis and co-workers provided an alternative solution to the difficulty of nucleating AuNPs by simply using higher generation dendrimers, which contain more amine groups.[641] These authors found that while low-generation PAMAM dendrimers (G2−G4) were more likely to behave as capping ligands, higher generation versions (G6−G10) were able to accommodate Au precursor ions and act as templates to control the growth of monodisperse AuNPs. Using this strategy while adding "magic number" equivalents of $HAuCl_4$ to PAMAM dendrimers, significantly more monodisperse 1−2 nm AuNPs could be formed by virtue of their greater thermodynamic stability.[642] Finally, through the use of either simultaneous metal

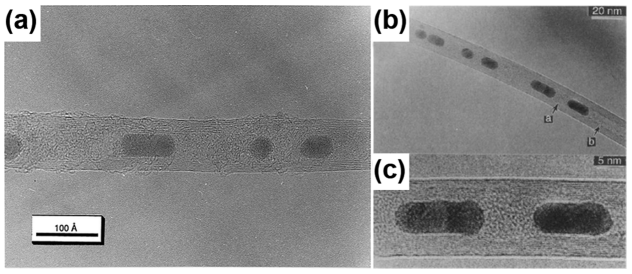

Figure 26. TEM images of Ag nanostructures that have been grown inside the hollow cavity of carbon nanotubes by (a) high-temperature decomposition of $AgNO_3$ and (b, c) electron beam reduction of $AgNO_3$. (a) Adapted with permission from ref 90. Copyright 1996 American Chemical Society. (b, c) Adapted with permission from ref 650. Copyright 1996 American Association for the Advancement of Science.

ion encapsulation and reduction or sequential metal ion encapsulation and reduction, a number of bimetallic alloy or core−shell nanoparticles, respectively, have been synthesized with dendrimer scaffolds using combinations of Au and Pd,[643] Au and Ag,[644] or Au and Pt.[645]

3.5.8. Carbon Nanotubes. Carbon nanomaterials represent another interesting class of non-self-assembled structures that have been used extensively as templates for the synthesis of plasmonic materials. Although carbon has a number of different allotropes, here we will focus on carbon nanotubes (CNTs), as they are most often the morphology used to template metallic nanostructures.[475,646] Interestingly, almost immediately after the discovery of CNTs, researchers realized that these nanoscale wires could function as scaffolds for the deposition of other materials.[647] Although not shown with plasmonic metals, these initial attempts introduced the idea of using the hollow interior of the CNTs as 1-D nanoscale pores into which new nanostructures could be grown.[647,648] Importantly, as-synthesized CNTs typically possess hemispherical end caps that prevent access to the inner cavity of the nanotubes by most chemical species. To solve this problem, Green and co-workers introduced an important and now widely used procedure involving refluxing of CNTs in a nitric acid solution that selectively "opened" the ends, allowing access to the nanotube interior.[648] Sloan and co-workers were among the first to use this method to open CNTs and use them as templates for the synthesis of Au and Ag nanostructures (Figure 26a).[90] Incubation of these opened CNTs with aqueous solutions of $AgNO_3$ or $AuCl_3$, followed by a high-temperature calcination step to decompose the precursors, resulted in the formation of Au or Ag nanocrystals encapsulated within the interior of the CNTs. Although these particles varied in length from 3.5 to 8.5 nm, they typically adopted the same diameter as the innermost carbon tube. When this high-temperature decomposition approach was applied with $HAuCl_4$, extremely thin (1−1.4 nm), high aspect ratio Au nanowires could be synthesized within the CNT templates that exhibited both transverse and longitudinal plasmon resonances.[649] In a similar procedure, de Heer and collaborators showed that $AgNO_3$ could be melted and drawn into ∼4 nm diameter CNTs by capillary forces.[650] Subsequent reduction by a TEM electron beam resulted in 10−15 nm long Ag nanorod segments separated by pockets of NO_2 and O_2 gas that were byproducts of the $AgNO_3$ decomposition (Figure 26b,c). Green and co-workers showed similar results by allowing capillary forces at high temperatures to draw ionic liquids of AgCl, AgBr, and eutectic $AgCl_{0.2}AgBr_{0.8}$ into CNT interiors.[651] In particular, photolytic decomposition of AgCl-filled single-walled carbon nanotubes (SWNTs) resulted in the formation of continuous Ag nanowires. Using a particularly simple approach, Rao and co-workers showed that addition of metal salt during the nitric acid refluxing step resulted in filling of the inner cavity with reduced metal nanoparticles in a single step.[652] Finally, significant improvements to the morphology, length, and yield have also been shown using sonication,[652,653] chemical reduction,[652] and γ radiation reduction[654] methods.

Although several impressive examples have shown the growth of metals inside CNTs, this method remains challenging as it is difficult to achieve both continuous metal nanowires and a high yield of metal encapsulation. An alternative strategy which has also been quite popular is the nucleation and growth of plasmonic materials on the outside of the CNT template. Haushalter and co-workers first identified that the nitric acid treatment used to open the nanotubes also produced several reactive functional groups along the CNT that could be used as redox centers to generate metal NPs.[655] Using X-ray photoelectron spectroscopy, the authors revealed the presence of carboxylic, carbonyl, and hydroxyl groups on the nanotube surface that were able to facilitate, with the aid of formaldehyde, the nucleation of ∼10 nm AgNPs along the length of the template. Similar results were found by Rao and co-workers nucleating AuNPs onto CNT templates using tetrakis(hydroxymethyl)phosphonium chloride as a reducing agent.[656] Although several other chemical reduction methods have been shown,[657,658] Dai and co-workers demonstrated that the redox reaction alone was capable of generating nanoparticles on CNTs, but only for sufficiently noble metals such as Au and Pt.[659] This restriction was later circumvented using a process called substrate-enhanced electroless deposition, which allowed less noble metals (e.g., Ag and Cu) to be reduced onto CNT templates.[660] By using a substrate with a lower reduction potential than the desired metal, deposited CNTs acted as the cathode while the substrate acted as the anode. For example, CNTs dispersed on a Zn substrate (Zn^{2+}/Zn, −0.76 V vs SHE) were able to facilitate the nucleation of Ag (Ag^{2+}/Ag, +0.373 V vs SHE) or Cu (Cu^{2+}/Cu, +0.34 V vs SHE) nanoparticles by this mechanism.[660] Several researchers have subsequently adopted and modified this spontaneous redox protocol for producing AuNP-decorated CNTs and have shown that the donation of electrons to reduce the metal leaves the structure electron deficient (or equivalently results in hole injection), resulting in significant modifications to the electronic structure of the nanotubes.[661] More recently, this protocol has been used to generate a continuous 4−8 nm thick Au coating around CNT templates.[662] The resulting particles, having diameters of ∼11 nm and lengths of ∼100 nm, show transverse and longitudinal plasmon resonances and have been used as NIR imaging contrast agents (Figure 27). Numerous alternative strategies have also utilized CNTs as templates for metallization, some of which include alternative reduction methods,[663−665] chemical modification with thiolated[666,667] or dendrimeric[668,669] ligands, and electron beam evaporation.[670,671]

4. SYNTHESIS WITH POROUS TEMPLATES

Porous materials and membranes are routinely used to fabricate nanostructures of all types and geometries with a host of properties and applications. Pores that permeate the structures can be filled or coated with a variety of materials, such as metals,[672−678] polymers,[674,675,678−683] and semiconductors,[678,684,685]

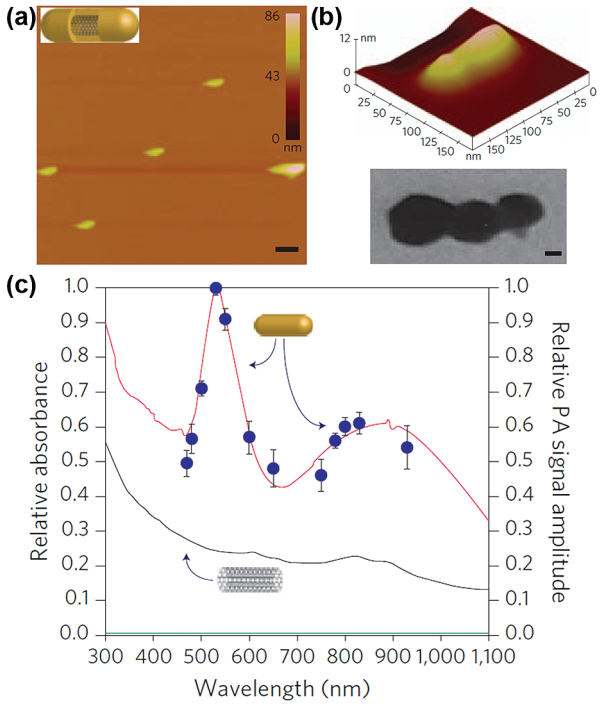

Figure 27. Au overgrowth of carbon nanotube templates: (a, b) AFM and TEM characterization of $HAuCl_4$ that has been reduced onto shortened CNTs (scale bars 100 nm for AFM images and 10 nm for TEM images), (c) extinction spectra show the appearance of both transverse and longitudinal plasmon bands in the Au-coated CNT structure. Adapted with permission from ref 662. Copyright 2009 Nature Publishing Group.

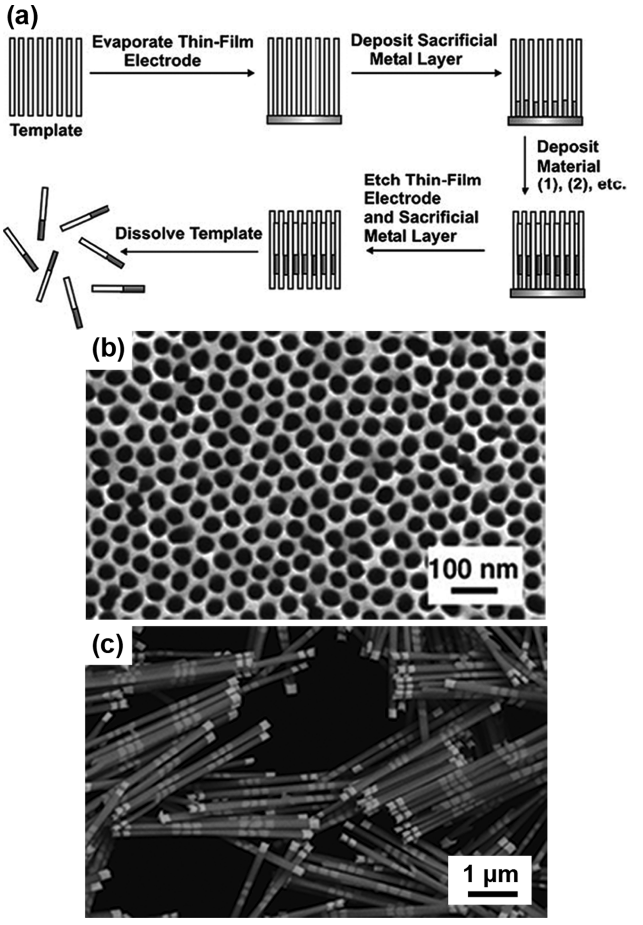

Figure 28. Template-based electrochemical deposition of metal nanowires: (a) synthetic scheme describing the synthesis of multicomponent nanowires, (b) SEM image of the AAO porous membrane template used for nanowire synthesis, highlighting the pore monodispersity and density; (c) SEM image of multicomponent Au−Ni−Ag metal nanowires grown using the scheme in (a). (a, b) Adapted with permission from ref 678. Copyright 2006 Wiley-VCH Verlag GmbH & Co. KGaA.

to produce nanostructures with a final size and shape dispersity dictated by the size and shape of the template. Since many of the methods to produce these porous materials lead to high pore densities with low pore size dispersities, nanostructures with controlled geometries can be routinely synthesized in high yield with these methods.[678] Many different porous materials have been used as templates to synthesize nanostructures, including mica,[686] glass,[687] zeolites,[688,689] and nanoporous solids,[690] but for metal structures with interesting plasmonic properties, track-etched polymer and anodic aluminum oxide (AAO) membranes and mesoporous materials are the most common and will be the focus of this section.[678]

4.1. Porous Membranes for 1-D Nanostructures

Track-etched and AAO templates are nanoporous membranes with uniform cylindrical pores running throughout that can serve as templates for 1-D nanowires, nanorods, and nanotubes. Track-etched polymer membranes are fabricated by bombarding a thin polymer film with ions to create randomly spaced tracks through the films, which are then chemically etched to form uniform pores with diameters ranging from approximately 10 nm to 10 μm.[675] Polycarbonate or polyester films are both readily available, but often contain pores in random locations across the surface of the template. This can lead to significant intersection of the pores, which adversely affects the monodispersity, yield, and control of the nanomaterials synthesized inside.[678] AAO templates are less prone to this issue and are generally the template of choice for most nanosynthetic applications.

AAO templates are most commonly fabricated by a two-step anodization process on a thin aluminum metal electrode pioneered by Masuda and co-workers, among others.[691−695] Briefly, the aluminum electrode is polished and anodized in an acidic electrolyte solution, leading to the formation of a film of aluminum oxide containing a high density of cylindrical pores throughout the material (Figure 28b).[694] Unlike the track-etched templates, these pores are not random and are periodically spaced in a hexagonal arrangement, limiting the amount of intersection between adjacent pores and greatly increasing the utility of AAO templates for the synthesis of monodisperse nanostructures.[678] Furthermore, this hexagonal arrangement is transferred to the nanostructures fabricated inside and can lead to important coupling or ensemble effects, especially for plasmonic structures. By controlling the temperature and choice of acid etchant, AAO templates with pore sizes ranging from approximately 10 to 400 nm can be synthesized and are available commercially. Similarly, changing the anodization time affects the thickness of the membrane, which allows one to control the length of the pores available for nanostructure growth or deposition.[678] In recent years, there have also been several examples of controlling the shape of these pores, which could eventually be used to create nanostructures with unique geometries.[696−698]

4.1.1. Electroless Deposition of Metal Nanotubes. For metals, there are two primary methods for synthesizing nanostructures in membrane templates: electrochemical deposition and electroless deposition.[675] Electrochemical deposition is commonly used to synthesize structures that fill the entirety of the pores, such as nanowires and nanorods. Conversely, electroless deposition is most commonly used to synthesize materials where only the pore walls are coated with the deposited material (i.e., nanotubes and core−shell structures[699]). Electroless deposition of metal into membrane templates was first pioneered by Martin and co-workers on polycarbonate membrane templates by altering a process established in the electroplating industry for electroless silver deposition known as the Rochelle salt method.[700,701] Briefly, Sn^{2+} ions were adsorbed onto the polycarbonate pore walls by sonicating the membrane in a 0.2% solution of $SnCl_2$ in 0.02 M HCl, sensitizing the pore walls for metal deposition.[700] After the activation process, membranes were then soaked in a silver salt solution, where the Sn^{2+} ions act as reaction sites by being oxidized to Sn^{4+}, producing Ag particles on the pore walls. Finally, electroless Ag or Au plating solutions comprised of a metal salt and a reducing agent were used to deposit metal on the nanoparticle-coated pore walls, producing nanotubes that span the length of the pore walls with wall thicknesses controlled by the electroless deposition time.[700] The silver layer and membrane could then be dissolved to disperse the nanowires in solution or left in the pores to study coupled effects. As ensemble structures left in the pores, these Au nanotubes have been studied in the context of optical properties,[702] and several novel membrane applications using the Au-coated pores have been developed.[703,704]

4.1.2. Electrodeposition of Single-Component Nanorods. While it is possible to increase the reaction time required for closed nanowires to be formed by electroless deposition, electrodeposition using membrane templates provides several key advantages for nanowire synthesis, including improved length and composition control. Electrodeposition involves the electrochemical reduction of metal ions inside the pores of the membrane templates (Figure 28a). By first depositing a thin film of metal on one side of the templates, a working electrode and electrical contact are created to allow deposition of metal ions into the now half-closed templates. Applying a potential to this metal film in the presence of an electrolyte containing the metal ions to be deposited allows reduction of the metal ions on the surface of the working electrode and controlled bottom-up growth of nanowires in the pores of the template. By controlling the charge passed during synthesis, the length of the resulting nanowire segments is finely controlled with less than 10% variation (Figure 28c). Furthermore, by thoroughly rinsing and changing the electrolyte solution to deposit a different metal, multisegmented nanowires can be grown.[678] After synthesis of the nanowires, the template and deposited working electrode metal can be dissolved, leaving dispersed nanowires with controlled diameters and lengths in solution (Figure 28a). Of course, neither of these dissolution steps is required, and retaining the template structure can lead to interesting emergent properties for plasmonic materials, particularly for the densely packed, periodic arrangement of nanowires produced in AAO templates.[705−707]

Pioneered by Moskovits[672,676,708] and Martin,[673−675,677,709] electrodeposition of metal nanostructures in membrane templates has been an important force in the development of plasmonic materials for fundamental and applied studies. Due to the cylindrical shape of the pores, electrodeposition is most commonly used to synthesize nanowires with highly tailorable compositions and geometries by altering the parameters described previously. While other methods exist for creating metal nanowires, template-synthesized structures (typically Au and Ag) have led to many important discoveries pertaining to the optical properties of anisotropic metal nanomaterials due to the extent to which nanowire diameters and lengths can be controlled.[676,677,710−712] With diameters ranging from approximately 10 nm to as large as 400 nm and lengths between a few nanometers and tens of micrometers,[678] membrane-template-synthesized nanowires have been tailored to have specific optical properties across the visible spectrum. As dispersed nanowires or coupled structures, these properties have been harnessed for many important applications, including chemical and biological detection[706,713] and the synthesis of metamaterials.[705]

4.1.3. Structures Derived from Multicomponent Nanorods. In addition to this fine geometry control, the compositions of the structures have also been uniquely tailored to affect the optical properties with membrane-template-synthesized nanowires. Using Au and Ag as an example, multicomponent nanowires have been created in two different ways. By preparing an electrolyte bath with both metal ions in solution, AuAg alloy nanowires were synthesized, where the relative amounts of Au and Ag are controlled by the concentrations in solution and the applied field during deposition.[444,445] Alternatively, multisegmented Au−Ag nanowires made up of separate segments of Au and Ag have been synthesized by sequential deposition of Au and Ag during synthesis, leading to structures that are particularly interesting and difficult to synthesize by other methods (Figure 28c). Natan and co-workers have taken advantage of this unique tailorability to make striped nanowires comprised of a variety of materials for nanoscale encoding and detection applications where the difference in the reflectivity between neighboring metal segments is used to identify the structures.[714−716] Providing an example of using these structures for plasmonic applications, Park and co-workers recently studied the effects of relative segment sizes and compositions of Au and Ag on the optical properties of these multisegmented nanowires.[717] By successively depositing thin segments of Au and Ag with varying lengths by monitoring the charge passed during deposition, the authors observed the relative effects of both the composition and geometry on the optical properties of metal nanowires. Interestingly, multiple plasmon resonances resulting from interactions between the two metals were observed, highlighting an effect that had not been seen with previously reported nanowires.[717]

The unique ability to control the composition down the length of these nanowires has also been leveraged to create interesting coupled plasmonic systems based on the interaction of closely spaced nanowire segments.[718,719] Rather than creating multisegmented structures with two functional materials (such as the Au−Ag structures described above), these structures have electrodeposited sacrificial segments in the nanowires to act as placeholders in the structure. By dissolving the template to disperse the wires in solution and then depositing a thin support layer onto the nanowires, the sacrificial layers were selectively etched to create structures with controllable gaps between the desired metal segments. Mirkin and co-workers pioneered this synthetic strategy with the development of on-wire lithography (OWL; Figure 29).[719] In OWL, nanowires with the desired geometry based on Au, Ag, Pt, and sacrificial Ni segments are synthesized in AAO membranes, released into solution, and drop cast onto substrates (Figure 29a). A thin (∼50 nm) support layer

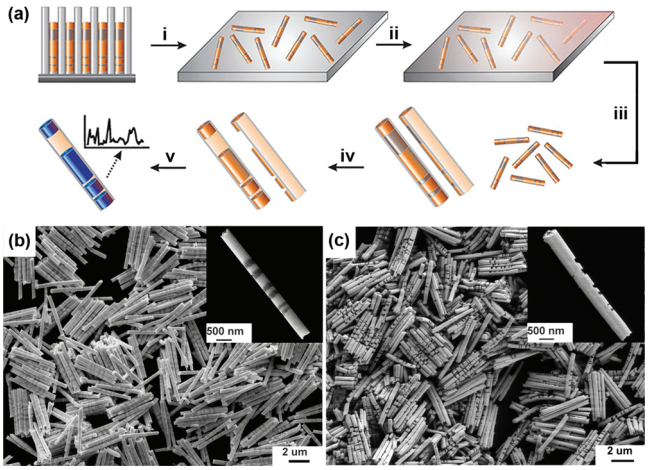

Figure 29. Synthesis of gapped metal nanorod arrays using on-wire lithography: (a) OWL synthetic scheme describing (i) dispersal of multicomponent nanowires grown in AAO onto a substrate, (ii) line-of-sight deposition of a thin backing layer (i.e., SiO_2 or Ti/Au) on the nanowires, (iii) sonication to disperse the wires back into solution, (iv) selective etching of sacrificial segments, and (v) functionalization and use of structures for SERS. (b) and (c) depict SEM images of Au−Ag nanowires before etching and gapped Au nanowires after etching, respectively. (b, c) Adapted with permission from ref 719. Copyright 2005 American Association for the Advancement of Science.

is then deposited by a physical or chemical vapor deposition method (typically SiO_2 by plasma-enhanced chemical vapor deposition) onto the exposed side of the dried nanostructures. Ultrasonication is used to recover the nanowires into solution, where the difference in reactivities between the desired and sacrificial metals can be exploited to selectively etch the Ni segments. The support film holds the remaining metal segments together so that their length, width, and relative spacing remain unchanged after the removal of Ni. This allows for unique geometries to be synthesized that are inaccessible via other nanowire synthesis methodologies. By using AAO membranes with different pore sizes, the diameters of the structures have been tailored to range from 360 to 35 nm.[720] The length and spacing of the nanowire segments have similarly been shown to be tunable by controlling the charge passed during deposition of the desired and sacrificial segments, respectively (Figure 29 b,c). Tuning these parameters has enabled the synthesis of metal segments between 6 nm and several micrometers in length, with gap thicknesses between 1 nm and several micrometers, allowing unique tailorability of the optical properties of OWL-generated nanostructures to yield particular plasmon resonances or field enhancement capabilities.[720] Examples of this include the optimization of the geometry of Au and Ag nanodisk dimers for SERS to create a powerful system for both detection and encoding[713,721−723] and a systematic study of the variation of field enhancement in nanoscale gaps as a function of the length of the Au nanowire segments comprising the structures.[724,725]

OWL has also been used to create unique heterostructures to probe plasmonic properties that are difficult to study using other methods. By designing a structure with two desired materials (i.e., Au and Ag with Ni sacrificial segments or Au and Ni with Ag sacrificial segments), OWL-generated structures consisting of Ni and Ag nanowire segments located at controlled distances away from enhancing Au disk dimers have been synthesized.[726,727] For the Au−Ag structures, Ni was selectively etched with H_3PO_4 or HCl to allow demonstration of nonlinear energy transfer from the excited Au dimers to the out-of-resonance Ag segments that were separated from the Au dimers by 100 nm.[727] Similarly, the Au−Ni structures were synthesized by selectively etching Ag sacrificial segments in a 4:1:1 mixture of methanol, 28% NH_4OH, and 30% H_2O_2.[726] Through selective functionalization only on the Ni segment using a carboxyl-terminated Raman chromophore, these structures allowed the authors to probe how far the enhancement extended away from the Au dimers by systematically studying the Raman signal on the nonenhancing Ni segments as a function of the distance from the Au dimers. Surprisingly, it was determined that this signal was detectable with separations between the Au dimer and Ni segments up to 100 nm, which is significantly longer than reports about the nature of decaying plasmonic fields.[726]

In addition to these examples from multisegmented nanowires, selective etching has also been harnessed to demonstrate structural control in alloy nanowires. By simultaneously depositing two metals from the same plating bath, alloy structures can be synthesized where the relative concentrations of each metal in the nanowires are dictated by the concentrations of precursor ions in solution. Similar to the previous examples, one can take advantage of the relative reactivities of each component of the alloy to selectively etch the less noble element. Ji and Searson first demonstrated this with AuAg alloy nanowires in 2002.[444,445] By varying the relative concentrations of Au and Ag, the authors found that the size of the resulting Au and Ag segments of the alloy could be controlled.[445] Selectively etching the Ag regions with concentrated nitric acid provided a means of producing controllably porous Au nanowires with varying surface areas. Subsequent work extended this idea to new systems, including work by Park and co-workers to create Pt-coated porous Au nanowires.[728] AuAg alloy nanowires were synthesized on a Au electrode, and the Ag regions were selectively removed in nitric acid. With the working electrode not dissolved in this case, a thin layer of Cu was deposited on the surface of the porous Au nanowires using an electrochemical underpotential deposition method.[728] Finally, a galvanic replacement reaction was utilized to replace the Cu with Pt in a 5 mM solution of Na_2PtCl_6.

4.1.4. Modified Pore Morphologies for Electrodeposition of Complex Structures. Adding to the complexity of these metal nanowires, Stucky and co-workers have incorporated another template material into the pores of an AAO membrane to synthesize Au and Ag nanowire structures with helical morphologies.[729] First, the AAO pores are dip coated into a precursor solution containing TEOS, poly(ethylene oxide)-*b*-poly(propylene oxide)-*b*-poly(ethylene oxide) block copolymer $EO_{20}PO_{70}EO_{20}$ (Pluronic P123), diluted hydrochloric acid (pH 2), and ethanol, with a molar ratio of 1 TEOS:0.0096 P123:6 H_2O:8.8 ethanol:0.001 HCl.[730] Upon evaporation, this mixture forms a self-assembled mesoporous silica network in each AAO pore that is then calcined at 400−500 °C to produce solid mesoporous structures. Typical electrodeposition methods were then employed to deposit Au or Ag metal in the interstitial areas of the mesoporous films, resulting in hierarchical nanowire structures with ordered helix morphologies upon removal of the AAO and mesoporous silica membrane materials.[729] The authors characterize different helix shapes using electron microscopy and demonstrate how the helical ordering of the Ag structures can be harnessed to act as strongly enhancing

structures for SERS where the closely spaced surfaces along the turns in the helices lead to plasmon coupling.

Although most of the work to synthesize plasmonic nanostructures using electrochemical deposition has been done in alumina and track-etched membrane templates, one recent example using a novel lithographic process has led to complex Au nanostructures with metamaterial applications.[731] In this work, direct laser writing is used to create an array of helix-shaped pores in a positive-tone photoresist on an indium tin oxide (ITO) surface. Au is then electrodeposited in these pores from a sulfite-based Au plating solution with the ITO surface serving as the working electrode, similar to the method for electrodepositing nanorods in AAO. Removal of the polymer resist resulted in a 2-D array of gold helices, producing an ensemble arrangement of hierarchical structures that is very difficult to produce with other methods.[731] The authors demonstrate novel applications of these structures as metamaterial broad-band circular polarizers; for the case of propagation along the axes of the helices, light that has a circular polarization with the same handedness as the structures is blocked, whereas light with the opposite polarization is transmitted.[731] With the ability to tune the structures to a variety of wavelengths and synthesize them over large areas, this work represents an important step forward in developing metamaterial optical circuit components.

Most of the methods for creating metal nanotubes in membrane templates involve electroless deposition of material on the pore walls, which limits control of the length and composition. However, several groups have developed novel methods to overcome these limitations by electrodepositing metal nanotubes to create multisegmented structures.[732−735] One such method involves replicating the shape of the membrane pores to physically create an annular region in the pores, which can be filled with metal ions during electrodeposition in the AAO.[735] A second approach demonstrated the fabrication of nanotubes by slowing the deposition rate so that the metal was deposited only along the pore walls, which is the preferred initial growth location of the solid metal.[733] Others have demonstrated how this method can be improved by functionalizing the pores of the AAO membrane with silane molecules with functional groups that bind to the metal being plated.[673] The lengths of the structures produced using this method were limited to a few micrometers before the structures closed up and began depositing as nanowires. Chemically, the most interesting approach was developed by Gosele and co-workers, who produced controlled multisegmented Au−Ni nanotubes up to tens of micrometers in length by seeding the pore walls of AAO membranes with Ag nanoparticles.[732] It was believed that the nanoparticles served to direct preferential growth along the pore walls by creating a small conducting path between the growing nanotube ends and the next nearest nanoparticles, making deposition of metal along these conducting paths preferred compared to growth in the center of the tubes. It is important to note that this nanoparticle layer was not dense enough to create a conducting path along the entire nanopore surface, which allowed the bottom-up and multisegmented growth of Au−Ni nanotubes by changing the electrolyte. In this case, the nanoparticles were grown on the surface of the AAO pores by sequential exposure of the template to aqueous solutions of $SnCl_2$ and $AgNO_3$, where Sn^{2+} attached to the AAO surface and was subsequently oxidized to Sn^{4+} to produce Ag metal nanoparticles upon exposure to $AgNO_3$.[732]

4.2. Mesoporous Templates

In addition to membrane templates, the tunable geometries of organic and ceramic mesoporous templates have also been used to control the synthesis of nanomaterials. Because of their large surface areas, mesoporous templates have been most commonly used to synthesize catalytic nanostructures, such as Pd and Pt nanoparticles and nanowires.[736−744] More recently, the advent of plasmonics has led to more examples of the synthesis and optical characterization of Au and Ag structures made using mesoporous materials,[745] but the decreased control and structural complexity available with these methods have limited their impact compared to other more advanced methods. For these reasons, researchers have primarily chosen AAO templates over mesoporous templates for plasmonic studies, but one important advantage of using mesoporous materials instead of AAO is the minimum pore size available (sub 1 nm compared to 10−20 nm).[745]

Although the first mesoporous materials were patented in 1971,[746] there was little activity in the field until Beck and co-workers synthesized an important mesoporous silica material, MCM-41, in 1992.[746,747] Calcination of aluminosilicate gels in the presence of surfactants led to the synthesis of MCM-41, which possessed a hexagonal geometry dictated by the surfactant micelles formed in solution. In this case, quaternary amine-containing surfactants were used with varying alkyl chain lengths to control the pore sizes between 1.6 and 10 nm.[689,747] A second class of mesoporous silica materials, termed SBA-15, was developed by Stucky and co-workers using amphiphilic triblock copolymers as templates to produce hexagonally ordered pores in the silica gels.[748] In this case, triblock copolymers of poly(ethylene oxide)-*b*-poly(propylene oxide)-*b*-poly(ethylene oxide) were assembled in water into hexagonal micellar rods, which templated the formation of mesoporous silica upon calcination similarly to MCM-41. Pore sizes and wall thicknesses could be tailored by changing the temperature used during heating, producing larger pore sizes (up to 30 nm) and thicker walls than those of MCM-41.[748] Similar work also showed that other phases of mesoporous materials, such as cubic and lamellar, could be formed by adding nonionic ethylene oxide surfactants to these mixtures.[749,750] While many other mesoporous materials have been synthesized, including zeolites, metal−organic frameworks (MOFs), and other organic templates, variations of these silica materials represent the most often used mesoporous templates for the synthesis and assembly of nanostructures and will be the focus of this section.[745,751]

4.2.1. Chemical and Thermal Reduction for Metal Nanowire Synthesis. Like membrane templates, the cylindrical nature of the pores in mesoporous materials naturally led to the predominance of nanowires and spherical nanoparticles as the most commonly synthesized nanostructures using this method. Each variation on the synthesis of metal structures in mesoporous templates has followed the same basic steps: infiltration of the pores with metal ions by solution- or vapor-phase methods, chemical or thermal reduction of the metal ions to solid metal, and optional removal of the template to recover free-standing metal nanostructures. This concept was first demonstrated in 1996 with the deposition of Pt nanowires in cationic-surfactant-synthesized mesoporous silica materials to image the geometry of the pores.[737,752] In these studies, $Pt(NH_3)_4(NO_3)_2$ was mixed with the preformed mesoporous material, rinsed with distilled water, and dried. $Pt(NH_3)_4^{2+}$ ions were incorporated on the surface of the template by ion exchange

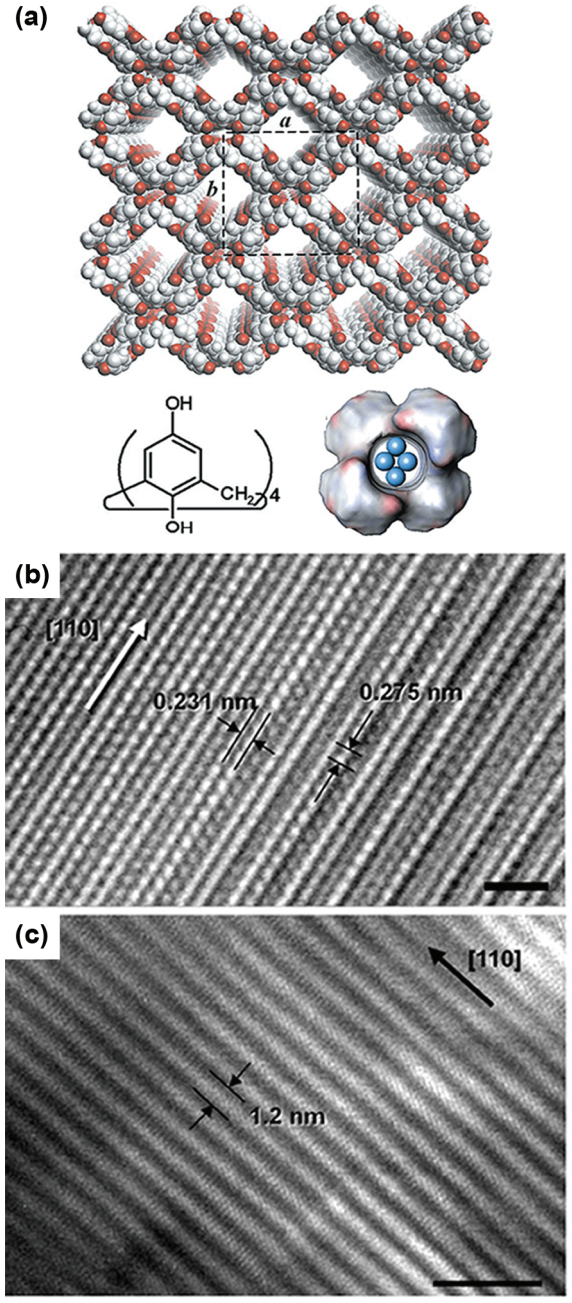

Figure 30. Synthesis of ultrathin Ag nanowires in calix[4]hydroquinone templates: (a) Schematic of calix[4]hydroquinone templates from X-ray data with the molecular structure of the monomer (bottom left) and cross-section of a single-crystalline Ag wire inside the template (bottom right). (b) and (c) depict high-resolution TEM images of aligned Ag nanowires grown in the templates. Scale bars for (b) and (c) are equal to 2 and 5 nm, respectively. Adapted with permission from ref 758. Copyright 2001 American Association for the Advancement of Science.

at elevated temperatures and activated by further heating in O_2. Finally, Pt nanowires were formed in the pores upon the reduction of Pt ions in H_2, highlighting one primary route taken to convert the precursors to metal: chemical reduction.[752] Similarly, it was shown that the reduction of Pt cationic species could be induced by irradiation with light to produce nanowires with diameters of 1.5−2 nm.[743,744] Although this technique has primarily been used for nanoparticle synthesis, there have also been several reports of using high temperatures in various gas environments to thermally precipitate metal from adsorbed precursors.[743,744] While most of the published examples utilized solution-phase infiltration methods to incorporate the metal precursors, there are also cases of vapor-phase techniques.[753]

In 1998, Zhang and co-workers were among the first to study the optical properties of metal nanostructure−mesoporous template hybrid materials with their synthesis of Ag nanostructures in mesoporous silica.[754] After infiltration of the pores of the silica with $AgNO_3$, the membrane was dried and heated to 773 K for 30 min in air, providing enough thermal energy to precipitate Ag metal and form nanoparticles in the template to study the semiconducting optical properties of the hybrid material.[754] In a similar study, Ricolleau and co-workers synthesized Ag nanoparticles on a surface-bound mesoporous silica film and characterized the plasmonic optical properties of the resultant films at different calcination temperatures.[755] Extending this work, Yang and co-workers developed methods for the synthesis of high aspect ratio, 5−6 nm diameter Ag nanowires in SBA-15.[756] Importantly, the researchers determined that the relative water and ethanol concentrations used for the $AgNO_3$ infiltration solution affected the Ag loading in the block copolymer-derived templates and, consequently, whether Ag nanoparticles or nanowires were formed upon thermal decomposition.[756] Also using SBA-15, Stucky and co-workers followed a very similar procedure except with H_2 reduction to form Au, Ag, and Pt nanowires with diameters around 7 nm.[757] Silver nanowires have also been synthesized with mesoporous materials other than silica. Using calix[4]hydroquinone (CHQ) nanotube templates, Kim and co-workers have demonstrated the ability to synthesize 0.4 nm diameter single-crystalline silver nanowires (Figure 30).[758] CHQ nanotubes assemble as ordered mesoporous arrays in aqueous solutions (Figure 30a). Because the inner surfaces of the pores present π faces and OH groups, water and Ag^+ ions are able to infiltrate the pores and be reduced to Ag metal by the hydroquinone groups on the membrane.[758]

4.2.2. Electrochemical and Electroless Deposition of Metal Nanowires. More closely related to the methods used in the synthesis of nanowires with membrane templates, mesoporous materials have also been used to template nanostructure growth via electrochemical and traditional electroless depositions.[759−762] Among the first approaches using electroless plating techniques, Shen and co-workers implanted Pd nanoparticles in the pores of SBA-15 by thermally decomposing $[Pd(NH_3)_4]^{2+}$ ions. The Pd nanoparticles were then used to catalyze the deposition of Cu or Ni from Cu and Ni electroless plating baths. Using a more established approach, other researchers have used silver-catalyzed electroless depositions to form Au nanoparticles in the pores.[760] In this case, Sn^{2+} ions were first bound to the surface of SBA-15, which served as reduction sites for Ag nanoparticles formed from a $AgNO_3$ solution. Finally, a commercially available electroless Au plating solution was used to grow Au nanoparticles from the small Ag nanoparticle seeds.[760] Also previously demonstrated with AAO films, electrodeposition in mesoporous oxide materials was achieved by first contacting the porous template to a conductive film on one or both sides. Using the methods described in section 4.1.2, metal was then electrodeposited to fill the pores from an electrolytic solution of metal ions. In one case, Ag conductive paste was applied to the porous template to serve as the working electrode;[762] in the other, the triblock copolymer-derived

template was spin coated onto conductive glass substrates prior to electrodeposition.[761] While these examples produced structures that were smaller in diameter than those produced by electrodeposition in AAO, the control, monodispersity, and robustness demonstrated using AAO methods have not been shown with mesoporous materials to date.

Using many of the same methods described in this section, there have been several other examples of the synthesis of metal nanoparticles anchored on mesoporous templates.[740,763−774] Because of these likenesses and the lack of demonstrated plasmonic properties that arise from the order of the mesoporous templates these nanoparticles are anchored on, we will not cover these in detail in this review. While the high surface area of these templates combined with the small size of the synthesized nanoparticles could lead to important applications in catalysis and separations, use of mesoporous templates for the synthesis of plasmonic materials has not demonstrated the same level of control or complexity as other methods. Consequently, researchers interested in the fundamental study or application of plasmonic nanostructures have focused on other methods, such as AAO templates or solution-phase methods (see relevant sections in this review).

5. SYNTHESIS WITH SURFACE MASK TEMPLATES

One of the most common ways to produce nanostructured metal surfaces is through use of a surface template. For each of these approaches, the general scheme is the same: a surface is patterned using one of a variety of methods to create a template, physical deposition is then used on and around the patterned structure, and finally, the template may be removed to produce free-standing metal nanoparticles or films. Typically, traditional lithography methods, such as photolithography or electron beam lithography, are used for the patterning and are part of a large body of literature in the fabrication of plasmonic structures for a variety of studies, including those related to plasmonic metamaterials,[775] waveguides,[8,776] and SERS sensors.[777] Because of the expansiveness of these approaches, we will instead focus on several more unconventional, templated methods for producing surface masks, including use of deposited colloidal particles and porous templates as masks for the synthesis of ordered nanostructured films and arrays of discrete nanostructures.

5.1. Colloidal Lithography for Discrete Nanostructure Arrays

Similar to the methods already described for using colloidal particles as templates in solution (see section 3.2), monodisperse samples of size-tailorable nanoparticles have been utilized to create highly controlled plasmonic nanostructures on surfaces. In each of these methods, known collectively as colloidal lithography, a substrate is coated with solution-synthesized nanostructures, which serve as a physical mask for the deposition of a nanostructured metal film using line-of-sight deposition methods (typically thermal or electron beam evaporation) whose geometry derives from the pattern of nanoparticles on the surface. In this case, the particle size, shape, ordering, and angle of deposition can be controlled to create large-area plasmonic films for a variety of applications. Thus far, colloidal SiO_2 and polymer particles have been used most often and can be either selectively removed to produce an inverse metal substrate or retained to produce a conformal film that maintains the form of the nanoparticle array.

5.1.1. Close-Packed Colloid Templates. Developed by Deckman and Dunsmuir in 1982, the first colloidal lithographic

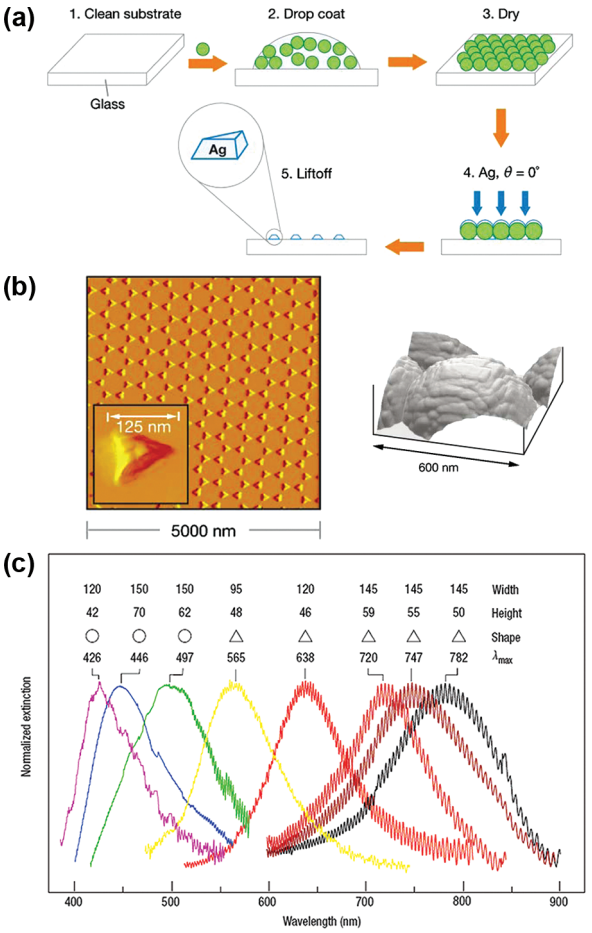

Figure 31. Fabrication of triangular periodic particle arrays using nanosphere lithography: (a) scheme depicting the fabrication steps of drop-coating template particles in a close-packed film and depositing the plasmonic metal (usually Ag or Au) into the interstices to form triangular particles, (b) AFM images of the resulting Ag triangular particles (left) and metal coating on the spheres before removal of the template (right), (c) extinction spectra of various sizes and shapes of Ag particle arrays fabricated by NSL. (a, b) Adapted with permission from ref 72. Copyright 2007 Annual Reviews. (c) Adapted with permission from ref 39. Copyright 2005 Materials Research Society.

method demonstrated that 300−800 nm polystyrene (PS) spherical particles could be assembled into hexagonally close-packed, ordered arrays on surfaces to serve as masks for the deposition of nanostructured Ag films using thermal evaporation.[778] After the spheres were dissolved in CH_2Cl_2, arrays of triangular Ag particles remained from the interstitial regions between PS particles. In 1995, Van Duyne and coworkers demonstrated the controllability of this method, now termed nanosphere lithography (NSL), by creating nanostructure arrays with tailorable size, shape, and composition (Figure 31).[779] In this work, single and double layers of 264 nm diameter PS spheres were spin coated onto a substrate of interest to produce hexagonally close-packed films. Like the work by Deckman et al., metal films of Au, Ag, and Cr were deposited by thermal evaporation to create ordered nanostructure arrays upon dissolution of the polymer spheres. In the case of a single layer of particles, triangular interstices were formed, yielding arrays of triangular prism nanoparticles (Figure 31b). On the other hand, the double-layer film created circular

dx.doi.org/10.1021/cr1004452 |Chem. Rev. 2011, 111, 3736–3827

interstices due to the particle overlap and produced spherical particles on the surface.[779] In subsequent work, the authors studied how the spacing and height of the particles could be controlled by varying the diameter of the PS spheres and thickness of evaporated metal layer, respectively.[780] Importantly, it was also demonstrated that altering the PS particle diameter changed the thickness of the patterned particles, because the volume of the interstitial areas depends on the template particle diameter.

Because of the ability to easily tune these structural parameters by changing the nanosphere size, assembly, and metal coating, NSL has been used to study the optical properties of coupled nanoparticles over large areas for plasmonic particles arrays made up of Ag, Au, Pt, Cu, and Al.[781] For each material, the synthetic differences are minor and only involve changing the source material for the metal deposition step in the thermal or electron beam evaporation. In terms of optical properties, Au,[782] Cu,[783] and Al[784] have been studied in depth to determine the effect of changing the structural parameters (particle spacing, thickness, and height) on the location of the LSPR peaks, but Ag has been most extensively studied due to its superior plasmonic properties across the visible spectrum (Figure 31c).[780,782,785,786] Using these properties, NSL substrates have been harnessed for two important plasmonic sensing technologies: LSPR and SERS. Taking advantage of the sensitive dependence of the LSPR wavelength on the refractive index, NSL-generated substrates have been used to detect biological and chemical analytes down to the ultrasensitive level of monitoring protein conformational changes on the surface of the particles.[73,787−790] Furthermore, since the particles are spaced closely together, large electromagnetic field enhancements have been observed, leading to sensitive SERS substrates.[39,791]

In addition to studies focused on varying the particle spacing and shape by controlling the nanosphere size and assembly, it has also been demonstrated that the angle of incidence for the metal deposition plays an important role in controlling the geometry.[792] Changing the angle of the substrate relative to the metal source alters the size, shape, and spacing of the deposited particles to allow one to further tune the optical properties of the plasmonic substrate. In another example, Van Duyne and co-workers used three successive metal depositions at three different angles to achieve a repeating array of three closely spaced triangular particles with distances controlled by the angle difference between each deposition. This structure led to new angle-dependent dichroic optical properties.[793] Taking this idea further, Giersig and colleagues produced ordered arrays of several complex morphologies by controlling both the angle of incidence and the rotation of the substrate during the deposition.[794,795] The authors used different combinations of angle and rotation during deposition to create Ni cup-like structures, rods, and wires.[794] Like the previous work, they demonstrated how multiple depositions could be used to create patterns of higher complexity and structures comprised of more than one material. Additionally, it was shown how this method could be combined with a microwave-assisted annealing procedure to allow even more complex nanostructure geometries, such as partially opened rings, dots, and rod-like structures made up of Co and Fe.[795] While none of the materials from the last two examples are plasmonic, it is easy to imagine how these methods could be used to produce complex plasmonic materials simply by changing the deposited metal.

5.1.2. Non-Close-Packed Colloid Templates. Using a similar method, several groups have used colloidal particles that are not assembled into ordered close-packed arrays to produce highly controlled and reproducible plasmonic nanoparticle surfaces. The advantage of these methods is that they are not as sensitive to nanosphere mask assembly conditions and can be used more easily to fabricate larger area plasmonic arrays with uniform, albeit less dense, optical features. In this method, the deposition and assembly of PS spheres on a variety of substrates is achieved by controlled electrostatic interactions.[796,797] Using layer-by-layer assembly, the authors first deposited the positively charged polymer poly(diallyldimethylammonium chloride) (PDDA) on the negatively charged substrate. Subsequent layers of negatively charged poly(sodium 4-styrenesulfonate) (PSS) and positively charged aluminum chloride hydroxide create a positively charged surface that is around 1 nm thick.[796] By placing this substrate into a solution of negatively charged PS spheres, electrostatic forces cause the particles to bind, resulting in a nanosphere-covered surface. While this produces a substrate with particles randomly adsorbed on the surface, the authors go on to show that NaCl can be added to the colloid solution to affect the interparticle spacing of the arrangement by screening the repulsive electrostatic interactions between adjacent particles.[796] Following this procedure on a Au substrate, arrays of Au nanodisks with various particle densities were prepared to study the effects of interparticle spacing on the optical properties.[797] In this case, the nanosphere substrates were annealed at 106−120 °C to induce deformation of the particles, resulting in circular interaction areas between the PS and the Au substrate. Ar ion beam etching was then used to etch the uncovered Au regions, and ozone plasma was used to remove the PS spheres, leaving Au nanodisks with diameters equal to the circular interaction areas and heights equal to the thickness of the Au film on the substrate.[797] Interestingly, it has also been shown that plasmonic Au nanorings can be fabricated by following this same procedure without heating the substrate.[798−800] In this case, a secondary deposition of Au occurs along the sides of the spheres during Ar ion beam etching, which is not favorable on the flattened spheres created by heating. These nanoring arrays demonstrate many interesting plasmonic phenomena, including biosensing properties in the near-infrared[799] and dark plasmon modes due to their anisotropy.[801]

Taking advantage of the ability to control the angle of deposition, researchers have also demonstrated the ability to make nanocrescent structures from colloidal masks.[802−804] In the first example, demonstrated by Lee and co-workers, PS spheres were dried on a spin-coated photoresist film.[803] Au was then deposited at controlled angles to coat the spheres on their exposed sides to form a crescent shape around the spheres. A liftoff procedure was then used to dissolve the polymer film and recover the Au-coated spheres. The structures were then centrifuged and resuspended in toluene to remove the PS particle cores, resulting in Au nanocrescent shell particles. The authors then studied the plasmonic field enhancement at the tips of the structures, finding that single nanocrescents could produce SERS enhancements that were larger than 10^{10}.[803] In subsequent work, multilayer nanocrescent structures were prepared by depositing Fe and Ag in addition to Au to produce magnetically addressable SERS structures for biological applications.[805] Using this idea of controlled-angle metal deposition, other researchers have developed a colloidal lithographic method to produce nanocrescent shapes with sharp tips and controllable sizes on surfaces (Figure 32 A−E).[802,804] In this method, PS spheres were dried on a silicon wafer followed by evaporation of Au at an oblique

angle.[802] Finally, the substrate was placed in an Ar ion beam that was perpendicular to the surface, removing any Au that was not masked by the PS particles. Upon removal of the spheres, crescent-shaped Au nanoparticles resulted due to the different angles used between the metal deposition and Ar ion milling steps; metal deposited at the base of the spheres due to the oblique deposition angle was masked by the spheres during the perpendicular Ar ion milling step.[802] The authors prepared nanocrescent substrates of different sizes and shapes by varying the size of the PS spheres and deposition angle, respectively.[802] In addition, the optical properties of these structures were studied as a function of size, shape, and polarization for potential applications in LSPR detection (Figure 32 F,G).[802,804] For 194 nm templated nanocrescents, a detection sensitivity based on the change in plasmon resonance due to the dielectric environment of 480 nm/refractive index unit (RIU) was measured.[804]

5.1.3. Colloid-Derived Polymeric Hole Mask Templates. Similar to NSL, later work extended this method to produce more complex nanostructures by the physical deposition of plasmonic materials onto these colloid-derived templates. In a method termed hole-mask colloidal lithography (HCL), researchers assembled the spheres on a sacrificial, spin-coated polymer film instead of on a Au surface.[806] A mask layer consisting of a material resistant to oxygen plasma etching was then deposited on and around the spheres, and the spheres were subsequently removed using tape, leaving a mask with a pattern inverse to that of the particles. An oxygen plasma etch was then used to transfer the pattern through the underlying polymer film to create the final mask. After deposition of the plasmonic metal of interest on the template using a number of techniques and selectively dissolving the polymer mask, controlled arrays of nanodisks were formed.[806] The authors also showed how making minor changes to this method allows one to produce interesting, more complex structures, such as nanocone arrays, coupled nanodisk pair arrays made up of two different materials, and embedded nanodisk arrays.[806] Like NSL, the materials generality of HCL was harnessed to study the optical properties and interparticle spacing effects of arrays of Al, Pd, Pt, and Au−SiO_2−Au sandwich nanodisks.[807−809]

Using these and similar techniques, several groups have also created unique solution-dispersible structures consisting of asymmetrically metal-coated template colloids or half-shells of metal when these colloids are removed.[810−813] In a particularly interesting example of this, Whitesides, Xia, and co-workers deposited 600 nm silica spheres on a surface and evaporated a 25−40 nm thick Au layer (with a thin Ti/W adhesion layer) on the exposed side of each sphere.[812] These substrates were then annealed at 700 °C for 3 h to cause the Au film to dewet and agglomerate into a particulate structure that was attached to the much larger silica spheres. Sonication was then used to remove the silica spheres and transfer the metal structures into solution and study their morphologies with TEM.

5.2. Colloidal Mask Templates for Nanostructured Films

5.2.1. Nanostructured Metal Films over Close-Packed Colloids. In addition to discrete nanostructure arrays, colloidal lithographic methods have also been used to fabricate large-area films with periodic nanostructured features. While the primary application of discrete nanoparticles is LSPR sensing, nanostructured films have most often been used for SERS and plasmonic crystal materials. One of the most powerful methods of producing these films is NSL, where minor alterations can be made to

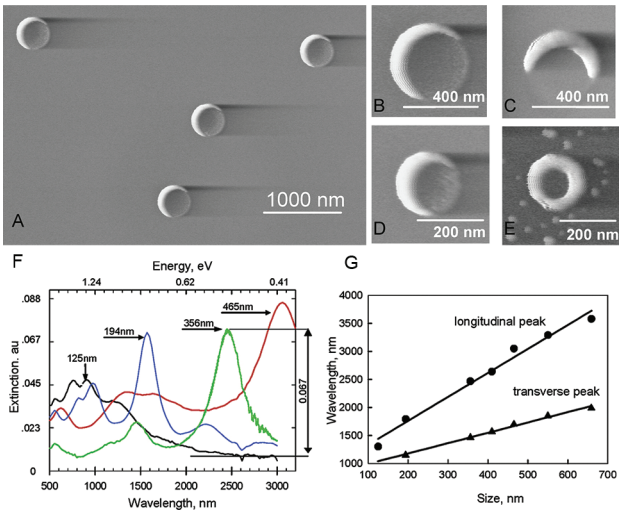

Figure 32. Au nanocrescent particles fabricated by colloidal lithography: (A−E) SEM images of Au nanocrescent structures of various sizes (356, 194, and 125 nm template particles for (A)−(C), (D), and (E), respectively), (F) extinction spectra of 125 nm (black), 194 nm (blue), 356 nm (green), and 465 nm (red) Au nanocrescent structures, (G) longitudinal and transverse plasmon wavelengths as a function of the particle size. Adapted with permission from ref 804. Copyright 2007 American Chemical Society.

the scheme already presented to prepare textured surfaces such as nanowell arrays[814] or conformal films over nanosphere substrates.[815] In the latter, more common method, a thicker (~200 nm instead of ~50 nm) metal film is deposited on the close-packed colloid surface, and unlike the other NSL examples, the colloid template is not removed.[815] Thus, the metal deposits as a conformal coating over the colloid surface, producing a metal film with a repeating, ordered texture known as a film over nanospheres (FON). Most commonly prepared with a Ag coating because of its superior plasmonic properties, these structures were first demonstrated by Van Duyne and co-workers as a capable, large-area substrate for SERS.[816] Indeed, at each point between adjacent spheres, large SERS enhancements are observed, leading to reproducible enhancement factors as large as 10^6.[817] It should be noted that this value is lower than that found with the discrete NSL-generated particles (~10^8), but the overall signal is larger for Ag FONs because of the significantly larger surface area available for chemical functionalization.[817] Harnessing these large enhancements, several important biological and chemical SERS detection assays have been demonstrated on Ag FONs, including in vivo detection of glucose in mice[817] and anthrax detection on ultrastable substrates coated with Al_2O_3 by atomic layer deposition that were sensitive for up to nine months.[34,818] Importantly, Van Duyne and co-workers have also demonstrated that the large-area Ag FON SERS substrates can be used with a hand-held, nonconfocal Raman spectrometer, greatly increasing its utility for point-of-use detection in the field.[818]

5.2.2. Nanohole Arrays. Similarly, sparse colloidal lithographic methods where the particles are not close packed have also led to interesting nanostructured films, particularly nanohole arrays.[59] In this work, PS spheres were assembled on a glass substrate using the electrostatic method described previously, and a thin Au layer was deposited on and around the nanospheres. The sphere masks were subsequently removed from the

dx.doi.org/10.1021/cr1004452 |*Chem. Rev.* 2011, 111, 3736–3827

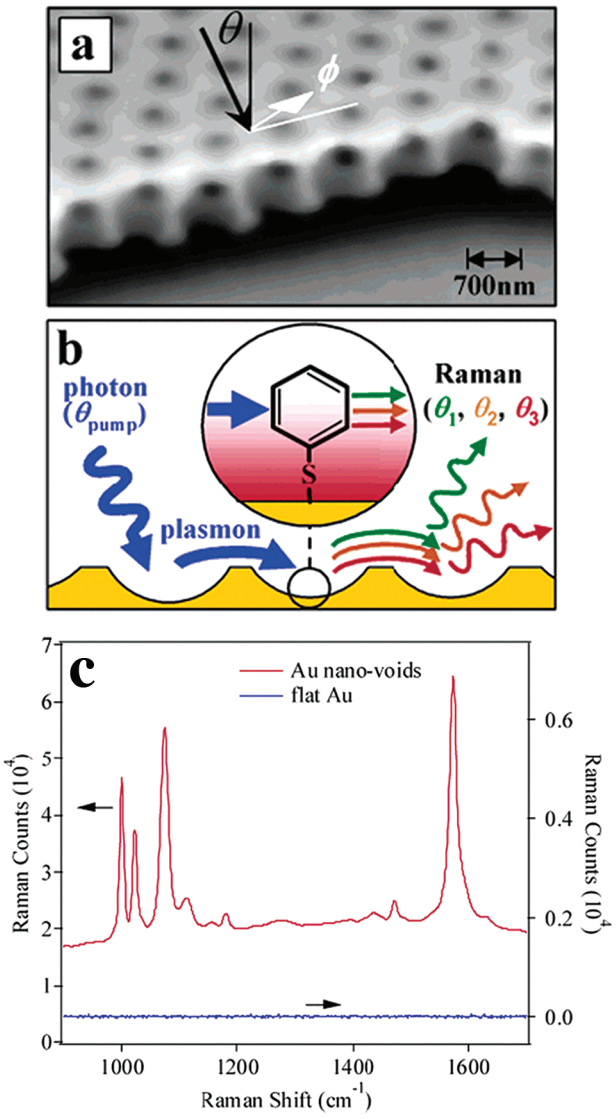

Figure 33. Eletrodeposited Au nanovoid arrays from colloidal templates: (a) SEM image of Au nanovoid arrays used in this study. (b) Scheme depicting the SERS enhancement mechanism in the nanovoid arrays: light is coupled into a plasmon which interacts with the Raman reporter molecule on the surface (benzenethiol) and is scattered back into a photon. (c) Raman signal of benzenethiol on the Au nanovoid arrays (red, left axis) compared to a flat Au film (blue, right axis). Adapted with permission from ref 830. Copyright 2005 American Chemical Society.

surface using tape, much like the previous discrete particle examples.[59] The optical properties of the resulting Au nanohole arrays were then studied as a function of geometry, and it was determined that the scattering from the holes is about 5 times higher than that of comparable nanodisk arrays. Not surprisingly, it was also found that the plasmon resonance red-shifted with increasing hole size and increasing refractive index of the medium. The authors also observed a pronounced blue-shift in the resonance for decreasing particle spacings, suggesting that there was enhanced coupling between neighboring holes as a result of propagating surface plasmon polaritons.[59] Subsequent work has focused on how these surfaces could be used for LSPR sensing and modeling of the plasmon physics around each hole.[819,820] Recently, a method has been developed for the fabrication of plasmonic, ordered hole arrays of controlled shape based on the slow O_2 etching of close-packed PS spheres.[821] By etching the spheres to make them smaller, the necessary separation between the spheres is obtained to create ordered nanohole arrays upon evaporation of a Ag film and subsequent removal of the spheres.

5.2.3. Nanovoid Arrays from Electrodeposition. Another powerful technique for producing nanostructured films from colloidal particle templates that has not yet been discussed involves electrodepositing metal around particles in a method similar to that used to synthesize nanowires in porous templates.[822−826] Developed by Bartlett and co-workers, colloidal particles were first assembled in a close-packed array on a gold electrode by allowing the spheres to order and dry over a period of 5−7 days.[823] This gold electrode was then used as the working electrode to electrodeposit metal (originally Co, Pt, and Pd) around the assembled colloidal particles, where the thickness of the film could be controlled by monitoring the amount of charge passed during deposition. After removal of the PS particles in toluene, the resulting nanostructured film consisted of ordered nanoscale voids that followed the size, shape, and contours of the assembled colloid template (Figure 33a).[823] In an effort to study the optical properties of these films, the authors fabricated Au and Pt nanovoid arrays with different geometries with varying thicknesses and diameters (dictated by the nanospheres used for the template) and studied how the SPR was affected by the azimuthal angle and light polarization by measuring reflectance spectra.[57,827,828] By altering these parameters, it was determined that the SPR of these unique films could be varied across the visible from the UV to the near-infrared. Importantly, the plasmonic properties of these structures were studied both experimentally and theoretically, and it was determined that the strong plasmon fields generated around the voids in the metal films were a result of the interaction between localized surface plasmons and surface plasmon polaritons (Figure 33 b,c).[829,830] These strong fields have been used for several SERS applications, including studying the importance of resonance conditions on SERS,[830] demonstrating one of the first reproducible, tailorable SERS substrates based on Pt or Pd,[831] and measuring single-base mismatches in DNA sequences using controlled duplex melting from a nanovoid array.[832] Further, it has been shown how the strong fields and long-range ordering available with this method can be harnessed to develop new plasmonic band gap materials.[833]

5.2.4. Nanoporous Materials from Chemical Reduction. Utilizing a similar method to deposit material into the interstices of colloidal particle assemblies, several groups have also chemically reduced metal ions to produce porous plasmonic structures. In this case, metal salts or oxides are impregnated into the interstitial regions of the colloidal templates and thermally or chemically reduced to produce nanoporous metal materials when the templating colloids are removed.[826] Among the first examples, nanoporous Ni films were formed from the thermal treatment of Ni^{2+}-impregnated close-packed 660 nm PS spheres in nitrogen.[834] Extending this concept to plasmonic materials, Mallouk and co-workers used a similar method to create nanoporous Au and Pt structures.[835] Using 30−75 nm silica spheres that were pelletized at high pressure and temperature as a template, a solution of $H_2PtCl_6 \cdot H_2O$ or $AuCl_3$ was added to impregnate metal ions in the interstitial regions of the assembly. The template was then heated to 150 °C to reduce these ions and placed in HF to remove the silica spheres to produce nanoporous Pt and Au materials with pore sizes resembling those of the

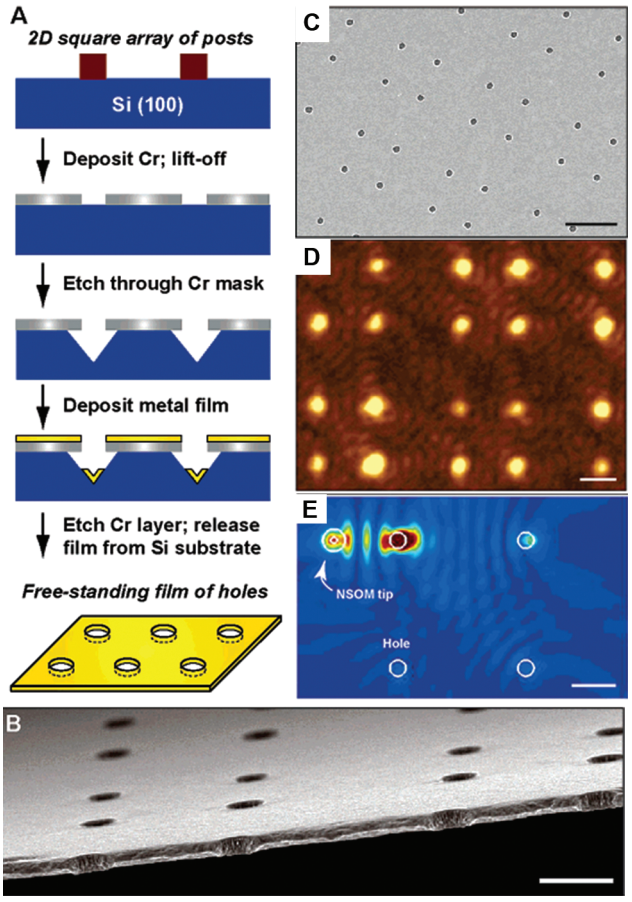

Figure 34. Fabrication and characterization of Au nanohole arrays: (A) schematic depiction of fabrication of Au nanohole arrays, (B) SEM image of the resulting, free-standing Au nanohole array film (100 nm thick with 250 nm diameter holes, scale bar 500 nm), (C) SEM image of the Au nanohole array, showing uniformity and yield (scale bar 2 μm), (D) NSOM optical image of the 100 nm thick Au nanohole array film on a glass substrate, showing enhancement at the holes and propagating plasmon patterns in the Au (scale bar 1 μm), (E) calculated near-field SPP standing wave pattern for a given NSOM tip position (scale bar 500 nm). Adapted with permission from ref 841. Copyright 2005 American Chemical Society.

original template spheres.[835] Colvin and co-workers also used this method of metal salt impregnation and thermal reduction to produce metal structures from colloid-derived polymer templates.[836] In an alternative method, Zhou and co-workers assembled a close-packed film of polyelectrolyte-coated PS spheres and subsequently removed the PS core with toluene.[409] The polyelectrolyte shell was then impregnated with $AgNO_3$, where the Ag^+ ions bound to the anionic polyelectrolyte and the Ag ions were chemically reduced to Ag metal through use of Tollen's reagent.[409] Differing from previous examples, material was not deposited in the interstitial regions of the template and was instead incorporated throughout the ordered, porous polyelectrolyte film. Recently, another important example of this concept was developed by Kuroda and co-workers for the creation of 2- and 3-D porous Au materials.[837,838] In this case, a vapor-phase reduction of $HAuCl_4$ with dimethylamine−borane was used to control the morphology of the resulting Au structures formed in 3-D 40 nm silica nanosphere assemblies.

5.3. Patterned Surface Mask Templates

In addition to colloidal particles, many surface structures have been used as masks for the fabrication of plasmonic nanostructures. Traditional lithographic methods (e.g., photolithography, electron beam lithography, and focused ion beam lithography) are particularly prevalent examples, but only unique variations that have led to novel plasmonic structures will be covered here. Also like colloidal lithography, many of these methods are particularly interesting because of the ability to create large-area, ordered surfaces that can more easily be used for many important applications such as band gap materials and large-area sensors.

5.3.1. Nanohole Arrays Using Soft-Lithography-Fabricated Masks. Of the many structures made by these methods, nanohole arrays have particularly interesting optical properties and have been synthesized using several different techniques. Among the first to fabricate and study the properties of metal nanohole arrays, Ebbesen and co-workers used focused ion beam lithography to create plasmonic films in 1998.[77,839] Surprisingly, the authors found enhanced transmission and band gap behavior in these films,[839] leading to a flurry of new studies and synthetic methods to create these materials. One example that has already been discussed is collodial lithography, which is summarized in section 5.2. In recent years, two soft lithography methods have also been developed and have led to easier and higher throughput syntheses of plasmonic nanohole arrays. Developed by Whitesides and co-workers, soft lithography utilizes an elastomeric stamp to pattern materials over large areas.[19,840] Molded from a lithographically generated master, poly(dimethylsiloxane) (PDMS) is the most commonly used elastomer for the stamp and can be used to make micro- and nanoscale features.[840]

Among the first to utilize soft lithography to fabricate nanostructured ordered plasmonic films, Odom and co-workers demonstrated the ability to prepare large-area, free-standing Au nanohole arrays in 2005 (Figure 34).[841] In this method, the authors first used phase-shift photolithography with high-resolution PDMS stamps as the masks to fabricate 2-D arrays of ~250 nm photoresist posts on Si substrates. Cr was then deposited by electron beam evaporation, and the photoresist was subsequently removed, producing a thin Cr nanohole array film (Figure 34A). A KOH/isopropyl alcohol (IPA) mixture was then used to anisotropically etch the Si holes into pyramidal pits. Au films were subsequently deposited on top of these holes, and a liftoff process was used to remove the Cr and release free-standing Au nanohole arrays (Figure 34B). The authors fabricated Au and Au−Ni multicomponent nanohole arrays and studied the surface plasmon propagation with near-field scanning optical microscopy (NSOM; Figure 34 C−E).[841,842] In each case, enhanced transmission was observed at the nanoholes, which was attributed to localized surface plasmons coupling resonantly with the excitation light (Figure 34D). Furthermore, fringe patterns on the metal films were also observed, which were attributed to standing waves from propagating surface plasmon polaritons. As was expected, these fringes were only observed in the Au−Ni nanohole arrays when Au was facing the excitation source. In subsequent work, Odom and co-workers focused on studying the effects of the thickness of the Au film on plasmon propagation and were able to very clearly observe the wavelength of propagation with NSOM.[843]

Adding complexity to this method, it was also demonstrated that these nanohole arrays could be patterned into micrometer patches of holes that were ordered with respect to each other.[844]

dx.doi.org/10.1021/cr1004452 |*Chem. Rev.* 2011, 111, 3736–3827

In this case, a second exposure through a Cr mask (in addition to the initial exposure through the PDMS) is used to limit the photoresist posts to the areas covered by the Cr on the mask. Compared to the "inifinite" nanohole array, these micropatterned nanohole arrays have strikingly different optical properties. Importantly, these differences can be harnessed to improve the refractive index sensing of these materials (313 nm/RIU instead of 286 nm/RIU). Furthermore, the authors demonstrated the ability to use these nanohole arrays as masks to create nanopost arrays on a different substrate.[844] As a proof-of-concept, the optical properties of Au, Cu, Ag, and Si nanopost arrays were studied with dark-field scattering.

It has also been demonstrated that this method can be used to change the geometry of the individual holes in the array.[845−847] One important example of this was demonstrated in 2007 with the fabrication of Au nanohole arrays comprised of elliptical and slit-like holes.[845] To fabricate these structures, a small change is made to the phase-shift photolithography step through the PDMS masks. Instead of doing the second deposition with the line mask rotated by 90° as is typically done, the line mask is rotated by 15° and 45° for slit-like and elliptical holes, respectively. In a subsequent study, Odom and co-workers found that 1-D arrays of these slit-like nanoholes have interesting optical properties characterized by 1-D surface plasmon polariton Bloch wave modes. Studying their refractive index sensitivity, the authors found a linear shift of 560 nm/RIU for small refractive index changes, which is on the same order as 2-D nanohole arrays.[846] Also affecting the shape of the holes, 3-D protruding nanohole arrays have been recently prepared by taking advantage of the indented nature of the pyramidal pits serving as the holes in the mask.[847] Similar to the use of a nanohole array as a mask to deposit nanoposts, these materials have also been transferred to PDMS masks and used as nanostencil masks for the fabrication of plasmonic structures on other substrates.[848]

In another soft lithographic route to produce plasmonic nanohole arrays, Rogers and co-workers used a PDMS stamp to pattern holes into a polyurethane film and then cured it by exposure to 350−380 nm UV light.[849] Au is then deposited by thermal evaporation on top of a Ti adhesion layer. In this work, a nanohole array consisting of holes with diameters and depths of 545 and 300 nm, respectively, and with a periodicity of 700 nm were prepared and studied as plasmonic crystals with optical band gaps.[849] Subsequent experiments used these nanohole arrays as plasmonic crystal sensors for the detection of biochemical binding events, such as fibrinogen.[850] Taking this a step further, Rogers and co-workers created multispectral biosensors of these materials based on the interaction of the nanoholes with the Au nanodisks formed at the base of every hole.[5,399,850] These materials display many unique spectral features that are all highly sensitive to changes in the local environment. In this case, the authors monitored the transmission at several resonance wavelengths as a function of the poly(ethylene glycol) concentration and observed very high sensitivity, even at low concentrations. Furthermore, they went on to study a biotin−avidin system with a microfluidic device to pattern and detect nonspecific fibrinogen binding.[399]

5.3.2. Discrete Nanoparticle Arrays Using Soft-Lithography-Fabricated Masks. In addition to nanoholes, both of these soft lithography methods have also been used to pattern positive plasmonic features on surfaces.[842,851] For the method developed by Odom and co-workers, use of their nanohole arrays as a secondary mask or template for the patterning of positive plasmonic features has already been described.[844,848,852] However, there is also a unique class of nanoparticles that are synthesized directly on a patterned Si surface in a slightly altered procedure than the one used to fabricate the nanohole arrays. In this case, the anisotropy of the pits formed from the KOH/IPA etch in the Si is utilized to fabricate plasmonic pyramidal nanoparticles.[852−856] After the previously described process for producing nanohole arrays (including lift-off to recover the nanohole array film) is followed, the only remaining structures on the Si substrate are pyramidal-shaped particles formed in the pits during metal deposition. By placing the substrate in a secondary solution of KOH/IPA to etch the Si support layer, these can be recovered into solution as interesting pyramidal nanoparticles with sharp tips. Initially, this was demonstrated for the synthesis of Au, Ni, and Au−Ni multicomponent nanopyramids with tips having a radius of curvature down to below 2 nm, providing a material with both interesting optical properties and unique multicomponent functionality.[853] Subsequent work focused on the optical properties of Au pyramidal nanoshells by fabricating arrays of these materials and encapsulating them in PDMS.[854] As was expected, the authors found that immobilized arrays of these anisotropic structures produced orientation-dependent optical properties. Taking advantage of the ability to create multicomponent structures, Odom and co-workers have also studied the optical properties of Au−Ni nanopyramids.[855] In this case, the authors demonstrated the ability to selectively functionalize the Au portion of the structures in different geometries and study the effect of coupling between nanopyramids in assembled linear chains due to the magnetic Ni components. Importantly, the Odom group has also used these pyramidal features formed from anisotropic Si etching to create plasmonic pyramidal gratings (Au, Ag, and Pd) to study angle-dependent optical properties of different materials in the context of refractive index sensing and measured dispersion diagrams.[857,858]

5.3.3. Block Copolymer-Derived Mask Templates. While many of these methods have produced highly ordered arrays of nanostructures, synthesis of structures smaller than 50 nm (in terms of both size and spacing) has proven to be difficult. One method that has been used to get around the limitations of using surface masks has taken advantage of the small features available with block copolymer films.[859,860] Among the first to show evaporation of material through a mask derived from a block copolymer film, Adamson and co-workers demonstrated the ability to use polystyrene-*b*-polyisoprene (PS-*b*-PI) block copolymer films as templates for the deposition of gold nanodot arrays.[859] By synthesizing the PS-*b*-PI copolymer by sequential high-vacuum anionic polymerization, it adopts a microstructure consisting of spherical PI domains in a body-centered-cubic lattice within a PS matrix. The size and periodicity of these domains are on the order of 10 nm and provide a geometry conducive to generating smaller nanodot patterns. The authors fabricate these patterns by first creating a multilayer film consisting of subsequently deposited 52 nm polyimide, 23 nm silicon nitride, and 65 nm PS-*b*-PI.[859] Spin coating from a 2% solution in toluene and annealing at 175 °C for 24 h produced hexagonally ordered spherical PI domains in the PS film (20 nm spherical regions with a periodicity of 40 nm). Taking advantage of the relative reactivities of PS and PI segments, ozonation was used to selectively remove the PI regions by predominantly reacting with the carbon−carbon double bonds along the PI backbone, creating ordered voids in the polymer film. A series of dry etching

processes in O_2 and CF_4 were then used to transfer this pattern of holes to the silicon nitride and polyimide film all the way down to the underlying Si substrate. Thermal evaporation was subsequently used to deposit Au in these holes, resulting in Au nanodots with their size and ordering dictated by the original PI spherical regions.[859] Extending this work, Russell and co-workers used poly(styrene-*b*-methyl methacrylate) (PS-*b*-PMMA) in a similar method where ordered cylindrical PMMA regions formed in the PS matrix.[860] After irradiation with UV light and washing with acetic acid and water, an array of 16 nm holes was formed in the PS film (Figure 35a). Similar to the previous method, this was used to create 16 nm Au nanodot arrays (Figure 35 b,c). By changing the relative volume ratios of PS and PMMA, PS cylindrical regions could be formed in PMMA matrixes to produce cylindrical nanoposts of PS instead of the nanohole arrays produced previously. In this case, Au nanohole arrays could be created with 21 nm holes and center-to-center spacings of 42 nm (Figure 35d).[860]

A related deposition strategy was reported by Ansari and Hamley in which osmium tetroxide was used to selectively stain isoprene segments in a poly(styrene-*b*-isoprene-*b*-styrene) copolymer, followed by sputtering of Au.[861] In this method, Au atoms migrated selectively to these stained segments and formed a nonuniform film of nanoparticles. Russell and co-workers have used a similar approach, utilizing either a poly(styrene-*b*-ferrocenylsilane) diblock copolymer or a PS-*b*-P4VP polymer.[862] The first (iron-containing) block copolymer phase separated in a manner similar to that of PS-*b*-PMMA copolymers and, upon reactive ion etching, was converted into an inorganic nanostructure. Sputter coating of Ag on top of this surface generated SERS-active substrates. When using PS-*b*-P4VP, the authors reported the generation of nanodot, nanohole, and nanoring-like arrays.[863] Further work by Zschech et al. reported the patterning of both a plasmonic material (Au) and the underlying semiconductor (Si_3N_4) substrate using a PS-*b*-PMMA block copolymer system.[864] After solvent annealing and PS-*b*-PMMA film formation on the Si_3N_4 substrate, the PMMA domains were removed with UV curing and an acetic acid wash. The remaining PS segments were stained with RuO_4 (to slow degradation in the subsequent step), and the entire substrate underwent reactive ion etching (CHF_3/Ar). This etching effectively transferred the block copolymer cylindrical morphology to the Si_3N_4 surface, which was then further patterned through Au evaporation, resulting in a Au nanodot array.

5.4. Porous Surface Mask Templates

Another material that is ideally suited for the fabrication of ordered, plasmonic films is AAO.[865−868] One early example of using AAO membranes as a mask for the deposition of ordered arrays of 40 nm Au nanoparticles was demonstrated by Masuda and co-workers.[865] Instead of the thicker AAO membranes used for nanowire and nanotube growth described in section 4.1, these templates were only a few hundred nanometers thick and were used as masks for evaporation or sputtering of nanoparticles. More recently, this has been extended to the ability to create complex coupled nanoparticle surfaces by two sequential depositions of the metal(s) into each pore.[866] In this work, the authors used membranes with pore diameters and depths of 60 and 300 nm, respectively. Instead of depositing exactly perpendicular to the surface, Au was deposited at an angle that resulted in coating of the substrate only near the wall of the AAO. For the second deposition, this angle was changed to deposit only on the other side of the pore wall to produce two discrete nanoparticles in each pore. This was demonstrated for Au nanoparticles with different geometries and for the fabrication of closely spaced Au and Ag particles where different metal sources were used for the metal depositions.[866] Importantly, this concept was applied by Atwater and co-workers in 2008 for the fabrication of plasmon-enhanced solar cells.[867] In this case, AAO templates were used as masks for the deposition of 110 nm diameter Ag nanoparticles onto the window layer of GaAs solar cells to produce ordered arrays of nanoparticles. The heights of these particles were easily controlled by changing the thickness of the Ag deposited through the AAO, leading to anisotropic particles on the surface. The authors studied the effects of annealing, thickness, and shape on the optical properties and absorption of these films and determined that the Ag particles increase the optical path of the incident light in the absorbing layer, increasing the short circuit current density by up to 8%.[867] In a slightly different method, Whitesides and co-workers have also taken advantage of shadow evaporation through AAO membranes to prepare Au nanotubes by evaporating at an angle while rotating the substrate to ensure even deposition.[869] Arrays of Au nanotubes with diameters between 20 and 200 nm and lengths up to 1.5 μm were prepared and used in proof-of-concept experiments as SERS substrates with enhancement factors up to 5×10^5. In a similar manner, mesoporous thin-films have also been used as masks to create porous plasmonic arrays by coating the top surface of the template, which has also been particularly interesting for SERS applications.[870−873]

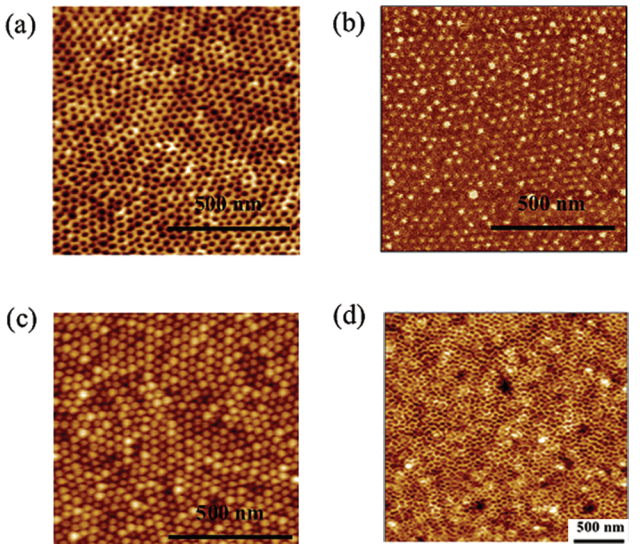

Figure 35. Tapping mode AFM images of the use of block copolymer-derived masks for fabrication of metal nanohole and nanodot arrays: (a) porous PS film after etching of the PMMA regions of a block with UV exposure, (b) phase image of the Au/Cr film evaporated into the pores of the PS template in (a), (c) resulting Au nanodot array after removal of the PS template, (d) porous Cr nanohole array made using a similar method but with a larger percentage of PMMA in the block copolymer film. Adapted from ref 860. Copyright 2002 American Chemical Society.

5.5. Vertically Aligned Nanowire Templates

Contrasting with AAO pores used as hole masks, vertically aligned nanowire and nanorod arrays have been used to template the deposition of high aspect ratio, anisotropic metal nanostructure arrays. Because they are not plasmonic themselves but have

dx.doi.org/10.1021/cr1004452 |*Chem. Rev.* 2011, 111, 3736–3827

highly controllable geometric properties, vapor−liquid−solid (VLS) grown semiconductor nanowire arrays are most commonly used for this purpose. While there has been some work with using the metal catalyst particles atop the nanowires for SERS applications,[874,875] most of the plasmonic studies have involved using the arrays of nanowires as templates to deposit high aspect ratio metal structures.[876−881] In these cases, metal ions are chemically reduced or metal nanoparticles are deposited around the semiconductor material to produce roughened metal shells around the nanowires. While most of the examples involve Si nanowire arrays, ZnO nanowires have also been used.[876,881] Ag and Au structures have been generated from coating processes based on galvanic replacement,[877] electroless deposition,[879] and hydrothermal reduction.[881] Because of the morphology of the arrays (closely spaced metal surfaces on adjacent nanowires) and the roughness of the deposited metal films on top of the nanowires, these materials have been considered primarily as SERS substrates.

5.6. Biological Surface Mask Templates

In addition to many of these patterned and inorganic materials, biological materials have also been used to mask the fabrication of metal structures and films with nanoscale features.[476] Because of the small sizes of these materials, these methods have led to metal feature sizes and densities that are difficult to achieve with other masking methods. Among the first examples of creating nanoscale plasmonic structures on surfaces with biological masks, Kohler and co-workers utilized microtubules adsorbed onto 30 nm Au films.[882] Dry etching was then used to remove the Au film except for where the microtubules masked the surface, producing Au nanowires on the surface with the same dimensions as the microtubules. In a similar method, Douglas and co-workers used proteins to mask the deposition of Au onto a substrate.[883] In this case, a thin film of Au was deposited onto a protein-adsorbed surface, wherein the surface adjacent to the proteins was masked and not coated with Au. Dry etching was then used to transfer this pattern to the substrate, allowing them to create small Au nanostructures in these voids by depositing another layer of metal. More recently, using very similar methods, DNA[884,885] and diatoms[886] have also been used as masks for the fabrication of Au nanostructures on surfaces.

6. ASSEMBLY WITH BIOLOGICAL TEMPLATES

The large number of biomolecular structures available via both chemical synthesis and in vivo synthetic methods present a wide array of templates for plasmonic nanostructures.[75,464−468,471,476,887−891] Different chemical groups that occur in natural biological molecules can be used to bind or synthesize nanoparticles (the latter has been discussed in section 3.5), and synthetic modification strategies can be used to add functional moieties to these structures. Furthermore, many different 1-, 2-, and 3-D structures can be created from different biomolecule building blocks. This structural diversity and synthetic programmability provide an obvious means for creating templates; in this section, we specifically focus on biomolecules and biological objects used to direct the assembly of preformed nanoparticles.

6.1. DNA or Oligonucleotides

DNA strands provide a natural option for templating the assembly of nanostructures, as oligonucelotides can be readily synthesized via automated procedures, the base-pairing

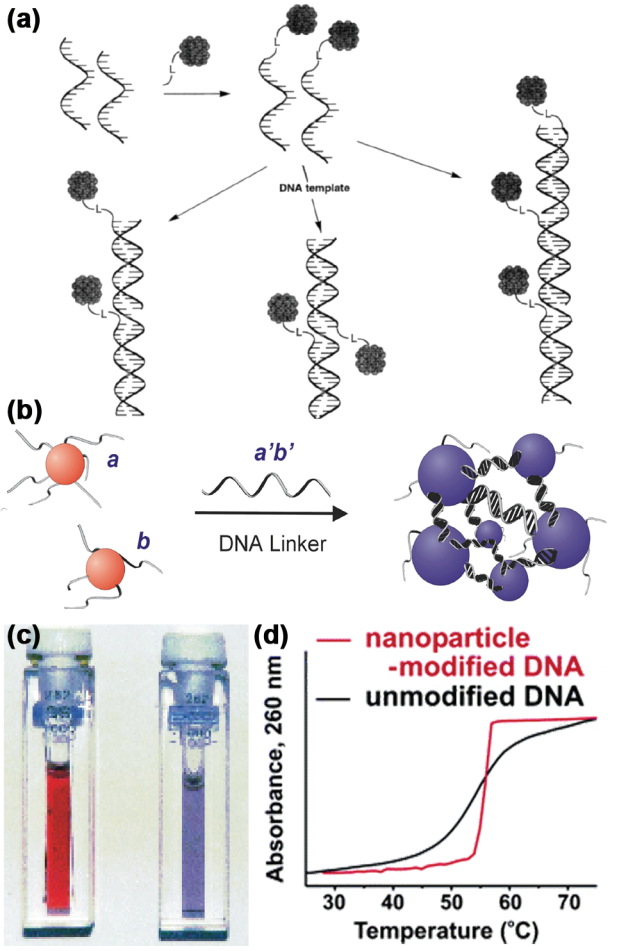

Figure 36. Nanostructure assembly induced by sequence-specific DNA binding events: (a) discrete clusters of AuNPs synthesized using a single DNA strand as a template, (b) polyvalent DNA−AuNP conjugates organized into extended aggregates via the addition of multiple DNA linking strands, (c) solution color change from red to purple due to plasmon coupling upon DNA-templated assembly of AuNPs, (d) the change in absorbance of DNA duplexes upon thermal dissociation shows a sharp melting transition for assembled DNA−AuNP conjugates and can be used to distinguish single-base mismatches with high fidelity. (a) Adapted with permission from ref 892. Copyright 1996 Nature Publishing Group. (b) Adapted with permission from ref 910. Copyright 2000 American Chemical Society. (c) Adapted with permission from ref 911. Copyright 2003 American Chemical Society. (d) Adapted with permission from ref 912. Copyright 1997 American Association for the Advancement of Science.

interactions provide a means of simple programming of interactions, and different chemical functionalities can be easily added to the oligonucleotides to allow for interactions with a variety of different materials. Two of the first examples of using DNA to template the formation of discrete nanoparticle structures were demonstrated by Mirkin and Alivisatos in 1996 (Figure 36).[62,892] Although these two groups presented similar ideas for conjugating DNA strands to the surfaces of nanoparticles to generate nanoparticle assemblies, they adopted two very different strategies for using DNA as the templating agent. As a result, the types of materials one can realize with each of these strageties are radically different. Alivisatos and co-workers conjugated a single DNA strand to the surface of the nanoparticles, providing the

capability of creating discrete nanoparticle clusters. Conversely, Mirkin and co-workers attached many DNA strands to the nanoparticle surface, creating a polyvalent DNA−AuNP conjugate that can be used to form macroscopic colloidal crystal lattices and other structures which have a wide variety of uses. While both of these examples are comprised of the same basic components and have led to important templating strategies, the fundamental properties of these two materials are notably different. In this section, we will first focus on discrete plasmonic clusters of nanoparticles and then discuss methods for creating extended nanoparticle arrays. We will also address the use of non-base-pair interactions (such as electrostatic attraction) to mediate nanoparticle assembly and the synthesis of complex, large-scale DNA-based scaffolds as templates; many of these examples also utilize the DNA−AuNP conjugates developed by Alivisatos and Mirkin as building blocks.

6.1.1. Discrete DNA−Nanoparticle Clusters. In the initial work by Alivisatos and co-workers, small clusters of gold nanocrystal "molecules" were synthesized by programmed DNA-recognition interactions using a single DNA strand as a template (Figure 36a).[892] Here, 1.4 nm gold particles, functionalized with a single *N*-propylmaleimide molecule, were reacted with short synthetic oligonucleotides that contained a thiol group at either the 3′ or 5′ terminus. It is worth noting that this maleimide conjugation strategy has been employed in many of the examples covered in this section to generate AuNP−oligonucleotide conjugates and thus will be referred to often. These bionanoparticle conjugate structures were then assembled onto single-stranded DNA templates via complementary base-pair interactions. Gel electrophoresis and TEM were used to confirm the presence of DNA−AuNP conjugates bound to the template strand, and electron microscopy showed that dimers were only synthesized in the presence of the DNA template.

This work was expanded upon in 1999, where more sophisticated DNA-programmed interactions were used to create a larger variety of structures.[893] The generalizability and programmability of DNA sequences are fully evident in this work, as the nanoparticles were assembled in a large number of arrangements with a high degree of precision. Both 5 and 10 nm AuNPs were functionalized with single oligonucleotides by the addition of DNA strands in submolar quantities; each DNA strand contained a single thiol group, at either the 3′ or 5′ terminus or on the C5 position of a 2′-deoxyuridine nucleotide. Unlike the previous strategy which employed a chemical reaction between thiol and maleimide groups, the thiols on these DNA strands were found to directly adsorb onto the particle surface via covalent gold−sulfur bonds. The DNA−NPs were then assembled into homodimeric, heterodimeric, homotrimeric, and heterotrimeric species, where the positions of the NPs relative to one another were determined by the DNA sequences utilized to template the cluster formation. Interestingly, while the relative positions of nanoparticles were always conserved, the assemblies were found to be flexible, with the resulting clusters often adopting bent geometries instead of straight chains assembled along a linear DNA helix.

A similar strategy has been employed by both the Alivisatos group and others in subsequent studies, creating a diverse array of 1- and 2-D structures. Different cluster structures have been synthesized both by incorporating branched DNA structures as templates[894] and by arranging different numbers of AuNPs around a central DNA-functionalized quantum dot.[895] Methods also have been developed to control the number of DNA strands bound to the nanoparticles,[896] purify DNA-templated clusters via gel electrophoresis,[897] and chemically ligate the DNA strand templates so that a single oligonucleotide serves to bind two nanoparticles together.[898] Nanoparticle−streptavidin−biotin constructs have also been created that utilize single-stranded DNA as a template.[899] Rolling chain polymerization, a biomolecule synthesis technique that creates very long strands of DNA, has likewise been used to create long, linear templates that bind many DNA−AuNPs;[900] telomeric DNA has also been used to create 1-D arrangements of particles.[901] This DNA-templating strategy also can be used to create small clusters of nanoparticles with very short (∼1 nm) interparticle distances, which exhibit interesting plasmonic effects.[902,903] Interestingly, Polman and co-workers demonstrated that these assembled clusters could be used to construct plasmonic nanolenses that were theoretically shown to enhance the local electromagnetic field by up to 4 orders of magnitude.[902]

More complex NP assemblies were created by the Alivisatos group in 2009, where the same basic concept was applied to the synthesis of a 3-D structure.[904] Here, 5 nm gold nanoparticles were functionalized with a single strand of DNA and subsequently purified using gel electrophoresis to separate and obtain DNA−AuNPs monofunctionalized with very long (∼90 base) DNA strands. Four sets of DNA−NP conjugates were made, each containing a unique DNA sequence that programmed specific binding interactions to the other three particle conjugates. When combined, the DNA sequences on the four different AuNPs hybridized to each other and formed a tetrahedron with each nanoparticle positioned at a corner and each DNA strand tracing the outline of one of the tetrahedron's triangular faces. These 3-D structures were obtained both in a stepwise growth method where individual nanoparticle types were added sequentially and in a one-pot reaction where all the nanoparticles were combined simultaneously. No difference in yield or number of off-target products was noticed in either process, highlighting the robust, selectively programmable nature of DNA as a templating agent. Further sophistication was introduced to the system by making chiral tetrahedra that incorporated 5, 10, 15, and 20 nm nanoparticles in either *R* or *S* enantiomers. In this case, switching the position of the 5 and 10 nm particles by conjugating them with opposite strands controlled the chirality of the pyramids. It is projected that such structures could prove useful as 3-D plasmonic rulers, where the plasmonic coupling between nanoparticles can be altered upon the addition of an input signal. The use of chiral assemblies of nanoparticles increases the capability of the system compared with previous plasmon-based rulers,[905] as changes in the DNA−NP position due to some input signal would break the symmetry of the system and change plasmonic coupling in a manner that is specific to the 3-D structure of the NP cluster.

While DNA binding interactions can be tailored via Watson−Crick or non-Watson−Crick base-pairing interactions, the ability to chemically functionalize DNA with non-natural groups provides another means to increase the diversity of DNA templates. In 2006, Sleiman and co-workers covalently attached organic linker molecules to synthesized DNA strands.[906] In this work, they utilized chemical reactions that have been well established for the automated synthesis of synthetic oligonucleotides to insert a bisterphenyl moiety in the center of a growing DNA strand in place of a standard nucleobase. The bisterphenyl moiety forms a rigid, 120° angle, which allowed it to be used as a molecular "corner". Because double-stranded (ds) DNA naturally forms a linear chain, this allowed for bends in a dsDNA

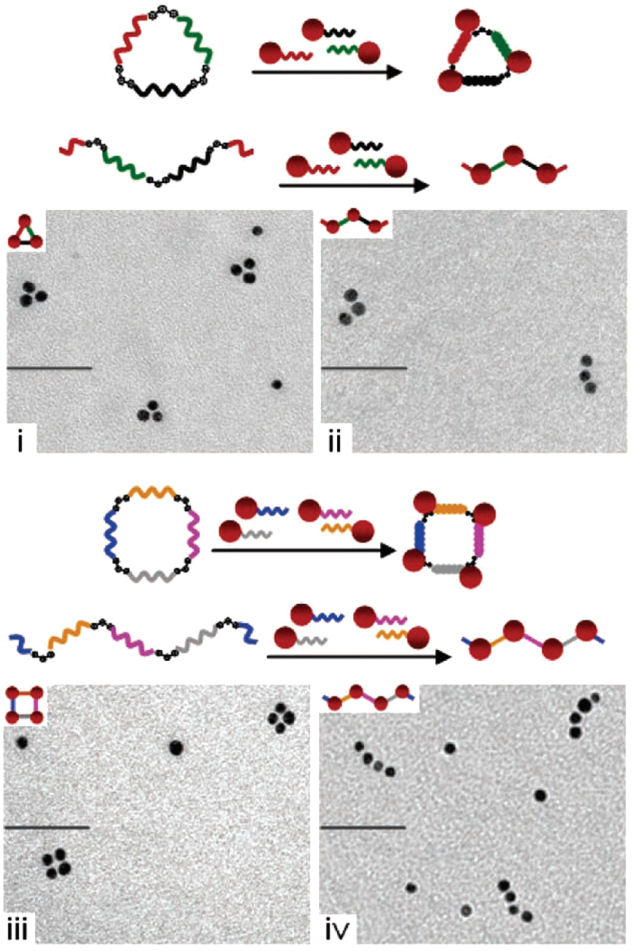

Figure 37. Bisterphenyl moieties, inserted in the middle of a DNA strand during synthesis, are used to create "molecular corners" in oligonucleotides. The addition of nanoparticles functionalized with appropriate DNA strands results in linear, triangular, square, or other types of 2-D geometries. Scale bars are 50 nm. Adapted with permission from ref 907. Copyright 2007 American Chemical Society.

structure to be programmably inserted into a DNA sequence. Sleiman and co-workers synthesized six different oligonucleotides containing these organic corners, and when the DNA strands on either end of the organic corner hybridized to other strands, the end result was a rigid hexagonal structure. They confirmed the presence of discrete hexagons through both gel electrophoresis and the addition of mung bean nuclease (MBN), an enzyme that cleaves only single-stranded DNA. It was found that the DNA strands in the hexagon were not degraded by MBN, indicating that the hexameric structures obtained were comprised of full duplexes and, therefore, formed a closed hexagon, rather than just a linear chain. These structures were subsequently made plasmonically active by covalently modifying the ends of each monomeric DNA strand with a 1.4 nm AuNP monofunctionalized with a succinimidyl ester moiety.

This work was taken a step further in 2007, where a similar strategy was used to create nanoparticle triangles, squares, rectangles, and trapezoids, and was also used to demonstrate a sequential write and erase feature for the discrete structures (Figure 37).[907] Initially, building blocks consisting of organic molecule corners covalently attached to two DNA arms were assembled into triangular (three building blocks) or square (four building blocks) shapes via the addition of linker DNA strands. The strands were then ligated, and the linker strands were removed, resulting in a fully cyclical but single-stranded DNA template. Five and fifteen nanometer particles, each functionalized with a single strand of DNA, were then added to these templates, creating isolated NP clusters with specific geometries. By controlling the DNA sequences attached to the nanoparticles, different sized AuNPs could be added to specific vertices of the DNA template. After assembly, these nanoparticles could also be "erased" from a cluster and different nanoparticles could be "rewritten" in their place by the stepwise addition of different oligonucleotide sequences or DNA–NP conjugates. Furthermore, when the templating DNA strands contained an internal segment of DNA that was not complementary to the DNA–AuNP sequence, the DNA–NPs hybridized to only the outermost sections of the side of the polygonal templates. This brought two of the nanoparticles in the cluster closer together than if the template DNA were fully hybridized to the DNA–AuNPs, providing a means of creating trapezoids and rectangles.

As with the previous examples presented by Alivisatos and coworkers, this strategy was later extended to the formation of 3-D assemblies.[908,909] In this work, the DNA-triangle templates were assembled as before, but rather than directly hybridizing to DNA–AuNPs, the triangles were themselves assembled via the addition of DNA linkers, creating long 1-D tubes consisting of joined trigonal prisms. By changing the DNA sequences used to assemble the DNA triangles and prisms, the dimensions of the tubes could be varied from 7 to 14 nm on each triangular side. The authors found that when these tubes were assembled in the presence of excess citrate-capped AuNPs, the particles were encapsulated within the DNA nanotubes, resulting in long 1-D chains of nanoparticles. Interestingly, the AuNPs were shown not to diffuse into the trigonal prismatic cavities after a DNA nanotube had already been formed, and the sizes of the AuNPs needed to be commensurate with the nanotube cavities for the particles to be enclosed within a tube during synthesis. Furthermore, these AuNPs could be released upon the addition of single-stranded DNA that was complementary to the DNA holding the nanotubes together. The plasmonic properties of these nanotubes were measured, and it was shown that when the nanoparticles were close together, a longitudinal plasmon band could be observed due to coupling between the assembled AuNPs. This was later extended to create DNA nanotubes of controllable length.[909]

6.1.2. Extended DNA–Nanoparticle Assemblies. One of the most prolific areas of DNA-templated assembly involves the polyvalent oligonucleotide–nanoparticle conjugate. This structure consists of a single particle with numerous surface-bound DNA strands which can be used to template the formation of extended nanoparticle aggregates. The first example of this type of conjugate assembly was presented by Mirkin et al. in 1996 (Figure 36b–d).[62] In this work, two sets of nanoparticles functionalized with different non-complementary DNA strands were combined with linker oligonucleotides that assembled them into macroscopic polymeric aggregates. A striking red to blue color change was observed as a consequence of plasmonic coupling between the inorganic particles in the assembled state (Figure 36c). It was later shown that the collective plasmon resonance of the assembly could be tailored by changing the DNA linker length.[910] Importantly, it was shown that the polyvalent nature of the DNA–AuNP conjugate resulted in increased DNA

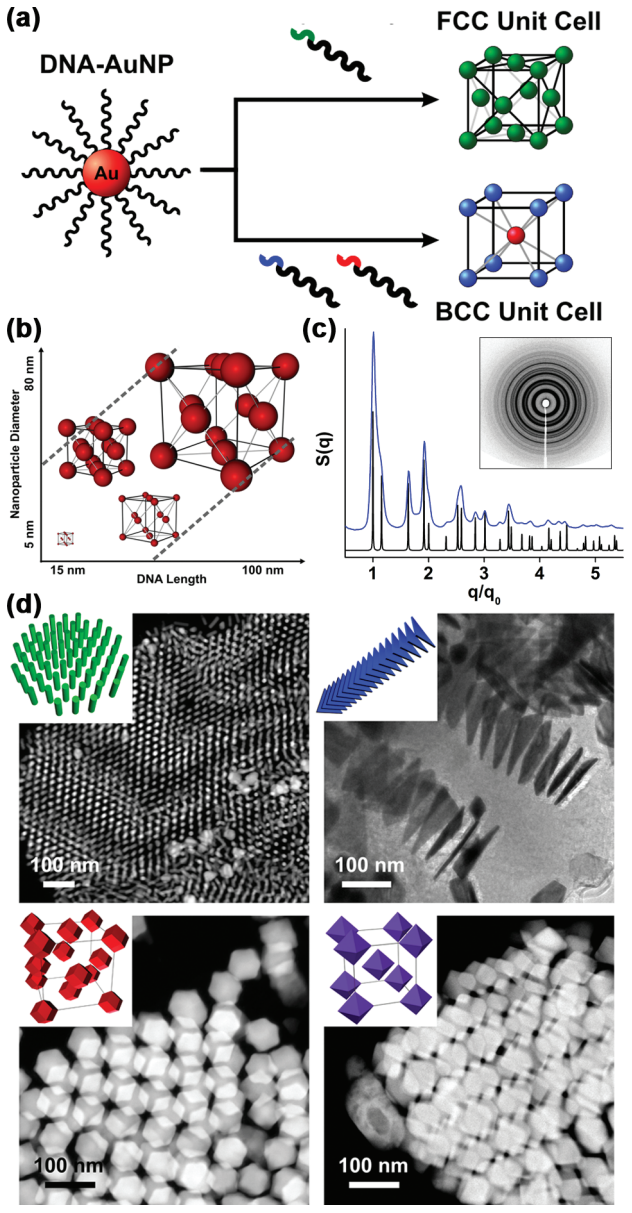

Figure 38. DNA-templated assembly of AuNPs: (a) ordering of particles into fcc lattices (top) or bcc lattices (bottom) using self- and non-self-complementary DNA linkers, respectively, (b) fcc lattices can be synthesized with independent control over both the DNA length and nanoparticle size, (c) small-angle X-ray scattering pattern of 5 nm AuNPs assembled into an fcc superlattice, offset by the pattern for a perfect fcc crystal (the inset shows the same data represented by diffraction rings), (d) TEM images showing that nanoparticle shape dictates the crystal symmetry for 2-D hexagonal sheets (rods), 1-D columns (triangular prisms), and fcc (rhombic dodecahedra) and bcc (octahedra) lattices. (a) Adapted with permission from ref 943. Copyright 2008 Nature Publishing Group. (b, c) Adapted with permission from ref 949. Copyright 2010 Wiley-VCH Verlag GmbH & Co. KGaA. (d) Adapted with permission from ref 950. Copyright 2010 Nature Publishing Group.

hybridization strength and greater selectivity against mismatched sequences than in free DNA duplex systems (Figure 36d).[911] These properties have led to highly functional materials and devices for protein and oligonucleotide detection, including commercially useful FDA-cleared medical diagnostic tools.[912−919]

Using the polyvalent DNA−nanoparticle as a building block and oligonucleotides as the templating strands, many different assemblies have been achieved. DNA has been used to construct both extended assemblies of binary networks of different particle sizes[920] and discrete "satellite" structures, where a number of smaller nanoparticles surround a large DNA-functionalized particle.[921−924] DNA has also been utilized in the templating of aggregates that can switch between different binding states, where reversibility is imparted through changes in pH[925] or the addition of short oligonucleotide sequences.[926] Further, assemblies incorporating oligonucleotides and proteins[927,928] or utilizing protein interactions to assemble and disassemble particles[929,930] have been studied. In addition to Watson−Crick base-pairing interactions, G-quartet binding motifs have also been used to create DNA-templated structures.[819,931] Asymmetric functionalization of spheres to template different cluster morphologies,[932−934] functionalization of nanoparticles with multiple different templating strands,[935] and DNA-based hybridization of different shapes and surfaces have provided access to more sophisticated assembled structures.[936−940]

Although initial aggregates described in the works above exhibited, in certain cases, only preliminary signs of long-range ordering of the nanoparticles,[941] advances were subsequently made to control the position of nanoparticles within a specific crystal lattice. Indeed, a major advance in using DNA to template the assembly of nanoparticle building blocks came in 2008 with the synthesis of ordered colloidal crystals (Figure 38).[942,943] In back-to-back publications, the Mirkin and Gang groups developed different but complementary methods to synthesize nanoparticle superlattices. Gang and co-workers utilized a strategy similar to the initial DNA-templated synthesis developed by Mirkin in 1996 to achieve body-centered-cubic (bcc) crystals, where two nanoparticles were assembled by the addition of single-stranded DNA templates.[942] The major advance in this work came from the addition of long flexible regions to the DNA template that allowed for nanoparticles to remain somewhat mobile even after binding to the linker oligonucleotides. On the other hand, the DNA templates utilized by Mirkin and coworkers presented an entirely new strategy where the linkers consisted of primarily rigid, double-stranded DNA with a weak binding region placed at the DNA terminus away from the particle surface.[943] Interestingly, this strategy enabled the use of the sequence programmability of DNA to template the formation of different crystallographic arrangements from the same AuNP building blocks, highlighting one of the distinct advantages of DNA-based nanoparticle assembly (Figure 38a). When the DNA sequence templating the assembly of crystals contained a self-complementary binding region (indicating that all particles could bind to all other particles equally), a face-centered-cubic (fcc) arrangement of particles was obtained. However, when two sets of nanoparticles were functionalized with DNA sequences that were complementary to each other, a bcc crystal was obtained. This points out an interesting aspect of DNA-based templating: while most DNA templates only provide a physical backbone to direct assembly, in this work, the structural identity (in terms of DNA length and number and position of DNA strands) of the DNA was not changed significantly, but rather it was the actual identity of the DNA sequences themselves that directed the formation of different nanoparticle superlattices.

This work has since been built upon by multiple groups, wherein lattice parameters have been controlled with nanometer-scale precision via changes in the DNA length,[944,945] the fundamental

pathway and kinetics of ordered crystal formation has been established,[946] and drying effects and DNA-hairpin schemes have been utilized to tune the lattice parameters.[947,948] Recently, by utilizing nanoparticles of different sizes and DNA of different lengths, interesting phase behavior has been observed (Figure 38b).[949] It has been demonstrated that the ratio between the nanoparticle size and the DNA length has a significant impact on the formation of ordered colloidal crystals. When spherical particles were utilized, only DNA strands of certain lengths were able to facilitate the assembly of fcc crystals. DNA that was too short was sterically constrained, indicating that the most thermodynamically stable structure was not a crystalline arrangement of particles. Conversely, when the DNA strands were too long, the kinetics of crystal formation were sufficiently hindered to prevent superlattice formation. Although in this case the DNA strands may have been able to template a thermodynamically stable crystal, the kinetics of crystallization were too slow to observe ordered structures over the time scales investigated. This understanding has led to improvements in the quality of nanoparticle superlattices assembled by this method and has allowed an even greater degree of control over nanoparticle placement in a crystal, as evidenced by X-ray diffraction techniques (Figure 38c).

Interestingly, by using anisotropic particles, Mirkin and coworkers showed that a type of valency could be introduced into the nanoparticle conjugates. Specifically, it was found that the shape of the particle dictated the resulting crystallographic symmetry of the nanoparticle superlattice (Figure 38d).[950] For example, flat, triangular prisms formed ordered 1-D stacks, and long rod-like structures formed primarily 2-D sheets. These structures were obtained because the particle shape dictated the directionality of the DNA interactions. The most stable arrangement in each case was found to be the one that maximized commensurate, parallel face-to-face interactions between particles. In this example, both the DNA and the particle shape template the symmetry of the final crystal, where the relative importance of each component in dictating the assembly of different crystals varied as a function of the DNA length. This was most evident in the assembly of octahedra: at short DNA lengths, no order was observed, whereas at intermediate DNA lengths, a bcc arrangement was observed, with all particles exhibiting the same rotational orientation. At long DNA lengths, the DNA became very flexible, and the particle's shape anisotropy was lost, resulting in fcc arrangements of octahedra with no rotational order.

6.1.3. DNA-Constructed Scaffolds as Templates. A separate method of creating extended DNA templates is through the use of DNA origami, wherein DNA sequences are programmed so that they fold into intricate geometries. Typically, these templates program the position of nanoparticles by the placement of single-stranded binding regions that are complementary to DNA sequences covalently attached to a particle. Kawai and co-workers were among the first to utilize this principle, demonstrating limited ordering of gold nanoparticles on a DNA scaffold.[951] Kiehl and colleagues later improved upon this in 2004, creating larger arrays with significantly improved ordering of the nanoparticles (Figure 39).[952] Here, a large 2-D template was assembled by the combination of four different DNA tiles, where each tile consisted of several long sequences of DNA that were internally complementary, as well as short sequences ("sticky ends") that were complementary to similar "sticky ends" on other tiles. Each tile was ~2 × 4 × 16 nm in size, and the assembly of these tiles resulted in large 2-D arrays with tiles of a particular type aligned in long rows. One of the tile types

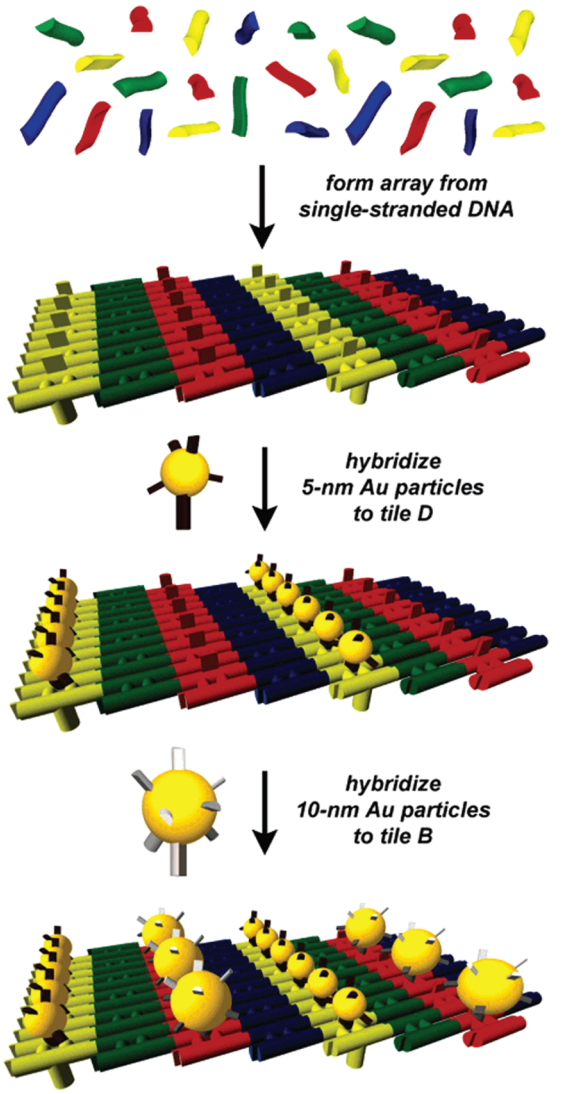

Figure 39. Schematic of a DNA origami scaffold that presents binding sites for DNA-functionalized gold nanoparticles. The DNA template arranges the particles into alternating rows of 5 and 10 nm AuNPs. Adapted with permission from ref 953. Copyright 2005 American Chemical Society.

contained a long polyadenosine sequence designed to be unhybridized upon assembly of the 2-D array, thereby allowing it to be used as an anchor for particle binding. Six nanometer AuNPs were then functionalized with multiple strands of 3′-thiolated polythymine DNA, which allowed the NPs to bind to the polyadenosine sequences on the 2-D DNA tile arrays. Atomic force microscopy (AFM) and TEM images confirmed the assembly of large (micrometer-sized) arrays of AuNPs aligned in rows with ~63 nm between rows and ~20 nm between particles within a row. In areas where the AuNPs were most densely packed, the spacing between AuNPs was ~12 nm, which was predicted to be the effective size of a single DNA-functionalized AuNP. Kiehl and co-workers later expanded upon this work by encoding different binding regions onto two tiles in the scaffold to hybridize 5 and 10 nm NPs at select points on the 2-D array (Figure 39).[953] This resulted in parallel, alternating rows of 5 and 10 nm NPs spaced by ~32 nm. The 5 nm NP rows were more densely packed and linear than the 10 nm NPs, but there was no cross-contamination between the two types of nanoparticles.

Since this early work, major advances have been made, particularly by Seeman and co-workers, using DNA tiles that were triangular, rather than rectangular.[954] Monofunctionalized 5 and 10 nm NPs assembled onto these substrates formed rows, hexagonal grids, or alternating rows of differently sized NPs, depending on the DNA sequences used to template the assembled structures. Another example was given by Bokor and coworkers, where discrete linear arrays of particles were assembled onto a DNA template.[955,956] In this case, rather than creating extended DNA scaffolds, discrete structures were synthesized as templates for just a few nanoparticles. By creating a DNA origami triangle that presented DNA binding sites along one of its sides, 5, 10, and 15 nm AuNPs were assembled in a six-nanoparticle chain. The positions of these particles were controlled so that all assembled structures aligned AuNPs in a 15−10−5−5−10−15 nm array with ±2 nm precision in particle placement. Importantly, the plasmon focusing effects that arise from this particular arrangement of particles have been proposed as a method to create plasmonic nanolenses. In addition to these works, DNA-based scaffolding techniques have been refined and extensively utilized to assemble different arrangements of nanoparticles in recent years.[156,955,957−963]

An interesting recent example utilized steric and electrostatic repulsion between AuNPs to create extended helices of nanoparticles.[964] The DNA templates utilized in these structures consisted of four distinct DNA tiles assembled in a repeating A−B−C−D fashion to create long arrays of DNA templates. The first tiles in these assemblies contained a dangling oligonucleotide sequence that was hybridized to a DNA−AuNP monofunctionalized with a complementary DNA sequence, and the third tiles contained a stem−loop structure that provided a steric counterbalance to the bound NPs. Due to repulsive forces between NPs stacked next to each other, the tile arrays tended to curl up into tubes with the nanoparticles located on the outside. Depending on the degree of twisting in the DNA tube, the AuNPs formed ring structures, helices, or multiple nested helices, leading to structures exhibiting both left- and right-handed chirality. Depending on the sizes of the NPs used and the presence or absence of the stem−loop, different dominant architectures were formed. When neither NPs nor the stem−loop were present, flat ribbons were obtained, as no steric or electrostatic repulsive forces were present to induce curvature in the DNA array. Nested helices were only observed as a noticeable product when the stem−loop was present, and increasing the size of the NPs bound to the array drove the assembly toward a greater number of stacked ring structures, as opposed to helical formations.

It is also possible to create extended DNA templates that adsorb nanoparticles without hybridization of a target DNA sequence, typically by using the DNA strand as a physical template to position binding units at specific locations or by creating a scaffold to which nanoparticles can bind via electrostatic interactions. Examples of this include functionalization of AuNPs with DNA-intercalating moieties,[965,966] using protein and small-molecule interactions to assemble AuNPs onto a DNA template,[967−969] and electrostatic binding of positively charged AuNPs to DNA.[970−974]

6.2. Peptides and Proteins

Peptides and proteins present an interesting class of biomolecule for the purpose of synthesizing nanomaterial templates since they naturally exhibit varying degrees of order, as different peptide sequences can form structures such as α helices, β sheets, or more complex 3-D arrangements.[464−467] These proteins can, through the same set of interactions, also assemble into highly ordered 1-, 2-, and 3-D arrays. The complex assembly methods involved in these processes are not nearly as well understood as in the case of DNA, primarily because of the significantly larger number of modular building blocks (amino acids), which contain a much more diverse set of chemical functionalities. However, this complexity does give rise to very ornate nano-objects whose structures can be used to dictate the assembly of discrete nanoparticle conjugates (through encapsulation or adsorption of particles). Furthermore, the programmability afforded by utilizing a diverse set of chemical functional groups allows for highly selective interactions between nanomaterials or small-molecule-conjugated nanomaterials.

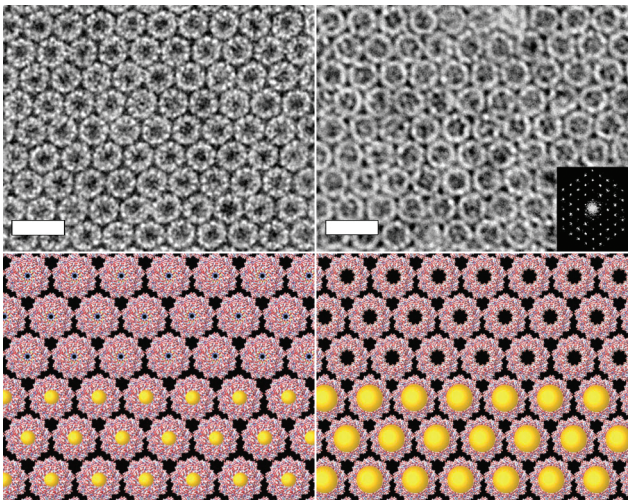

Figure 40. Arrays of chaperonin proteins serve as binding sites for different sizes of particles. Top: TEM images, with the electron diffraction pattern inset. Bottom: Schematics of protein arrays and AuNP binding sites. Scale bars are 30 nm. Adapted with permission from ref 975. Copyright 2002 Nature Publishing Group.

6.2.1. 1- and 2-D Arrays as Templates. An early example of the assembly of arrays of proteins and plasmonic structures was shown by McMillin et al., where chaperonin proteins were used to template 2-D arrays of nanoparticles (Figure 40).[975] Chaperonins are semispherical proteins that consist of 14−18 subunits that assemble into stacked-ring structures ∼15−20 nm in diameter. In this work, the proteins were modified to specifically express cysteine residues at selected points on their surface. Depending on the site of alteration, these cysteine modifications were arranged in rings that were either 3 or 9 nm in diameter. Under reducing conditions, these proteins formed a template of disk-like, hexagonally close-packed (hcp) crystals with a total size of ∼20 μm. These crystals were then exposed to BSPP-coated gold nanoparticles with diameters of 5, 10, or 15 nm, resulting in large hcp nanoparticle arrays. Interestingly, the sizes of the cysteine rings that bound the nanoparticles had a distinct impact on the sizes of AuNPs that could associate with the template. The 3 nm rings bound only 5 nm AuNPs, while the 9 nm rings bound only 10 nm AuNPs. This was projected to be a consequence of the accessibility and positioning of individual cysteines in the assembled chaperonin template. Interestingly, these arrays could also be formed by preconjugating 1.4 nm AuNPs to individual subunits prior to chaperonin assembly. In this case,

the non-native structures were reacted with AuNPs containing a single maleimide functional group. Chaperonin proteins were then assembled, forming protein−NP conjugates comprised of 2-D hcp arrays, where the AuNPs were localized preferentially within the cores of the individual proteins at the sites of the non-native cysteine residues. Since this work, other examples of cross-linked protein arrays have been demonstrated by several research groups.[569,976,977]

Proteins on the outer surface of some bacterial cell envelopes create a 2-D porous membrane known as an S-layer. Synthetic S-layers provide a natural template for assembling nanomaterials, as they form ordered 2-D arrays of repeating subunits with different symmetries and lattice constants on the order of 3−30 nm, typically containing pores that are 2−6 nm in diameter. In the previous section regarding biotemplated synthesis, examples of particle formation using S-layers are given (see section 3.5.3). From an assembly standpoint, one of the first examples of the use of an S-layer to position preformed nanoparticles was presented by Mann and co-workers.[978] In this work, the hexagonally packed intermediate (HPI) S-layer of *Deinoccous radiodurans* was used to assemble gold nanoparticles of different sizes into hexagonal arrays with specific interparticle spacings. The HPI of this particular bacterium displayed *p6* symmetry with a lattice constant of 18 nm, where each hexameric subunit consisted of a hollow cone with a 2 nm wide, positively charged central channel. To generate nanoparticle superlattices, monolayers of proteins were assembled onto a hydrophobic TEM grid and then exposed to an aqueous solution of negatively charged AuNPs with diameters of either ∼5 or ∼10 nm. In both instances, the nanoparticles formed hexagonal arrays over micrometer-sized domains with center-to-center distances between particles of ∼18 nm. Interestingly, the pores exhibited some size selection in the case of the 10 nm AuNPs, as the average size of assembled NPs was ∼8 nm, indicating that the small size of the positively charged pore channel in each of the protein subunits selectively bound smaller AuNPs. No size selection was observed in the 5 nm AuNP case, but a 1:1 mixture of 5 and 10 nm AuNPs showed that the 5 nm AuNPs were selectively incorporated into ordered superlattices, while the 10 nm particles were observed at random positions across the HPI surface.

This work was later built upon by Batt and co-workers,[979] who examined the effects of the solution ionic strength and orientation of the HPI. It was shown that, while both sides of the HPI could bind negatively charged particles, only the extracellular face was observed to facilitate the formation of ordered nanoparticle arrays. In addition, under low ionic strength, the nanoparticles could bind only at every other vertex in the HPI. However, by increasing the concentration of NaCl in solution, the authors were able to screen the repulsive forces between particles, resulting in the adsorption of particles to nearly every vertex point in the lattice in a nearly continuous hexagonal array of particles. They also later developed methods to pattern different S-layer proteins into lattices with different interparticle spacings and superlattice geometries.[980] Other membrane proteins (purple membrane protein) have been shown to exhibit this behavior and have been successfully used for the assembly of gold nanoparticles.[981]

Rather than use extended 2-D protein crystals, Willner and colleagues have utilized 1-D actin monofilaments to synthesize nanowire assemblies.[558] Actin monomers were first polymerized into a long actin wire and then reacted with 1.4 nm AuNPs monofunctionalized with a maleimido group to form a linear assembly of particles. These multimeric structures were then dissociated by dialysis to remove the ATP, Na^+, and K^+ responsible for filament formation and then reassembled and subjected to gold ion reduction, resulting in long nanorods 80−100 nm in diameter and 2−3 μm in length, depending on the exposure time to the growth solution (see section 3.5.3). It was shown that polymerization of actin monomers prior to AuNP conjugation was necessary, as functionalization of individual monomers resulted in a lack of actin filament polymerization. This was attributed to the indiscriminate binding of AuNPs during the functionalization step, resulting in blocking of some of the active binding residues on the monomers necessary for filament formation. Finally, by feeding the actin polymerization reaction with sequential additions of AuNP-modified and natural actin monomers, a segmented linear nanoparticle assembly could be synthesized with controllable segment lengths.

In 2008, Pochan and co-workers demonstrated a methodology for creating ordered linear arrays of nanoparticles by using templates of β sheet fibrils.[982] The peptides involved in this work exhibited an alternating sequence of hydrophobic and hydrophilic amino acids consisting of primarily valines (hydrophobic) and lysines (hydrophilic, positively charged). In solution, these naturally formed β sheets, which subsequently formed laminated fibrils consisting of β sheets stacked on top of each other in an ordered fashion. When 2 nm AuNPs were introduced into solution during the fibril formation process, they were selectively captured by the peptides, with the negatively charged surface of the AuNPs associating with the lysine residues. The end result was parallel, linear arrays of particles along the length of the fibril with regular periodicity across the fibril's width. The inclusion of these particles served to increase the spacing between β sheets from 2.5 to 3.9 nm. Importantly, it was shown that the ordered nanoparticles needed to be commensurate in size with the periodicity of the β sheet fibrils to make ordered arrays. For instance, when 12 nm diameter particles were used during the assembly process, they still associated with the fibrils but in a random fashion.

One of the main advantages of protein- and peptide-based assembly is that there are a large number of structural motifs that can be accessed by different amino acid sequences. For example, Woolfson[983,984] and Langer[985] have both used leucine zipper motifs, and others have shown helix−loop−helix,[986−988] β sheet,[989] double-helix,[96,534,990] and single-chain[990] structures to be successful for nanoparticle assembly. Peptide superstructures such as cylindrical tubules,[991−993] hollow spheres,[536,994] and coaxial nanowires[537] have also served as templates for plasmonic nanoparticles.

Rosi and co-workers have recently devised a strategy to simultaneously synthesize and assemble gold nanostructures using peptide−small-molecule constructs (Figure 22; see also section 3.5.2).[96,534,536] Here, the template building blocks consisted of a small 12-carbon alkyl chain covalently conjugated to a 12-mer peptide that had been shown to exhibit high affinity for gold surfaces. Due to the hydrophobic nature of the alkyl chain, the peptide−organic molecule conjugates assemble in solution into long ribbon-like structures (∼4 μm by 6.1 nm), exhibiting a left-handed twist with a pitch of ∼84 nm. Circular dichroism and IR spectroscopy experiments allowed Rosi and co-workers to project that the structures consisted of a double helix of peptides, where the hydrophobic alkyl tails are sequestered at the center of the helix and the peptide components form parallel β sheets. Varying the assembly and synthesis conditions allowed for the

formation of double helices,[96] continuous 1-D arrays,[534] and hollow spheres[536] with tailorable particle sizes and interparticle distances.

6.2.2. Antibody−Small Molecule Templates. Unique templating strategies that take advantage of well-established molecular recognition schemes and protein interactions (i.e., antibody−antigen) have also been demonstrated. One of the first examples was provided by Fitzmaurice and co-workers, where disulfide−biotin analogues were attached to gold nanoparticles and subsequently assembled with the addition of streptavidin, a molecule known to bind to biotin with extremely high affinity.[995] Another interesting early example is the work of Murphy and colleagues, who used the highly specific and efficient biotin−streptavidin interaction to template long 1-D arrays of nanorods joined in an end-to-end fashion.[996] Highly anisotropic CTAB-coated nanorods (aspect ratio ∼18) were first immersed in a solution of biotin and then divided into two aliquots. One of these aliquots was suspended in a saturated solution of streptavidin (SA), thereby ensuring that all surface-bound biotin molecules were coated in SA, while the other was unaltered and therefore remained coated in biotin. The two aliquots were then recombined and analyzed by TEM. It was found that the nanorods primarily assembled in an end-to-end fashion, with only a few end-to-side or side-to-side pairings observed (interparticle spacings were typically ∼5 nm). It was proposed that the biotin was only able to attach to the tips of the nanorods where the CTAB surfactant layer was less dense. In this case, the biotin−SA interactions were only able to template the assembly of linear chains of rods. Kotov and collaborators, on the other hand, have recently developed a method to template end-to-end or side-to-side assembly of nanorods using antibody−small-molecule interactions.[997] Several other examples of antibody-templated nanoparticle assembly strategies have also been shown,[998] such as the incorporation of DNA with SA−biotin interactions,[999−1001] electrostatic assembly on SA templates,[1002,1003] and reversible particle assemblies.[1004]

6.2.3. Large-Scale 3-D Assemblies of Particles. In 2005, Rotello and co-workers devised a strategy to create large 3-D aggregates of nanoparticles using the interaction between a lysozyme protein and a gold nanoparticle surface to tune interparticle spacings, thereby affecting the aggregate morphology and plasmonic behavior.[1005] Lysozyme was chosen as it is well characterized and resistant to denaturation and presents different binding modes to negatively charged surfaces depending upon system parameters such as temperature and degree of nanoparticle surface coverage. Varying stoichiometries of lysozyme and ∼7 nm AuNPs were assembled at both room temperature and 50 °C. An increase in interparticle spacing with increasing amounts of protein was observed, with variations in particle−particle distances ranging from 7.3 to 13.6 nm for room temperature assemblies and from 7.3 to 12.1 nm for assemblies at elevated temperature. This was attributed to different adsorption orientations under different conditions, where lower amounts of protein at room temperature preferred side-on adsorption and end-on orientations were preferred at higher temperatures. Importantly, it was demonstrated that these variations could be used to tune the plasmonic response of the particle assemblies. The composites prepared at room temperature were less compact and, as a result, displayed brown-colored aggregates. Conversely, the high-temperature composites displayed a smooth, purple film composed of a dense packing of AuNPs. Furthermore, changing the protein density around particles within an aggregate showed two different effects on the collective plasmon peak of the aggregates. Increased interparticle spacings were observed to result in a blue-shift of the plasmon peak. Interestingly, when this increase in particle spacing was achieved via a denser packing of proteins, the greater protein concentration also resulted in an increased refractive index of the environment around the particles, and the net impact on the plasmon band was only a nominal blue-shift of the peak position, even at the larger interparticle spacings. By utilizing these different effects, the SPR was varied over a 127 nm range, from 548 to 675 nm. The same group has also investigated similar effects using proteins that denature upon binding to the nanoparticles.[1006]

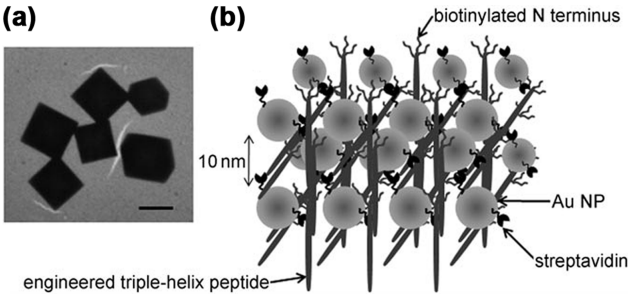

Figure 41. Large-scale peptide-templated assembly: (a) TEM image and (b) schematic of 3-D AuNP arrays assembled by synthetic collagen-like peptides. Scale bar is 2 μm. Adapted with permission from ref 1007. Copyright 2010 Wiley-VCH Verlag GmbH & Co. KGaA.

One of the important challenges in making useful templated nanostructures is the development of assembled materials that are large enough to be integrated with macroscale devices. A recent example of utilizing proteins as templates to create large nanostructured materials was provided by Matsui and co-workers, where collagen fibers were used to assemble gold nanoparticles into micrometer-sized 3-D arrays (Figure 41).[1007] The peptides used in this work consisted of 63 residues from the α1 chain of type I collagen which provided structure to the template, a foldon domain that served to correctly fold the peptides into the proper structure, and a cys-knot sequence that connected peptides via disulfide bridges. The designer peptides were expressed in *Escherichia coli* cells to achieve a sufficient amount of material; while in the cells, endogenous bacterial biotin ligase (BirA) added a biotin moiety to a lysine residue that would later enable assembly. The purified assembled templates were monodisperse 4 × 40 nm protein rods, as confirmed by TEM. These collagen fibers were then added to a solution of streptavidin-coated 10 nm AuNPs, resulting in cubic structures whose sizes could be tailored from ∼100 nm to 2 μm in diameter by altering the relative concentrations of peptides and nanoparticles. Interparticle spacing within these cubes was found to be ∼7 nm, and the nanoparticles were arranged in a cubic superlattice. When larger 30 nm AuNPs were used, micrometer-sized hexagons were formed. It was projected that the larger NPs changed the interactions between collagen peptides and nanoparticles, thereby forming a different, noncubic unit cell, which in turn caused the growth of a hexagonal crystal.

6.3. Microorganisms

In addition to using biological molecules as programmable nanomaterial templates, biological organisms present interesting scaffolds for materials assembly. The complex shapes created by

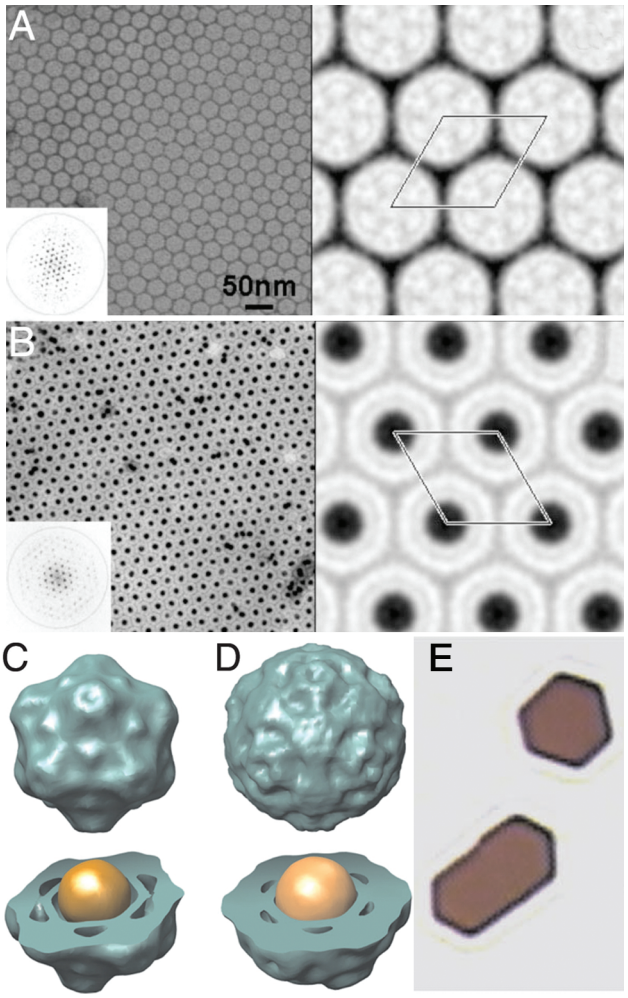

Figure 42. Templating large-scale nanoparticle arrays using virus-like particles (VLPs): (A, B) TEM images of 3-D arrays of assembled VLPs without (A) and with (B) AuNPs inside the virus cores, (C, D) different virus protein coating structures are obtained when different sizes of AuNPs are inserted into the hollow cores of the VLPs, (E) optical micrograph of crystals obtained by assembling VLPs with embedded AuNPs. Adapted with permission from ref 1011. Copyright 2007 The National Academy of Sciences of the USA.

microorganisms often have unique features that would be difficult to replicate by top-down fabrication techniques, and their self-replication or self-assembly properties can be used to scale up template syntheses. For example, viruses are nanoscale biological objects with well-defined, highly monodisperse shapes and sizes that can be controlled via genetic modifications. Diatoms create silica shells with ornate designs that are unique to each particular species. Living organisms also present dynamic structures that can be altered even after the initial templating of materials. The structural diversity and tailorability that biological organisms present provides access to many different template structures, limited only by our ability to manipulate the organisms at the genetic or molecular level.

6.3.1. Virus Templates. Viruses are discrete nanoscale objects of predictable sizes and shapes and therefore represent a natural choice to template materials assembly.[471,887−890] In 2004, Ratna and co-workers utilized the cowpea mosaic virus (CPMV) as a template for gold nanoparticles, creating discrete clusters of AuNPs attached to a single virus template.[1008] They engineered three different mutant viruses to present cysteine residues positioned at different sites (rings of cysteines either centered directly around a 5-fold icosahedron axis or dispersed uniformly around the virus surface) and then exposed the viruses to 5 or 2 nm AuNPs. The different locations of the cysteines provided a means of controlling interparticle distances, which were predicted to be between 2 and 8 nm. For the mutant virus that exhibited cysteines centered at the 5-fold axes of the icosahedral protein coat, the majority of samples showed vertices with only a single nanoparticle attached. In some cases, the 5 nm particles were attached off-center from the axis, allowing two AuNPs to bind per vertex, but these were found to be less common than the singly bound sites. Depending upon the sites of the cysteine residues, controllable interparticle spacings for viruses of 6.4 and 8.4 nm were demonstrated. In related work, Ratna and co-workers have demonstrated a purification methodology for these composite materials,[1009] and Finn[1010] and Balci[582] have demonstrated conceptually similar strategies for achieving nanoparticle assembly.

Because viruses are essentially hollow structures utilized for the carrying of nucleic acid cargos, it is also possible to template plasmonic materials by encapsulating them within individual virus structures.[1011−1014] In 2007, Sun et al.[1011] utilized the brome mosaic virus, a 28 nm icosahedron consisting of 180 identical protein subunits, to encapsulate PEG-COOH-functionalized gold nanoparticles (Figure 42). Nanoparticles with diameters ranging from 6 to 18 nm were incubated in a solution of protein subunits, and virus capsids were observed to naturally assemble around the nanoparticles with up to 70% efficiency (the remaining capsids assembled without any material at their core); maximum efficiency was obtained with 12 nm AuNPs. These virus−AuNP materials were subsequently assembled into both 2-D and 3-D arrays, and their plasmonic properties were analyzed (Figure 42A,B). The 2-D arrays possessed hexagonal symmetry with a lattice constant of ∼25 nm, approximately equal to that of a 2-D crystal consisting of virus capsids with no nanoparticle core, demonstrating that the AuNP cargo did not disrupt the recognition or assembly properties of the virus. The authors then cocrystallized both hollow and AuNP-containing viruses into 3-D structures that appeared red in color (Figure 42E), with the intensity of the UV−vis signal being proportional to the relative amount of AuNP-containing viruses incorporated within the crystal. Interestingly, while the free AuNP−virus hybrid structures exhibited a peak at 526 nm in solution, once assembled, two peaks were observed at 481 and 608 nm. This was attributed to multipolar coupling between gold cores leading to the formation of a plasmonic band gap, making these 3-D virus−nanoparticle assemblies excellent examples of optical metamaterials.

The diversity of shapes afforded by different viruses enables the development of many different templated structures beyond just icosahedra. As an example, Belcher and co-workers have exploited the long, rod-like M13 virus as a template for the growth of monodisperse nanowires that can be assembled into macroscopic materials.[1015] These viruses were used to facilitate the formation of negative electrode materials for lithium ion batteries. Co_3O_4 nanoparticles were grown on the surface of a genetically engineered virus; when assembled, these materials exhibited voltage/capacity curves similar to those of other Co_3O_4-nanoparticle-based electrodes. However, when the viruses were also engineered to display binding motifs for gold nanoparticles, the incorporation of AuNPs resulted in higher

initial and reversible lithium storage capacity. These virus assemblies were subsequently organized onto a working, centimeter-scale electrode, demonstrating the scalability of the technique. Subsequent work by the authors has demonstrated other extended arrays of virus templates, including various branched morphologies and liquid crystalline materials containing viruses and gold nanoparticles.[533,1016] In addition, Ward and co-workers have used viruses as templates to bind small nanoparticles, followed by gold reduction to create gold nanoshells.[587] Applications of these virus-templated plasmonic materials include structures designed for therapeutics,[1017] spectroscopic enhancement,[1018] and pathogen detection strategies.[1019]

6.3.2. Living Organisms as Templates. Previously in this review, we presented examples of living organisms aiding in the synthesis of plasmonically active nanomaterials (see section 3.5.4). However, there have also been examples of living organisms being used to template the assembly of nanomaterials by providing a physical structure to which extracellular materials can adhere. These represent an interesting class of templates, as they provide a means for creating adaptable, responsive material scaffolds that can continue to grow or respond to stimuli during or after the assembly process.

In 2003, Mirkin and co-workers used growing fungi to template the assembly of gold nanoparticles.[1020] Spores of the filamentous fungus *Aspergillus niger* were grown in a culture solution containing DNA-functionalized gold nanoparticles. Initially, this solution was a bright red color due to the SPR band of the particles. However, after the fungal spores germinated, the hyphae grew and branched, presenting a surface upon which the AuNPs could assemble, resulting in a red-purple solid precipitating from solution. TEM images confirmed that the tube-shaped hyphae were loaded with a very dense layer of AuNPs, and sectioned samples of the fungi showed that NPs were assembled only around the edges of the hyphae, creating a hollow, tube-like structure. Other fungi were also used (*Penicillium notatum*, *Mucor hiemalis*, and *Streptomyces venezuelae*) and demonstrated tube-shaped AuNP assemblies ranging from 12 to 0.8 μm in diameter and tens of micrometers in length. While the interactions between the DNA strands and the fungal surfaces were not investigated, the DNA coating the AuNPs could be used to template a secondary layer of DNA−AuNPs of a different size through specific hybridization interactions (13 nm NPs attached to the fungi that were subsequently hybridized to 30 nm NPs). Interestingly, the DNA−AuNPs did not appear to inhibit the growth of the fungi; by moving the fungi from a solution containing 13 nm NPs to a solution containing 5 nm NPs, structures with variation in NP composition along a hyphae surface could be obtained, indicating that the fungi were still growing as the AuNPs attached to the fungal surfaces. Several others have demonstrated similar results using bacterial flagellae, fungi, or diatoms as templates to create complex 3-D structures of assembled nanoparticles.[561,1021,1022]

A unique example of utilizing living organisms as templates was presented by Saraf and co-workers,[1023] where electrically active wires were synthesized via templated assembly by living viruses. *Bacillus cereus* bacteria are rod-shaped organisms that are ~5 μm long and ~0.9 μm in diameter and exhibit a high affinity for lysine residues. In this work, living *B. cereus* bacteria were deposited on a substrate containing gold electrodes and then washed with 1 M NaOH to remove extracellular surface proteins and expose the largest possible amount of negatively charged peptidoglycan surface. These devices were then exposed to lysine-coated 30 nm AuNPs for 12 h, resulting in highly uniform AuNP coatings across the bacteria's surface. Interestingly, it was found that the bacteria needed to be both alive and in the logarithm phase of their growth process for this deposition procedure to create a dense coverage of nanoparticles. This was confirmed in a control experiment which showed that autoclaved bacteria (which killed the bacteria while preserving their 3-D structure) did not exhibit full monolayer coverage of AuNPs. Additionally, the bacterial affinity for lysine was critical, as control experiments with positively charged, polymer-coated NPs resulted in reduced AuNP coverage of the bacterial surfaces. Electrical measurements on synthesized devices showed that conductivity could be improved by "annealing" the templates with an applied electric field. This result was attributed to small movements of the AuNPs on the surfaces of the living bacteria, resulting in a larger number of branched pathways between electrodes.

7. ASSEMBLY WITH ORGANIC TEMPLATES

In this work, we define organic templates to include a variety of structures that consist primarily of carbon-containing compounds. The advantage of these materials lies in the atom-level control that chemists routinely wield over the position of various chemical groups in a molecule. It is hoped that this degree of precision can be brought to bear on the assembly of nanostructures by using these molecules as templates. While nanoparticle assembly via small molecules or carbon nanomaterials depends on the symmetry of the discrete species, assembly via supramolecules or polymeric species typically relies on the symmetry of their self-assembled ordered phases to template the placement of plasmonic materials. This distinction practically manifests in the observation that the former class of templates lead mostly to symmetric clusters of nanostructures (sections 7.1 and 7.2),[1024,1025] while the latter class of templates lead to extended 2- or 3-D architectures (sections 7.3 and 7.4),[1026,1027] although this is not always the case. As a result, use of these templates allows one to manipulate nanoparticle ordering across several length scales, taking advantage of both short- and long-range plasmonic effects to dictate material properties.

7.1. Small Molecules

There are many instances in the literature of small molecules that are capable of arranging nanoparticles into larger aggregate materials. For example, excess of a simple dithiol molecule can randomly link AuNPs into a disordered superstructure.[1028] However, only those examples where the symmetry of the molecule or molecular assembly clearly dictates the shape or symmetry of the final assembled structure will be covered here. As a result, these materials usually consist of small clusters of nanoparticles, whose arrangement is dependent on the symmetry of the binding interactions of the molecular templates used to induce nanoparticle association.

One of the first examples of small-molecule-templated assembly is work by Feldheim and co-workers,[1024,1029−1031] wherein rigid thiol-functionalized phenylacetylene molecules were used as assembly agents. Although their initial work showed the formation of AuNP dimers and trimers,[1024] a more sophisticated example can be found in their subsequent work, where these small molecules templated the formation of nanoparticle dimers, trimers, and tetramers with pseudo-$D_{\infty h}$, D_{3h}, and T_d symmetries, respectively.[1030] Both small AuNPs (>10 nm) and larger AgNPs (~30 nm) were assembled, and the resulting structures were

characterized by both TEM and UV−vis, with the latter being compared with theoretical calculations. Importantly, the interparticle distances could be varied by changing the number of phenylacetylene moieties in a single template molecule. In counting ∼100 structures in the samples analyzed via TEM, the AuNP cluster yields were 50% for the dimers, 30% for the trimers, and 10% for the tetramers, with the remainder of particles predominantly being uncoupled. UV−vis measurements demonstrated noticeable differences for the 30 nm silver particles as a function of the number of phenylacetylene moieties in the template molecules. While the isolated AgNPs exhibited a plasmon resonance at 420 nm, addition of the linker molecules to create particle dimers caused both a red-shifting of this peak and the appearance of new peaks. When the linking molecule contained nine phenylacetylene units, this peak red-shifted only slightly, while seven phenylacetylene units resulted in the appearance of a peak at 450 nm and a shoulder at 420 nm. A molecule containing three phenylacetlyene units resulted in both the short-wavelength peak shifting to 370 nm and the appearance of a weak band at ∼600 nm. The results in this work were expanded upon by the same group,[1029] wherein hyper-Raleigh scattering was used to measure the collective nonlinear optical properties of the materials. Exceptionally large responses (compared with those of molecular chromophores) were observed, and both the symmetry ($D_{\infty h}$, D_{3h}, T_d, and D_{4h}) and interparticle distance were observed to have a significant impact on the cluster's nonlinear optical behavior. The electronic properties of these materials were also later measured.[1031]

Recently, van der Boom and co-workers have demonstrated similar results using linkers that contained between one and four pyridyl moieties to construct different clusters of nanoparticles.[1032] In this work, the number of pyridyl moieties and the stiffness of the molecular chains affected the clustering behavior of the nanoparticles. In separate work, Kotov and colleagues have utilized the chromonic material disodium chromoglycate (DSCG) to assemble CTAB-coated nanorods.[1033] When the positively charged nanorods were mixed with DSCG, side-to-side assembly was observed due to attraction of the negatively charged stacks of DSCG. On the other hand, when the nanorods were coated with negatively charged poly(acrylic acid) (PAA) and mixed with DSCG, end-to-end assembly was observed, since PAA was able to bind the positively charged CTAB-coated sides of the nanorods but not the tips, which were left to interact with DSCG via electrostatic or van der Waals forces. pH was also used to disassemble the rods after the initial formation of stacks. Shifts in the optical spectra, consistent with end-to-end and side-to-side assembly of nanorods, were observed from bulk samples in solution.

An ideal strategy for templating the formation of nanoparticle assemblies would be to place molecular recognition agents at discrete sites on a nanoparticle surface. Although, to the best of our knowledge, no generalizable strategy has been developed to site-specifically place small molecules at an arbitrary location on a nanostructure, an interesting example that pairs self-assembled monolayers (SAMs) and particle shape with small-molecule templates to create nanoparticle superstructures is exemplified by the work of Stellacci and co-workers (Figure 43).[1034] In this case, the authors demonstrated the ability to position two individual molecules at opposite poles of a spherical gold nanoparticle and use these molecules to direct the formation of linear nanoparticle chains. These bifunctionalized nanoparticles are created by first forming a mixed monolayer on the surface of

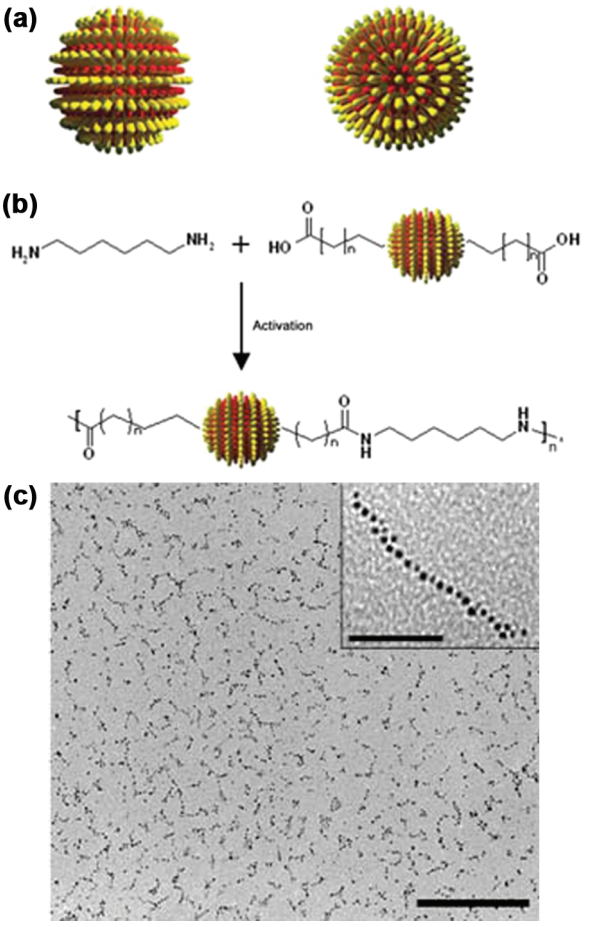

Figure 43. Small-molecule-templated assembly via divalent metal nanoparticles: (a) Co-loading of different thiolated molecules on the surface of a AuNP drives the formation of ring-like phase separation, (b) schematic demonstrating the covalent cross-linking of AuNPs with diametrically opposed linker sites, (c) TEM of linear arrays of AuNPs obtained after cross-linking. Scale bars are 200 and 50 nm (inset). Adapted with permission from ref 1034. Copyright 2007 American Association for the Advancement of Science.

nanoparticles consisting of 1-nonanethiol and 4-methylbenzenethiol. These two molecules then self-assembled into ordered rings of alternating phases on the surface of the nanoparticle, creating two diametrically opposed SAM defect points on the particle surface. The SAM-coated NPs were then exposed to a solution containing linking molecules that selectively replaced the small molecules at the defect points and allowed for a precipitate to form (Figure 43b). When the precipitate was analyzed via TEM, a large number of linear NP chains were observed, containing between 3 and 20 AuNPs (Figure 43c). They observed a very low fraction of branched chains and no 3-D aggregates, indicating that the particles were indeed selectively functionalized at only the defect points on opposite hemispheres. The average yield of nanoparticles incorporated in chains was ∼20%, compared with 3−5% chains and a large number of 3-D aggregates in different control experiments. The authors also demonstrated the ability to change the interparticle distance, using nanoparticles of different sizes, and make continuous films as large as 1 cm^2 by depositing large numbers of the chains at a water−toluene interface. Similar work was conducted by Mann and colleagues, who utilized a ditopic molecule (2-mercaptoethanol)

dx.doi.org/10.1021/cr1004452 |*Chem. Rev.* 2011, 111, 3736–3827

to assemble linear structures of nanoparticles.[1035] In this work, the structures were branched, rather than singular chains, where the extent of branching was observed to be dependent upon the number of 2-mercaptoethanol molecules on the surfaces of the particles.

In addition to the small molecules presented above that possess unique symmetries to be taken advantage of as templates, significant research has been invested in the development of molecules that can be dynamically modulated with external stimuli. An excellent example of this is the work by Stoddart and co-workers, which uses pseudorotaxane molecules to reversibly assemble and disassemble nanoparticles using electric or chemical stimuli.[1036] The pseudorotaxane molecules in this work were based upon the preferential binding of cyclobis(paraquat-*p*-phenylene) ($CBPQT^{4+}$) with an electrochemically activated diethylene glycol-disubstituted tetrathiafulvalene (TTF-DEG). The TTF-DEG molecules can undergo a reversible oxidation process to create a cationic species, which activates the dissociation of the complex via like-charge repulsion between the two species. The authors synthesized three different complexes that contained two, three, and four $CBPQT^{4+}$ moieties in roughly linear, triangular, and square shapes, respectively. AuNPs were functionalized with a mixture of thiolated TTF-DEG molecules and thiolated molecules that lacked the TTF-DEG moiety. The molar ratios of these two complexes were highly skewed toward the latter so as to prevent uncontrolled aggregation of large particle clusters with multiple $CBPQT^{4+}$−TTF-DEG interactions. Upon addition of the $CBPQT^{4+}$-containing molecules, the nanoparticles were observed to assemble into dimers, trimers, and tetramers with ∼5−10% yields. Oxidation and reduction of the TTF molecule demonstrated that the AuNP clusters could be dynamically assembled and disassembled via electrochemical stimuli.

A similar strategy using host−guest interactions has been employed recently by Secchi and co-workers using calixarene molecules.[1037] In this work, larger clusters that exhibited no reversibility were created, but the size of the clusters was dependent upon the identity of the guest molecule. An interesting counterexample to the works presented above (with small-molecule-templated nanoparticle structures) was achieved by Amabilino and co-workers,[1038] where gold nanoparticles served as a template to assemble small molecules into supramolecular fiber structures. In this work, tetrathiafulvalene-capped gold nanoparticles induced the formation of large arrays of fibrous materials that exhibited interesting electronic characteristics.

7.2. Carbon Nanotubes

Elemental carbon can exist in many different allotropes, including different discrete nanostructured shapes, such as fullerenes and nanotubes. While the former have been used to aggregate nanoparticles, the latter is the primary focus of this section. CNTs present natural choices for templating 1-D nanostructures, as they exhibit highly linear shapes that can be up to several micrometers long and can be chemically modified to present functional groups for the binding of nanomaterials.

An early example of CNT-based nanoparticle assembly was presented by Fitzmaurice and co-workers (Figure 44).[1025] Tetraoctylammonium bromide-stabilized gold nanocrystals (6 ± 1 nm) were first added to a solution of carbon nanotubes. Although initially bright red due to the surface plasmon resonance of the AuNPs, the solution eventually faded in color, and a precipitate formed at the bottom of the reaction vessel that was subsequently

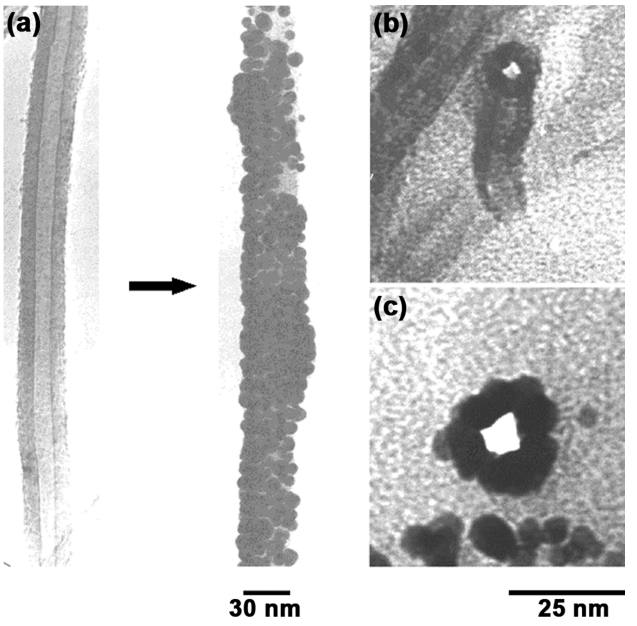

Figure 44. Adsorption of plasmonic nanoparticles to carbon nanotube templates: (a) TEM images before and after assembly of AuNPs onto CNT templates, (b, c) magnification of cross sections of CNTs coated with nanoparticles. Adapted with permission from ref 1025. Copyright 2000 Wiley-VCH Verlag GmbH & Co. KGaA.

analyzed using TEM. The authors observed CNTs up to 10 μm in length with near monolayer coverage of AuNPs. These assemblies consisted of long, composite structures comprised of individual nanoparticles separated by a layer of the surface ligand. Continuous gold nanowires were obtained by firing these assembled structures in air at 300 °C for a few minutes. TEM measurements taken at different time points in the annealing process revealed that the surface atoms of the nanoparticles melted within ∼30 s, followed by nanoparticle coalescence. Extended heating times (up to ∼120 s) resulted in less regular, polycrystalline samples.

A more recent example that has probed the phenomenon of AuNP adsorption to CNT templates is the work by Rance et al.,[1039] who looked at using van der Waals forces to assemble AuNPs on CNTs. In this case, citrate-capped nanoparticles of a known concentration were added to a solution of multiwalled carbon nanotubes with a known surface area. The solution was allowed to equilibrate, resulting in the formation of a nanotube−nanoparticle precipitate, which decreased the intensity of the red color in solution. UV−vis spectroscopy was used to quantify the number of nanoparticles remaining in solution, and this was used to characterize the degree of binding between particles and carbon nanotubes. The authors note that because the nanoparticles are capped with citrate and the nanotubes are partially oxidized, both exhibit a negative surface charge, and thus, any forces driving them to associate with one another must inherently be short-range van der Waals in nature. The coverage of nanoparticles adsorbed to the surface of the nanotubes was shown to increase exponentially with increasing surface area. Specifically, there was a strong quadratic relationship between the CNT surface area and the number of bound nanoparticles. Although this was unexpected, it was attributed to van der Waals interactions becoming increasingly efficient with increasing carbon nanotube concentration, which was consistent with

previous literature precedent regarding van der Waals forces with fullerenes. Two different sizes of particles were used, both showing this same effect. It was also demonstrated that although larger nanoparticles exhibit higher surface charge, they also exhibit stronger van der Waals forces, resulting in greater nanoparticle adherence to the nanotube surface. Different nanotube parameters were also probed, with longer and wider multiwalled nanotubes resulting in greater nanoparticle coverage than shorter and thinner nanotubes, respectively. Using these data, they were able to define a mathematical relationship between system design parameters (such as those discussed above) and the degree of nanoparticle coverage, allowing for the density of 1-D chains of nanoparticles to be tuned.

An interesting example of CNT-based templating has been demonstrated by Liz-Marzán and co-workers, wherein the 1-D CNTs are used to assemble nanorods.[1040] In this work, the nanorods were deposited by a layer-by-layer technique that had been previously used to assemble Au and Au@SiO_2 NPs onto CNTs.[1041,1042] The nanorods were synthesized in CTAB, which was subsequently exchanged with poly(vinylpyrrolidone). The carbon nanotubes were first wrapped with negatively charged poly(styrenesulfonate) and then with positively charged poly(diallyldimethylammonium chloride). When these two solutions were combined, the nanorods were shown to preferentially associate with the CNTs with their long axes parallel to the long axis of the nanotube. Interestingly, rather than forming a uniform layer across the entire tube, the nanorods formed stripes on either side of the CNT. This lack of full coverage was attributed to the anisotropic surface potential of the nanorods, which decays more rapidly at the highly curved nanorod tips. Furthermore, the optical properties reflected uniaxial plasmon coupling, indicating that the nanorods were aligned along the CNTs in an end-to-end fashion only. Rods with different aspect ratios were used, and the UV−vis measurements demonstrated that the longitudinal plasmon band of the nanorods broadened and red-shifted upon assembly, while the transverse plasmon band remained relatively unchanged. By embedding the assembled materials in a polymer and then stretching and gently heating the polymer film, they also demonstrated the ability to align the nanorod assemblies relative to one another. Importantly, polarization of the light used to probe the sample at an angle parallel to the rods' long axes resulted in suppression of the transverse plasmon band, while polarization of the light perpendicular to this direction resulted in suppression of the rods' longitudinal band.

Naik and co-workers have developed methods to use biomolecules (DNA and peptides) to template the assembly of gold nanoparticles on CNTs in a chemically reversible manner.[1043] Here, the authors used dielectrophoresis to position DNA-coated CNTs on electrode patterns, followed by the addition of Pt^{2+} ions and peptide-stabilized AuNPs to coat the surface of the CNTs. Electrostatic interactions between the positively charged platinum ions and the negatively charged DNA and peptides directed the AuNP assembly process. The addition of ethylenediaminetetraacetic acid removed the Pt^{2+} ions, thereby removing the AuNPs from the surface of the CNT. McCall and co-workers have also demonstrated the use of DNA to template gold nanoparticles on CNTs, although they used DNA-based recognition interactions instead of electrostatics.[1044] Other methods to coat CNTs with nanoparticles include sonication-assisted deposition,[1045] chemical functionalization strategies,[1046−1049] hydrophobic and hydrogen-bonding interactions,[1050−1052] and electrostatic interactions.[1053]

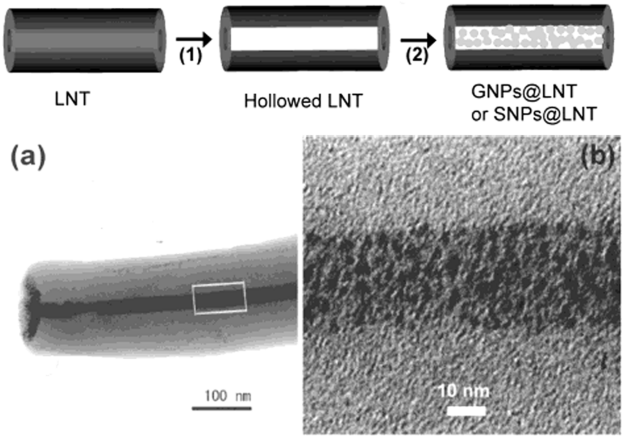

Figure 45. Schematic and TEM images of hollow lipid nanotubules that are filled with gold or silver nanoparticles. The box in (a) is the magnified area in (b). Adapted with permission from ref 1054. Copyright 2004 American Chemical Society.

7.3. Supramolecular Assemblies

Supramolecular templates can be created by arranging small molecules into defined nanometer-scale shapes, or extended arrays, and subsequently using these objects as scaffolds to assemble plasmonic nanoparticles. An excellent example given by Shimizu and co-workers used hollow nanotubes of assembled glycolipids as a template to form 1-D arrays of both gold and silver nanoparticles (Figure 45).[1054] When placed in an aqueous environment, the lipids naturally assemble with near 100% efficiency into tubes that vary in length from tens to hundreds of micrometers. The width of the tubes is highly monodisperse, with the outer diameter being ∼200 nm and the diameter of the hollow inner portion ranging from 30 to 50 nm. This corresponded with a tube that is ∼16 lipid bilayers in thickness, which gave the tubules structural rigidity, even in the absence of water. Solutions of nanoparticles were initially not found to readily enter the tubules when dispersed in water. However, by first lyophilizing the tubules to remove all solvent and then redispersing them in a solution containing nanoparticles, capillary forces allowed the nanoparticles to penetrate into the hollow tubule interior. The yield of this infiltration was found to be ∼30% for particles smaller than 4 nm in diameter and 10% for particles that were 15−20 nm in diameter, and no infiltration was observed for particles that were 50 nm in diameter (larger than the size of the tubule's hollow interior). TEM images revealed that the nanoparticles remained discrete once inside the tubule, forming long 1-D arrays of individual nanoparticles. The authors then probed the use of this template as a means of creating long, continuous 1-D structures by thermally decomposing both the tubule and the nanoparticles. By firing in air at different temperatures, nanowire-like gold nanoparticle assemblies, chains of discrete nanoparticles, and continuous polycrystalline gold wires were obtained.

Lvov et al. also presented a method to template nanoparticles onto tubules using zwitterionic lipids, although in this case, when AuNPs were used, the nanoparticles typically formed caps at the end of the tube structure.[1055] Alternatively, Korgel and co-workers have assembled sub 2 nm diameter dodecanethiol-coated Au nanoparticles inside phosphatidylcholine lipid vesicles made by an extrusion process.[1056] Here, the nanoparticles assembled into the hydrophobic core of the lipid bilayer without

disrupting their structure, thereby forming hollow pseudospherical nanoshell structures.

Liquid crystals formed from small-molecule components are another type of molecular assembly template that, rather than creating discrete assembled objects, can be used to create large-scale assemblies of plasmonic materials.[1057] While the ordering of nanoparticles within these matrixes is generally not as precise as other methodologies, they provide the distinct advantage of inducing particle alignment over large areas, which allows interesting optical effects to be probed for bulk-scale materials. A recent example of this is the work by Smalyukh and colleagues, who aligned gold nanorods in surfactant-based liquid crystals.[1026] The specific system examined was a mixture of CTAB, benzyl alcohol, and water, with which they were able to create both nematic and hexagonal liquid crystal phases. The difference between these two is that the nematic phase exhibits only orientational ordering and the hexagonal phase exhibits both orientational and hexagonal planar ordering. After addition of a solution of gold nanorods to these mixtures, the samples were aligned by either shearing the material between two glass plates or putting the sample under a strong magnetic field. Freeze-fracture TEM images demonstrated that the nanorods were well dispersed and aligned in a single direction along their long axes, but exhibited no long-range, 3-D order. Because nematic liquid crystals can be aligned by applying magnetic fields, this allowed for the optical properties of this system to be modulated and examined. When placed under a 11.7 T magnetic field, the particles and the surrounding rod-like micelles of the surfactant oriented along the field and preserved this orientation once the field was turned off. When the plasmonic properties of these materials were measured with polarized light, it was found that the longitudinal and transverse SPR peaks were nearly completely suppressed for rods aligned perpendicular and parallel to the direction of the light polarization, respectively. Similar work has been conducted by several others who have demonstrated methods to tune the plasmonic properties of gold nanoparticles in liquid crystals via the application of an electric field.[1058,1059]

Because of the diversity of these interactions, a huge variety of liquid crystal phases and nanoparticle combinations have been demonstrated. For example, demixed nematic lyotropic liquid crystalline phase formations in dispersions of long (6.8 μm) silver nanowires and spherical nanoparticle aggregates in mixtures of ethylene glycol and water have recently been reported by Davis and colleagues.[1060] In addition, Hegmann and co-workers have provided examples of nematic liquid crystals consisting of gold nanoparticles and chiral molecules[1061] and liquid crystals of gold nanoclusters in bolaamphiphilic liquid solutions.[1062] Both Kanayama et al.[1063] and In et al.[1064] have developed methods to covalently attach molecules that induce liquid crystal ordering directly to the surface of gold nanoparticles. Finally, in an interesting application-based investigation, Boyd and co-workers demonstrated a method for using liquid crystal-templated nanorod assemblies as potential drug delivery vehicles.[1065] By irradiating nanorods at their plasmon resonance, local heating of the liquid crystals induced a phase transformation from inverse bicontinuous cubic to hexagonal to inverse micellar, which was projected to be useful as a drug-release mechanism.

7.4. Polymeric Molecules

In addition to assemblies of molecules, polymers present an obvious choice of organic molecules to template the formation of plasmonic materials, as they are readily synthesized and have tailorable chemical functionalities. The majority of polymer-based templating of plasmonic structures is done with block copolymers, but important examples exist with other varieties of single-component polymers that can be used to template distinct sizes or shapes of assembled nanostructures.

7.4.1. Single-Component Polymer Templates. An early example of utilizing polymers to template nanoparticle assemblies of controllable sizes was shown by Rotello and co-workers.[1066] In this work, 2 nm AuNPs functionalized with alkanethiol-modified thymine molecules were templated on polystyrene modified with diaminotrizine (DAT) moieties. DAT and thymine are known to associate via three hydrogen bonds, creating a stable interaction between the particles and the polymer. When combined, solutions of polymer and AuNPs in organic solvent (such as dichloromethane or chloroform) resulted in the rapid formation of a black solid. The precipitate was insoluble in nonpolar solvents, but polar liquids such as tetrahydrofuran and methanol could be used to dissolve a large portion (>80%) of the solid. Small-angle X-ray scattering demonstrated that the distance between particles adhered to the polymer template was approximately 6.4 nm. The proposed mechanism of formation was one of nanoparticle-induced polymer unfolding. In nonpolar solvents, the DAT-functionalized polystyrene molecules fold into a highly compact structure due to hydrogen bonding between the DAT units. As the nanoparticles were introduced, they bound to the DAT moieties in a multivalent fashion, causing the polymer to unzip and expose more DAT molecules to the solution to bind more nanoparticles. The resulting spherical clusters were ~100 nm in diameter with ~20% polydispersity, correlating to ~3000−7000 nanoparticles per sphere. By using temperature to control the thermodynamics and kinetics of assembly, different sizes of aggregates could be synthesized. At 10 °C, large networks were formed instead of discrete spheres, and at −20 °C, larger spherical particles (~500−1000 nm) were formed. This indicates that the large networks are possible intermediate structures on the way to discrete assemblies.

Srivsatava, Frankamp, and Rotello have provided another example of tunable, plasmonically active materials, using PAMAM dendrimers to control interparticle spacing.[1067] In this process, a solution of AuNPs was added to a large excess of dendrimer in methanol. Electrostatic attraction between the terminal amines on the dendrimer and the carboxylic functionalization of the AuNPs facilitated the formation of a NP−dendrimer complex. Because the amount of dendrimer greatly exceeded that of the AuNPs, complete surface coverage of each AuNP was achieved. By varying the generation of the dendrimer (G0−G4), the spacing of 6.2 nm AuNPs was varied between 0.6 nm for G0 dendrimers to 1.9 nm for G4 dendrimers. UV−vis studies revealed that the SPR of the assembled AuNPs red shifted, with the greatest change in peak position being observed for the shortest dendrimers. While the G0 SPR was red-shifted nearly 60 nm relative to the SPR of AuNPs free in solution, the G4 SPR was much closer to the standard solution SPR (red shifted by about 15 nm), implying that interparticle spacings of >3 nm are sufficient to prevent plasmon-coupling interactions in particles of this size.

In contrast to the above examples, a number of surface-based methods have been combined with polymer templates to generate interesting nanoparticle assemblies. For example, Li and Li have reported an approach to polymer-based surface patterning

in which single crystals of thiol-capped polyethylene oxide (PEO) were used to control the localization and interparticle spacing of AuNPs.[1068,1069] In these examples, the authors utilized the fact that many long-chain polymers will fold onto themselves upon crystallization (from either a melted or solution-dissolved state), forming 5−20 nm wide quasi-2-D lamellae. This folding was used to control the density of thiol groups on the surface of the crystal, to which AuNPs could be grafted. As higher molecular weight polymers have proportionally fewer thiol groups, the AuNP decoration density was proportional to the weight of the polymer used. Initially, simple square-shaped regions of AuNPs were patterned, but in subsequent studies, an iterative PEO crystallization process was used to generate more complex structures such as square-shaped rings of varying thicknesses and single-crystal structures with different nanoparticle types confined into different regions of the superstructure.[1069] In an alternative approach, Bockstaller and colleagues have demonstrated a polymer-based method to assemble gold nanoparticles into semiordered arrays.[1070] When both gold and silica nanoparticles were functionalized with polymers and dried onto a substrate, they obtained hexagonal local ordering of the silica particles, with the gold nanoparticles filling into interstitial areas in a disordered fashion. Additional work has been carried out by Prasad and co-workers, who have shown a method to create chirally ordered polymer−nanoparticle composites that exhibit chiral optical activity at the wavelengths corresponding to the plasmon band of the nanoparticles.[1071] Furthermore, Zubarev and co-workers have developed a method to assemble polymer-coated nanorods into 2-D, circular rings via phase separation and drying effects.[1072]

Several groups have used polymeric templates to create dynamic assemblies that are sensitive to the environmental conditions. For example, Akamatsu et al. have developed a PVP-based microgel that responds to changes in the local pH.[1073] In addition, Gupta et al. have developed responsive polymer−NP systems and employed them as solvent sensors.[1074] In this work, the authors selectively swelled and collapsed polystyrene brushes through changing the solvent (for example, toluene vs acetone). As the polymer brush contracted due to changes in solvent, the plasmonic interaction of the neighboring AuNPs bound to the brush caused shifts in the SPR. The location of the SPR peak was used to determine the composite's local solvent environment.

7.4.2. Block Copolymer Templates. Block copolymers (BCP) are a particularly well suited class of materials for use as templates for generating nanoscale architectures, as tailoring the number and relative position of monomer units dictates the properties of a BCP−NP composite.[1075−1082] Specifically, spatial control over discrete chemical moieties allows one to direct the assembly of polymeric structures or thin films with different morphologies and to selectively incorporate plasmonic materials to different areas within the final BCP structure. In addition, chemical control over the individual substituents provides a means to influence the interactions between the BCP and nanoparticle components. Here, we will briefly discuss important advances in the synthesis of BCP−NP composites, focusing on the different ways chemical and physical morphologies of the polymers have led to unique nanoparticle assemblies with interesting optical propeties[1083] that have proven useful in many plasmonic systems.[1084]

Despite some early examples of nonplasmonic BCP−nanoparticle composites (see above citations for a detailed summary), Schrock and co-workers were among the first to demonstrate the integration of plasmonically active NPs into the microdomains of a BCP as early as 1992.[1085−1087] In these studies, the authors synthesized a family of modified cyclodecene-*b*-diphenylphosphine-biscycloheptane copolymers. Metal salts (Ag, Au, Pd, or Pt) were added to a solution of the polymer and selectively complexed with the phosphinated block. The copolymer was then allowed to phase separate and after thermal annealing, the resulting metal nanoclusters were confined to either lamellar or cylindrical domains corresponding to the biscycloheptane-based block. Similar work carried out by Saito et al. employed a more conventional poly(styrene-*b*-vinylpyridine) (PS-*b*-PVP) copolymer to assemble Ag nanoparticles.[1088] After domains were formed through phase separation, Ag ions selectively entered the lamellar PVP domains and were subsequently reduced with hydroquinone, producing ordered arrays of Ag nanoparticles.

In addition to metallic nanostructures being generated within phase-separated BCP films, the formation of nanoparticles prior to BCP-mediated assembly provides an additional means to both control the reaction conditions during the particle synthesis and better modulate the plasmonic properties of the final structure. For example, Möller and co-workers demonstrated the sequential complexation of metal precursors into BCP micelles followed by nanoparticle synthesis and polymer phase separation as a means to obtain an ordered array of nanoparticles within a BCP film.[1089] Sita and colleagues investigated an alternative approach of selective attachment of presynthesized nanoparticles to phase-separated microdomains of a PS-*b*-PMMA BCP.[1090] Building on this early work, Acharya et al. used a PS-*b*-P4VP BCP micelle in a two-step process to create a more complex Ag/Au nanoparticle composite film.[1091] In this case, the Ag nanoparticles were generated through in situ reduction of Ag ions and the Au nanoparticles were synthesized separately and added during the BCP film formation. As a result, the AgNPs were localized in the core of the BCP micelles while the AuNPs decorated the periphery of the structures. By varying the ratio of the initial Ag ions to AuNPs, the final ratio of the Ag to Au nanoparticles could be controlled. Unsurprisingly, the characteristic SPR band of the sample varied linearly (over a range of approximately 100 nm) with the relative amount of AgNPs and AuNPs present in the composite. Furthermore, the authors varied the molecular weight of the copolymer separating these two particle types to control the interparticle spacing and plasmon coupling. Interestingly, it was found that the SPR peak of the composite film red shifted with increasing interparticle distance due to decreased plasmon coupling. These examples represent a powerful method of BCP-based templating of plasmonic particles as the ability to integrate fully formed NPs into BCP templates allows for the possibility of creating more complex nanostructures.

Zubarev et al. have used amphiphilic polymers to assemble tubule structures of gold nanoparticles via chemical attachment of the polymer to the nanoparticle surface (Figure 46).[1092] A V-shaped polystyrene-*b*-poly(ethylene oxide) amphiphile was synthesized, containing a centrally located carboxylic group that was used to attach the polymer to phenol-functionalized ∼2 nm gold and silver particles. When these polymer nanoconjugates were placed in a THF solution and water was added in a dropwise fashion, they assembled into hollow cylindrical tubules approximately 20 nm wide and 100 nm long. The addition of methanol to the solution, on the other hand, induced the formation of spherical and short rod-like assemblies. It was also shown that the assembly process required that the length of the polymer be

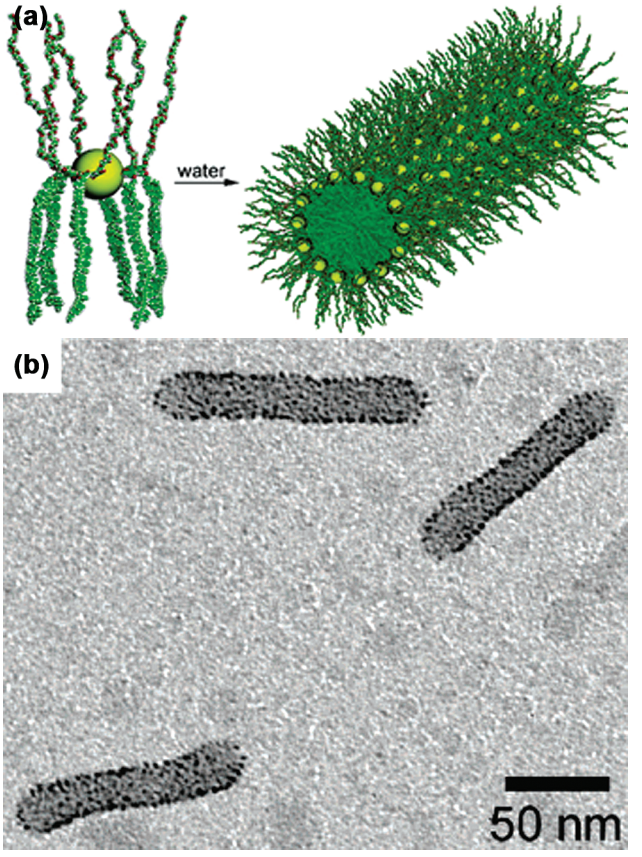

Figure 46. Block copolymer-templated assembly of discrete nanostructures: (a) schematic and (b) TEM image of AuNPs functionalized with a block copolymer that drives the assembly of tubule structures in the correct solvent conditions. Adapted with permission from ref 1092. Copyright 2006 American Chemical Society.

significantly longer than the diameter of the particles; otherwise the assembly process resulted in the formation of disordered aggregates.

Major advances in the intricacy of BCP-templated metallic nanostructures have been achieved through several diverse approaches. Examples include the demonstration of hierarchical assembly across molecular, nanometer, and micrometer length scales,[1066,1093] fabrication of multilayer structures containing plasmonic particles,[1094] the use of metal ion doping to create continuous metal sections rather than nanoparticles in microdomains,[631] and the early development of nanoparticle arrays with more precise ordering.[1095] In a particularly elegant example, Bockstaller et al. devised a synthesis methodology to make ternary BCP−NP mixtures.[1027] In this case, small (<4 nm) AuNPs were selectively localized at the junctions of poly(styrene-*b*-ethylene propylene) microdomains, while larger (>20 nm) silica particles were localized in the center of the ethylene/propylene phase (Figure 47). Although both particles were coated with aliphatic side chains, the authors reasoned that the selective localization was purely a result of the particle size. These conclusions were supported by other groups' theoretical calculations, which showed that interfacial segregation of particles is expected to occur for particles with diameters less than 20% of the characteristic BCP lamellar microdomain width.[1096] Conversely, particles with diameters greater than 30% of the microdomain width are expected to localize near the centers of the domains.

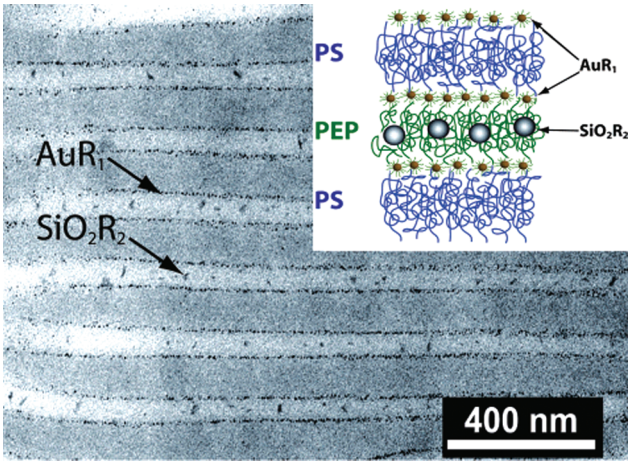

Figure 47. TEM image of block copolymer-templated assembly of Au and SiO_2 nanoparticles into lamellar arrays. Inset: Schematic of the particle distribution within the template. Adapted with permission from ref 1027. Copyright 2003 American Chemical Society.

Others have improved upon the traditional BCP−NP assembly strategy by reporting that more precise control over particle localization in a BCP can be achieved by rationally designing chemical monolayers on the NP surface.[1097] Au particles that were uniformly functionalized with a homopolymer (e.g., polystyrene) and then added to a BCP (e.g., PS-*b*-PVP) were found to localize in the center of lamellar domains. This is because the BCP ends are commonly localized in the center of the mircodomain, and the homopolymer monolayer on the AuNPs preferentially interacts with the BCP ends. Conversely, if the AuNPs were functionalized with a mixture of PS and PVP, the particles were found to localize at the junction of two lamellar microdomains. Emrick, Russell, and co-workers demonstrated similar control through careful use of AuNP monolayer and processing conditions (e.g., spin coating vs dip coating).[1098]

The applicability of BCP−NP assemblies has been demonstrated through the construction of complex materials with unique physical properties, such as the first examples of BCP−NP composite based photonic structures.[1099] Bockstaller and colleagues demonstrated that polystyrene-functionalized Au nanoparticles could be confined to the lamellar sections of a poly(styrene-*b*-ethylene propylene) (PS-*b*-PEP) BCP.[1027] These AuNPs served to increase the dielectric contrast between microdomains of the materials, leading to more dramatic photonic properties. As a result, the reflection of light was increased at visible wavelengths over that of the non-AuNP-doped sample. This work was expanded upon in 2003, when the authors revisited the system and synthesized a variety of lamellar PS-*b*-PE/PPE copolymers.[1100] As before, adding oligostyrene-functionalized nanoparticles to the BCP during solvent annealing led to the localization of NPs to the PS lamellae. By varying the volume fraction of AuNPs in the polymer from $\phi = 0$ to $\phi = 0.12$, the peak reflectivity red-shifted from ~550 to ~630 nm. To understand this effect, the authors modeled the system with a Gaussian-broadened polynomial superposition parametric dispersion model centering on effective medium concepts; their results confirmed that polydispersity in particle size strongly impacts the validity of the calculated results and that dielectric functions of bulk materials cannot be substituted for nanostructures.

Additional functionality can be imparted to plasmonic structures templated with BCPs by introducing methods to dynamically control interparticle spacing in domains containing the plasmonically active components.[1101] Liz-Marzán and co-workers have reported one example where gel microsphere cores of an *N*-isopropylacrylamide−allylacetic acid copolymer surrounded by Au nanorods form a pH- and temperature-responsive assembly.[1102] In this work, they demonstrated that the collapse of the microgel core enhances the plasmonic interactions between the nanorods and, above a critical packing density, causes the longitudinal SPR of the Au nanorods to red-shift by approximately 55 nm.

While the work presented so far has primarily described the assembly of spherical nanoparticles on BCP templates, several notable reports have described incorporation of anisotropic metal nanoparticles into BCP microdomains, allowing the more complex optical properties inherent to these materials to be harnessed in BCP−NP composites. One example can be found in the work of Deshmukh, Liu, and Composto, who synthesized Au nanorods functionalized with polyethylene glycol brushes.[1103] These nanorods were first added to a PS-*b*-PMMA BCP prior to solvent annealing. After 2 days, lamellar films were generated with nanorods localized in the PMMA domains; these rods were localized in the interior of the thin film, rather than being localized on its surface. Interestingly, since the width of the PMMA domains (∼34 nm) was chosen to be less than the length of the rods (∼48 nm) but slightly larger than their diameter (∼18 nm), the nanorods self-aligned with a preferential orientation parallel to the lamellar structure. Additionally, these structures were more localized to the lower surface of the films, and it was proposed that this was a result of the natural solvent gradient that occurs during annealing when solvent evaporates from the surface first, driving rods to lower portions of the film.

Park, Achermann, and others have provided another excellent example of how one can use BCPs to create a template for the formation of highly anisotropic nanomaterials with interesting plasmonic properties.[1104] In their work, PS-*b*-P4VP was solvent annealed to produce cylindrical arrays which were subsequently immersed in a Au salt solution to complex Au ions with the P4VP domains, and both $NaBH_4$ and oxygen plasma were used in different experiments to reduce the Au ions. In the latter case, the plasma removed the entire BCP template and generated an array of AuNPs that were each 17 nm wide and 13 nm tall and were separated by 43 nm; scanning force microscopy (SFM), extinction measurements, and theoretical calculations were used to confirm the particle dimensions. The authors then adapted this synthesis by blending PS-*b*-PEO with a PS-*b*-P2VP copolymer. Through several solvent annealing steps and sequential addition of $LiAuCl_4$ and $AgNO_3$, Au ions were selectively localized in PEO microdomains, while Ag ions were locally sequestered into P2VP sections. Similar to the previous experiment, scanning electron microscopy (SEM) and optical measurements confirmed the generation of asymmetric, separate Ag and Au particles in a quasi-hexagonal array. By generating these AuNP arrays on top of SiO_2-coated Ag film substrates, the researchers could control the degree of interaction between the BCP−NP SPRs and the SPPs of the underlying Ag film by tuning the thickness of the SiO_2 layer. Compared to Ag-film-only samples, SPPs in the hybrid BCP−NP composite films exhibited larger angle-resolved SPP coupling wavelengths and dispersion relations that corresponded to larger wave vectors. Additionally, increasing the spacer layer thickness also led to larger angles and wave vectors. Since increased wave vectors imply slower wave propagation and, therefore, larger field enhancements, the authors state that this approach could prove useful in systems or properties reliant on high electromagnetic fields.

8. ASSEMBLY WITH PHYSICAL TEMPLATES

Physical templates are defined in this work as those that function as a scaffold onto which preformed plasmonic materials can be deposited or assembled. Therefore, it is the physical shape of the template that defines the geometry of the final composite structure and, as a result, its collective plasmonic properties. To function in this manner, such templates are usually significantly larger than the nanomaterial being deposited and are typically made of inorganic materials, although some polymer-based templates will also be highlighted. The advantage of using these types of templates is the range of shapes that can be utilized to pattern plasmonic materials. They can exist as large arrays, for example, the pores of AAO,[1105,1106] as discrete particles in solution, such as colloidal suspensions of silica spheres,[1107,1108] or even as more exotic shapes, such as CdTe tetrapods.[1109] Unlike some of the templates covered in previous sections, wherein the chemical groups used to assemble particles are responsible for their geometric arrangement, these physical templates typically rely on nonspecific adhesion of the particles to the surface of the template. As a result, this type of assembly strategy is extremely straightforward to implement and is generalizable to many different plasmonic nanostructures.

8.1. Solution-Phase Templates

Similar to the work discussed in section 3.2, where nanoparticles are nucleated at the surface of colloidal silica spheres, a significant amount of research has been conducted on the use of colloidal structures to template the assembly of nanoparticles. In this section, we will discuss physical templates that are solution-dispersed nano- or microscale objects. A typical example of a colloidal template is a solution of microspheres, although other examples exist. These templates can generally be divided into two classes on the basis of their shape: spherical or pseudosperical templates and anisotropic templates with distinct morphologies.

8.1.1. Spherical Colloidal Templates. Spherical and pseudospherical templates present the most common form of colloidal structure for assembling plasmonic nanomaterials, as they are easily prepared by a large number of methods with a diverse array of compositions. One of the most commonly used templates is a silica sphere, early examples of which have been provided by Halas and co-workers.[264,1107] In each of these cases, gold nanoparticles and gold nanoparticle clusters were assembled on silica spheres approximately 100 nm in diameter. In the first example,[264] silica spheres were prepared in ethanolic solution and functionalized with different silicon-containing molecules and then added to a solution of gold nanoparticles. When the silica spheres were coated with APTMS, the gold nanoparticle coverage was ∼30%, with individual particles well separated from each other. When the gold nanoparticle solutions were diluted with various mixtures of ethanol and water prior to addition of silica spheres, the gold nanoparticles were found to form small clusters consisting of tens of particles, and these clusters assembled at the surface of the spheres. Varying ratios of APTMS to PTMS, along with varying ratios of water to ethanol, resulted in different morphologies, ranging from discrete nanoparticles to nanoparticle clusters. It was found that high amounts of ethanol were necessary to form clusters, with larger amounts of APTMS

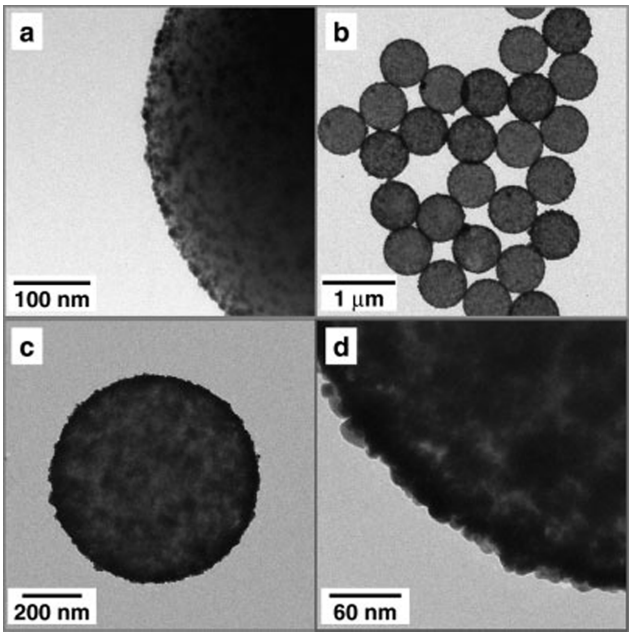

Figure 48. TEM images of silica particles used as templates for the assembly of sparse (a, b) and dense (c, d) coatings of AuNPs. Adapted with permission from ref 1108. Copyright 2002 Wiley-VCH Verlag GmbH & Co. KGaA.

resulting in less ethanol necessary to induce this effect. While amine-containing small molecules exhibited heavy coverage of nanoparticles, thiol- and phosphate-containing molecules exhibited limited or no coverage, and molecules with only methyl groups were not able to bind with the gold nanoparticles at all. It was proposed that the ethanol in the solution affected the nanoparticle binding and clustering capabilities by both changing the dielectric constant of the medium surrounding the particles and inducing more local effects such as hydrogen bonding between small molecules at the surface of the particles. Similar results have been found by Ma and co-workers,[1110] Wei and co-workers,[1111] and Osterloh and co-workers.[1112]

Further progress enabled the development of methods to template the assembly of AuNPs on colloidal spherical particles with full coverage of the spheres. Previous limitations were predominantly due to Coulombic interactions, where electrostatic repulsive forces prevented dense nanoparticle coverage. Caruso and colleagues presented a means to overcome this problem with a single deposition step in 2002 by using polyelectrolyte coatings on the surface of the template spheres (Figure 48).[1108] Gold nanoparticles were first synthesized in toluene and then transferred to an aqueous phase via the addition of 4-dimethylaminopyridine making them positively charged. The polystyrene spheres used as templates were negatively charged, and introduction of these templates to a solution of gold nanoparticles for 12 h resulted in approximately 30% coverage of the spheres. More dense coverage was obtained by first assembling four layers of polyelectrolytes on the surface of the polystyrene, creating a 5 nm thick layer that terminated in a negatively charged surface. Upon addition of gold nanoparticles, a 10−15 nm thick layer of nanoparticles was observed, indicating that the nanoparticles were able to infiltrate the polyelectrolyte coating. This was confirmed by changing the number of layers of polyelectrolyte, which resulted in different degrees of nanoparticle loading. They were also able to create solid coatings using these spheres through electroless deposition of gold.

Caruso et al. have demonstrated a similar technique, wherein a thin layer of silica-coated gold particles were assembled on polystyrene microspheres via a layer-by-layer assembly approach.[1113] Alternating depositions of the Au@SiO_2 particles and poly(diallyldimethylammonium chloride) allowed for the formation of shells of tunable thickness. Initial polystyrene spheres were ∼640 nm in diameter and were primed with polyelectrolyte films to create a smooth featureless surface. After the spheres were coated with one, three, or five layers of Au@SiO_2 particles, the diameters increased to 700, 760, and 825 nm, respectively; this correlated to an individual layer thickness (either Au@SiO_2 or polyelectrolyte) of ∼16 nm. Although individual gold particles exhibited an extinction peak at ∼520 nm, increasing the thickness of the assembled shells red shifted the plasmon resonance to 588, 618, and 642 nm. Interestingly, calcination of these structures resulted in the formation of hollow spheres. Heating the samples to 450 °C facilitated both the removal of the polystyrene core and the sintering of the silica layers coating the gold nanoparticles. The resulting hollow spheres were observed to be mesoporous for shells up to three layers thick, after which complete spheres were observed. Due to the thinness of the silica shells that were used, some of the gold spheres were observed to fuse together, resulting in slight red shifting of the plasmon peak. A similar process involving AuNPs embedded in SiO_2 spheres has also been demonstrated by Graf et al.[1114] This work is distinct from the synthesis of Au@SiO_2 particles, as it involved a layer-by-layer type of assembly of AuNPs on SiO_2 templates, followed by an overgrowth of silica to create silica particles with multiple embedded AuNPs. Caruso and co-workers have also demonstrated the assembly of these AuNP-coated polystyrene templates into ordered arrays.[1115] On the other hand, Braun and co-workers have recently demonstrated an opposing technique, wherein the assemblies were created first and then used as templates for gold nanoparticles.[1116] Several additional examples of these types of templates are covered in section 8.2.2. Finally, nanoparticles of different material compositions (such as silver) have also been assembled on both silica spheres[1117,1118] and polystyrene spheres.[224,1119]

Wang and colleagues have recently presented an example of how spherical colloidal templates can be used to tune the optical response of plasmonic materials.[1120] Hollow mesoporous silica microspheres (HMSMSs) of sizes ranging from 1.04 to 2.53 μm with a ∼100 nm thick silica shell were used as templates for the assembly of gold nanoparticles, including both spheres and rods of different dimensions (diameter ∼20−30 nm, aspect ratio 1−4). The nanoparticles were coated in thiol-terminated polyethylene glycol molecules and attached to the surface of the spheres by mixing the two components together. Light scattering spectra were first obtained for the silica spheres alone, demonstrating that they matched calculated Fabry−Perot interference patterns. Upon addition of the gold nanoparticles, the scattering spectra were observed to shift considerably, with scattering peaks at shorter wavelengths decreasing in intensity and peaks at longer wavelengths increasing significantly. Interestingly, this enhanced region coincides nearly completely with the SPR of the adsorbed nanoparticles. It was hypothesized that the localization of the excitation light at wavelengths corresponding to the SPR peak of the AuNPs facilitated coupling into the HMSMSs, giving the observed enhancement effect. Furthermore, the scattering

enhancement factors were as high as 127 times those of the bare HMSMS particles and were found to be in direct correlation with the AuNP surface density on the HMSMS spheres.

In addition to spherical colloidal templates with interesting photonic properties, plasmonic nanoparticles have also been coupled to nanostructures with unique magnetic properties. An example is the work of Wang and co-workers, who utilized Fe_3O_4 particles as templates.[1121] Iron oxide nanospheres approximately 300 nm in diameter were first synthesized and coated with a thin layer of APTMS. This APTMS layer was then used to adsorb different nanoparticles, including gold, silver, and gold−platinum hybrid particles, via electrostatic interactions. Each of these hybrid materials was shown to have unique properties that may benefit different applications: Au/Fe_3O_4 hybrid materials were proposed as NIR adsorption materials that could be localized in living tissues by magnetic fields for photothermal therapies, Au/Pt/Fe_3O_4 materials were proposed as recyclable catalysts, and Au/Ag/Fe_3O_4 particles were proposed as SERS substrates. In all cases, relevant physical properties (NIR adsorption, high saturation magnetization, catalytic activity, and SERS enhancement) were measured and demonstrated that these materials showed promise in all of the proposed applications. Further examples of spherical templated structures with unique magnetic characteristics have been shown by a number of other groups.[1122−1124]

As an interesting counterpoint to the majority of the examples above which utilize templates of ∼100 nm or greater, Chen and co-workers have used gold nanoparticles as spherical templates for the assembly of other nanoparticles of commensurate sizes.[1125] Interestingly, in this size regime (20−40 nm), the particle size and electrostatic repulsion play a large role in dictating the symmetry of the resulting small clusters. By varying the solution ionic strength, discrete clusters with linear, trigonal, and tetrahedral geometries have been synthesized. These clusters were subsequently purified in high yields by density gradient centrifugation. Similar work was done by Grzybowski and colleagues wherein small spherical gold particles were attached to larger Fe_3O_4 particles and assembled with homobifunctional cross-linkers.[1126] The steric bulk of the Fe_3O_4 particles forced the assemblies into dimers, trimers, or tetramers, depending on the difference in size between the gold and iron oxide particles.

8.1.2. Anisotropic Colloidal Templates. Although spherical and pseudospherical particles are the most readily accessible colloidal structures, there are many different anisotropic shapes that can be made as templates, from relatively simple structures such as rods to highly complex architectures. Often, these anisotropic templates are made of materials that have interesting plasmonic effects themselves or other interesting optical properties that are affected by the presence of plasmonic nanostructures.

One example of such a structure has been synthesized by Kotov and co-workers and consists of a CdTe nanowire surrounded by plasmonic particles.[1127] This assembly provides a means to create and tune interesting optical phenomena as a result of the coupling between the two optically active components. Cysteine-stabilized CdTe nanowires (∼6 nm in diameter and ∼1 μm in length) and gold nanoparticles (∼4 nm in diameter) were synthesized and functionalized with biotin and streptavidin, respectively. As has been covered elsewhere (see section 6.2.2), the high affinity of biotin for streptavidin allows for the production of highly conjugated structures. This property was used to tune the local environment surrounding the CdTe nanowires and control their optical features. When solutions of the two particles were mixed, a 5-fold enhancement of the luminescence intensity, along with a concomitant gradual blue-shift of the luminescence peak, of the CdTe nanowires was observed. The extent of this enhancement could be tuned by adding different amounts of nanoparticles, with the 5-fold enhancement corresponding to a saturation of all the binding sites on the CdTe wire. These phenomena were examined with theoretical models, and the authors concluded that they were the result of the stimulation of photon emission by the high local electromagnetic field surrounding the AuNPs. The resulting assembly was also shown to be reversible via the addition of excess streptavidin, which resulted in AuNPs dissociating from the nanowire surface. This work was later expanded upon by the same group to create a protein-detection system.[1128] Gold nanoparticles were attached to CdTe nanowires via PEG molecules that were covalently bound to antibodies. Because the average length of this linker is dependent on the bound/unbound state of the antibody (through conformational changes in the antibody structure), the proximity of the AuNPs to the CdTe wire changed upon antigen binding. This could be monitored by emission wavelength shifts from the CdTd nanowires and was used to monitor the reaction progress. A shift of ∼8 nm was observed upon target binding, and this shift was reversed upon target release, providing a prototype system for protein or small-molecule detection. The same group has also developed CdTe−AgNP conjugated materials.[1129]

Long nanowires have also been used as templates for the assembly of other plasmonically active materials, such as in the work by Tsukruk and co-workers in 2008.[1130] Here, 65 nm diameter and several micrometer long silver nanoparticles were functionalized with a three-arm star polymer presenting azides at its tips. After exposure of this to a solution of 4 nm gold nanoparticles capped with propynyl 11-mercaptoundecanoate, click chemistry was used to couple the materials together. SEM, energy-dispersive X-ray spectroscopy (EDX), and high-resolution transmission electron microscopy (HR-TEM) were used to confirm the successful templating of the nanostructures, with nanoparticle grafting densities of approximately 80 nm^2 per particle (corresponding with ∼250 nanoparticles per 100 nm length of the silver rod). These rods were then examined by Raman spectroscopy, demonstrating that the composite materials exhibited significant enhancement of the signal intensity. Compared with undecorated silver wires, which only exhibited Raman signal enhancement at the intersection of two overlaid wires, the Raman scattering for the gold-nanoparticle-coated wires exceeded this scattering by an order of magnitude, and enhancement was observed across the length of the entire rod. Other examples of similar SERS enhancements from templated plasmonic nanostructures on silver and gold wires have been demonstrated by multiple groups.[1131−1135] $LiMo_3Se_3$ wires have also been used to template the assembly of gold nanoparticles,[1136] and conversely, gold nanorods have been used to template the assembly of iron oxide particles,[1137] where the plasmonic properties of the rods were used in photothermal ablation.

A more complex anisotropic template has been synthesized by Alivisatos and co-workers, consisting of CdTe tetrapod-shaped nanoparticles (Figure 49).[1109] Tetrapods are branched particles consisting of four equally long arms (tunable from 20 to 200 nm) extending in a tetrahedral arrangement from a single point. To utilize these particles as templates, the researchers synthesized CdTe tetrapods and deposited them on a silicon surface. Upon

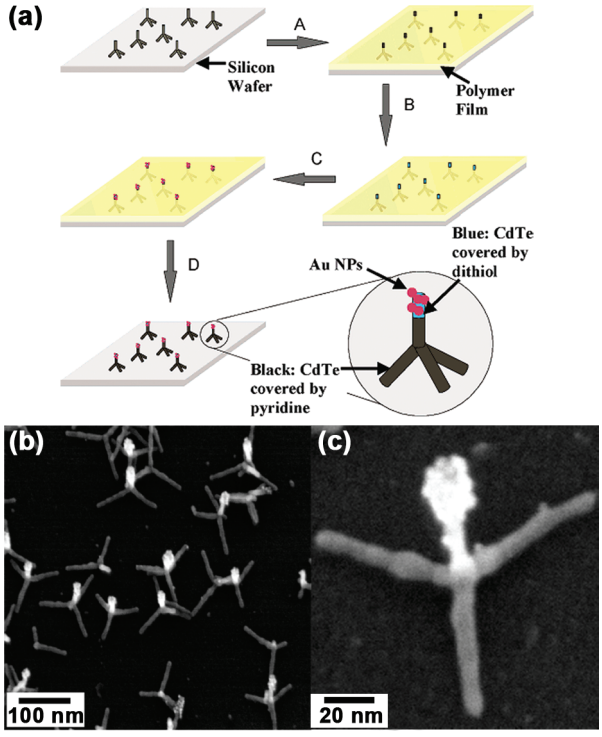

Figure 49. Assembly of nanoparticles onto an anisotropic template: (a) schematic of the coating of CdTe tetrapods with AuNPs on a single arm of the template, (b, c) SEM images of the assembled structures. Adapted with permission from ref 1109. Copyright 2004 Americal Chemical Society.

deposition, three arms of each tetrapod were in contact with the surface, with the fourth arm pointing in a direction perpendicular to the surface. The substrate was then spin coated with a thin layer of polymer, which covered only the bottom three arms of the tetrapod, leaving the top arm exposed for functionalization. The surface was then treated with an excess of hexanedithiol, which reacted with the exposed CdTe arm, leaving one remaining thiol available for binding to a separate particle. Exposure to trioctylphosphine-coated AuNPs (5 or 10 nm in diameter) resulted in nanoparticle conjugation to the CdTe tetrapods. The polymer films were then dissolved by the addition of organic solvents, and the samples were examined by SEM, confirming that the tetrapods were selectively functionalized with gold nanoparticles at the top of the previously exposed tetrapod arm (Figure 49b,c). Interestingly, applying mechanical force to the sample (by pressing a TEM grid onto the surface) usually resulted in the modified arms breaking off of the CdTe tetrapod. This created CdTe nanowires that were asymmetrically functionalized with gold nanoparticles only on a single end.

Another example of anisotropically functionalized semiconductor nanorods is the work by the Banin group, who have created discrete clusters of gold-tipped rods in a number of different arrangements.[355,1138] In their first work (see section 3.3.1), they developed a method to synthesize gold nanoparticles at the tips of CdSe nanorods and then assembled the rods via the addition of hexanedithiol molecules.[355] A more complex and controllable approach was later presented that utilized biotin disulfide and avidin proteins, where the relative stoichiometries of the individual components (biotin, avidin, and CdSe rods) dictated the formation of linear, branched, and flower-like structures.[1138] When the avidin molecules were added to the nanorods in a 1:2:2 (biotin:avidin:nanorod) ratio, they were able to achieve dimer structures, while adding equal amounts of each of the molecules resulted in both dimers and trimers. "Flower-like" assemblies were achieved via the addition of biotin and avidin molecules to smaller CdSe nanorods, where the reduced steric hindrance allowed multiple rods to complex around a single avidin cross-linking unit.

In a more recent example, Kumacheva and co-workers have shown that nanorods with faceted ends dictate the assembly of linear, branched, and circular chains.[1139] The nanorod structures in this work were synthesized to contain arrowhead tips, where each end had four specific facets. When these tips were functionalized with thiol-terminated polystyrene and the rods were subsequently added to solutions of dimethylformamide and 15% water, the polystyrene molecules on neighboring nanorods associated to minimize interactions with the aqueous phase. This resulted in the observation of linear chains of nanorods that increased in their degree of polymerization as a function of time, reaching a maximum of ~20 nanorods per chain. Due to the faceted nature of the nanorod tips, the majority of the assembled structures had rods aligned end to end, with two adjacent rods aligned in either a parallel or a perpendicular conformation. In groupings of three adjacent rods, equivalent numbers of cis and trans confirmations were observed, and for assemblies with only a small amount of polymerization of the nanorods, cyclic structures were occasionally seen. Larger, extended assemblies also formed branched structures containing nanoparticles arranged in all three possible branching combinations (parallel−parallel, parallel−perpendicular, and perpendicular−perpendicular).

8.2. Surface-Based Templates

Similar to these solution-phase templates, many of the surface-based templates used to synthesize nanostructures have also been used for assembly. One of the main advantages of these techniques, which is also harnessed in the synthesis examples, is the ability to introduce longer range order on the basis of the morphology of the template or surface being used, potentially allowing many of the important coupling effects necessary for plasmonic applications. Examples covered in this section include porous templates (AAO and mesoporous) and assembled colloid surfaces. General descriptions of the morphologies, properties, and syntheses of each of these templates can be found in their respective synthesis sections (sections 4.1, 4.2, 5.1, and 5.2). Like in previous sections, although lithographic methods have provided an effective route to producing surface templates for the assembly of plasmonic nanostructures,[1140−1142] these methods will not be covered in this section.

8.2.1. Porous Materials. Like synthetic strategies, assembly of plasmonic nanostructures in porous membranes is primarily accomplished using AAO templates. In addition to the high density and order of the pores in AAO, which improves the plasmonic properties of the resulting structures, the walls can be functionalized using a variety of chemical and physical methods to facilitate the anchoring of metal nanostructures onto the walls. Among these methods, the two most common types of molecular anchors are those that chemically bind the nanoparticles through covalent bonds and those that physically bind the nanoparticles through electrostatic interactions. While initial research was focused on the development of chemical anchors based on silanization of the templates with thiol- and amine-containing

dx.doi.org/10.1021/cr1004452 |*Chem. Rev.* 2011, 111, 3736–3827

molecules, recent work has shifted to the physical attachment of AuNPs and AgNPs with charged polymers using developed layer-by-layer methodologies.

Among the first to template the assembly of plasmonic NPs on AAO, Schmid and co-workers functionalized the walls of AAO templates with mono-, di-, and trialkoxysilane molecules by heating in toluene solutions.[1105] Thiol and amine terminal groups were chosen for this work because of their affinity for and ability to bind AuNPs, which was demonstrated in similar studies on planar glass surfaces.[1143,1144] Vacuum filtration was then used to flow 13 nm AuNPs through the template to anchor particles onto the amine and thiol moieties on the molecules. TEM and absorbance measurements were used to confirm that particles had bound to the surface of the AAO, with coverage estimated to be 25% of a full monolayer. Importantly, absorbance measurements showed only a single peak at 525 nm, which suggests that only dispersed, nonaggregated NPs are on the template.[1105] In a subsequent study, the authors demonstrated a similar concept with more complex anchor molecules to Au and Pt particles.[1145] Similar to the preceding report, absorption measurements suggested the formation of dispersed AuNPs in the template pores.

Following up on these reports, Rubinstein and co-workers demonstrated the ability to use APTMS to create dense NP films on AAO pore walls that coalesce into free-standing NP nanotubes (Figure 50).[1106,1146] After initially modifying 220 nm diameter pore AAO templates with APTMS, citrate-stabilized 14 nm AuNPs were vacuum filtered through the pores until the efflux solution changed from clear to a deep red color, which is indicative of NPs passing through the already fully covered pores (Figure 50a). After drying, the AAO membrane was dissolved in 1.0 M NaOH, resulting in free-standing nanotubes comprised of coalesced AuNPs. Studies with SEM and TEM confirmed the particulate nature of the nanotubes (Figure 50 b−d), and optical studies in solution and immobilized on surfaces showed significantly red-shifted plasmon resonances (>650 nm) due to the coupling of particles in the nanotubes (Figure 50e).[1106] In these and in future studies, Ag, Pd, and mixed-metal NP nanotubes also have been and will be demonstrated.[1106,1146] Interestingly, by studying the morphology of these structures at different stages of formation, the authors were able to determine that the NP coalescing process began during the final stages of NP filtration and continued during drying.[1146] Recently, the complexity of these structures has been greatly enhanced by Voelcker and co-workers, who demonstrated the ability to controllably create discrete regions of NP coverage separated by regions of no NPs down the length of the pores.[1147]

In another method of attaching plasmonic NPs onto AAO pore walls, several research groups have utilized layer-by-layer deposition methodologies to physically bind the NPs using electrostatic interactions. In these methods, alternating layers of cationic and anionic polymers are bound to the AAO membrane and subsequently used to attach the NPs of interest. Commonly used cationic polymers include poly(allylamine hydrochloride) (PAH) and PDDA, and commonly used anionic polymers include PSS and PAA. Among the first to extend these concepts developed on flat surfaces to AAO membranes were Bruening and co-workers, who demonstrated the attachment of 12 nm AuNPs onto 230 nm diameter pore AAO membranes using alternating PAH and PAA for catalytic applications.[1148,1149] In their system, 0.02 M PAA was flowed through to bind to the positively charged AAO surface, followed by 0.02 M PAH to produce a more positively charged surface. The nanoparticles were then flowed through and attached to the surface, resulting in dispersed AuNPs decorating the AAO pore surface. As was expected, the Au colloid and PAH layers could be alternated for multiple iterations to produce an even denser coating of particles.[1148]

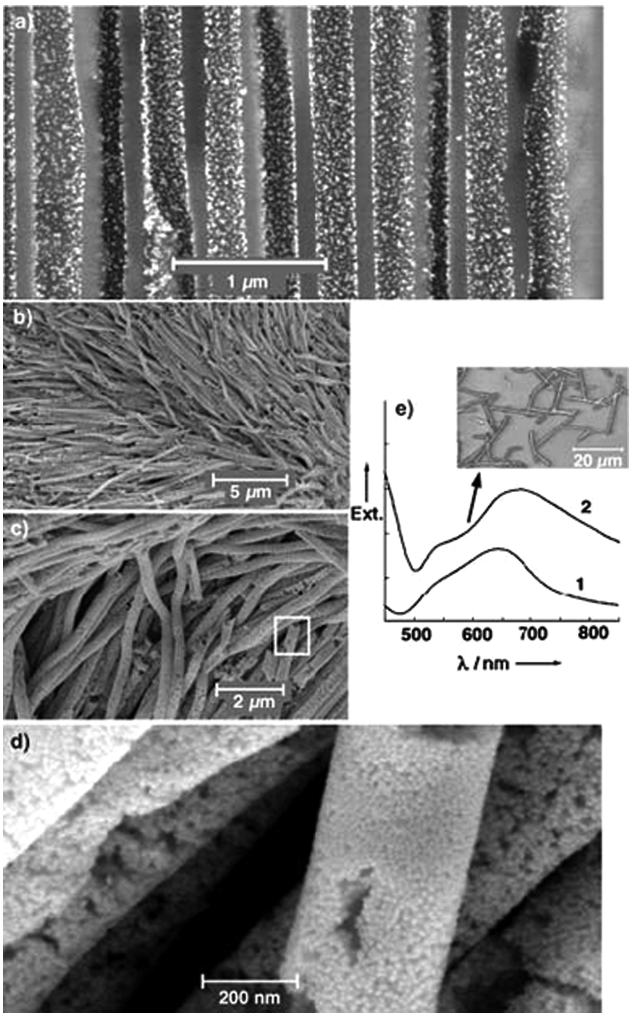

Figure 50. Fabrication of Au nanoparticle nanotubes in AAO: (a) SEM cross-sectional image of the AAO membrane template with 14 nm AuNPs chemically adsorbed to the walls, (b-d) SEM images of coalesced nanoparticle nanotubes after removal of the AAO template, (e) extinction spectra of Au nanoparticle nanotubes in solution (1) and dried on a glass surface (2). Adapted with permission from ref 1106. Copyright 2003 Wiley-VCH Verlag GmbH & Co. KGaA.

Importantly, Tsukruk and co-workers have recently used these polyelectrolyte layer-by-layer methods to assemble NPs in AAO for chemical detection using SERS.[1151,1150] In both examples, the membranes were found to be highly sensitive SERS sensors based on the arrangement of the particles in the pores, which act as optical waveguides to increase the Raman signal to unexpectedly high levels. In the first example, AAO membranes were decorated with AuNPs by first coating the templates with PDDA by spin coating from a 0.2% aqueous solution, followed by the introduction of 32 nm CTAB-stabilized AuNPs.[1150] SEM confirms the adsorption of dispersed, individual NPs down the length of the pores. 2,4-Dinitrotoluene (DNT), a model

nitroaromatic compound for trinitrotoluene (TNT)-based plastic explosives that is usually more difficult to detect because of its smaller Raman cross-section, was then drop evaporated on the membrane and detected using SERS. The DNT molecules are adsorbed to the AuNPs through interactions of the electron-donating amine groups in PDDA with the electron-deficient NO_2 groups in DNT, providing a detection limit of 10 fg with 785 nm laser excitation.[1150] In a subsequent report, Tsukruk and co-workers adsorbed the same CTAB-stabilized AuNPs onto AAO membranes coated with poly(ethylenimine).[1151] In this work, the CTAB concentration was varied to control the aggregation of particles on the pore walls by affecting the electrostatic repulsion between the particles and the positively charged pore walls. By controllably assembling the particles into immobilized dimers and trimers, the previous results taking advantage of the optical waveguiding were improved by more than 6 orders of magnitude, leading to detection limits for DNT and TNT of 15−30 molecules.[1151]

In addition to AAO, mesoporous materials have also been used to assemble plasmonic nanoparticles. Because of the small size of the pores in mesoporous templates, synthesis is a more common method to deposit nanostructures in the pores (section 4.2). However, there have been several important examples of assembling plasmonic nanostructures into mesoporous silica templates. Among the first to accomplish this, Samorjai and co-workers included 2, 5, and 20 nm AuNPs in the reaction system to form mesoporous silica materials.[1152] In the case of the 2 and 5 nm particles, they were incorporated into the channels of the mesoporous matrix, whereas the 20 nm particles produced no NPs in the matrix because of their size. The authors used these materials to study their properties and potential catalytic applications. While there has been some incorporation of NPs into mesoporous materials in this way, the most powerful use of mesoporous materials for templating the assembly of plasmonic materials has come by using AuNPs as the micelles in the formation of the porous material itself. In recent work by Brinker and co-workers, AuNPs were chemically functionalized with surfactants to create structures that mimic micelles used in the formation of mesoporous structures.[1153−1155] Upon addition of the other reactants for the formation of mesoporous silica, the AuNPs assembled to form an fcc-ordered array inside the SiO_2 matrix in a way analogous to that of the micelles that would form the pores in the mesoporous case.[1153] Extending this work, the authors used standard conditions that had been established for mesoporous materials in the past to spin coat thin films of the highly ordered AuNPs on silicon surfaces.[1154] In this case, the pH of the reaction solution was changed from basic to acidic to slow the condensation of the silica matrix and prepare high-quality thin films of ordered AuNPs by preventing overcondensation of the film. The optical properties of the resulting films were studied and found to have well-defined plasmon resonances around 518 nm.[1154] In another alteration of the process, Brinker and co-workers changed the processing conditions to create interesting SiO_2 microspheres with irregular and polydisperse morphologies that contained highly ordered AuNPs.[1155] By controlling the surfactant used during synthesis (CTAB and cetyltriethylammonium bromide, CTEAB), the morphology could be controlled from well-formed spheres (CTEAB) to highly irregular agglomerations of particles (CTAB). Interestingly, in each case, the assembled AuNPs within the matrix particles were highly ordered as evidenced by TEM and X-ray diffraction.[1155]

8.2.2. Colloidal Surface Assembly. While these same adsorption methods can be used to assemble AuNPs and AgNPs onto close-packed polystyrene and silica spheres,[341,1115,1116,1156] colloidal lithographic templates also allow for a unique way to assemble plasmonic NPs into ordered arrays. Initially demonstrated by Kaler and co-workers, ordered arrangements of NPs can be achieved by an assembly process that occurs after crystallization of larger PS and silica spheres dried on surfaces.[1157−1159] In this method, both 15−25 nm AuNPs and ∼300 nm PS spheres are filtered onto a polycarbonate membrane that has pores to allow both particle types to accumulate on the surface while allowing the solvent to flow through.[1159] The spheres are then carefully dried, allowing the PS colloids to crystallize and form hexagonally close-packed arrays, similar to nanosphere lithography (described in section 5). The difference in this case is that the AuNPs, which are significantly smaller than the polymer spheres, assemble into the interstitial regions of the colloidal crystal to occupy the available space.[1158] At this point, two techniques can be employed to remove the colloid template and produce ordered, nanoporous arrays of AuNPs with different properties: calcination at elevated temperatures (300 °C) causes the particles to coalesce, producing a film with bulk Au properties, and chemical dissolution of the PS produces nanoporous materials that are comprised of individual AuNPs with interesting plasmonic properties.[1159] To study the effectiveness of this material for SERS, the authors compared the SERS signal from this porous material to that from randomly drop-cast AuNPs and smooth and electrochemically roughened Au films, finding that the templated nanoparticle assembly was significantly more enhancing.[1158]

Olev and co-workers expanded on this work by combining the two assembly steps (polymer spheres and AuNPs) into a single step where both sets of particles were filtered and dried from a single solution.[1160] The authors also study the effects of nanoporosity on the SERS properties of these materials by annealing the samples to different temperatures between 200 and 500 °C, where higher temperatures cause the nanoparticles to fuse together and decrease the nanoparticulate nature of the films. As expected, the authors report a monotonic decrease in the SERS signal intensity with increasing annealing temperature.[1160] Similarly, Paik and co-workers used this binary mixture of colloidal particles to assemble Au nanorods into the interstitial regions.[1161] 25 nm diameter Au nanorods with an aspect ratio of 15 were assembled between 495 nm PS spheres, with the concentration of Au rods varied between 0.03 and 0.1 wt % to change the number of nanorods between each sphere.

Another interesting alteration of this method was demonstrated by Caruso and co-workers in their coassembly of PS spheres with Au@SiO_2 core−shell NPs (Figure 51).[1162] Au@SiO_2 NPs were synthesized with 15 nm Au cores and shell thicknesses varying from 8 to 28 nm, leading to total particle diameters approximately equal to 30, 50, and 70 nm. Each of these particles was then mixed in a binary solution with 640 nm PS spheres and carefully dried to assemble the smaller Au@SiO_2 NPs in the interstices of the larger PS spheres in a manner similar to that of the previous examples. Upon heating the array at 500 °C, the PS spheres were removed and SiO_2 layers on adjacent Au@SiO_2 were sintered together, producing ordered arrays of Au@SiO_2 particles with three AuNPs in each particle (Figure 51). The authors studied the effect of the SiO_2 layer thickness on the Au interparticle spacing and order and the resulting optical properties of the array (plasmon resonances around 535 nm).[1162]

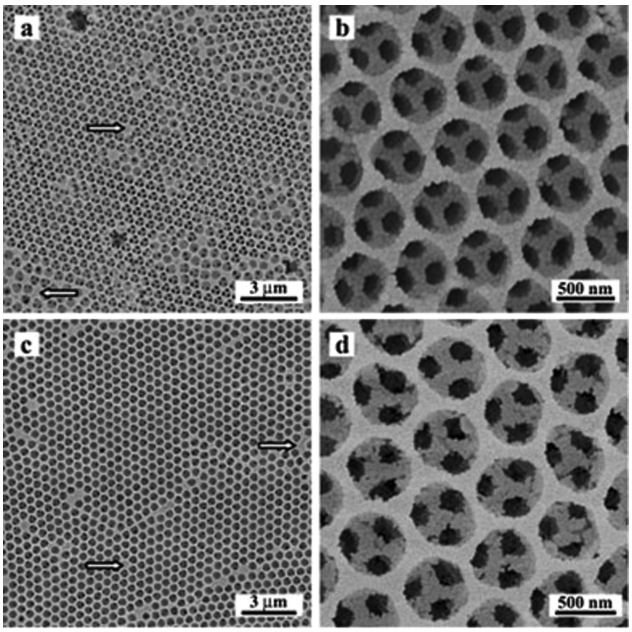

Figure 51. Lower (left) and higher (right) resolution SEM images of gold−silica inverse opals formed by templating colloidal crystals of 640 nm PS spheres with 70 nm (a, b) and 50 nm (c, d) Au@SiO_2 nanoparticles. While not present for smaller core−shell particles, long-range order is observed in both of these samples (left), with defect domains highlighted by white arrows. Adapted with permission from ref 1162. Copyright 2002 Wiley-VCH Verlag GmbH & Co. KGaA.

9. PROPERTIES AND APPLICATIONS

A direct result of the structural complexity inherent to many templated nanostructures is the appearance of several fascinating new properties relating to plasmonic effects. Some of these are relatively new and have only recently been observed for the first time, while others have been studied for decades and serve as the foundation for industrial or medical technologies. In this section, we will briefly highlight some of the most prominent examples where templated plasmonic nanostructures have contributed to the discovery of new physical phenomena or have been applied toward technological issues of societal significance. We will not attempt to be comprehensive and limit our discussion to only the most topical papers so as to give the reader a sense of the current state of the art in each field. In all cases, the construction of these nanomaterials has been covered in their respective synthesis or assembly section where additional examples pertaining to their properties and applications can be found.

9.1. Surface-Enhanced Raman Scattering

As one of the most intensely researched areas of plasmonics, the synthesis and fabrication of SERS substrates have evolved a great deal in the past 30 years. From electrochemically roughened metal surfaces to random nanoparticle aggregates and finally to rationally designed nanostructures, the ability to controllably create closely spaced Au and Ag nanostructure hot spots has led to many important studies and applications pertaining to SERS, including the ability to detect molecules of interest down to the single-molecule level.[1163,1164] Because many of the template-derived methods discussed in this review inherently produce ordered and closely spaced plasmonic nanostructures, these techniques have proven to be ideally suited for the preparation and optimization of sensitive SERS materials.

One class of materials that has been particularly important in the development of biological and chemical SERS sensors is the Ag FON developed by Van Duyne and co-workers. To prepare a Ag FON sample, a conformal Ag film is deposited on top of carefully assembled close-packed colloids, preserving the geometry of the template and creating hot spot regions of closely spaced metal surfaces between adjacent particles in the arrays (section 5.2.1).[815] After initially characterizing the plasmonic properties of these structures through functionalization with typical Raman reporter molecules, Van Duyne and co-workers applied this technique to develop the first systematic, quantitative glucose sensor based on SERS.[1165] In this case, a partition layer (1-decanethiol) was first functionalized on the Ag FON to stabilize the surface and help preconcentrate the glucose analyte near the high electromagnetic fields around the surface of the metal. After incubation in glucose at various concentrations (between 0 and 250 mM; up to 25 mM is biologically relevant), characteristic Raman shifts (1123 and 1064 cm^{-1}) that were expected for the analyte were observed when measured with confocal Raman microscopy. A detailed analysis of the data led to a model for quantitative and qualitative detection of glucose using SERS.[1165] Subsequent work has led to further optimization of the system and quantitative, real-time detection of glucose in bovine plasma.[1166] Importantly, in recent years, Van Duyne and co-workers have also made strides in incorporating Ag FONs into implantable glucose detection devices by demonstrating real-time glucose monitoring in rats.[817,1167] In another potential application for these materials, Ag FON SERS sensors have also been used for the ultrasensitive detection of anthrax spores down to a detection limit of 2.6×10^3 spores per sample.[34,818] Greatly improving on previous anthrax SERS studies, this work is both more sensitive and requires less laser power, which are both important considerations for usable systems. Van Duyne and co-workers took an important step toward this goal in demonstrating that a field-deployable, portable Raman spectrometer could be used to detect 10^4 spores within 5 s on a 30-day-old sample.[818]

Using a similar synthetic method, a novel SERS-based DNA detection method has recently been developed by Bartlett and co-workers using plasmonic Au nanovoid arrays.[832] In this case, the close-packed colloids were used as a template, instead of a mask, for the electrochemical growth of metal around the particles, producing a nanovoid array upon dissolution of the template (section 5.2.3). After preparation of the plasmonic material, the surface was functionalized with a thiolated oligonucleotide probe, followed by passivation with mercaptohexanol to prevent nonspecific binding of the target strands. Raman chromophore-labeled target strands were then hybridized onto these probe strands, bringing the chromophore close to the Au nanovoid surface and allowing detection of the label (fluorophores Cy3, Cy5, and Texas Red) with SERS. By finely controlling the temperature or applied potential to this surface, the duplex DNA on the surface of the nanovoid was melted at a specific temperature or potential, and the SERS signal from the label was lost. Importantly, because this process only dehybridizes the duplex on the surface and does not desorb the probe DNA strands, the authors showed that these surfaces can be reused to bind target DNA. Through a host of experiments correlating the applied temperature or potential to the expected duplex melting temperature, the authors also demonstrated a powerful example of the sensitivity of this technique: the ability

to distinguish between the wild type, a single-base point mutation, and a triple-base deletion in the cystic fibrosis transmembrane conductance regulator gene down to the 0.02 attomole level.[832]

Recently, a new methodology for using assembled, closely spaced nanoparticle monolayers as SERS substrates was demonstrated with templated Au@SiO_2 or Au@Al_2O_3 core−shell nanoparticles (section 3.1.4).[158] Through controlled synthesis of a 2 nm thick oxide shell around 55 nm Au nanoparticles, assembly of a dense monolayer of particles leads to very closely spaced Au surfaces for SERS. Because these structures do not require any further modification or processing after assembly, the authors demonstrate the ability to assemble these particles on arbitrary surfaces. Instead of functionalizing or adsorbing the molecules of interest directly on the particle as is done in most SERS examples, this method allows one to probe the SERS characteristics of nonplasmonic surfaces and materials in a way similar to that of tip-enhanced Raman scattering (TERS). After proof-of-concept work detecting hydrogen adsorption on Pt{111} and Si{111} surfaces, Tian and co-workers demonstrate two important real-world applications by coating their structures on yeast cells to study the proteins in the cell wall and an orange to observe the residue of a pesticide, methyl parathion.[158]

Because of one's ability to finely control the geometry and composition with nanometer precision, electrodeposition in alumina (AAO) membrane templates has also led to the development of powerful and interesting SERS materials. In particular arrays of closely spaced metal nanodisk dimers with large SERS enhancements at each dimer have been developed by Mirkin and co-workers. On-wire lithography (OWL) allows one to produce arrays of Au and Ag nanodisk dimers with gap sizes down to ∼2 nm (section 4.1.3).[719] After a set of optimization experiments, 120 nm thick Au disks spaced by a 30 nm gap were found to produce maximum SERS enhancements at 633 nm excitation.[721] Due to the nature of the process, arrays of these optimum dimers were then pursued for novel applications in chemical and biological sensing and encoding.[713] By controlling the relative distance between adjacent dimers in an array (Figure 52A), nanodisk codes (NDCs) were developed as a binary-reporting encoding scheme capable of high sensitivity, multimodal reporting, and detection. In this case, the presence of an enhancing dimer structure at a location in the array is considered a "1" and the absence a "0" in the physical readout. Upon preparation of these arrays and subsequent functionalization with a Raman chromophore of interest, the signal pattern of the binary code is easily observed using confocal Raman microscopy. Interestingly, because Raman spectroscopy allows for the identification of the chromophore complementary or redundant chemical information can be used to enhance the sophistication of the system. Due to the large enhancement of each dimer in the array (∼10^8), NDCs were also used to detect labeled DNA down to 100 fM in a three-strand sandwich assay (Figure 52 D−F).[713] Recently, the development of Ag NDCs has produced larger enhancements that led to an order of magnitude decrease in this limit of detection for DNA.[1168] Further, because the Ag structures produce significantly larger signals than Au (∼10^3) at 532 nm excitation, Mirkin and co-workers have now expanded the sophistication of NDCs to a multicomponent system where the larger signals from Ag structures are read as a "2" in the encoding scheme (Figure 52 G−I).

9.2. SPR/LSPR Sensing

Like the SERS materials, which also produced important sensing examples, the large-area order inherent to many of the templated methods for producing plasmonic surfaces makes them particularly well suited as surface plasmon resonance-based sensors. Colloidal lithographic methods are one of the most common examples, and are most often used to create arrays of discrete particles, leading to LSPR as the primary sensing methodology for these materials. In recent years, several novel applications related to chemical and biological sensing with templated LSPR sensors have been reported and will be the focus of this section. In each example, the basic physical phenomenon is the same: a binding event changes the local refractive index around the particles to cause a reproducible shift in the LSPR wavelength.

Similar in synthesis to the Ag film over nanosphere materials described in the SERS section (9.1), colloidal lithography-generated discrete nanoparticle arrays (section 5.1.1) have been one of the primarily studied LSPR substrates for biosensing. Van Duyne and co-workers have demonstrated two important examples of this ability with nanosphere lithography. By synthesizing arrays of triangular Ag nanoparticles and functionalizing the surface of the particles with a mixed monolayer of a passivating molecule and a functional molecule to bind antibodies, the authors are able to detect specific proteins on the basis of their interactions with antibodies. One example of this was first shown in 2004 with the detection of antibodies for amyloid-derived diffusible ligands (ADDLs), markers for Alzheimer's disease.[790] In this case, ADDL proteins were first bound to the functionalized Ag nanoparticles, causing a slight red-shift of the LSPR wavelength due to a local refractive index change. Upon exposure to anti-ADDLs (antibodies), a second shift was observed which was determined to be from binding of anti-ADDLs to the ADDL molecules adsorbed on the surface of the particles. Because anti-ADDLs are considered important in prohibiting the development of Alzheimer's disease, this development as both an anti-ADDL sensor and a tool to study fundamental binding chemistry between ADDLs and anti-ADDLs represents an important advancement in research on Alzheimer's disease. Importantly, the authors extended this concept in a subsequent report to directly detect ADDLs from extracts of human brain and cerebrospinal fluid from healthy and diseased patients, finding increased levels among the diseased patients.[789]

In a second example of protein binding and detection studies with these materials, Van Duyne and co-workers demonstrated ultrasensitive LSPR sensors capable of detecting not only protein binding but also protein conformational changes.[788] In this case, the Ag nanoparticle array surface was functionalized with a mixed monolayer of thiolated PEG-OH and PEG-phosphonate molecules. Cutinase−calmodulin−cutinase protein constructs were then adsorbed onto the surface of the particles through an interaction between one cutinase protein and the phosphonate groups, yielding a protein-functionalized surface and concomitant red-shift in the LSPR wavelength due to the refractive index change. Upon addition of Ca^{2+}, the construct underwent a known conformational change and caused a red-shift in the peak wavelength.[788] Subsequent chelation with EGTA reversed this conformational change and shift in the resonance. In addition to obvious importance to biodetection and binding studies, these changes were reversible for multiple iterations and were also envisioned as useful for potential plasmonic switches in devices. Of course, biodetection with LSPR has also been demonstrated

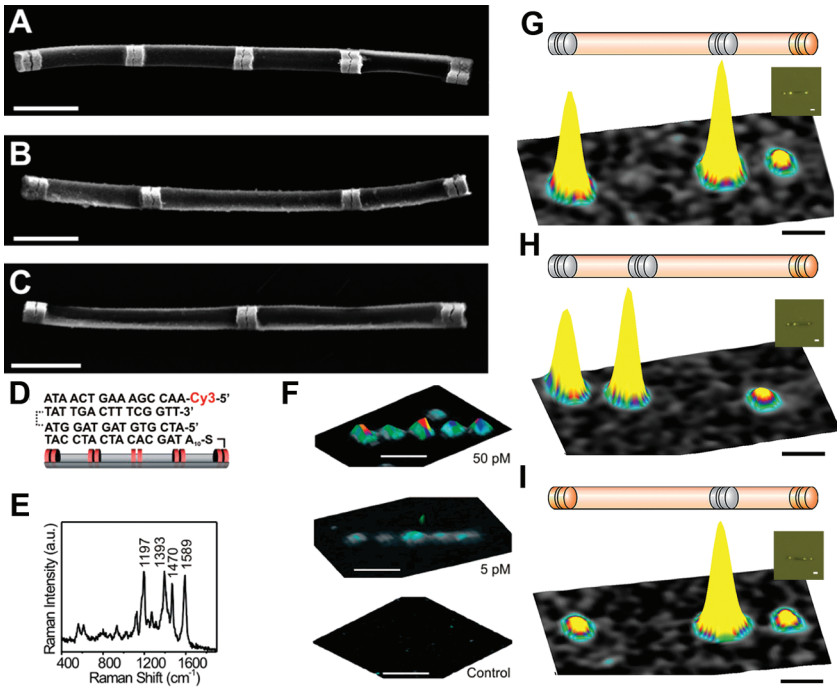

Figure 52. Nanodisk codes (NDCs) generated by on-wire lithography: (A−C) SEM images of 11111, 11011, and 10101 nanodisk codes, respectively (scale bars 1 μm). (D−F) DNA detection down to 5 pM with NDCs: (D) scheme showing the three-strand sandwich assay used for detection with a 11111 code, (E) representative Raman spectrum of Cy3, which serves as the Raman reporter for readout on the reporter strand, (F) scanning confocal Raman images of samples with target DNA concentrations of 50 and 5 pM and a control with no target DNA (top to bottom, 633 nm excitation, scale bars 2 μm). (G−I) Increase in encoding sophistication with multicomponent Ag−Au NDCs, where the larger signals from Ag structures provide a third option ("2") at each encoding location: scanning confocal Raman images with 532 nm excitation for 2021 (G), 2201 (H), and 1021 (I) code structures (scale bars 1 μm). (A−F) Adapted with permission from ref 713. Copyright 2007 American Chemical Society. (G−I) Adapted with permission from ref 1168. Copyright 2010 American Chemical Society.

on other colloidal lithography-generated surfaces, including Au nanohole[1169] and nanodisk[1170] arrays.

In addition to these important examples of biodetection, chemical detection for applications such as catalysis, hydrogen storage, and gas sensing have also been areas of interest using template-synthesized LSPR sensors. Kasemo and co-workers have demonstrated two important examples using hole-mask colloidal lithography (HCL) to fabricate metal nanodisks of uniform size and shape on a surface (section 5.1.3).[1171,1172] The first example studied the absorption of H_2 into Pd nanodisks measuring 300 nm in diameter and 20 nm in height formed by HCL.[1171] After preparation of the Pd nanoparticle substrate, the optical absorbance of the film was monitored as a function of increasing H_2 gas pressure. After the system was allowed to equilibrate at each successively higher pressure, an absorbance spectrum was collected, showing a significant red-shift broadening, and dampening of the resonance peak (1180−1260 nm for hydrogen pressures of 0−150 Torr) and yielding interesting pressure−LSPR-response isotherms. These peak shifts were attributed to changes in the electronic and physical structure of the disks as hydrogen was absorbed and diffused through the Pd matrix.[1171] Similar results were also observed for smaller Pd nanodisks (190 nm × 20 nm) in this study. In a second report, Kasemo and co-workers used HCL-generated Au nanodisks as a nanoplasmonic probe to monitor the progress of catalytic reactions near the Au surfaces.[1172] After fabrication of Au nanodisks measuring 76 nm in diameter and 30 nm in height, the structures were coated with a 10 nm SiO_2 film to act as a buffer and support for the subsequent deposition of 5−20 nm Pt nanoparticles by electron beam evaporation (insets of Figure 53). The structures are designed in this way to realize an indirect sensing scheme, where the Au nanoparticles sense changes in the refractive index from the chemical transformation occurring at the Pt nanoparticle surfaces.[1172] Using these substrates, the oxidations of hydrogen (Figure 53A) and carbon monoxide (Figure 53B) were both studied by monitoring the changes in the Au nanodisk resonance and temperature resulting from the exothermic reactions. For both reactions, the concentration of the reactant (H_2 or CO) was swept back and forth from low to high, resulting in concomitant blue-shifts in the resonance and peaks in the temperature at the kinetic phase transition between Pt nanoparticles covered in oxygen and those covered in H or CO (parts A and B, respectively, of Figure 53). Similarly, Au nanodisks measuring 105 nm in diameter and 30 nm in height were coated with 30 nm BaO and used to monitor the absorption and reduction of NO_x over Pt/BaO catalysts.[1172]

While the plasmonic materials in each of these examples have been derived from colloidal templates, a different example has utilized Au nanowires deposited in AAO templates (section 4.1.2).[706] In this case, Au nanowires measuring 25 nm in diameter and 380 nm in length, with a 60 nm center-to-center spacing, were grown and supported in AAO membranes. In measuring the optical properties of this nanowire film in transmission mode, the authors observed the expected longitudinal and transverse modes and measured a decrease in the longitudinal mode magnitude with decreasing excitation angle. However, in studying the optical properties in a total internal reflection (ATR) geometry that is used for many SPR detection

dx.doi.org/10.1021/cr1004452 |*Chem. Rev.* 2011, 111, 3736–3827

experiments, a new guided mode appeared in the infrared part of the spectrum (~900−1000 nm). Interestingly, this mode was found to be similar to bulk modes in metal films but with unique features arising from the anisotropic metal slabs comprising the structure. In particular, this metamaterial structure acts like a Au film with its permittivity determined by the coupling of individual nanowire plasmon modes. Unlike the longitudinal and transverse modes, this guided mode was found to be sensitive to dielectric changes even while surrounded by the host AAO matrix. Studying the effect of varying refractive index, the surface was found to have a very large figure of merit sensitivity of 30 000 nm/RIU in a glycerine−water gradient experiment.[706] As a proof-of-concept, the authors used their nanowire film to detect the binding of biotin to streptavidin at a biotin concentration below 300 nM, which is well below the 100 μM or higher concentrations required for most other SPR sensors.[706]

9.3. Emergent Plasmonic Phenomena

As of the time of this writing, the past several years have seen the publication of several fascinating reports of the appearance of new optical properties from templated nanostructures that arise as a result of plasmonic effects. Interestingly, many of these new phenomena have been observed in templated structures that were first synthesized well over a decade prior and have been studied thoroughly since. Innovations in the technical ability of researchers to measure these properties and a greater fundamental understanding of these complex systems have been largely responsible for these findings. This seems to suggest that while significant advances have been made in being able to synthesize complex plasmonic structures, there is still much to learn regarding their emergent and coupled optical behavior.

One particularly simple templated nanostructure, that of a AuNP core with an organic dye-embedded silica shell (see section 3.1.4), has recently been shown by Noginov et al. to exhibit surface-plasmon-based lasing behavior.[159] In direct analogy to a laser, the stimulated emission of coherent surface plasmons placed next to a gain medium is known as a "spaser". In this case, ~14 nm gold nanoparticle cores are capable of supporting the plasmon oscillations while adjacent dye molecules (Oregon Green 488) in a ~15 nm thick concentric SiO_2 coating act as the gain medium. Importantly, spectral overlap between the emission band of the dye molecules ($\lambda_{em} \approx 520$ nm) and the plasmon band of the AuNPs ($\lambda_{SPR} \approx 520$ nm) is crucial for achieving resonant energy transfer from the dye to the plasmon oscillations (Figure 54a).[159] Here, the authors showed that the coherent spaser modes are capable of outcoupling to photonic modes, resulting in the emission of coherent, monochromatic light, thus allowing these structures to act also as nanoscale lasers. This feature allowed for the convenient detection of far-field light to confirm the physical behavior of the system. For example, it was demonstrated that when using a nanosecond pulsed laser to pump the gain medium (dye), a threshold energy was required to achieve coherent emission of photons ($\lambda \approx 530$ nm) from the system (Figure 54b). This observation can be explained as the dramatic appearance of narrow, laser-like emission above a threshold is a hallmark indicator of stimulated emission. However, unlike conventional lasers, the stimulated emission is, in this case, of surface plasmons, which subsequently outcouple to photons and are responsible for the lasing behavior of the system. Furthermore, this same lasing response was observed even for a 100-fold diluted sample, demonstrating that the effect was active

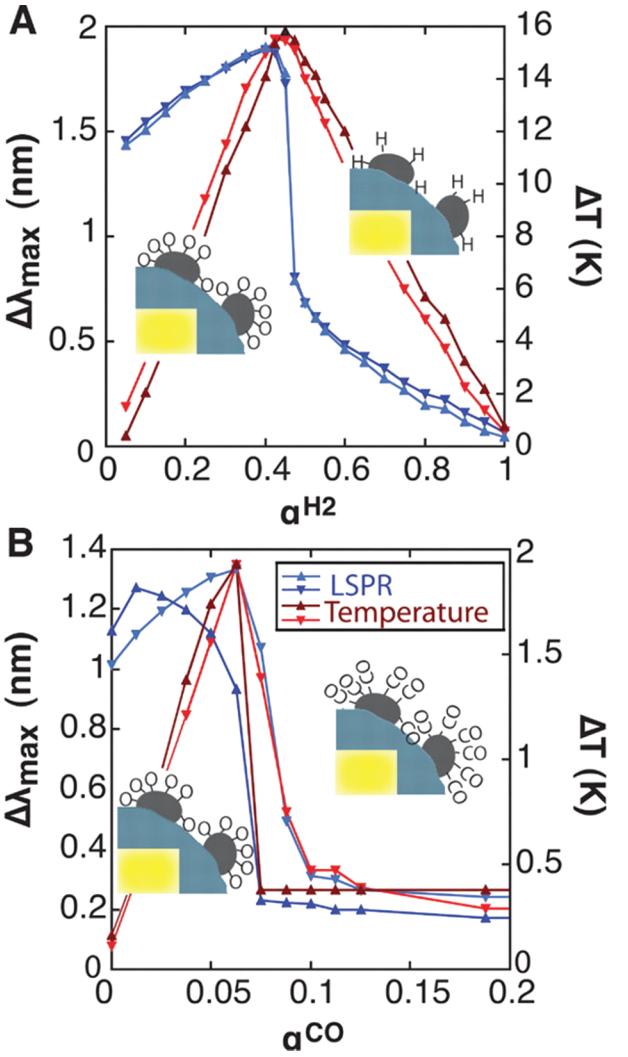

Figure 53. LSPR probes for monitoring the progress of catalytic reactions fabricated by hole-mask colloidal lithography: plasmon peak shifts (blue, left axis) and temperature variation (red, right axis) as a function of a^{H_2} (A) and a^{CO} (B) sweeps for the monitoring of the oxidation of hydrogen and carbon monoxide over Pt nanoparticle catalysts, respectively. The insets depict structure morphologies: Au nanodisk (yellow) coated with a 10 nm SiO_2 layer (blue) and 12 nm Pt nanoparticles adsorbed on top. Plasmon shifts occur from transitions to hydrogen (A) or carbon monoxide (B) coverage on the Pt nanoparticles, and temperature variation results from the exothermic reactions. Adapted with permission from ref 1172. Copyright 2009 American Association for the Advancement of Science.

at the single-particle level and did not require coupling between structures. The capability of incorporating two or more chemically disparate materials into one nanoscale volume is one of the major advantages of templated synthesis methods, which is elegantly illustrated by this work.

Another interesting example that takes advantage of plasmonic and excitonic coupling interactions has recently been shown by Ouyang and co-workers.[160] Here, the authors demonstrated spin manipulation in Au@CdSe nanostructures for possible quantum information processing applications via resonant coupling between plasmons in the Au core and excitons in the CdSe

dx.doi.org/10.1021/cr1004452 |Chem. Rev. 2011, 111, 3736–3827

shell. Starting with a Au core around 4.3 nm and a quantum-confined CdSe shell 2.8 nm in thickness, the signatures of a hybrid exciton were observed, indicated by modifications to the absorption spectrum. By tuning the exciton energy to lie within the continuum of states of the plasmon oscillation, resonant coupling was observed. This, in turn, led to significant enhancements to the optical Stark effect (OSE), a fundamental light–matter interaction that is typically weak in colloidal semiconductor quantum dots, but is measurable in this case because of the proximity to the concentrated optical near field due to the metallic nanoparticle core. Importantly, the authors observed that this resonantly enhanced OSE showed a strong dependence on the polarization of the excitation light, which could be used to induce a powerful spin splitting of electrons and a subsequent light-induced magnetic field along the laser direction. It is this field which is set up within the particle that provides the external tool for spin manipulation in the semiconductor by allowing for the application of a torque capable of rotating spins from their original polarization. It is important to note that this impressive level of control over the quantum state of the nanostructure is critically dependent on the inclusion of the plasmonic core, as this component provides the necessary enhancement to observe and utilize the OSE to achieve these light-mediated magnetic fields.

In addition to these coupling effects between different excited states in hybrid systems, Halas and co-workers have demonstrated the appearance of newly observed plasmonic Fano resonances in a variety of structures.[280,321] Although observed in many atomic and quantum systems, Fano resonances have only more recently been discovered and studied in the context of plasmonic materials.[11] In all cases, they arise in instances of constructive and destructive interference between a sharp, narrow resonance (discrete state) and a broad, diffuse resonance (continuum of states) that overlap in energy.[11] In plasmonic structures, this can occur via the spectral overlap of bright (superradiant) and dark (subradiant) resonance modes and results in an asymmetric peak and dip profile, characteristic of a Fano resonance.[1173] This behavior was observed by Halas in symmetric heptameric clusters of Au nanoshells (see section 3.2.2) assembled onto a substrate (Figure 55).[280] Functionalization of the colloidal nanoshells with a short polymer determines their interparticle separation and deposition onto a hydrophobic surface results in capillary organization into clusters of varying symmetry and size that can be probed individually using dark-field spectroscopy. In the case of a symmetric heptamer of nanoshells, the central particle has approximately the same dipole moment as a hybridization of the six surrounding particles, so the system can be thought of in terms of interactions between the central nanoshell plasmons and the hybridized ring plasmons (Figure 55A, insets). The resulting bonding mode between these two is broad and superradiant, acting as the continuum, while the antibonding mode is sharp and subradiant, acting as the discrete state. The interference between these two results in the appearance of a pronounced dip in the scattering spectra, indicative of the plasmonic Fano resonance. Eliminating the need for an assembly step, Halas and collaborators have also shown the emergence of Fano resonances from isolated nanostructures having a concentric AuNP core–SiO_2 shell–Au shell (see section 3.2.3) morphology.[321] Because the conditions of the Fano resonance are such that little energy is lost to the emission of outcoupled photons, local field strengths can be quite high, making structures that support this effect interesting for

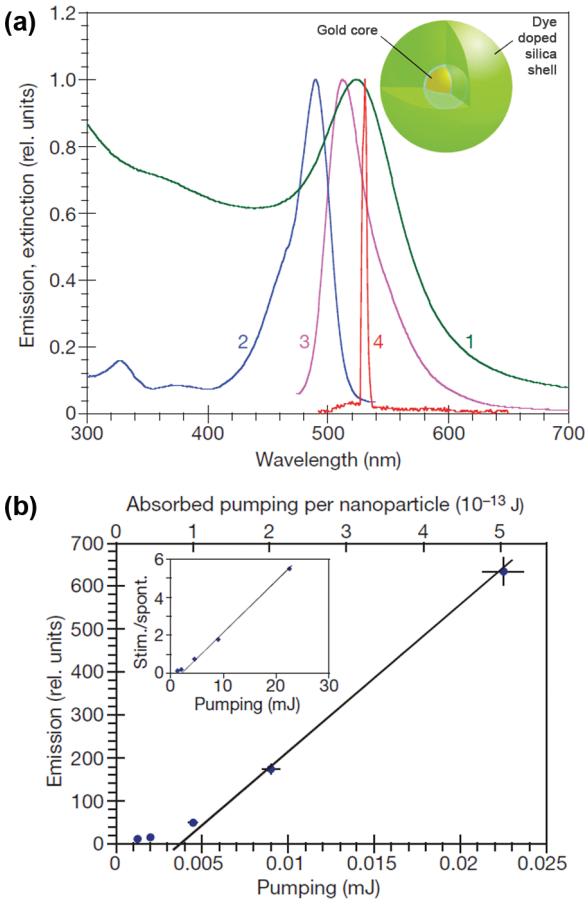

Figure 54. Evidence of surface-plasmon-based lasing behavior from dye-impregnated Au@SiO_2 nanoparticles: (a) When the dye is excited, overlap between its emission band (trace 3) and the absorption band of the AuNPs (trace 1) results in resonant energy transfer from the dye to coherent plasmon oscillations in the particles that can outcouple as monochromatic photons (trace 4). (b) A threshold energy is observed for pumping the gain medium (dye) to detect emission from the system, which suggests a stimulated emission and lasing mechanism is responsible. Adapted with permission from ref 159. Copyright 2009 Nature Publishing Group.

virtually any plasmonic-enhancement-based application (vida supra) such as SERS, LSPR detection, or surface plasmon lasers (spasers).[1173]

The examples presented thus far have highlighted instances of modern observations of novel plasmonic effects that have well-understood atomic analogues. As the underlying principles are often the same, this illustrates the power of such an approach to discovering new optical properties. However, the burgeoning field of metamaterials, which seeks to understand materials that derive their properties from mesoscale structure rather than composition, typically deals with phenomena which have no natural counterparts (e.g., negative index of refraction, reverse Doppler shift, and others).[84] Plasmonic nanostructures have played an important role in the development of advanced metamaterials, and consequently, so have templated methods for their construction. For example, Zhang and co-workers recently demonstrated the synthesis of Ag nanowires in AAO templates that exhibited negative index of refraction behavior at optical frequencies (Figure 56a).[705] Negative

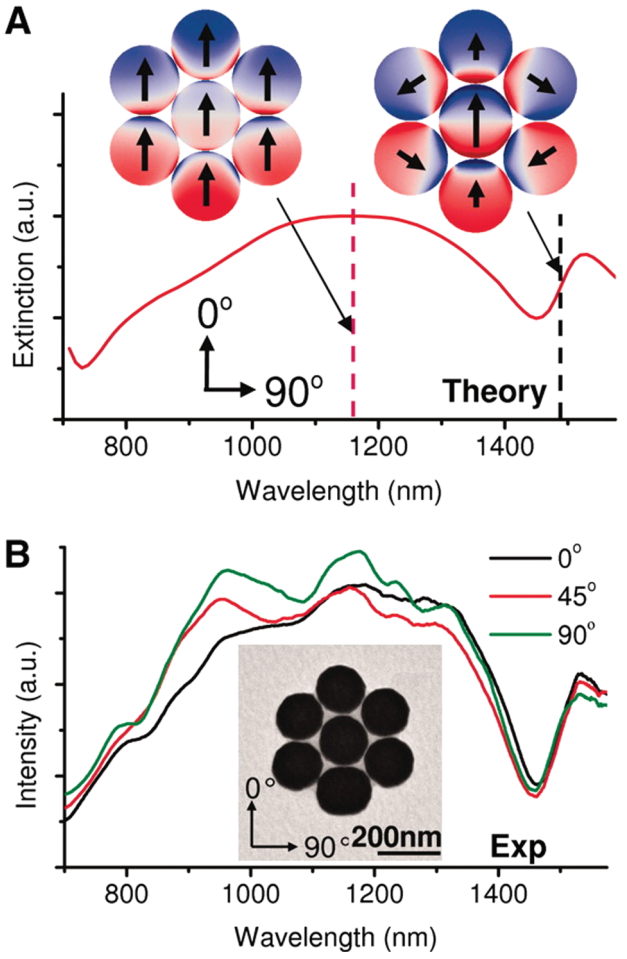

Figure 55. Fano resonance arising from heptameric clusters of Au nanoshells: (A) Calculated extinction spectrum showing the presence of a bright mode at ~1160 nm and the characteristic Fano minimum at ~1450 nm. Insets show charge density plots at each resonance. (B) Experimental single-cluster extinction plots collected by dark-field spectroscopy at several incidence angles all demonstrating the dip resulting from suppression of the bright mode at the Fano resonance. Adapted with permission from ref 280. Copyright 2010 American Association for the Advancement of Science.

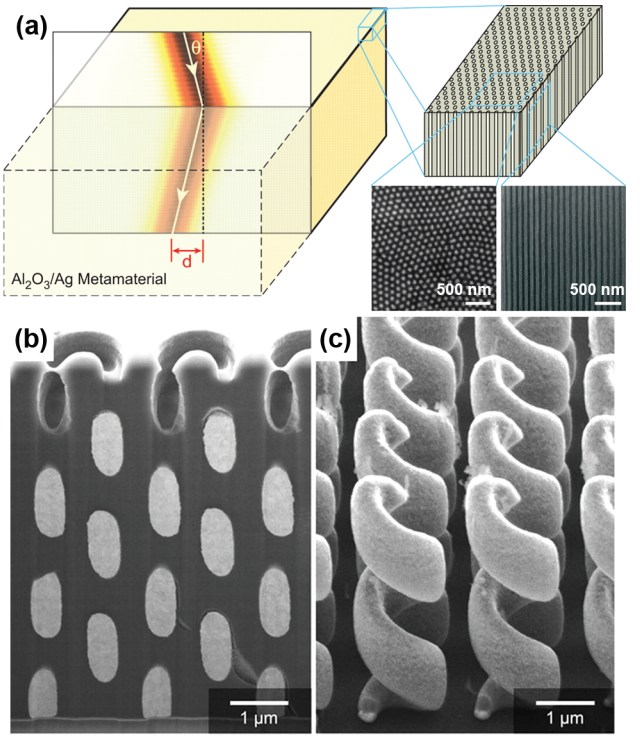

Figure 56. Optical metamaterials fabricated by templated methods: (a) Ag nanowires grown in porous aluminum oxide membranes exhibit negative index of refraction behavior. (b, c) Au helicies grown in a photolithography-generated template act as broad-band filters for circularly polarized light of the same chirality as the helicies. (a) Adapted with permission from ref 705. Copyright 2008 American Association for the Advancement of Science. (b, c) Adapted with permission from ref 731. Copyright 2009 American Association for the Advancement of Science.

index of refraction usually occurs when the effective electric permittivity ε and the effective magnetic permeability μ are both negative and is manifest by Snell's law in the refraction of light on the same side of the normal as the incident light.[84] Using straightforward electrochemical methods to grow the nanowires (see section 4.1.2), the composite AAO−Ag nanowire metamaterial was shown to form an effective medium capable of shifting transverse-magnetic-polarized transmitted light to the same side as the incident source, corresponding to effective negative index behavior.[705] In a separate example, Wegener and co-workers have shown the synthesis of helical Au nanostructures which act as broad-band circular polarizer metamaterials (Figure 56b).[731] Electrodeposited from a unique photolithography-generated template in an ordered 2-D array (see section 4.1.4), these structures showed selective blocking of circularly polarized light with the same handedness as the Au helices, while allowing transmission of light having the opposite handedness. These examples serve to briefly highlight the role that templated nanostructures can play in generating metamaterials with unique optical properties.

9.4. Photothermal Therapy and Imaging

Because many biological processes occur on the nanoscale, integration with synthetic nanomaterials has become an extensive area of research. Templated nanostructures with plasmonic properties have made significant contributions to this field for two primary reasons. First, with many being highly anisotropic, their resonances can be tuned to the near-infrared region of the electromagnetic spectrum where absorption by biological tissues is minimal, making them externally addressable. Second, and most importantly, they exhibit a property known as the photothermal effect which results in light to heat conversion under laser irradiation at their SPR.

The mechanism for this energy conversion is quite interesting and has, itself, garnered considerable interest.[1174,1175] In essence, the energy relaxation mechanism for electrons in metal nanoparticles excited by a pulsed laser (usually femto-, pico-, or nanosecond pulse widths) follows three (approximately) sequential processes: (1) electron−electron scattering, (2) electron−phonon coupling, and (3) phonon−phonon interactions.[1175] During the first process, electrons that are initially promoted into excited states above the Fermi level exhibit a nonequilibrium energy distribution. Progression of the system

dx.doi.org/10.1021/cr1004452 |*Chem. Rev.* 2011, 111, 3736–3827

from this nonequilibrium state to an equilibrium one occurs by a process known as thermalization whereby elastic electron−electron scattering redistributes the electron energies so as to conform to Fermi−Dirac statistics. This new distribution develops over a time scale of ∼500 fs and can be described mathematically by a higher effective "electronic" temperature that can be on the order of 1000 K. Following these purely elastic interactions is the first relaxation process by coupling of these excited electrons to phonons in the nanoparticle lattice. This can be thought of as an equilibration process between two coupled systems at different temperatures, the result of which is heating of the lattice on time scales between 1 and 4 ps. Finally, the hot phonon bath is capable of relaxing further by coupling to the solvent or matrix via phonon−phonon interactions. This process results in heating of the external environment surrounding the excited nanoparticle and usually occurs on time scales of ∼100 ps. Importantly, because these relaxation processes are so fast, laser excitation of low energy or long pulse width can be dissipated immediately with little change to the thermal profile around the nanostructure. However, if the laser pulse is confined to time scales before which phonon−phonon coupling is an available relaxation mechanism, energy can accumulate in the lattice, resulting in heating of the particle. Indeed, if laser pulses are sufficiently short (femtosecond), and energetic (∼μJ), the melting temperature of the lattice can be achieved, resulting in shape transformation of the nanoparticle from anisotropic to spherical.[1175] Furthermore, the energy threshold for melting of the particle increases if picosecond or nanosecond pulses are used instead, as phonon−phonon interactions with the environment can now compete with the rate of lattice heating, resulting in a dissipation of the excitation energy. This explains the observation that when continuous-wave (CW) irradiation is used instead of pulsed methods, a laser power of ∼1 W or greater is often necessary to observe even moderate nanoparticle heating.

Taking advantage of this unique effect, active at near-infrared wavelengths because of the particle shape, many groups have shown the utility of nanoscale heating in biological settings. Among the first to apply this principle was Halas and co-workers, who showed, using a Au nanoshell resonant with a 820 nm NIR laser (see section 3.2.2), selective in vitro and in vivo destruction of cancer cells when exposed to a combination of particles and laser irradition.[199] Temperature changes in solid tumors as high as ∼37 °C were reported in as little as minutes, representing an input of energy more than sufficient to cause immediate cell death in the area surrounding the laser spot. More recently, they have shown an innovative approach to achieving targeting of their nanoshells to a specific tumor environment using a "Trojan horse" delivery approach.[204] Here, cells known as monocytes, which are naturally recruited to the hypoxic regions within tumors by a chemotractive gradient, are preloaded with nanoshells. Once introduced to a breast cancer tumor spheroid, these cells are capable of penetrating the periphery and differentiating into cells known as tumor-associated macrophages which then enter the central hypoxic region. Subsequent photothermal treatment resulted in tumor ablation and cell death, demonstrating the feasibility of such an approach. Importantly, it is crucial to the success of this strategy that the therapeutic component, which will ultimately be responsible for the cell death, remain dormant until the cargo-filled monocytes have differentiated and entered the hypoxic tumor microenvironment. The external addressability facilitated by the photothermal effect and the possibility of NIR excitation are both instrumental components that help to fulfill these requirements. Halas and co-workers have been particularly prolific in investigating these concepts and have started to see these ideas transition from the laboratory to more clinical settings.[205] However, Xia and collaborators have also shown both in vitro[403] and in vivo[404] efficacy of Au nanocages (see section 3.4.3) in photothermal cancer treatment. In these cases, the hollow structures likewise have NIR resonances for adequate tissue penetration but are significantly smaller overall (50−60 nm edge length)[403,404] compared to nanoshells with the same resonance wavelength (90−120 nm diameter),[199,204] which may have implications for cell uptake or tumor penetration considerations.

Rather than use photothermally generated local heating to destructively kill cells, several groups have instead used this effect to show light-triggered release of drugs or biomolecules. For example, Xia and co-workers have used the hollow interiors of the Au nanocages to encapsulate molecular species that can then be released through the pores upon NIR laser irradiation (Figure 57).[405] To accomplish this, nanocages were coated in a poly(*N*-isopropylacrylamide) (pNIPAM)-based polymer that undergoes a reversible conformational transition between swollen and collapsed states as a function of temperature (this temperature can be tuned to lie between 32 and 50 °C on the basis of the incorporation of an acrylamide block in the polymer chain). Below the transition temperature, the polymer is hydrophilic and swells to cover the pores on the nanocage, trapping the cargo inside. Above the transition temperature, the polymer becomes hydrophobic and collapses, allowing diffusion of the encapsulated species out from the interior. By incubating these structures in the "open" state (higher temperatures, collapsed polymer) with a fluorescent dye molecule, followed by a fast "closing" step (lower temperatures, swollen polymer), the authors were able to achieve efficient encapsulation by the nanocage. Further, it was demonstrated that heat generated via photothermal conversion of NIR light could provide the necessary energy to enable the polymer conformational change and release of the trapped dye. Variables such as the laser power and irradiation time were also shown to provide the capability to modulate the release profile of the molecule (Figure 57b). Importantly, the authors also demonstrated the release of a cancer drug (doxorubicin) and a protein enzyme (lysozyme), showing the method to be generalizable to many possible agents and gentle enough to maintain the activity of sensitive biomolecules.

Halas and co-workers have used a similar nondestructive strategy to demonstrate the release of oligonucleotides from nanoshells under NIR laser irradiation.[278] By conjugating a thiolated oligonucleotide to the surface of Au nanoshells, followed by hybridization of a complementary strand, DNA duplexes were formed which could subsequently be loaded with DAPI (4′,6-diamidino-2-phenylindole), a well-known fluorescent molecule that intercalates double-stranded DNA. After incubation of these conjugates with lung cancer cells, irradiation with NIR light at their SPR resulted in the release of DAPI from the nanoparticles, after which it could diffuse to the cell nucleus and bind the genomic DNA. This observation was shown to be a result of dehybridization of the DNA duplexes bound to the nanoshell mediated by photothermally generated heat and illustrates a potential means to trigger the release of both drugs and oligonucleotides by light.

Imaging contrast is another area of recent interest in which the photothermal properties of templated nanostructures have

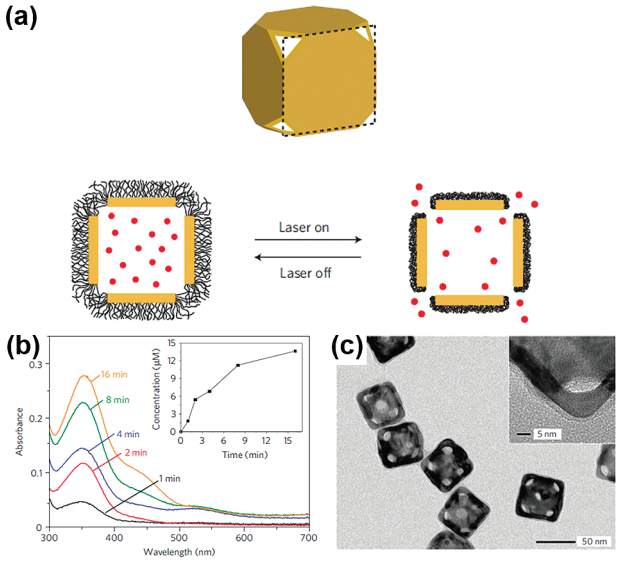

Figure 57. Photothermally triggered release of small molecules and proteins from hollow Au nanostructures: (a) Schematic illustration demonstrating the encapsulation role played by the thermoresponsive polymer coating on Au nanocages. At sufficient photothermally generated temperatures, a conformational transition in the polymer causes it to become hydrophobic and collapse, allowing release of the trapped cargo. (b) Release of a fluorescent dye as a function of the irradiation time. (c) TEM image of the polymer-coated porous Au nanocages. Adapted with permission from ref 405. Copyright 2009 Nature Publishing Group.

facilitated significant contributions. Two major imaging modalities have made use of these particles as contrast agents- optical coherence tomography (OCT) and photoacoustic tomography (PAT). OCT is capable of detecting the spatial variation in tissue scattering from sections through a biological sample by monitoring the interference pattern between light passed through the sample and through a reference mirror, originating from a single source.[203,207] In cases where this technique is made phase sensitive, small temperature gradients generated by photothermal excitation of contrast agent nanostructures cause a shift in the optical path length which can be readily detected. Fujimoto and co-workers have recently applied this technique successfully, using NIR-resonant Au nanoshells as contrast agents, to the ex vivo imaging of human breast tissue, which is typically challenging to image because it is highly scattering.[207] PAT, on the other hand, operates by generating detectable acoustic pressure waves as a result of local temperature gradients and subsequent thermoelastic expansion of tissues.[407,408] Consequently, PAT detects spatial variation in the optical absorption of tissues which can be greatly enhanced through the use of NIR photothermal contrast agents. In fact, Xia and co-workers have recently shown such enhancements to this imaging modality using Au nanocages in noninvasive detection of sentinel lymph nodes, which are indicators of cancer metastasis.[407] Importantly, Xia has also shown that, through bioconjugation, active targeting of the nanocages to melanomas resulted in a ~300% higher photoacoustic signal compared to that of nanocages that accumulated passively.[408] These results highlight the possibility that early detection of cancer through targeting and/or imaging contrast enhancement might be possible with such optically active nanostructures.

10. CONCLUSIONS AND FUTURE OUTLOOK

Throughout this review, we have attempted to unify a number of nanostructure synthesis and assembly methodologies by showing that they can all be categorized as following the same basic principle of templating. Instead of relying on surfactant—metal surface interactions that give rise to anisotropic nanostructures or relatively nonspecific nanoparticle assembly interactions (to name a few), templated techniques take advantage of prefabricated nanostructures with well-defined geometries to guide the formation of plasmonic materials that mimic the symmetry of the template. This approach, however, is then obviously linked to methods to better control the dimensions, morphology, and monodisperty of the template materials. As a result, advances in templated synthesis and assembly methods may coincide with advances in template fabrication. In the case of templated synthesis, this will require the ability to generate colloidal nanostructures and porous membranes with higher yields and a greater degree of size and shape control. For templated assembly, more complex natural (biomolecules) and synthetic (polymers/supramolecules) materials that can guide the formation of ordered structures across macroscopic length scales are required. Fortunately, because the range of available materials is so broad, new nanostructures that could serve as templates for the preparation of plasmonic materials are frequently generated.

While the sections of this review describe significant advances made in the development of various templating methodologies, the combination or two or more of these individual methods should also enable new and more sophisticated plasmonic structures. For example, merging several of the synthetic methods addressed in sections 3—5 may allow one to generate more complex nanostructures than any one approach might offer. Indeed, porous-membrane-synthesized segmented nanorods (section 4.1.3) can act as sacrificial templates (section 3.4) to create 1-D structures with positive and negative features that have been used as powerful SERS substrates (section 9.1) due to their superior plasmonic properties.[713,719,721] Along with the many well-developed techniques to controllably synthesize complex nanostructures using colloidal templates (section 3), the ability to assemble these materials into strongly coupled systems with well-defined symmetry and dimensionality (sections 6—8) could lead to large-area, easily fabricated plasmonic materials for a variety of applications, especially energy harvesting and SERS. Initial results suggest that even relatively simple templated nanostructures organized into symmetric clusters or superlattices can give rise to new optical phenomena that occur in no known naturally occurring materials (section 9.3).[11,280,731]

Finally, one of the enormous advantages of templated methods which is challenging with other processes is the ability to incorporate dissimilar materials into a single nanostructure. This often has the effect of allowing for coupling between materials that have complementary optical properties that can interact in novel ways. Plasmonic structures are uniquely suited for such effects, as adjacent dielectric and metal structures can affect their resonance conditions. Alternatively, the enhanced local fields generated under resonance can strongly affect other optically active materials, such as semiconductors and molecular dyes, providing avenues to new light-mediated and -enhanced properties.[159,160] While these disciplines are only just beginning, they represent some of the most promising areas

of scientific inquiry into the field of plasmonics, and templated methods are poised to contribute significantly to their future progress.

AUTHOR INFORMATION

Corresponding Author

*Fax: (847) 467-5123. E-mail: chadnano@northwestern.edu.

BIOGRAPHIES

Matthew R. Jones received his B.S. in materials science and engineering and biomedical engineering from Carnegie Mellon University in 2007 with university, college, and departmental honors. He is currently pursuing his Ph.D. in materials science and engineering under the guidance of Prof. Chad A. Mirkin at Northwestern University. His research interests include the synthesis and assembly of nanomaterials and understanding the emergent properties that arise from ordered nanoparticle systems.

Kyle D. Osberg received his B.S. degree in chemical engineering from the University of Texas at Austin (UT-Austin) in 2007. While graduating with high honors at UT-Austin, he studied thin films for the development of imprint lithography under the supervision of Prof. C. Grant Willson. Also in 2007, he joined Prof. Chad A. Mirkin's group at Northwestern University to pursue his Ph.D. in materials science and engineering, which he is presently working toward. His research interests include synthesis and fabrication of nanomaterials, plasmonics, biological and chemical sensors, and emerging energy technologies.

Robert J. Macfarlane received his B.A. in biochemistry with honors from Willamette University in 2004 and received his M.S. in inorganic chemistry from Yale University in 2006. In 2007, Robert joined the laboratory of Prof. Chad A. Mirkin at Northwestern University, working toward his Ph.D. in chemistry with a focus on inorganic and bionanomaterials. He is currently researching methods for the DNA-directed assembly of nanoparticles, where his work has enabled the synthesis of ordered superlattices and elucidated the fundamental parameters of DNA-directed particle assembly.

Mark R. Langille studied chemistry at Carnegie Mellon University, earning his bachelor's degree in 2008. He is now conducting Ph.D. research at Northwestern University under the guidance of Prof. Chad A. Mirkin. His research focuses on developing synthetic methods for the generation of noble-metal nanostructures.

Chad A. Mirkin is the Director of the International Institute for Nanotechnology, the George B. Rathmann Professor of Chemistry, Professor of Chemical and Biological Engineering, Professor of Biomedical Engineering, Professor of Materials Science and Engineering, and Professor of Medicine at Northwestern University. He is known for his invention and development of nanoparticle-based biodetection schemes, dip-pen nanolithography, and the weak-link approach to supramolecular coordination chemistry. He is the author of over 450 papers and over 370 patents and applications and the founder of three companies, Nanosphere, NanoInk, and AuraSense. He is a Member of the President's Council of Advisors on Science & Technology (PCAST; Obama Administration), a Member of the Institute of Medicine, the National Academy of Sciences, the National Academy of Engineering, and the American Academy of Arts and Sciences.

ACKNOWLEDGMENT

C.A.M. acknowledges the Department of Energy (through the Non-equilibrium Energy Research Center), National Science Foundation (NSF), Air Force Office of Scientific Research, and Department of Defense (National Security Science and Engineering Faculty Fellowship) for supporting this work. M.R.J. acknowledges the NSF for a Graduate Research Fellowship and Northwestern University for a Ryan Fellowship. K.D.O. acknowledges the NSF for a Graduate Research Fellowship and Northwestern University for a Ryan Fellowship. R.J.M. acknowledges Northwestern University for a Ryan Fellowship.

REFERENCES

(1) Rosi, N. L.; Mirkin, C. A. *Chem. Rev.* **2005**, *105*, 1547.
(2) Ghosh, S. K.; Pal, T. *Chem. Rev.* **2007**, *107*, 4797.
(3) Kelly, K. L.; Coronado, E.; Zhao, L. L.; Schatz, G. C. *J. Phys. Chem. B* **2003**, *107*, 668.
(4) Schuller, J. A.; Barnard, E. S.; Cai, W.; Jun, Y. C.; White, J. S.; Brongersma, M. L. *Nat. Mater.* **2010**, *9*, 193.
(5) Stewart, M. E.; Anderton, C. R.; Thompson, L. B.; Maria, J.; Gray, S. K.; Rogers, J. A.; Nuzzo, R. G. *Chem. Rev.* **2008**, *108*, 494.
(6) Homola, J. *Chem. Rev.* **2008**, *108*, 462.
(7) Lal, S.; Link, S.; Halas, N. J. *Nat. Photonics* **2007**, *1*, 641.
(8) Maier, S. A.; Brongersma, M. L.; Kik, P. G.; Meltzer, S.; Requicha, A. A. G.; Atwater, H. A. *Adv. Mater.* **2001**, *13*, 1501.
(9) Atwater, H. A.; Polman, A. *Nat. Mater.* **2010**, *9*, 205.
(10) Ferry, V. E.; Munday, J. N.; Atwater, H. A. *Adv. Mater.* **2010**, *22*, 4794.
(11) Luk'yanchuk, B.; Zheludev, N. I.; Maier, S. A.; Halas, N. J.; Nordlander, P.; Giessen, H.; Chong, C. T. *Nat. Mater.* **2010**, *9*, 707.
(12) Yadong, Y.; Alivisatos, A. P. *Nature* **2005**, *437*, 664.
(13) Daniel, M.-C.; Astruc, D. *Chem. Rev.* **2003**, *104*, 293.
(14) Cushing, B. L.; Kolesnichenko, V. L.; O'Connor, C. J. *Chem. Rev.* **2004**, *104*, 3893.
(15) Xia, Y.; Xiong, Y.; Lim, B.; Skrabalak, S. *Angew. Chem., Int. Ed.* **2009**, *48*, 60.
(16) Burda, C.; Chen, X.; Narayanan, R.; El-Sayed, M. A. *Chem. Rev.* **2005**, *105*, 1025.
(17) Sau, T. K.; Rogach, A. L. *Adv. Mater.* **2010**, *22*, 1781.
(18) Wallraff, G. M.; Hinsberg, W. D. *Chem. Rev.* **1999**, *99*, 1801.
(19) Xia, Y.; Rogers, J. A.; Paul, K. E.; Whitesides, G. M. *Chem. Rev.* **1999**, *99*, 1823.
(20) Gates, B. D.; Xu, Q.; Stewart, M.; Ryan, D.; Willson, C. G.; Whitesides, G. M. *Chem. Rev.* **2005**, *105*, 1171.
(21) Menard, E.; Meitl, M. A.; Sun, Y.; Park, J.-U.; Shir, D. J.-L.; Nam, Y.-S.; Jeon, S.; Rogers, J. A. *Chem. Rev.* **2007**, *107*, 1117.
(22) Faraday, M. *Philos. Trans. R. Soc. London* **1857**, *147*, 145.
(23) Mie, G. *Ann. Phys.* **1908**, *25*, 377.
(24) Raether, H. *Surface Plasmons on Smooth and Rough Surfaces and on Gratings*; Springer: New York, 1988.
(25) Maier, S. A. *Plasmonics: Fundamentals and Applications*; Springer: New York, 2007.
(26) Kerker, M. *The Scattering of Light and Other Electromagnetic Radiation*; Academic Press: New York, 1969.
(27) Bohren, C. F.; Huffman, D. R. *Absorption and Scattering of Light by Small Particles*; Wiley Interscience: New York, 1983.
(28) Kreibig, U.; Vollmer, M. *Optical Properties of Metal Clusters*; Springer: Berlin, 1995.
(29) Ritchie, R. H. *Phys. Rev.* **1957**, *106*, 874.
(30) Knobloch, H.; Brunner, H.; Leitner, A.; Aussenegg, F.; Knoll, W. *J. Chem. Phys.* **1993**, *98*, 10093.
(31) Knoll, W. *Annu. Rev. Phys. Chem.* **1998**, *49*, 569.
(32) Brockman, J. M.; Nelson, B. P.; Corn, R. M. *Annu. Rev. Phys. Chem.* **2000**, *51*, 41.
(33) Wark, A. W.; Lee, H. J.; Corn, R. M. *Anal. Chem.* **2005**, *77*, 3904.
(34) Zhang, X. Y.; Zhao, J.; Whitney, A. V.; Elam, J. W.; Van Duyne, R. P. *J. Am. Chem. Soc.* **2006**, *128*, 10304.
(35) Freunscht, P.; Van Duyne, R. P.; Schneider, S. *Chem. Phys. Lett.* **1997**, *281*, 372.
(36) Sanders, A. W.; Routenberg, D. A.; Wiley, B. J.; Xia, Y. N.; Dufresne, E. R.; Reed, M. A. *Nano Lett.* **2006**, *6*, 1822.
(37) Oulton, R. F.; Sorger, V. J.; Genov, D. A.; Pile, D. F. P.; Zhang, X. *Nat. Photonics* **2008**, *2*, 496.
(38) Ditlbacher, H.; Hohenau, A.; Wagner, D.; Kreibig, U.; Rogers, M.; Hofer, F.; Aussenegg, F. R.; Krenn, J. R. *Phys. Rev. Lett.* **2005**, *95*, 257403.
(39) Haes, A. J.; Haynes, C. L.; McFarland, A. D.; Schatz, G. C.; Van Duyne, R. P.; Zou, S. L. *MRS Bull.* **2005**, *30*, 368.
(40) Lee, K. S.; El-Sayed, M. A. *J. Phys. Chem. B* **2006**, *110*, 19220.
(41) Ghosh, S. K.; Nath, S.; Kundu, S.; Esumi, K.; Pal, T. *J. Phys. Chem. B* **2004**, *108*, 13963.
(42) Underwood, S.; Mulvaney, P. *Langmuir* **1994**, *10*, 3427.
(43) Miller, M. M.; Lazarides, A. A. *J. Phys. Chem. B* **2005**, *109*, 21556.
(44) Mock, J. J.; Barbic, M.; Smith, D. R.; Schultz, D. A.; Schultz, S. *J. Chem. Phys.* **2002**, *116*, 6755.
(45) Halas, N. J. *MRS Bull.* **2005**, *30*, 362.
(46) Perez-Juste, J.; Pastoriza-Santos, I.; Liz-Marzán, L. M.; Mulvaney, P. *Coord. Chem. Rev.* **2005**, *249*, 1870.
(47) Link, S.; El-Sayed, M. A. *J. Phys. Chem. B* **1999**, *103*, 8410.
(48) Link, S.; Mohamed, M. B.; El-Sayed, M. A. *J. Phys. Chem. B* **1999**, *103*, 3073.
(49) Novo, C.; Gomez, D.; Perez-Juste, J.; Zhang, Z. Y.; Petrova, H.; Reismann, M.; Mulvaney, P.; Hartland, G. V. *Phys. Chem. Chem. Phys.* **2006**, *8*, 3540.
(50) Schmucker, A. L.; Harris, N.; Banholzer, M. J.; Blaber, M. G.; Osberg, K. D.; Schatz, G. C.; Mirkin, C. A. *ACS Nano* **2010**, *4*, 5453.
(51) Myroshnychenko, V.; Rodriguez-Fernandez, J.; Pastoriza-Santos, I.; Funston, A. M.; Novo, C.; Mulvaney, P.; Liz-Marzán, L. M.; de Abajo, F. J. G. *Chem. Soc. Rev.* **2008**, *37*, 1792.
(52) Jin, R. C.; Cao, Y. W.; Mirkin, C. A.; Kelly, K. L.; Schatz, G. C.; Zheng, J. G. *Science* **2001**, *294*, 1901.
(53) Millstone, J. E.; Park, S.; Shuford, K. L.; Qin, L. D.; Schatz, G. C.; Mirkin, C. A. *J. Am. Chem. Soc.* **2005**, *127*, 5312.
(54) Millstone, J. E.; Hurst, S. J.; Metraux, G. S.; Cutler, J. I.; Mirkin, C. A. *Small* **2009**, *5*, 646.
(55) Wannemacher, R. *Opt. Commun.* **2001**, *195*, 107.
(56) Yin, L.; Vlasko-Vlasov, V. K.; Rydh, A.; Pearson, J.; Welp, U.; Chang, S. H.; Gray, S. K.; Schatz, G. C.; Brown, D. B.; Kimball, C. W. *Appl. Phys. Lett.* **2004**, *85*, 467.
(57) Coyle, S.; Netti, M. C.; Baumberg, J. J.; Ghanem, M. A.; Birkin, P. R.; Bartlett, P. N.; Whittaker, D. M. *Phys. Rev. Lett.* **2001**, *87*, 176801.
(58) Genet, C.; Ebbesen, T. W. *Nature* **2007**, *445*, 39.
(59) Prikulis, J.; Hanarp, P.; Olofsson, L.; Sutherland, D.; Kall, M. *Nano Lett.* **2004**, *4*, 1003.

(60) Su, K. H.; Wei, Q. H.; Zhang, X.; Mock, J. J.; Smith, D. R.; Schultz, S. *Nano Lett.* **2003**, *3*, 1087.
(61) Hao, E.; Schatz, G. C. *J. Chem. Phys.* **2004**, *120*, 357.
(62) Mirkin, C. A.; Letsinger, R. L.; Mucic, R. C.; Storhoff, J. J. *Nature* **1996**, *382*, 607.
(63) Shalaev, V. M.; Botet, R.; Jullien, R. *Phys. Rev. B* **1991**, *44*, 12216.
(64) Bharadwaj, P.; Deutsch, B.; Novotny, L. *Adv. Opt. Photonics* **2009**, *1*, 438.
(65) Haynes, C. L.; McFarland, A. D.; Van Duyne, R. P. *Anal. Chem.* **2005**, *77*, 338A.
(66) Jensen, T. R.; Van Duyne, R. P.; Johnson, S. A.; Maroni, V. A. *Appl. Spectrosc.* **2000**, *54*, 371.
(67) Geddes, C. D.; Aslan, K.; Gryczynski, I.; Malicka, J.; Lakowicz, J. R. *Rev. Fluoresc.* **2004**, *1*, 365.
(68) Kneipp, K.; Moskovits, M.; Kneipp, H.; Bohr, H. *Surface-Enhanced Raman Scattering*; Springer: Berlin, Heidelberg, 2006; p 261.
(69) Kneipp, J.; Kneipp, H.; Kneipp, K. *Chem. Soc. Rev.* **2008**, *37*, 1052.
(70) Nie, S. M.; Emery, S. R. *Science* **1997**, *275*, 1102.
(71) Kneipp, K.; Wang, Y.; Kneipp, H.; Perelman, L. T.; Itzkan, I.; Dasari, R.; Feld, M. S. *Phys. Rev. Lett.* **1997**, *78*, 1667.
(72) Willets, K. A.; Van Duyne, R. P. *Annu. Rev. Phys. Chem.* **2007**, *58*, 267.
(73) Anker, J. N.; Hall, W. P.; Lyandres, O.; Shah, N. C.; Zhao, J.; Van Duyne, R. P. *Nat. Mater.* **2008**, *7*, 442.
(74) Cooper, M. A. *Nat. Rev. Drug Discovery* **2002**, *1*, 515.
(75) Katz, E.; Willner, I. *Angew. Chem., Int. Ed.* **2004**, *43*, 6042.
(76) Gramotnev, D. K.; Bozhevolnyi, S. I. *Nat. Photonics* **2010**, *4*, 83.
(77) Barnes, W. L.; Dereux, A.; Ebbesen, T. W. *Nature* **2003**, *424*, 824.
(78) Giannini, V.; Fernández-Domínguez, A. I.; Sonnefraud, Y.; Roschuk, T.; Fernández-García, R.; Maier, S. A. *Small* **2010**, *6*, 2498.
(79) Maier, S. A.; Atwater, H. A. *J. Appl. Phys.* **2005**, *98*, 011101.
(80) Ozbay, E. *Science* **2006**, *311*, 189.
(81) Gao, H. W.; Zhou, W.; Odom, T. W. *Adv. Funct. Mater.* **2010**, *20*, 529.
(82) Yao, J. M.; Le, A. P.; Gray, S. K.; Moore, J. S.; Rogers, J. A.; Nuzzo, R. G. *Adv. Mater.* **2010**, *22*, 1102.
(83) Notomi, M. *Phys. Rev. B* **2000**, *62*, 10696.
(84) Smith, D. R.; Pendry, J. B.; Wiltshire, M. C. K. *Science* **2004**, *305*, 788.
(85) Shalaev, V. M. *Nat. Photonics* **2007**, *1*, 41.
(86) Cai, W. S.; Chettiar, U. K.; Kildishev, A. V.; Shalaev, V. M. *Nat. Photonics* **2007**, *1*, 224.
(87) Sau, T. K.; Rogach, A. L.; Jackel, F.; Klar, T. A.; Feldmann, J. *Adv. Mater.* **2010**, *22*, 1805.
(88) Wiley, B. J.; Im, S. H.; Li, Z. Y.; McLellan, J.; Siekkinen, A.; Xia, Y. A. *J. Phys. Chem. B* **2006**, *110*, 15666.
(89) Reches, M.; Gazit, E. *Science* **2003**, *300*, 625.
(90) Chu, A.; Cook, J.; Heesom, R. J. R.; Hutchison, J. L.; Green, M. L. H.; Sloan, J. *Chem. Mater.* **1996**, *8*, 2751.
(91) Mazumder, V.; Chi, M.; More, K. L.; Sun, S. *Angew. Chem., Int. Ed.* **2010**, *49*, 9368.
(92) Liz-Marzán, L. M.; Giersig, M.; Mulvaney, P. *Langmuir* **1996**, *12*, 4329.
(93) Oldenburg, S. J.; Averitt, R. D.; Westcott, S. L.; Halas, N. J. *Chem. Phys. Lett.* **1998**, *288*, 243.
(94) Yang, J.; Elim, H. I.; Zhang, Q.; Lee, J. Y.; Ji, W. *J. Am. Chem. Soc.* **2006**, *128*, 11921.
(95) Chen, J.; McLellan, J. M.; Siekkinen, A.; Xiong, Y.; Li, Z.-Y.; Xia, Y. *J. Am. Chem. Soc.* **2006**, *128*, 14776.
(96) Chen, C.-L.; Zhang, P.; Rosi, N. L. *J. Am. Chem. Soc.* **2008**, *130*, 13555.
(97) Henglein, F.; Henglein, A.; Mulvaney, P. *Ber. Bunsen-Ges. Phys. Chem.* **1994**, *98*, 180.
(98) Henglein, A.; Mulvaney, P.; Linnert, T.; Holzwarth, A. *J. Phys. Chem.* **1992**, *96*, 2411.
(99) Henglein, A.; Holzwarth, A.; Mulvaney, P. *J. Phys. Chem.* **1992**, *96*, 8700.
(100) Henglein, A. *Chem. Rev.* **1989**, *89*, 1861.
(101) Sinzig, J.; Radtke, U.; Quinten, M.; Kreibig, U. *Z. Phys. D: At., Mol. Clusters* **1993**, *26*, 242.
(102) Mulvaney, P.; Giersig, M.; Henglein, A. *J. Phys. Chem.* **1993**, *97*, 7061.
(103) Hodak, J. H.; Henglein, A.; Giersig, M.; Hartland, G. V. *J. Phys. Chem. B* **2000**, *104*, 11708.
(104) Henglein, A. *J. Phys. Chem. B* **2000**, *104*, 2201.
(105) Henglein, A. *J. Phys. Chem. B* **2000**, *104*, 6683.
(106) Srnová-Šloufová, I.; Lednický, F.; Gemperle, A.; Gemperlová, J. *Langmuir* **2000**, *16*, 9928.
(107) Moskovits, M.; Srnová-Šloufová, I.; Vlčková, B. *J. Chem. Phys.* **2002**, *116*, 10435.
(108) Srnová-Šloufová, I.; Vlčková, B.; Bastl, Z.; Hasslett, T. L. *Langmuir* **2004**, *20*, 3407.
(109) Kumar, G. V. P.; Shruthi, S.; Vibha, B.; Reddy, B. A. A.; Kundu, T. K.; Narayana, C. *J. Phys. Chem. C* **2007**, *111*, 4388.
(110) Kim, Y.; Johnson, R. C.; Li, J.; Hupp, J. T.; Schatz, G. C. *Chem. Phys. Lett.* **2002**, *352*, 421.
(111) Yang, J.; Sargent, E.; Kelley, S.; Ying, J. Y. *Nat. Mater.* **2009**, *8*, 683.
(112) Xu, Z.; Hou, Y.; Sun, S. *J. Am. Chem. Soc.* **2007**, *129*, 8698.
(113) Wang, C.; Peng, S.; Chan, R.; Sun, S. *Small* **2009**, *5*, 567.
(114) Wang, L.; Yamauchi, Y. *J. Am. Chem. Soc.* **2010**, *132*, 13636.
(115) Wen, T.; Krishnan, K. M. *J. Phys. Chem. C* **2010**, *114*, 14838.
(116) Wang, C.; van der Vliet, D.; More, K. L.; Zaluzec, N. J.; Peng, S.; Sun, S.; Daimon, H.; Wang, G.; Greeley, J.; Pearson, J.; Paulikas, A. P.; Karapetrov, G.; Strmcnik, D.; Markovic, N. M.; Stamenkovic, V. R. *Nano Lett.* **2011**in press.
(117) Jin, R. C.; Cao, Y. C.; Hao, E. C.; Metraux, G. S.; Schatz, G. C.; Mirkin, C. A. *Nature* **2003**, *425*, 487.
(118) Xue, C.; Mirkin, C. A. *Angew. Chem., Int. Ed.* **2007**, *46*, 2036.
(119) Zhang, J.; Li, S. Z.; Wu, J. S.; Schatz, G. C.; Mirkin, C. A. *Angew. Chem., Int. Ed.* **2009**, *48*, 7787.
(120) Zhang, J.; Langille, M. R.; Mirkin, C. A. *J. Am. Chem. Soc.* **2010**, *132*, 12502.
(121) Pietrobon, B.; Kitaev, V. *Chem. Mater.* **2008**, *20*, 5186.
(122) Zheng, X.; Zhao, X.; Guo, D.; Tang, B.; Xu, S.; Zhao, B.; Xu, W.; Lombardi, J. R. *Langmuir* **2009**, *25*, 3802.
(123) Zhou, J.; An, J.; Tang, B.; Xu, S. P.; Cao, Y. X.; Zhao, B.; Xu, W. Q.; Chang, J. J.; Lombardi, J. R. *Langmuir* **2008**, *24*, 10407.
(124) Maillard, M.; Huang, P. R.; Brus, L. *Nano Lett.* **2003**, *3*, 1611.
(125) Callegari, A.; Tonti, D.; Chergui, M. *Nano Lett.* **2003**, *3*, 1565.
(126) Xue, C.; Métraux, G. S.; Millstone, J. E.; Mirkin, C. A. *J. Am. Chem. Soc.* **2008**, *130*, 8337.
(127) Wu, X. M.; Redmond, P. L.; Liu, H. T.; Chen, Y. H.; Steigerwald, M.; Brus, L. *J. Am. Chem. Soc.* **2008**, *130*, 9500.
(128) Lindstrom, C. D.; Zhu, X. Y. *Chem. Rev.* **2006**, *106*, 4281.
(129) Watanabe, K.; Menzel, D.; Nilius, N.; Freund, H. J. *Chem. Rev.* **2006**, *106*, 4301.
(130) Brus, L. *Acc. Chem. Res.* **2008**, *41*, 1742.
(131) Redmond, P. L.; Brus, L. E. *J. Phys. Chem. C* **2007**, *111*, 14849.
(132) Redmond, P. L.; Wu, X. M.; Brus, L. *J. Phys. Chem. C* **2007**, *111*, 8942.
(133) Lee, S. J.; Piorek, B. D.; Meinhart, C. D.; Moskovits, M. *Nano Lett.* **2010**, *10*, 1329.
(134) Wu, X. M.; Thrall, E. S.; Liu, H. T.; Steigerwald, M.; Brus, L. *J. Phys. Chem. C* **2010**, *114*, 12896.
(135) Xue, C.; Millstone, J. E.; Li, S. Y.; Mirkin, C. A. *Angew. Chem., Int. Ed.* **2007**, *46*, 8436.
(136) Langille, M. R.; Zhang, J.; Mirkin, C. A. *Angew. Chem., Int. Ed.* **2011**, *50*, 3543.
(137) Ah, C. S.; Hong, S. D.; Jang, D.-J. *J. Phys. Chem. B* **2001**, *105*, 7871.
(138) Song, J. H.; Kim, F.; Kim, D.; Yang, P. *Chem.—Eur. J.* **2005**, *11*, 910.

(139) Liu; Guyot-Sionnest, P. *J. Phys. Chem. B* **2004**, *108*, 5882.
(140) Huang, C.-C.; Yang, Z.; Chang, H.-T. *Langmuir* **2004**, *20*, 6089.
(141) Xiang, Y.; Wu, X.; Liu, D.; Li, Z.; Chu, W.; Feng, L.; Zhang, K.; Zhou, W.; Xie, S. *Langmuir* **2008**, *24*, 3465.
(142) Fernanda Cardinal, M.; Rodríguez-González, B.; Alvarez-Puebla, R. A.; Pérez-Juste, J.; Liz-Marzán, L. M. *J. Phys. Chem. C* **2010**, *114*, 10417.
(143) Cho, E. C.; Camargo, P. H. C.; Xia, Y. *Adv. Mater.* **2010**, *22*, 744.
(144) Seo, D.; Yoo, C. I.; Jung, J.; Song, H. *J. Am. Chem. Soc.* **2008**, *130*, 2940.
(145) Seo, D.; Park, J. H.; Jung, J.; Park, S. M.; Ryu, S.; Kwak, J.; Song, H. *J. Phys. Chem. C* **2009**, *113*, 3449.
(146) Jung, J.; Seo, D.; Park, G.; Ryu, S.; Song, H. *J. Phys. Chem. C* **2010**, *114*, 12529.
(147) Sanedrin, R. G.; Georganopoulou, D. G.; Park, S.; Mirkin, C. A. *Adv. Mater.* **2005**, *17*, 1027.
(148) Aherne, D.; Charles, D. E.; Brennan-Fournet, M. E.; Kelly, J. M.; Gun'ko, Y. K. *Langmuir* **2009**, *25*, 10165.
(149) Yoo, H.; Millstone, J. E.; Li, S.; Jang, J.-W.; Wei, W.; Wu, J.; Schatz, G. C.; Mirkin, C. A. *Nano Lett.* **2009**, *9*, 3038.
(150) Fan, F.-R.; Liu, D.-Y.; Wu, Y.-F.; Duan, S.; Xie, Z.-X.; Jiang, Z.-Y.; Tian, Z.-Q. *J. Am. Chem. Soc.* **2008**, *130*, 6949.
(151) Habas, S. E.; Lee, H.; Radmilovic, V.; Somorjai, G. A.; Yang, P. *Nat. Mater.* **2007**, *6*, 692.
(152) Lee, Y. W.; Kim, M.; Kim, Z. H.; Han, S. W. *J. Am. Chem. Soc.* **2009**, *131*, 17036.
(153) Lim, B.; Kobayashi, H.; Yu, T.; Wang, J.; Kim, M. J.; Li, Z.-Y.; Rycenga, M.; Xia, Y. *J. Am. Chem. Soc.* **2010**, *132*, 2506.
(154) Ma, Y.; Li, W.; Cho, E. C.; Li, Z.; Yu, T.; Zeng, J.; Xie, Z.; Xia, Y. *ACS Nano* **2010**, *4*, 6725.
(155) Lu, C.-L.; Prasad, K. S.; Wu, H.-L.; Ho, J. A.; Huang, M. H. *J. Am. Chem. Soc.* **2010**, *132*, 14546.
(156) Liz-Marzán, L. M.; Mulvaney, P. *J. Phys. Chem. B* **2003**, *107*, 7312.
(157) Mulvaney, P.; Liz-Marzán, L. M.; Giersig, M.; Ung, T. *J. Mater. Chem.* **2000**, *10*, 1259.
(158) Li, J. F.; Huang, Y. F.; Ding, Y.; Yang, Z. L.; Li, S. B.; Zhou, X. S.; Fan, F. R.; Zhang, W.; Zhou, Z. Y.; WuDe, Y.; Ren, B.; Wang, Z. L.; Tian, Z. Q. *Nature* **2010**, *464*, 392.
(159) Noginov, M. A.; Zhu, G.; Belgrave, A. M.; Bakker, R.; Shalaev, V. M.; Narimanov, E. E.; Stout, S.; Herz, E.; Suteewong, T.; Wiesner, U. *Nature* **2009**, *460*, 1110.
(160) Zhang, J.; Tang, Y.; Lee, K.; Ouyang, M. *Nature* **2010**, *466*, 91.
(161) Liz-Marzán, L. M.; Giersig, M.; Mulvaney, P. *Chem. Commun.* **1996**, 731.
(162) Stöber, W.; Fink, A.; Bohn, E. *J. Colloid Interface Sci.* **1968**, *26*, 62.
(163) Mulvaney, P.; Giersig, M.; Ung, T.; Liz-Marzán, L. M. *Adv. Mater.* **1997**, *9*, 570.
(164) Ung, T.; Liz-Marzán, L. M.; Mulvaney, P. *Langmuir* **1998**, *14*, 3740.
(165) Lu, Y.; Yin, Y.; Mayers, B. T.; Xia, Y. *Nano Lett.* **2002**, *2*, 183.
(166) Lu, Y.; Yin, Y.; Li, Z.-Y.; Xia, Y. *Nano Lett.* **2002**, *2*, 785.
(167) Pastoriza-Santos, I.; Perez-Juste, J.; Liz-Marzán, L. M. *Chem. Mater.* **2006**, *18*, 2465.
(168) Yin, Y.; Lu, Y.; Sun, Y.; Xia, Y. *Nano Lett.* **2002**, *2*, 427.
(169) Xue, C.; Chen, X.; Hurst, S. J.; Mirkin, C. A. *Adv. Mater.* **2007**, *19*, 4071.
(170) Banholzer, M. J.; Harris, N.; Millstone, J. E.; Schatz, G. C.; Mirkin, C. A. *J. Phys. Chem. C* **2010**, *114*, 7521.
(171) Sun, J. Y.; Wang, Z. K.; Lim, H. S.; Ng, S. C.; Kuok, M. H.; Tran, T. T.; Lu, X. *ACS Nano* **2010**, *4*, 7692.
(172) Kim, M.; Sohn, K.; Na, H. B.; Hyeon, T. *Nano Lett.* **2002**, *2*, 1383.
(173) Kamata, K.; Lu, Y.; Xia, Y. *J. Am. Chem. Soc.* **2003**, *125*, 2384.
(174) Mulvaney, S. P.; Musick, M. D.; Keating, C. D.; Natan, M. J. *Langmuir* **2003**, *19*, 4784.
(175) Zhang, F.; Braun, G. B.; Shi, Y.; Zhang, Y.; Sun, X.; Reich, N. O.; Zhao, D.; Stucky, G. *J. Am. Chem. Soc.* **2010**, *132*, 2850.
(176) Tang, F.; He, F.; Cheng, H.; Li, L. *Langmuir* **2010**, *26*, 11774.
(177) Mori, K.; Kawashima, M.; Che, M.; Yamashita, H. *Angew. Chem., Int. Ed.* **2010**, *49*, 8598.
(178) Pastoriza-Santos, I.; Koktysh, D. S.; Mamedov, A. A.; Giersig, M.; Kotov, N. A.; Liz-Marzán, L. M. *Langmuir* **2000**, *16*, 2731.
(179) Li, J.; Zeng, H. C. *Angew. Chem., Int. Ed.* **2005**, *44*, 4342.
(180) Mayya, K. S.; Gittins, D. I.; Caruso, F. *Chem. Mater.* **2001**, *13*, 3833.
(181) Oldfield, G.; Ung, T.; Mulvaney, P. *Adv. Mater.* **2000**, *12*, 1519.
(182) Tom, R. T.; Nair, A. S.; Singh, N.; Aslam, M.; Nagendra, C. L.; Philip, R.; Vijayamohanan, K.; Pradeep, T. *Langmuir* **2003**, *19*, 3439.
(183) Hirakawa, T.; Kamat, P. V. *Langmuir* **2004**, *20*, 5645.
(184) Hirakawa, T.; Kamat, P. V. *J. Am. Chem. Soc.* **2005**, *127*, 3928.
(185) Sudeep, P. K.; Takechi, K.; Kamat, P. V. *J. Phys. Chem. C* **2006**, *111*, 488.
(186) Kamat, P. V.; Shanghavi, B. *J. Phys. Chem. B* **1997**, *101*, 7675.
(187) Lu, W.; Wang, B.; Zeng, J.; Wang, X.; Zhang, S.; Hou, J. G. *Langmuir* **2005**, *21*, 3684.
(188) Yang, T.-T.; Chen, W.-T.; Hsu, Y.-J.; Wei, K.-H.; Lin, T.-Y.; Lin, T.-W. *J. Phys. Chem. C* **2010**, *114*, 11414.
(189) Lee, J.-S.; Shevchenko, E. V.; Talapin, D. V. *J. Am. Chem. Soc.* **2008**, *130*, 9673.
(190) Kuo, C.-H.; Hua, T.-E.; Huang, M. H. *J. Am. Chem. Soc.* **2009**, *131*, 17871.
(191) Sun, Z.; Yang, Z.; Zhou, J.; Yeung, M.; Ni, W.; Wu, H.; Wang, J. *Angew. Chem., Int. Ed.* **2009**, *48*, 2881.
(192) Zhang, J.; Tang, Y.; Lee, K.; Ouyang, M. *Science* **2010**, *327*, 1634.
(193) Aden, A. L.; Kerker, M. *J. Appl. Phys.* **1951**, *22*, 1242.
(194) Kerker, M.; Blatchford, C. G. *Phys. Rev. B* **1982**, *26*, 4052.
(195) Neeves, A. E.; Birnboim, M. H. *J. Opt. Soc. Am. B* **1989**, *6*, 787.
(196) Zhou, H. S.; Honma, I.; Komiyama, H.; Haus, J. W. *Phys. Rev. B* **1994**, *50*, 12052.
(197) Prodan, E.; Radloff, C.; Halas, N. J.; Nordlander, P. *Science* **2003**, *302*, 419.
(198) Wang, H.; Brandl, D. W.; Nordlander, P.; Halas, N. J. *Acc. Chem. Res.* **2006**, *40*, 53.
(199) Hirsch, L. R.; Stafford, R. J.; Bankson, J. A.; Sershen, S. R.; Rivera, B.; Price, R. E.; Hazle, J. D.; Halas, N. J.; West, J. L. *Proc. Natl. Acad. Sci. U.S.A.* **2003**, *100*, 13549.
(200) O'Neal, D. P.; Hirsch, L. R.; Halas, N. J.; Payne, J. D.; West, J. L. *Cancer Lett.* **2004**, *209*, 171.
(201) Loo, C.; Lin, A.; Hirsch, L.; Lee, M.-H.; Barton, J.; Halas, N.; West, J.; Drezek, R. *Technol. Cancer Res. Treat.* **2004**, *3*, 33.
(202) Loo, C.; Lowery, A.; Halas, N.; West, J.; Drezek, R. *Nano Lett.* **2005**, *5*, 709.
(203) Gobin, A. M.; Lee, M. H.; Halas, N. J.; James, W. D.; Drezek, R. A.; West, J. L. *Nano Lett.* **2007**, *7*, 1929.
(204) Choi, M.-R.; Stanton-Maxey, K. J.; Stanley, J. K.; Levin, C. S.; Bardhan, R.; Akin, D.; Badve, S.; Sturgis, J.; Robinson, J. P.; Bashir, R.; Halas, N. J.; Clare, S. E. *Nano Lett.* **2007**, *7*, 3759.
(205) Lal, S.; Clare, S. E.; Halas, N. J. *Acc. Chem. Res.* **2008**, *41*, 1842.
(206) Wang, Y.; Xie, X.; Wang, X.; Ku, G.; Gill, K. L.; O'Neal, D. P.; Stoica, G.; Wang, L. V. *Nano Lett.* **2004**, *4*, 1689.
(207) Zhou, C.; Tsai, T.-H.; Adler, D. C.; Lee, H.-C.; Cohen, D. W.; Mondelblatt, A.; Wang, Y.; Connolly, J. L.; Fujimoto, J. G. *Opt. Lett.* **2010**, *35*, 700.
(208) Oldenburg, S. J.; Westcott, S. L.; Averitt, R. D.; Halas, N. J. *J. Chem. Phys.* **1999**, *111*, 4729.
(209) Jackson, J. B.; Westcott, S. L.; Hirsch, L. R.; West, J. L.; Halas, N. J. *Appl. Phys. Lett.* **2003**, *82*, 257.
(210) Jackson, J. B.; Halas, N. J. *Proc. Natl. Acad. Sci. U.S.A.* **2004**, *101*, 17930.

(211) Talley, C. E.; Jackson, J. B.; Oubre, C.; Grady, N. K.; Hollars, C. W.; Lane, S. M.; Huser, T. R.; Nordlander, P.; Halas, N. J. *Nano Lett.* **2005**, *5*, 1569.
(212) Levin, C. S.; Bishnoi, S. W.; Grady, N. K.; Halas, N. J. *Anal. Chem.* **2006**, *78*, 3277.
(213) Huang, Y.; Swarup, V. P.; Bishnoi, S. W. *Nano Lett.* **2009**, *9*, 2914.
(214) Levin, C. S.; Kundu, J.; Barhoumi, A.; Halas, N. J. *Analyst* **2009**, *134*, 1745.
(215) Kundu, J.; Le, F.; Nordlander, P.; Halas, N. J. *Chem. Phys. Lett.* **2008**, *452*, 115.
(216) Wang, H.; Kundu, J.; Halas, N. J. *Angew. Chem., Int. Ed.* **2007**, *46*, 9040.
(217) Levin, C. S.; Kundu, J.; Janesko, B. G.; Scuseria, G. E.; Raphael, R. M.; Halas, N. J. *J. Phys. Chem. B* **2008**, *112*, 14168.
(218) Le, F.; Brandl, D. W.; Urzhumov, Y. A.; Wang, H.; Kundu, J.; Halas, N. J.; Aizpurua, J.; Nordlander, P. *ACS Nano* **2008**, *2*, 707.
(219) Tam, F.; Goodrich, G. P.; Johnson, B. R.; Halas, N. J. *Nano Lett.* **2007**, *7*, 496.
(220) Bardhan, R.; Grady, N. K.; Halas, N. J. *Small* **2008**, *4*, 1716.
(221) Bardhan, R.; Grady, N. K.; Cole, J. R.; Joshi, A.; Halas, N. J. *ACS Nano* **2009**, *3*, 744.
(222) Warshawsky, A.; Upson, D. A. *J. Polym. Sci., Part A: Polym. Chem.* **1989**, *27*, 2963.
(223) Tamai, H.; Sakurai, H.; Hirota, Y.; Nishiyama, F.; Yasuda, H. *J. Appl. Polym. Sci.* **1995**, *56*, 441.
(224) Dokoutchaev, A.; James, J. T.; Koene, S. C.; Pathak, S.; Prakash, G. K. S.; Thompson, M. E. *Chem. Mater.* **1999**, *11*, 2389.
(225) Tan, L.; Chen, D.; Liu, H.; Tang, F. *Adv. Mater.* **2010**, *22*, 4885.
(226) Mayer, A. B. R.; Grebner, W.; Wannemacher, R. *J. Phys. Chem. B* **2000**, *104*, 7278.
(227) Kobayashi, Y.; Salgueiriño-Maceira, V.; Liz-Marzán, L. M. *Chem. Mater.* **2001**, *13*, 1630.
(228) Kobayashi, Y.; Tadaki, Y.; Nagao, D.; Konno, M. *J. Colloid Interface Sci.* **2005**, *283*, 601.
(229) Oláh, A.; Hempenius, M. A.; Vancso, G. J. *Eur. Polym. J.* **2004**, *40*, 763.
(230) Schuetz, P.; Caruso, F. *Chem. Mater.* **2004**, *16*, 3066.
(231) Lou, X.; Yuan, C.; Rhoades, E.; Zhang, Q.; Archer, L. *Adv. Funct. Mater.* **2006**, *16*, 1679.
(232) Phonthammachai, N.; White, T. J. *Langmuir* **2007**, *23*, 11421.
(233) Choi, W. S.; Koo, H. Y.; Kim, D.-Y. *Langmuir* **2008**, *24*, 4633.
(234) Antipov, A. A.; Sukhorukov, G. B.; Fedutik, Y. A.; Hartmann, J.; Giersig, M.; Möhwald, H. *Langmuir* **2002**, *18*, 6687.
(235) Chen, Z.; Chen, X.; Zheng, L.; Gang, T.; Cui, T.; Zhang, K.; Yang, B. *J. Colloid Interface Sci.* **2005**, *285*, 146.
(236) Tian, C.; Wang, E.; Gao, L.; Kang, Z.; Zhang, C.; Wang, C.; Lan, Y. *Chem. Lett.* **2006**, *35*, 812.
(237) Jean, R.-D.; Chiu, K.-C.; Chen, T.-H.; Chen, C.-H.; Liu, D.-M. *J. Phys. Chem. C* **2010**, *114*, 15633.
(238) Wang, Y.; Shen, Y.; Xie, A.; Li, S.; Wang, X.; Cai, Y. *J. Phys. Chem. C* **2010**, *114*, 4297.
(239) Dawson, A.; Kamat, P. V. *J. Phys. Chem. B* **2001**, *105*, 960.
(240) Subramanian, V.; Wolf, E. E.; Kamat, P. V. *Langmuir* **2002**, *19*, 469.
(241) Cozzoli, P. D.; Comparelli, R.; Fanizza, E.; Curri, M. L.; Agostiano, A.; Laub, D. *J. Am. Chem. Soc.* **2004**, *126*, 3868.
(242) Kamat, P. V.; Flumiani, M.; Dawson, A. *Metal-Metal and Metal-Semiconductor Composite Nanoclusters*; Elsevier: Kidlington, U. K., 2002; p 269.
(243) Subramanian, V.; Wolf, E. E.; Kamat, P. V. *J. Phys. Chem. B* **2003**, *107*, 7479.
(244) Wood, A.; Giersig, M.; Mulvaney, P. *J. Phys. Chem. B* **2001**, *105*, 8810.
(245) Chen, C.-W.; Chen, M.-Q.; Serizawa, T.; Akashi, M. *Adv. Mater.* **1998**, *10*, 1122.
(246) Chen, C.-W.; Serizawa, T.; Akashi, M. *Langmuir* **1999**, *15*, 7998.
(247) Chen, C.-W.; Serizawa, T.; Akashi, M. *Chem. Mater.* **2002**, *14*, 2232.
(248) Flores, J. C.; Torres, V.; Popa, M.; Crespo, D.; Calderón-Moreno, J. M. *J. Non-Cryst. Solids* **2008**, *354*, 5435.
(249) Pol, V. G.; Srivastava, D. N.; Palchik, O.; Palchik, V.; Slifkin, M. A.; Weiss, A. M.; Gedanken, A. *Langmuir* **2002**, *18*, 3352.
(250) Pol, V. G.; Gedanken, A.; Calderón-Moreno, J. M. *Chem. Mater.* **2003**, *15*, 1111.
(251) Pol, V. G.; Grisaru, H.; Gedanken, A. *Langmuir* **2005**, *21*, 3635.
(252) Ye, X.; Zhou, Y.; Chen, J.; Sun, Y. *Appl. Surf. Sci.* **2007**, *253*, 6264.
(253) Barnickel, P.; Wokaun, A. *Mol. Phys.* **1989**, *67*, 1355.
(254) Averitt, R. D.; Sarkar, D.; Halas, N. J. *Phys. Rev. Lett.* **1997**, *78*, 4217.
(255) Averitt, R. D.; Westcott, S. L.; Halas, N. J. *J. Opt. Soc. Am. B* **1999**, *16*, 1824.
(256) Averitt, R. D.; Westcott, S. L.; Halas, N. J. *Phys. Rev. B* **1998**, *58*, R10203.
(257) Averitt, R. D.; Westcott, S. L.; Halas, N. J. *J. Opt. Soc. Am. B* **1999**, *16*, 1814.
(258) Westcott, S. L.; Averitt, R. D.; Wolfgang, J. A.; Nordlander, P.; Halas, N. J. *J. Phys. Chem. B* **2001**, *105*, 9913.
(259) Skirtach, A. G.; Dejugnat, C.; Braun, D.; Susha, A. S.; Rogach, A. L.; Parak, W. J.; Möhwald, H.; Sukhorukov, G. B. *Nano Lett.* **2005**, *5*, 1371.
(260) Raschke, G.; Brogl, S.; Susha, A. S.; Rogach, A. L.; Klar, T. A.; Feldmann, J.; Fieres, B.; Petkov, N.; Bein, T.; Nichtl, A.; Kürzinger, K. *Nano Lett.* **2004**, *4*, 1853.
(261) Norman, T. J.; Grant, C. D.; Magana, D.; Zhang, J. Z.; Liu, J.; Cao, D.; Bridges, F.; Van Buuren, A. *J. Phys. Chem. B* **2002**, *106*, 7005.
(262) Zhang, J. Z.; Schwartzberg, A. M.; Norman, T.; Grant, C. D.; Liu, J.; Bridges, F.; van Buuren, T. *Nano Lett.* **2005**, *5*, 809.
(263) Raschke, G.; Brogl, S.; Susha, A. S.; Rogach, A. L.; Klar, T. A.; Feldmann, J.; Fieres, B.; Petkov, N.; Bein, T.; Nichtl, A.; Kürzinger, K. *Nano Lett.* **2005**, *5*, 811.
(264) Westcott, S. L.; Oldenburg, S. J.; Lee, T. R.; Halas, N. J. *Langmuir* **1998**, *14*, 5396.
(265) Oldenburg, S. J.; Hale, G. D.; Jackson, J. B.; Halas, N. J. *Appl. Phys. Lett.* **1999**, *75*, 1063.
(266) Oldenburg, S. J.; Jackson, J. B.; Westcott, S. L.; Halas, N. J. *Appl. Phys. Lett.* **1999**, *75*, 2897.
(267) Graf, C.; van Blaaderen, A. *Langmuir* **2001**, *18*, 524.
(268) Shi, W.; Sahoo, Y.; Swihart, M. T.; Prasad, P. N. *Langmuir* **2005**, *21*, 1610.
(269) Brinson, B. E.; Lassiter, J. B.; Levin, C. S.; Bardhan, R.; Mirin, N.; Halas, N. J. *Langmuir* **2008**, *24*, 14166.
(270) West, J. L.; Halas, N. J. *Annu. Rev. Biomed. Eng.* **2003**, *5*, 285.
(271) Hirsch, L.; Gobin, A.; Lowery, A.; Tam, F.; Drezek, R.; Halas, N.; West, J. *Ann. Biomed. Eng.* **2006**, *34*, 15.
(272) Brongersma, M. L. *Nat. Mater.* **2003**, *2*, 296.
(273) Hirsch, L. R.; Jackson, J. B.; Lee, A.; Halas, N. J.; West, J. L. *Anal. Chem.* **2003**, *75*, 2377.
(274) Sershen, S. R.; Westcott, S. L.; Halas, N. J.; West, J. L. *J. Biomed. Mater. Res.* **2000**, *51*, 293.
(275) Sershen, S. R.; Westcott, S. L.; Halas, N. J.; West, J. L. *Appl. Phys. Lett.* **2002**, *80*, 4609.
(276) Sershen, S. R.; Westcott, S. L.; West, J. L.; Halas, N. J. *Appl. Phys. B: Lasers Opt.* **2001**, *73*, 379.
(277) Barhoumi, A.; Huschka, R.; Bardhan, R.; Knight, M. W.; Halas, N. J. *Chem. Phys. Lett.* **2009**, *482*, 171.
(278) Huschka, R.; Neumann, O.; Barhoumi, A.; Halas, N. J. *Nano Lett.* **2010**, *10*, 4117.
(279) Tam, F.; Moran, C.; Halas, N. *J. Phys. Chem. B* **2004**, *108*, 17290.
(280) Fan, J. A.; Wu, C.; Bao, K.; Bao, J.; Bardhan, R.; Halas, N. J.; Manoharan, V. N.; Nordlander, P.; Shvets, G.; Capasso, F. *Science* **2010**, *328*, 1135.

(281) Westcott, S. L.; Jackson, J. B.; Radloff, C.; Halas, N. J. *Phys. Rev. B* **2002**, *66*, 155431.
(282) Grady, N. K.; Halas, N. J.; Nordlander, P. *Chem. Phys. Lett.* **2004**, *399*, 167.
(283) Tam, F.; Chen, A. L.; Kundu, J.; Wang, H.; Halas, N. J. *J. Chem. Phys.* **2007**, *127*, 204703.
(284) Oubre, C.; Nordlander, P. *J. Phys. Chem. B* **2004**, *108*, 17740.
(285) Prodan, E.; Nordlander, P. *Nano Lett.* **2003**, *3*, 543.
(286) Prodan, E.; Nordlander, P.; Halas, N. J. *Nano Lett.* **2003**, *3*, 1411.
(287) Prodan, E.; Lee, A.; Nordlander, P. *Chem. Phys. Lett.* **2002**, *360*, 325.
(288) Prodan, E.; Nordlander, P.; Halas, N. J. *Chem. Phys. Lett.* **2003**, *368*, 94.
(289) Knight, M. W.; Wu, Y.; Lassiter, J. B.; Nordlander, P.; Halas, N. J. *Nano Lett.* **2009**, *9*, 2188.
(290) Wu, Y.; Nordlander, P. *J. Phys. Chem. C* **2009**, *114*, 7302.
(291) Lal, S.; Westcott, S. L.; Taylor, R. N.; Jackson, J. B.; Nordlander, P.; Halas, N. J. *J. Phys. Chem. B* **2002**, *106*, 5609.
(292) Prodan, E.; Nordlander, P. *J. Chem. Phys.* **2004**, *120*, 5444.
(293) Brandl, D. W.; Oubre, C.; Nordlander, P. *J. Chem. Phys.* **2005**, *123*, 024701.
(294) Lassiter, J. B.; Aizpurua, J.; Hernandez, L. I.; Brandl, D. W.; Romero, I.; Lal, S.; Hafner, J. H.; Nordlander, P.; Halas, N. J. *Nano Lett.* **2008**, *8*, 1212.
(295) Jackson, J. B.; Halas, N. J. *J. Phys. Chem. B* **2001**, *105*, 2743.
(296) Jiang, Z.-j.; Liu, C.-y. *J. Phys. Chem. B* **2003**, *107*, 12411.
(297) Tian, C.; Wang, E.; Kang, Z.; Mao, B.; Zhang, C.; Lan, Y.; Wang, C.; Song, Y. *J. Solid State Chem.* **2006**, *179*, 3270.
(298) Lim, Y. T.; Park, O. O.; Jung, H.-T. *J. Colloid Interface Sci.* **2003**, *263*, 449.
(299) Zhang, J.; Liu, H.; Wang, Z.; Ming, N. *Mater. Lett.* **2007**, *61*, 4579.
(300) Zhang, J.; Liu, J.; Wang, S.; Zhan, P.; Wang, Z.; Ming, N. *Adv. Funct. Mater.* **2004**, *14*, 1089.
(301) Tian, C.; Mao, B.; Wang, E.; Kang, Z.; Song, Y.; Wang, C.; Li, S. *J. Phys. Chem. C* **2007**, *111*, 3651.
(302) Wang, H.; Tam, F.; Grady, N. K.; Halas, N. J. *J. Phys. Chem. B* **2005**, *109*, 18218.
(303) Lu, L.; Sun, G.; Xi, S.; Wang, H.; Zhang, H.; Wang, T.; Zhou, X. *Langmuir* **2003**, *19*, 3074.
(304) Kim, J.-H.; Bryan, W. W.; Randall Lee, T. *Langmuir* **2008**, *24*, 11147.
(305) Ji, T.; Lirtsman, V. G.; Avny, Y.; Davidov, D. *Adv. Mater.* **2001**, *13*, 1253.
(306) Bardhan, R.; Chen, W.; Perez-Torres, C.; Bartels, M.; Huschka, R. M.; Zhao, L. L.; Morosan, E.; Pautler, R. G.; Joshi, A.; Halas, N. J. *Adv. Funct. Mater.* **2009**, *19*, 3901.
(307) Salgueiriño-Maceira, V.; Correa-Duarte, M. A.; Farle, M.; López-Quintela, A.; Sieradzki, K.; Diaz, R. *Chem. Mater.* **2006**, *18*, 2701.
(308) Ji, X.; Shao, R.; Elliott, A. M.; Stafford, R. J.; Esparza-Coss, E.; Bankson, J. A.; Liang, G.; Luo, Z.-P.; Park, K.; Markert, J. T.; Li, C. *J. Phys. Chem. C* **2007**, *111*, 6245.
(309) Park, K.; Liang, G.; Ji, X.; Luo, Z.-P.; Li, C.; Croft, M. C.; Markert, J. T. *J. Phys. Chem. C* **2007**, *111*, 18512.
(310) Zhang, Q.; Ge, J.; Goebl, J.; Hu, Y.; Sun, Y.; Yin, Y. *Adv. Mater.* **2010**, *22*, 1905.
(311) Stoeva, S. I.; Huo, F.; Lee, J.-S.; Mirkin, C. A. *J. Am. Chem. Soc.* **2005**, *127*, 15362.
(312) Kim, J.; Park, S.; Lee, J. E.; Jin, S. M.; Lee, J. H.; Lee, I. S.; Yang, I.; Kim, J.-S.; Kim, S. K.; Cho, M.-H.; Hyeon, T. *Angew. Chem., Int. Ed.* **2006**, *45*, 7754.
(313) Aguirre, C. M.; Moran, C. E.; Young, J. F.; Halas, N. J. *J. Phys. Chem. B* **2004**, *108*, 7040.
(314) Prasad, V.; Mikhailovsky, A.; Zasadzinski, J. A. *Langmuir* **2005**, *21*, 7528.
(315) Wang, H.; Goodrich, G. P.; Tam, F.; Oubre, C.; Nordlander, P.; Halas, N. J. *J. Phys. Chem. B* **2005**, *109*, 11083.
(316) Lassiter, J. B.; Knight, M. W.; Mirin, N. A.; Halas, N. J. *Nano Lett.* **2009**, *9*, 4326.
(317) Knight, M. W.; Halas, N. J. *New J. Phys.* **2008**, *10*, 105006.
(318) Schierhorn, M.; Liz-Marzán, L. M. *Nano Lett.* **2001**, *2*, 13.
(319) Xu, H. *Phys. Rev. B* **2005**, *72*, 073405.
(320) Hu, Y.; Fleming, R. C.; Drezek, R. A. *Opt. Express* **2008**, *16*, 19579.
(321) Mukherjee, S.; Sobhani, H.; Lassiter, J. B.; Bardhan, R.; Nordlander, P.; Halas, N. J. *Nano Lett.* **2010**, *10*, 2694.
(322) Radloff, C.; Halas, N. J. *Nano Lett.* **2004**, *4*, 1323.
(323) Bardhan, R.; Mukherjee, S.; Mirin, N. A.; Levit, S. D.; Nordlander, P.; Halas, N. J. *J. Phys. Chem. C* **2009**, *114*, 7378.
(324) Charnay, C.; Lee, A.; Man, S.-Q.; Moran, C. E.; Radloff, C.; Bradley, R. K.; Halas, N. J. *J. Phys. Chem. B* **2003**, *107*, 7327.
(325) Wang, H.; Wu, Y.; Lassiter, B.; Nehl, C. L.; Hafner, J. H.; Nordlander, P.; Halas, N. J. *Proc. Natl. Acad. Sci. U.S.A.* **2006**, *103*, 10856.
(326) Wang, H.; Brandl, D. W.; Le, F.; Nordlander, P.; Halas, N. J. *Nano Lett.* **2006**, *6*, 827.
(327) Wang, L.; Bai, J.; Li, Y.; Huang, Y. *Angew. Chem., Int. Ed.* **2008**, *47*, 2439.
(328) Goon, I. Y.; Lai, L. M. H.; Lim, M.; Munroe, P.; Gooding, J. J.; Amal, R. *Chem. Mater.* **2009**, *21*, 673.
(329) Zhou, X.; Xu, W.; Wang, Y.; Kuang, Q.; Shi, Y.; Zhong, L.; Zhang, Q. *J. Phys. Chem. C* **2010**, *114*, 19607.
(330) Chin, S. F.; Iyer, K. S.; Raston, C. L. *Cryst. Growth Des.* **2009**, *9*, 2685.
(331) Lim, J.; Eggeman, A.; Lanni, F.; Tilton, R. D.; Majetich, S. A. *Adv. Mater.* **2008**, *20*, 1721.
(332) Levin, C. S.; Hofmann, C.; Ali, T. A.; Kelly, A. T.; Morosan, E.; Nordlander, P.; Whitmire, K. H.; Halas, N. J. *ACS Nano* **2009**, *3*, 1379.
(333) Bardhan, R.; Grady, N. K.; Ali, T.; Halas, N. J. *ACS Nano* **2010**, *4*, 6169.
(334) An, C.; Peng, S.; Sun, Y. *Adv. Mater.* **2010**, *22*, 2570.
(335) Zhang, H.; Li, Y.; Ivanov, I. A.; Qu, Y.; Huang, Y.; Duan, X. *Angew. Chem., Int. Ed.* **2010**, *49*, 2865.
(336) Yu, H.; Chen, M.; Rice, P. M.; Wang, S. X.; White, R. L.; Sun, S. *Nano Lett.* **2005**, *5*, 379.
(337) Aaron, J. S.; Oh, J.; Larson, T. A.; Kumar, S.; Milner, T. E.; Sokolov, K. V. *Opt. Express* **2006**, *14*, 12930.
(338) Larson, T. A.; Bankson, J. A.; Aaron, J. S.; Sokolov, K. V. *Nanotechnology* **2007**, *18*, 325101.
(339) Schotter, J.; Bethge, O.; Maier, T.; Brueckl, H. *Appl. Phys. Lett.* **2008**, *93*, 144105.
(340) Wang, L.; Park, H.-Y.; Lim, S. I.-I.; Schadt, M. J.; Mott, D.; Luo, J.; Wang, X.; Zhong, C.-J. *J. Mater. Chem.* **2008**, *18*, 2629.
(341) Lee, J. H.; Mahmoud, M. A.; Sitterle, V.; Sitterle, J.; Meredith, J. C. *J. Am. Chem. Soc.* **2009**, *131*, 5048.
(342) Mohammad, F.; Balaji, G.; Weber, A.; Uppu, R. M.; Kumar, C. S. S. R. *J. Phys. Chem. C* **2010**, *114*, 19194.
(343) Lyon, J. L.; Fleming, D. A.; Stone, M. B.; Schiffer, P.; Williams, M. E. *Nano Lett.* **2004**, *4*, 719.
(344) Wang, L.; Luo, J.; Maye, M. M.; Fan, Q.; Rendeng, Q.; Engelhard, M. H.; Wang, C.; Lin, Y.; Zhong, C.-J. *J. Mater. Chem.* **2005**, *15*, 1821.
(345) Wang, L.; Luo, J.; Fan, Q.; Suzuki, M.; Suzuki, I. S.; Engelhard, M. H.; Lin, Y.; Kim, N.; Wang, J. Q.; Zhong, C.-J. *J. Phys. Chem. B* **2005**, *109*, 21593.
(346) Lo, C. K.; Xiao, D.; Choi, M. M. F. *J. Mater. Chem.* **2007**, *17*, 2418.
(347) Mandal, M.; Kundu, S.; Ghosh, S. K.; Panigrahi, S.; Sau, T. K.; Yusuf, S. M.; Pal, T. *J. Colloid Interface Sci.* **2005**, *286*, 187.
(348) Park, H.-Y.; Schadt, M. J.; Wang, L.; Lim, S. I.-I.; Njoki, P. N.; Kim, S. H.; Jang, M.-Y.; Luo, J.; Zhong, C.-J. *Langmuir* **2007**, *23*, 9050.
(349) Wei, Q.; Song, H.-M.; Leonov, A. P.; Hale, J. A.; Oh, D.; Ong, Q. K.; Ritchie, K.; Wei, A. *J. Am. Chem. Soc.* **2009**, *131*, 9728.
(350) Song, H.-M.; Wei, Q.; Ong, Q. K.; Wei, A. *ACS Nano* **2010**, *4*, 5163.
(351) Jiang, J.; Gu, H.; Shao, H.; Devlin, E.; Papaefthymiou, G. C.; Ying, J. Y. *Adv. Mater.* **2008**, *20*, 4403.

(352) Choi, J.-s.; Jun, Y.-w.; Yeon, S.-I.; Kim, H. C.; Shin, J.-S.; Cheon, J. *J. Am. Chem. Soc.* **2006**, *128*, 15982.
(353) Xu, C.; Wang, B.; Sun, S. *J. Am. Chem. Soc.* **2009**, *131*, 4216.
(354) Li, Y.; Zhang, Q.; Nurmikko, A. V.; Sun, S. *Nano Lett.* **2005**, *5*, 1689.
(355) Mokari, T.; Rothenberg, E.; Popov, I.; Costi, R.; Banin, U. *Science* **2004**, *304*, 1787.
(356) Costi, R.; Cohen, G.; Salant, A.; Rabani, E.; Banin, U. *Nano Lett.* **2009**, *9*, 2031.
(357) Perro, A.; Reculusa, S.; Ravaine, S.; Bourgeat-Lami, E.; Duguet, E. *J. Mater. Chem.* **2005**, *15*, 3745.
(358) Gu, H.; Yang, Z.; Gao, J.; Chang, C. K.; Xu, B. *J. Am. Chem. Soc.* **2004**, *127*, 34.
(359) Wang, C.; Xu, C.; Zeng, H.; Sun, S. *Adv. Mater.* **2009**, *21*, 3045.
(360) Costi, R.; Saunders, A.; Banin, U. *Angew. Chem., Int. Ed.* **2010**, *49*, 4878.
(361) Cozzoli, P. D.; Pellegrino, T.; Manna, L. *Chem. Soc. Rev.* **2006**, *35*, 1195.
(362) Jun, Y.-w.; Choi, J.-s.; Cheon, J. *Angew. Chem., Int. Ed.* **2006**, *45*, 3414.
(363) Peng, X.; Wickham, J.; Alivisatos, A. P. *J. Am. Chem. Soc.* **1998**, *120*, 5343.
(364) Pacholski, C.; Kornowski, A.; Weller, H. *Angew. Chem., Int. Ed.* **2004**, *43*, 4774.
(365) Carbone, L.; Jakab, A.; Khalavka, Y.; Sönnichsen, C. *Nano Lett.* **2009**, *9*, 3710.
(366) Mokari, T.; Sztrum, C. G.; Salant, A.; Rabani, E.; Banin, U. *Nat. Mater.* **2005**, *4*, 855.
(367) Menagen, G.; Macdonald, J. E.; Shemesh, Y.; Popov, I.; Banin, U. *J. Am. Chem. Soc.* **2009**, *131*, 17406.
(368) Saunders, A. E.; Popov, I.; Banin, U. *J. Phys. Chem. B* **2006**, *110*, 25421.
(369) Menagen, G.; Mocatta, D.; Salant, A.; Popov, I.; Dorfs, D.; Banin, U. *Chem. Mater.* **2008**, *20*, 6900.
(370) Yong, K.-T.; Sahoo, Y.; Swihart, M. T.; Prasad, P. N. *Adv. Mater.* **2006**, *18*, 1978.
(371) Steiner, D.; Mokari, T.; Banin, U.; Millo, O. *Phys. Rev. Lett.* **2005**, *95*, 056805.
(372) Costi, R.; Saunders, A. E.; Elmalem, E.; Salant, A.; Banin, U. *Nano Lett.* **2008**, *8*, 637.
(373) Wetz, F.; Soulantica, K.; Falqui, A.; Respaud, M.; Snoeck, E.; Chaudret, B. *Angew. Chem., Int. Ed.* **2007**, *46*, 7079.
(374) Xu, C.; Xie, J.; Ho, D.; Wang, C.; Kohler, N.; Walsh, Edward, G.; Morgan, J. R.; Chin, Y. E.; Sun, S. *Angew. Chem., Int. Ed.* **2008**, *47*, 173.
(375) Yin, H.; Wang, C.; Zhu, H.; Overbury, S. H.; Sun, S.; Dai, S. *Chem. Commun.* **2008**, *44*, 4357.
(376) Pellegrino, T.; Fiore, A.; Carlino, E.; Giannini, C.; Cozzoli, P. D.; Ciccarella, G.; Respaud, M.; Palmirotta, L.; Cingolani, R.; Manna, L. *J. Am. Chem. Soc.* **2006**, *128*, 6690.
(377) Zeng, J.; Huang, J.; Liu, C.; Wu, C. H.; Lin, Y.; Wang, X.; Zhang, S.; Hou, J.; Xia, Y. *Adv. Mater.* **2010**, *22*, 1936.
(378) Shi, W.; Zeng, H.; Sahoo, Y.; Ohulchanskyy, T. Y.; Ding, Y.; Wang, Z. L.; Swihart, M.; Prasad, P. N. *Nano Lett.* **2006**, *6*, 875.
(379) Figuerola, A.; Franchini, I. R.; Fiore, A.; Mastria, R.; Falqui, A.; Bertoni, G.; Bals, S.; Van Tendeloo, G.; Kudera, S.; Cingolani, R.; Manna, L. *Adv. Mater.* **2009**, *21*, 550.
(380) Pang, M.; Hu, J.; Zeng, H. C. *J. Am. Chem. Soc.* **2010**, *132*, 10771.
(381) Wang, C.; Wei, Y.; Jiang, H.; Sun, S. *Nano Lett.* **2009**, *9*, 4544.
(382) Chen, T.; Chen, G.; Xing, S.; Wu, T.; Chen, H. *Chem. Mater.* **2010**, *22*, 3826.
(383) Shi, W.; Sahoo, Y.; Zeng, H.; Ding, Y.; Swihart, M. T.; Prasad, P. N. *Adv. Mater.* **2006**, *18*, 1889.
(384) Pazos-Pérez, N.; Gao, Y.; Hilgendorff, M.; Irsen, S.; Pérez-Juste, J.; Spasova, M.; Farle, M.; Liz-Marzán, L. M.; Giersig, M. *Chem. Mater.* **2007**, *19*, 4415.
(385) Gao, X.; Yu, L.; MacCuspie, R.; Matsui, H. *Adv. Mater.* **2005**, *17*, 426.
(386) Wei, Y.; Klajn, R.; Pinchuk, A. O.; Grzybowski, B. A. *Small* **2008**, *4*, 1635.
(387) Talapin, D. V.; Yu, H.; Shevchenko, E. V.; Lobo, A.; Murray, C. B. *J. Phys. Chem. C* **2007**, *111*, 14049.
(388) Mulvihill, M. J.; Ling, X. Y.; Henzie, J.; Yang, P. *J. Am. Chem. Soc.* **2009**, *132*, 268.
(389) Hao, E.; Li, S.; Bailey, R. C.; Zou, S.; Schatz, G. C.; Hupp, J. T. *J. Phys. Chem. B* **2004**, *108*, 1224.
(390) Sun, Y.; Mayers, B.; Xia, Y. *Adv. Mater.* **2003**, *15*, 641.
(391) Mahmoud, M. A.; Snyder, B.; El-Sayed, M. A. *J. Phys. Chem. C* **2010**, *114*, 7436.
(392) Mahmoud, M. A.; El-Sayed, M. A. *Nano Lett.* **2009**, *9*, 3025.
(393) Hunyadi, S. E.; Murphy, C. J. *J. Mater. Chem.* **2006**, *16*, 3929.
(394) Alvarez-Puebla, R. A.; Ross, D. J.; Nazri, G. A.; Aroca, R. F. *Langmuir* **2005**, *21*, 10504.
(395) Küstner, B.; Gellner, M.; Schütz, M.; Schöppler, F.; Marx, A.; Ströbel, P.; Adam, P.; Schmuck, C.; Schlücker, S. *Angew. Chem., Int. Ed.* **2009**, *48*, 1950.
(396) Sun, Y.; Xia, Y. *Anal. Chem.* **2002**, *74*, 5297.
(397) Mahmoud, M. A.; El-Sayed, M. A. *J. Am. Chem. Soc.* **2010**, *132*, 12704.
(398) Chen, J.; Wiley, B.; Li, Z.-Y.; Campbell, D.; Saeki, F.; Cang, H.; Au, L.; Lee, J.; Li, X.; Xia, Y. *Adv. Mater.* **2005**, *17*, 2255.
(399) Stewart, M. E.; Mack, N. H.; Malyarchuk, V.; Soares, J. A. N. T.; Lee, T.-W.; Gray, S. K.; Nuzzo, R. G.; Rogers, J. A. *Proc. Natl. Acad. Sci. U.S.A.* **2006**, *103*, 17143.
(400) Skrabalak, S.; Chen, J.; Au, L.; Lu, X.; Li, X.; Xia, Y. *Adv. Mater.* **2007**, *19*, 3177.
(401) Chen, J.; Yang, M.; Zhang, Q.; Cho, E. C.; Cobley, C. M.; Kim, C.; Glaus, C.; Wang, L. V.; Welch, M. J.; Xia, Y. *Adv. Funct. Mater.* **2010**, *20*, 3684.
(402) Chen, J.; Wang, D.; Xi, J.; Au, L.; Siekkinen, A.; Warsen, A.; Li, Z.-Y.; Zhang, H.; Xia, Y.; Li, X. *Nano Lett.* **2007**, *7*, 1318.
(403) Au, L.; Zheng, D.; Zhou, F.; Li, Z.-Y.; Li, X.; Xia, Y. *ACS Nano* **2008**, *2*, 1645.
(404) Chen, J.; Glaus, C.; Laforest, R.; Zhang, Q.; Yang, M.; Gidding, M.; Welch, M. J.; Xia, Y. *Small* **2010**, *6*, 811.
(405) Yavuz, M. S.; Cheng, Y.; Chen, J.; Cobley, C. M.; Zhang, Q.; Rycenga, M.; Xie, J.; Kim, C.; Song, K. H.; Schwartz, A. G.; Wang, L. V.; Xia, Y. *Nat. Mater.* **2009**, *8*, 935.
(406) Chen, J.; Saeki, F.; Wiley, B. J.; Cang, H.; Cobb, M. J.; Li, Z.-Y.; Au, L.; Zhang, H.; Kimmey, M. B.; Li, X.; Xia, Y. *Nano Lett.* **2005**, *5*, 473.
(407) Song, K. H.; Kim, C.; Cobley, C. M.; Xia, Y.; Wang, L. V. *Nano Lett.* **2008**, *9*, 183.
(408) Kim, C.; Cho, E. C.; Chen, J.; Song, K. H.; Au, L.; Favazza, C.; Zhang, Q.; Cobley, C. M.; Gao, F.; Xia, Y.; Wang, L. V. *ACS Nano* **2010**, *4*, 4559.
(409) Song, J. H.; Wu, Y.; Messer, B.; Kind, H.; Yang, P. *J. Am. Chem. Soc.* **2001**, *123*, 10397.
(410) Carbone, L.; Kudera, S.; Giannini, C.; Ciccarella, G.; Cingolani, R.; Cozzoli, P. D.; Manna, L. *J. Mater. Chem.* **2006**, *16*, 3952.
(411) Khalavka, Y.; Sönnichsen, C. *Adv. Mater.* **2008**, *20*, 588.
(412) Yang, J.; Peng, J.; Zhang, Q.; Peng, F.; Wang, H.; Yu, H. *Angew. Chem., Int. Ed.* **2009**, *48*, 3991.
(413) Sun, Y.; Mayers, B. T.; Xia, Y. *Nano Lett.* **2002**, *2*, 481.
(414) Sun, Y.; Xia, Y. *Nano Lett.* **2003**, *3*, 1569.
(415) Sun, Y.; Xia, Y. *J. Am. Chem. Soc.* **2004**, *126*, 3892.
(416) Lu, X.; Tuan, H.-Y.; Chen, J.; Li, Z.-Y.; Korgel, B. A.; Xia, Y. *J. Am. Chem. Soc.* **2007**, *129*, 1733.
(417) Shi, H.; Zhang, L. *J. Appl. Phys.* **2000**, *87*, 1572.
(418) Erlebacher, J.; Aziz, M. J.; Karma, A.; Dimitrov, N.; Sieradzki, K. *Nature* **2001**, *410*, 450.
(419) Yin, Y.; Erdonmez, C.; Aloni, S.; Alivisatos, A. P. *J. Am. Chem. Soc.* **2006**, *128*, 12671.
(420) Shukla, S.; Priscilla, A.; Banerjee, M.; Bhonde, R. R.; Ghatak, J.; Satyam, P. V.; Sastry, M. *Chem. Mater.* **2005**, *17*, 5000.

(421) Selvakannan, P.; Sastry, M. *Chem. Commun.* **2005**, *41*, 1684.
(422) Jin, Y.; Dong, S. *J. Phys. Chem. B* **2003**, *107*, 12902.
(423) Gao, J.; Ren, X.; Chen, D.; Tang, F.; Ren, J. *Scr. Mater.* **2007**, *57*, 687.
(424) Guo, S.; Dong, S.; Wang, E. *Chem.—Eur. J.* **2008**, *14*, 4689.
(425) Schwartzberg, A. M.; Olson, T. Y.; Talley, C. E.; Zhang, J. Z. *J. Phys. Chem. B* **2006**, *110*, 19935.
(426) Liang, H.-P.; Guo, Y.-G.; Zhang, H.-M.; Hu, J.-S.; Wan, L.-J.; Bai, C.-L. *Chem. Commun.* **2004**, *40*, 1496.
(427) Liang, H.-P.; Wan, L.-J.; Bai, C.-L.; Jiang, L. *J. Phys. Chem. B* **2005**, *109*, 7795.
(428) Schwartzberg, A. M.; Oshiro, T. Y.; Zhang, J. Z.; Huser, T.; Talley, C. E. *Anal. Chem.* **2006**, *78*, 4732.
(429) Guo, S.; Fang, Y.; Dong, S.; Wang, E. *J. Phys. Chem. C* **2007**, *111*, 17104.
(430) Skrabalak, S. E.; Chen, J.; Sun, Y.; Lu, X.; Au, L.; Cobley, C. M.; Xia, Y. *Acc. Chem. Res.* **2008**, *41*, 1587.
(431) Sun, Y.; Xia, Y. *Science* **2002**, *298*, 2176.
(432) Murphy, C. J. *Science* **2002**, *298*, 2139.
(433) Skrabalak, S. E.; Au, L.; Li, X.; Xia, Y. *Nat. Protoc.* **2007**, *2*, 2182.
(434) Chen, J.; Wiley, B.; McLellan, J.; Xiong, Y.; Li, Z.-Y.; Xia, Y. *Nano Lett.* **2005**, *5*, 2058.
(435) Lu, X.; Au, L.; McLellan, J.; Li, Z.-Y.; Marquez, M.; Xia, Y. *Nano Lett.* **2007**, *7*, 1764.
(436) Mahmoud, M. A.; El-Sayed, M. A. *J. Phys. Chem. C* **2008**, *112*, 14618.
(437) Sun, Y.; Xia, Y. *Adv. Mater.* **2003**, *15*, 695.
(438) Metraux, G. S.; Cao, Y. C.; Jin, R.; Mirkin, C. A. *Nano Lett.* **2003**, *3*, 519.
(439) Xu, S.; Tang, B.; Zheng, X.; Zhou, J.; An, J.; Ning, X.; Xu, W. *Nanotechnology* **2009**, *20*, 415601.
(440) Zou, X.; Ying, E.; Dong, S. *J. Colloid Interface Sci.* **2007**, *306*, 307.
(441) Seo, D.; Song, H. *J. Am. Chem. Soc.* **2009**, *131*, 18210.
(442) Sieb, N. R.; Wu, N.-c.; Majidi, E.; Kukreja, R.; Branda, N. R.; Gates, B. D. *ACS Nano* **2009**, *3*, 1365.
(443) Gu, X.; Xu, L.; Tian, F.; Ding, Y. *Nano Res.* **2009**, *2*, 386.
(444) Ji, C. X.; Searson, P. C. *Appl. Phys. Lett.* **2002**, *81*, 4437.
(445) Ji, C.; Searson, P. C. *J. Phys. Chem. B* **2003**, *107*, 4494.
(446) Laocharoensuk, R.; Sattayasamitsathit, S.; Burdick, J.; Kanatharana, P.; Thavarungkul, P.; Wang, J. *ACS Nano* **2007**, *1*, 403.
(447) Shin, T.-Y.; Yoo, S.-H.; Park, S. *Chem. Mater.* **2008**, *20*, 5682.
(448) Hangarter, C. M.; Lee, Y. I.; Hernandez, S. C.; Choa, Y. h.; Myung, N. V. *Angew. Chem., Int. Ed.* **2010**, *49*, 7081.
(449) Yang, J.; Lee, J. Y.; Too, H.-P. *J. Phys. Chem. B* **2005**, *109*, 19208.
(450) Lu, Z.; Prouty, M. D.; Guo, Z.; Golub, V. O.; Kumar, C. S. S. R.; Lvov, Y. M. *Langmuir* **2005**, *21*, 2042.
(451) Zhang, Q.; Xie, J.; Lee, J. Y.; Zhang, J.; Boothroyd, C. *Small* **2008**, *4*, 1067.
(452) Shon, Y.-S.; Dawson, G. B.; Porter, M.; Murray, R. W. *Langmuir* **2002**, *18*, 3880.
(453) Huang, T.; Murray, R. W. *J. Phys. Chem. B* **2003**, *107*, 7434.
(454) Zhao, M.; Crooks, R. M. *Chem. Mater.* **1999**, *11*, 3379.
(455) Lang, H.; Maldonado, S.; Stevenson, K. J.; Chandler, B. D. *J. Am. Chem. Soc.* **2004**, *126*, 12949.
(456) Zhang, Q.; Lee, J. Y.; Yang, J.; Boothroyd, C.; Zhang, J. *Nanotechnology* **2007**, *18*, 245605.
(457) Zhang, Q.; Xie, J.; Liang, J.; Lee, J. Y. *Adv. Funct. Mater.* **2009**, *19*, 1387.
(458) Sun, Y.; Wiley, B.; Li, Z.-Y.; Xia, Y. *J. Am. Chem. Soc.* **2004**, *126*, 9399.
(459) Chen, H. M.; Liu, R.-S.; Asakura, K.; Lee, J.-F.; Jang, L.-Y.; Hu, S.-F. *J. Phys. Chem. B* **2006**, *110*, 19162.
(460) Yang, J.; Lu, L.; Wang, H.; Zhang, H. *Scr. Mater.* **2006**, *54*, 159.
(461) Sun, Y.; Xia, Y. *Adv. Mater.* **2004**, *16*, 264.
(462) Hu, K.-W.; Liu, T.-M.; Chung, K.-Y.; Huang, K.-S.; Hsieh, C.-T.; Sun, C.-K.; Yeh, C.-S. *J. Am. Chem. Soc.* **2009**, *131*, 14186.
(463) Xiong, Y.; Wiley, B.; Chen, J.; Li, Z. Y.; Yin, Y.; Xia, Y. *Angew. Chem., Int. Ed.* **2005**, *44*, 7913.
(464) Chen, C.-L.; Rosi, N. L. *Angew. Chem., Int. Ed.* **2010**, *49*, 1924.
(465) Dickerson, M. B.; Sandhage, K. H.; Naik, R. R. *Chem. Rev.* **2008**, *108*, 4935.
(466) Behrens, S. S. *J. Mater. Chem.* **2008**, *18*, 3788.
(467) Lagziel-Simis, S.; Cohen-Hadar, N.; Moscovich-Dagan, H.; Wine, Y.; Freeman, A. *Curr. Opin. Biotechnol.* **2006**, *17*, 569.
(468) Niemeyer, C. M. *Angew. Chem., Int. Ed.* **2001**, *40*, 4128.
(469) Gazit, E. *FEBS J.* **2007**, *274*, 317.
(470) Becerril, H. A.; Woolley, A. T. *Chem. Soc. Rev.* **2009**, *38*, 329.
(471) Uchida, M.; Klem, M. T.; Allen, M.; Suci, P.; Flenniken, M.; Gillitzer, E.; Varpness, Z.; Liepold, L. O.; Young, M.; Douglas, T. *Adv. Mater.* **2007**, *19*, 1025.
(472) Shchukin, D. G.; Sukhorukov, G. B. *Adv. Mater.* **2004**, *16*, 671.
(473) Zhou, Y.; Shimizu, T. *Chem. Mater.* **2007**, *20*, 625.
(474) Scott, R. W. J.; Wilson, O. M.; Crooks, R. M. *J. Phys. Chem. B* **2004**, *109*, 692.
(475) Peng, X.; Chen, J.; Misewich, J. A.; Wong, S. S. *Chem. Soc. Rev.* **2009**, *38*, 1076.
(476) Sotiropoulou, S.; Sierra-Sastre, Y.; Mark, S. S.; Batt, C. A. *Chem. Mater.* **2008**, *20*, 821.
(477) Braun, E.; Eichen, Y.; Sivan, U.; Ben-Yoseph, G. *Nature* **1998**, *391*, 775.
(478) Eichen, Y.; Braun, E.; Sivan, U.; Ben-Yoseph, G. *Acta Polym.* **1998**, *49*, 663.
(479) Richter, J. *Physica E* **2003**, *16*, 157.
(480) Gu, Q.; Cheng, C.; Gonela, R.; Suryanarayanan, S.; Anabathula, S.; Dai, K.; Haynie, D. T. *Nanotechnology* **2006**, *17*, R14.
(481) Keren, K.; Krueger, M.; Gilad, R.; Ben-Yoseph, G.; Sivan, U.; Braun, E. *Science* **2002**, *297*, 72.
(482) Keren, K.; Berman, R. S.; Buchstab, E.; Sivan, U.; Braun, E. *Science* **2003**, *302*, 1380.
(483) Keren, K.; Berman, R. S.; Braun, E. *Nano Lett.* **2004**, *4*, 323.
(484) Nishinaka, T.; Takano, A.; Doi, Y.; Hashimoto, M.; Nakamura, A.; Matsushita, Y.; Kumaki, J.; Yashima, E. *J. Am. Chem. Soc.* **2005**, *127*, 8120.
(485) Park, S. H.; Prior, M. W.; LaBean, T. H.; Finkelstein, G. *Appl. Phys. Lett.* **2006**, *89*, 033901.
(486) Becerril, H. A.; Stoltenberg, R. M.; Monson, C. F.; Woolley, A. T. *J. Mater. Chem.* **2004**, *14*, 611.
(487) Ongaro, A.; Griffin, F.; Beecher, P.; Nagle, L.; Iacopino, D.; Quinn, A.; Redmond, G.; Fitzmaurice, D. *Chem. Mater.* **2005**, *17*, 1959.
(488) Harnack, O.; Ford, W. E.; Yasuda, A.; Wessels, J. M. *Nano Lett.* **2002**, *2*, 919.
(489) Cui, S.; Liu, Y.; Yang, Z.; Wei, X. *Mater. Des.* **2007**, *28*, 722.
(490) Berti, L.; Alessandrini, A.; Facci, P. *J. Am. Chem. Soc.* **2005**, *127*, 11216.
(491) Yan, H.; Park, S. H.; Finkelstein, G.; Reif, J. H.; LaBean, T. H. *Science* **2003**, *301*, 1882.
(492) Park, S. H.; Yan, H.; Reif, J. H.; LaBean, T. H.; Finkelstein, G. *Nanotechnology* **2004**, *15*, S525.
(493) Liu, D.; Park, S. H.; Reif, J. H.; LaBean, T. H. *Proc. Natl. Acad. Sci. U.S.A.* **2004**, *101*, 717.
(494) Park, S. H.; Barish, R.; Li, H.; Reif, J. H.; Finkelstein, G.; Yan, H.; LaBean, T. H. *Nano Lett.* **2005**, *5*, 693.
(495) Becerril, H. A.; Stoltenberg, R. M.; Wheeler, D. R.; Davis, R. C.; Harb, J. N.; Woolley, A. T. *J. Am. Chem. Soc.* **2005**, *127*, 2828.
(496) Stearns, L. A.; Chhabra, R.; Sharma, J.; Liu, Y.; Petuskey, W. T.; Yan, H.; Chaput, J. C. *Angew. Chem., Int. Ed.* **2009**, *48*, 8494.
(497) Zinchenko, A. A.; Yoshikawa, K.; Baigl, D. *Adv. Mater.* **2005**, *17*, 2820.
(498) Chen, N.; Zinchenko, A. A.; Yoshikawa, K. *Nanotechnology* **2006**, *17*, 5224.
(499) Samson, J.; Varotto, A.; Nahirney, P. C.; Toschi, A.; Piscopo, I.; Drain, C. M. *ACS Nano* **2009**, *3*, 339.
(500) Preston, T. C.; Signorell, R. *Langmuir* **2010**, *26*, 10250.

(501) Shemer, G.; Krichevski, O.; Markovich, G.; Molotsky, T.; Lubitz, I.; Kotlyar, A. B. *J. Am. Chem. Soc.* **2006**, *128*, 11006.
(502) Molotsky, T.; Tamarin, T.; Moshe, A. B.; Markovich, G.; Kotlyar, A. B. *J. Phys. Chem. C* **2010**, *114*, 15951.
(503) George, J.; Thomas, K. G. *J. Am. Chem. Soc.* **2010**, *132*, 2502.
(504) Fan, Z.; Govorov, A. O. *Nano Lett.* **2010**, *10*, 2580.
(505) Brown, S. *Nat. Biotechnol.* **1997**, *15*, 269.
(506) Slocik, J. M.; Moore, J. T.; Wright, D. W. *Nano Lett.* **2002**, *2*, 169.
(507) Slocik, J. M.; Wright, D. W. *Biomacromolecules* **2003**, *4*, 1135.
(508) Naik, R. R.; Jones, S. E.; Murray, C. J.; McAuliffe, J. C.; Vaia, R. A.; Stone, M. O. *Adv. Funct. Mater.* **2004**, *14*, 25.
(509) Selvakannan, P. R.; Mandal, S.; Phadtare, S.; Gole, A.; Pasricha, R.; Adyanthaya, S. D.; Sastry, M. *J. Colloid Interface Sci.* **2004**, *269*, 97.
(510) Slocik, J. M.; Stone, M. O.; Naik, R. R. *Small* **2005**, *1*, 1048.
(511) Bhargava, S. K.; Booth, J. M.; Agrawal, S.; Coloe, P.; Kar, G. *Langmuir* **2005**, *21*, 5949.
(512) Si, S.; Bhattacharjee, R. R.; Banerjee, A.; Mandal, T. K. *Chem.—Eur. J.* **2006**, *12*, 1256.
(513) Slocik, J. M.; Naik, R. R. *Adv. Mater.* **2006**, *18*, 1988.
(514) Tomczak, M. M.; Slocik, J. M.; Stone, M. O.; Naik, R. R. *Biochem. Soc. Trans.* **2007**, *035*, 512.
(515) Bassindale, A. R.; Codina-Barrios, A.; Frascione, N.; Taylor, P. G. *Chem. Commun.* **2007**, 2956.
(516) Wang, Z.; Chen, J.; Yang, P.; Yang, W. *Appl. Organomet. Chem.* **2007**, *21*, 645.
(517) Si, S.; Mandal, T. K. *Chem.—Eur. J.* **2007**, *13*, 3160.
(518) Carter, C. J.; Ackerson, C. J.; Feldheim, D. L. *ACS Nano* **2010**, *4*, 3883.
(519) Tan, Y. N.; Lee, J. Y.; Wang, D. I. C. *J. Am. Chem. Soc.* **2010**, *132*, 5677.
(520) Naik, R. R.; Stringer, S. J.; Agarwal, G.; Jones, S. E.; Stone, M. O. *Nat. Mater.* **2002**, *1*, 169.
(521) Shao, Y.; Jin, Y.; Dong, S. *Chem. Commun.* **2004**, *40*, 1104.
(522) Xie, J.; Lee, J. Y.; Wang, D. I. C.; Ting, Y. P. *ACS Nano* **2007**, *1*, 429.
(523) Shimizu, T.; Kogiso, M.; Masuda, M. *Nature* **1996**, *383*, 487.
(524) Shimizu, T.; Kogiso, M.; Masuda, M. *J. Am. Chem. Soc.* **1997**, *119*, 6209.
(525) Kogiso, M.; Ohnishi, S.; Yase, K.; Masuda, M.; Shimizu, T. *Langmuir* **1998**, *14*, 4978.
(526) Matsui, H.; Gologan, B. *J. Phys. Chem. B* **2000**, *104*, 3383.
(527) Djalali, R.; Chen, Y.-f.; Matsui, H. *J. Am. Chem. Soc.* **2002**, *124*, 13660.
(528) Djalali, R.; Chen, Y.-f.; Matsui, H. *J. Am. Chem. Soc.* **2003**, *125*, 5873.
(529) Yu, L.; Banerjee, I. A.; Matsui, H. *J. Am. Chem. Soc.* **2003**, *125*, 14837.
(530) Gao, X.; Matsui, H. *Adv. Mater.* **2005**, *17*, 2037.
(531) Gao, X.; Djalali, R.; Haboosheh, A.; Samson, J.; Nuraje, N.; Matsui, H. *Adv. Mater.* **2005**, *17*, 1753.
(532) Djalali, R.; Samson, J.; Matsui, H. *J. Am. Chem. Soc.* **2004**, *126*, 7935.
(533) Huang, Y.; Chiang, C.-Y.; Lee, S. K.; Gao, Y.; Hu, E. L.; Yoreo, J. D.; Belcher, A. M. *Nano Lett.* **2005**, *5*, 1429.
(534) Chen, C.-L.; Rosi, N. L. *J. Am. Chem. Soc.* **2010**, *132*, 6902.
(535) Hwang, L.; Chen, C.-L.; Rosi, N. L. *Chem. Commun.* **2011**, *47*, 185.
(536) Song, C.; Zhao, G.; Zhang, P.; Rosi, N. L. *J. Am. Chem. Soc.* **2010**, *132*, 14033.
(537) Carny, O.; Shalev, D. E.; Gazit, E. *Nano Lett.* **2006**, *6*, 1594.
(538) Brown, S.; Sarikaya, M.; Johnson, E. *J. Mol. Biol.* **2000**, *299*, 725.
(539) Zhou, Y.; Chen, W.; Itoh, H.; Naka, K.; Ni, Q.; Yamane, H.; Chujo, Y. *Chem. Commun.* **2001**, *37*, 2518.
(540) Burt, J. L.; Gutiérrez-Wing, C.; Miki-Yoshida, M.; José-Yacamán, M. *Langmuir* **2004**, *20*, 11778.
(541) Singh, A. V.; Bandgar, B. M.; Kasture, M.; Prasad, B. L. V.; Sastry, M. *J. Mater. Chem.* **2005**, *15*, 5115.
(542) Rangnekar, A.; Sarma, T. K.; Singh, A. K.; Deka, J.; Ramesh, A.; Chattopadhyay, A. *Langmuir* **2007**, *23*, 5700.
(543) Xie, J.; Lee, J. Y.; Wang, D. I. C. *J. Phys. Chem. C* **2007**, *111*, 10226.
(544) Zhang, L.; Swift, J.; Butts, C. A.; Yerubandi, V.; Dmochowski, I. J. *J. Inorg. Biochem.* **2007**, *101*, 1719.
(545) Bakshi, M. S.; Kaur, H.; Banipal, T. S.; Singh, N.; Kaur, G. *Langmuir* **2010**, *26*, 13535.
(546) Yamashita, I. *J. Mater. Chem.* **2008**, *18*, 3813.
(547) Harrison, P. M.; Arosio, P. *Biochim. Biophys. Acta, Bioenerg.* **1996**, *1275*, 161.
(548) Kramer, R. M.; Li, C.; Carter, D. C.; Stone, M. O.; Naik, R. R. *J. Am. Chem. Soc.* **2004**, *126*, 13282.
(549) Butts, C. A.; Swift, J.; Kang, S.-g.; Di Costanzo, L.; Christianson, D. W.; Saven, J. G.; Dmochowski, I. J. *Biochemistry* **2008**, *47*, 12729.
(550) Domínguez-Vera, J. M.; Gálvez, N.; Sánchez, P.; Mota, A. J.; Trasobares, S.; Hernández, J. C.; Calvino, J. J. *Eur. J. Inorg. Chem.* **2007**, *2007*, 4823.
(551) Shin, Y.; Dohnalkova, A.; Lin, Y. *J. Phys. Chem. C* **2010**, *114*, 5985.
(552) Kasyutich, O.; Ilari, A.; Fiorillo, A.; Tatchev, D.; Hoell, A.; Ceci, P. *J. Am. Chem. Soc.* **2010**, *132*, 3621.
(553) Behrens, S.; Rahn, K.; Habicht, W.; Böhm, K. J.; Rösner, H.; Dinjus, E.; Unger, E. *Adv. Mater.* **2002**, *14*, 1621.
(554) Behrens, S.; Wu, J.; Habicht, W.; Unger, E. *Chem. Mater.* **2004**, *16*, 3085.
(555) Behrens, S.; Habicht, W.; Wu, J.; Unger, E. *Surf. Interface Anal.* **2006**, *38*, 1014.
(556) Behrens, S.; Habicht, W.; Wagner, K.; Unger, E. *Adv. Mater.* **2006**, *18*, 284.
(557) Habicht, W.; Behrens, S.; Unger, E.; Dinjus, E. *Surf. Interface Anal.* **2006**, *38*, 194.
(558) Patolsky, F.; Weizmann, Y.; Willner, I. *Nat. Mater.* **2004**, *3*, 692.
(559) Scheibel, T.; Parthasarathy, R.; Sawicki, G.; Lin, X.-M.; Jaeger, H.; Lindquist, S. L. *Proc. Natl. Acad. Sci. U.S.A.* **2003**, *100*, 4527.
(560) Hamada, D.; Yanagihara, I.; Tsumoto, K. *Trends Biotechnol.* **2004**, *22*, 93.
(561) Kumara, M. T.; Tripp, B. C.; Muralidharan, S. *Chem. Mater.* **2007**, *19*, 2056.
(562) Bai, H.; Xu, K.; Xu, Y.; Matsui, H. *Angew. Chem., Int. Ed.* **2007**, *46*, 3319.
(563) Leroux, F.; Gysemans, M.; Bals, S.; Batenburg, K. J.; Snauwaert, J.; Verbiest, T.; Van Haesendonck, C.; Van Tendeloo, G. *Adv. Mater.* **2010**, *22*, 2193.
(564) Sára, M.; Sleytr, U. B. *J. Bacteriol.* **2000**, *182*, 859.
(565) Sleytr, U. B.; Messner, P.; Pum, D.; Sára, M. *Angew. Chem., Int. Ed.* **1999**, *38*, 1034.
(566) Pum, D.; Sleytr, U. B. *Trends Biotechnol.* **1999**, *17*, 8.
(567) Sleytr, U. B.; Sára, M.; Pum, D.; Schuster, B. *Prog. Surf. Sci.* **2001**, *68*, 231.
(568) Dieluweit, S.; Pum, D.; Sleytr, U. B. *Supramol. Sci.* **1998**, *5*, 15.
(569) Guli, M.; Lambert, E. M.; Li, M.; Mann, S. *Angew. Chem., Int. Ed.* **2010**, *49*, 520.
(570) Carney, C.; Harry, S.; Sewell, S.; Wright, D. *Biomineralization I*; Springer: Berlin, Heidelberg, 2007; p 155.
(571) Bruins, M. R.; Kapil, S.; Oehme, F. W. *Ecotoxicol. Environ. Saf.* **2000**, *45*, 198.
(572) Klaus, T.; Joerger, R.; Olsson, E.; Granqvist, C.-G. *Proc. Natl. Acad. Sci. U.S.A.* **1999**, *96*, 13611.
(573) Gericke, M.; Pinches, A. *Hydrometallurgy* **2006**, *83*, 132.
(574) Gardea-Torresdey, J. L.; Parsons, J. G.; Gomez, E.; Peralta-Videa, J.; Troiani, H. E.; Santiago, P.; Yacaman, M. J. *Nano Lett.* **2002**, *2*, 397.

(575) Kowshik, M.; Ashtaputre, S.; Kharrazi, S.; Vogel, W.; Urban, J.; Kulkami, S. K.; Paknikar, K. M. *Nanotechnology* **2003**, *14*, 95.
(576) Ahmad, A.; Senapati, S.; Khan, M. I.; Kumar, R.; Ramani, R.; Srinivas, V.; Sastry, M. *Nanotechnology* **2003**, *14*, 824.
(577) Mukherjee, P.; Ahmad, A.; Mandal, D.; Senapati, S.; Sainkar, S. R.; Khan, M. I.; Ramani, R.; Parischa, R.; Ajayakumar, P. V.; Alam, M.; Sastry, M.; Kumar, R. *Angew. Chem., Int. Ed.* **2001**, *40*, 3585.
(578) Shenton, W.; Douglas, T.; Young, M.; Stubbs, G.; Mann, S. *Adv. Mater.* **1999**, *11*, 253.
(579) Dujardin, E.; Peet, C.; Stubbs, G.; Culver, J. N.; Mann, S. *Nano Lett.* **2003**, *3*, 413.
(580) Knez, M.; Sumser, M.; Bittner, A. M.; Wege, C.; Jeske, H.; Kooi, S.; Burghard, M.; Kern, K. *J. Electroanal. Chem.* **2002**, *522*, 70.
(581) Knez, M.; Sumser, M.; Bittner, A. M.; Wege, C.; Jeske, H.; Martin, T. P.; Kern, K. *Adv. Funct. Mater.* **2004**, *14*, 116.
(582) Balci, S.; Noda, K.; Bittner, A. M.; Kadri, A.; Wege, C.; Jeske, H.; Kern, K. *Angew. Chem., Int. Ed.* **2007**, *46*, 3149.
(583) Nam, K. T.; Lee, Y. J.; Krauland, E. M.; Kottmann, S. T.; Belcher, A. M. *ACS Nano* **2008**, *2*, 1480.
(584) Slocik, J. M.; Naik, R. R.; Stone, M. O.; Wright, D. W. *J. Mater. Chem.* **2005**, *15*, 749.
(585) Lee, S.-Y.; Royston, E.; Culver, J. N.; Harris, M., T. *Nanotechnology* **2005**, *16*, S435.
(586) Lee, Y. J.; Lee, Y.; Oh, D.; Chen, T.; Ceder, G.; Belcher, A. M. *Nano Lett.* **2010**, *10*, 2433.
(587) Radloff, C.; Vaia, R. A.; Brunton, J.; Bouwer, G. T.; Ward, V. K. *Nano Lett.* **2005**, *5*, 1187.
(588) Payne, E. K.; Rosi, N. L.; Xue, C.; Mirkin, C. A. *Angew. Chem., Int. Ed.* **2005**, *44*, 5064.
(589) Kunitake, T. *Angew. Chem., Int. Ed. Engl.* **1992**, *31*, 709.
(590) Shimizu, T.; Masuda, M.; Minamikawa, H. *Chem. Rev.* **2005**, *105*, 1401.
(591) Burkett, S. L.; Mann, S. *Chem. Commun.* **1996**, 321.
(592) Yang, B.; Kamiya, S.; Yoshida, K.; Shimizu, T. *Chem. Commun.* **2004**, 500.
(593) Shimizu, T. *J. Polym. Sci., Part A: Polym. Chem.* **2006**, *44*, 5137.
(594) Zhan, C.; Wang, J.; Yuan, J.; Gong, H.; Liu, Y.; Liu, M. *Langmuir* **2003**, *19*, 9440.
(595) Yang, M.; Alvarez-Puebla, R. n.; Kim, H.-S.; Aldeanueva-Potel, P.; Liz-Marzán, L. M.; Kotov, N. A. *Nano Lett.* **2010**, *10*, 4013.
(596) Eisele, D. M.; Berlepsch, H. v.; Böttcher, C.; Stevenson, K. J.; Vanden Bout, D. A.; Kirstein, S.; Rabe, J. P. *J. Am. Chem. Soc.* **2010**, *132*, 2104.
(597) Zhang, X.; Li, D. *Angew. Chem., Int. Ed.* **2006**, *45*, 5971.
(598) Tian, J.; Liu, S.; Sun, X. *Langmuir* **2010**, *26*, 15112.
(599) Kurihara, K.; Kizling, J.; Stenius, P.; Fendler, J. H. *J. Am. Chem. Soc.* **1983**, *105*, 2574.
(600) Barnickel, P.; Wokaun, A. *Mol. Phys.* **1990**, *69*, 1.
(601) Barnickel, P.; Wokaun, A.; Sager, W.; Eicke, H. F. *J. Colloid Interface Sci.* **1992**, *148*, 80.
(602) Pileni, M. P. *J. Phys. Chem.* **1993**, *97*, 6961.
(603) Pileni, M. P. *Langmuir* **1997**, *13*, 3266.
(604) Pileni, M.-P. *Nat. Mater.* **2003**, *2*, 145.
(605) Petit, C.; Lixon, P.; Pileni, M. P. *J. Phys. Chem.* **1993**, *97*, 12974.
(606) Bagwe, R. P.; Khilar, K. C. *Langmuir* **1999**, *16*, 905.
(607) Taleb, A.; Petit, C.; Pileni, M. P. *Chem. Mater.* **1997**, *9*, 950.
(608) Cason, J. P.; Khambaswadkar, K.; Roberts, C. B. *Ind. Eng. Chem. Res.* **2000**, *39*, 4749.
(609) McLeod, M. C.; McHenry, R. S.; Beckman, E. J.; Roberts, C. B. *J. Phys. Chem. B* **2003**, *107*, 2693.
(610) Wang, Z.; Chen, M.; Wu, L. *Chem. Mater.* **2008**, *20*, 3251.
(611) Maillard, M.; Giorgio, S.; Pileni, M. P. *Adv. Mater.* **2002**, *14*, 1084.
(612) Maillard, M.; Giorgio, S.; Pileni, M.-P. *J. Phys. Chem. B* **2003**, *107*, 2466.
(613) Yener, D. O.; Sindel, J.; Randall, C. A.; Adair, J. H. *Langmuir* **2002**, *18*, 8692.
(614) Filankembo, A.; Pileni, M. P. *J. Phys. Chem. B* **2000**, *104*, 5865.
(615) Pileni, M. P. *Langmuir* **2001**, *17*, 7476.
(616) Pileni, M. P. *J. Exp. Nanosci.* **2006**, *1*, 13.
(617) Pileni, M. P. *J. Phys. Chem. C* **2007**, *111*, 9019.
(618) Bakshi, M. S.; Possmayer, F.; Petersen, N. O. *J. Phys. Chem. C* **2008**, *112*, 8259.
(619) Jana, N. R.; Gearheart, L.; Murphy, C. J. *J. Phys. Chem. B* **2001**, *105*, 4065.
(620) Jana, N. R.; Gearheart, L.; Murphy, C. J. *Chem. Commun.* **2001**, 617.
(621) Jana, N. R.; Gearheart, L.; Murphy, C. J. *Adv. Mater.* **2001**, *13*, 1389.
(622) Nikoobakht, B.; El-Sayed, M. A. *Chem. Mater.* **2003**, *15*, 1957.
(623) Pérez-Juste, J.; Liz-Marzán, L. M.; Carnie, S.; Chan, D. Y. C.; Mulvaney, P. *Adv. Funct. Mater.* **2004**, *14*, 571.
(624) Liu; Guyot-Sionnest, P. *J. Phys. Chem. B* **2005**, *109*, 22192.
(625) Vriezema, D. M.; Comellas Aragonès, M.; Elemans, J. A. A. W.; Cornelissen, J. J. L. M.; Rowan, A. E.; Nolte, R. J. M. *Chem. Rev.* **2005**, *105*, 1445.
(626) Kim, H.-C.; Park, S.-M.; Hinsberg, W. D. *Chem. Rev.* **2009**, *110*, 146.
(627) Antonietti, M.; Wenz, E.; Bronstein, L.; Seregina, M. *Adv. Mater.* **1995**, *7*, 1000.
(628) Seregina, M. V.; Bronstein, L. M.; Platonova, O. A.; Chernyshov, D. M.; Valetsky, P. M.; Hartmann, J.; Wenz, E.; Antonietti, M. *Chem. Mater.* **1997**, *9*, 923.
(629) Khullar, P.; Mahal, A.; Singh, V.; Banipal, T. S.; Kaur, G.; Bakshi, M. S. *Langmuir* **2010**, *26*, 11363.
(630) Glass, R.; Moller, M.; Spatz, J. P. *Nanotechnology* **2003**, *14*, 1153.
(631) Chai, J.; Buriak, J. M. *ACS Nano* **2008**, *2*, 489.
(632) Aizawa, M.; Buriak, J. M. *J. Am. Chem. Soc.* **2005**, *127*, 8932.
(633) Aizawa, M.; Buriak, J. M. *J. Am. Chem. Soc.* **2006**, *128*, 5877.
(634) Aizawa, M.; Buriak, J. M. *Chem. Mater.* **2007**, *19*, 5090.
(635) Mbenkum, B. N.; Díaz-Ortiz, A.; Gu, L.; Aken, P. A. v.; Schütz, G *J. Am. Chem. Soc.* **2010**, *132*, 10671.
(636) Balogh, L.; Valluzzi, R.; Laverdure, K. S.; Gido, S. P.; Hagnauer, G. L.; Tomalia, D. A. *J. Nanopart. Res.* **1999**, *1*, 353.
(637) Crooks, R. M.; Zhao, M.; Sun, L.; Chechik, V.; Yeung, L. K. *Acc. Chem. Res.* **2000**, *34*, 181.
(638) Esumi, K.; Suzuki, A.; Aihara, N.; Usui, K.; Torigoe, K. *Langmuir* **1998**, *14*, 3157.
(639) Garcia, M. E.; Baker, L. A.; Crooks, R. M. *Anal. Chem.* **1998**, *71*, 256.
(640) Esumi, K.; Suzuki, A.; Yamahira, A.; Torigoe, K. *Langmuir* **2000**, *16*, 2604.
(641) Grohn, F.; Bauer, B. J.; Akpalu, Y. A.; Jackson, C. L.; Amis, E. J. *Macromolecules* **2000**, *33*, 6042.
(642) Kim, Y.-G.; Oh, S.-K.; Crooks, R. M. *Chem. Mater.* **2003**, *16*, 167.
(643) Scott, R. W. J.; Wilson, O. M.; Oh, S.-K.; Kenik, E. A.; Crooks, R. M. *J. Am. Chem. Soc.* **2004**, *126*, 15583.
(644) Wilson, O. M.; Scott, R. W. J.; Garcia-Martinez, J. C.; Crooks, R. M. *J. Am. Chem. Soc.* **2004**, *127*, 1015.
(645) Yancey, D. F.; Carino, E. V.; Crooks, R. M. *J. Am. Chem. Soc.* **2010**, *132*, 10988.
(646) Singh, R.; Premkumar, T.; Shin, J.-Y.; Geckeler, K. E. *Chem.—Eur. J.* **2010**, *16*, 1728.
(647) Ajayan, P. M.; lijima, S. *Nature* **1993**, *361*, 333.
(648) Tsang, S. C.; Chen, Y. K.; Harris, P. J. F.; Green, M. L. H. *Nature* **1994**, *372*, 159.
(649) Govindaraj, A.; Satishkumar, B. C.; Nath, M.; Rao, C. N. R. *Chem. Mater.* **1999**, *12*, 202.
(650) Ugarte, D.; Chatelain, A.; de Heer, W. A. *Science* **1996**, *274*, 1897.
(651) Sloan, J.; M. Wright, D.; Bailey, S.; Brown, G.; P. E. York, A.; S. Coleman, K.; L. H. Green, M.; L. Hutchison, J.; Woo, H.-G. *Chem. Commun.* **1999**, 699.

(652) Satishkumar, B. C.; Govindaraj, A.; Mofokeng, J.; Subbanna, G. N.; Rao, C. N. R. *J. Phys. B: At., Mol. Opt. Phys.* **1996**, *29*, 4925.
(653) Borowiak-Palen, E.; Ruemmeli, M. H.; Gemming, T.; Pichler, T.; Kalenczuk, R. J.; Silva, S. R. P. *Nanotechnology* **2006**, *17*, 2415.
(654) Yu, H.; Peng, J.; Zhai, M.; Li, J.; Wei, G. *Physica E* **2008**, *40*, 2694.
(655) Ebbesen, T. W.; Hiura, H.; Bisher, M. E.; Treacy, M. M. J.; Shreeve-Keyer, J. L.; Haushalter, R. C. *Adv. Mater.* **1996**, *8*, 155.
(656) Satishkumar, B. C.; Vogl, E. M.; Govindaraj, A.; Rao, C. N. R. *J. Phys. D: Appl. Phys.* **1996**, *29*, 3173.
(657) Jiang, L.; Gao, L. *Carbon* **2003**, *41*, 2923.
(658) Niu, A.; Han, Y.; Wu, J.; Yu, N.; Xu, Q. *J. Phys. Chem. C* **2010**, *114*, 12728.
(659) Choi, H. C.; Shim, M.; Bangsaruntip, S.; Dai, H. *J. Am. Chem. Soc.* **2002**, *124*, 9058.
(660) Qu, L.; Dai, L. *J. Am. Chem. Soc.* **2005**, *127*, 10806.
(661) Kim, D. S.; Lee, T.; Geckeler, K. E. *Angew. Chem., Int. Ed.* **2006**, *45*, 104.
(662) Kim, J.-W.; Galanzha, E. I.; Shashkov, E. V.; Moon, H.-M.; Zharov, V. P. *Nat. Nanotechnol.* **2009**, *4*, 688.
(663) Raghuveer, M. S.; Agrawal, S.; Bishop, N.; Ramanath, G. *Chem. Mater.* **2006**, *18*, 1390.
(664) Samant, K. M.; Chaudhari, V. R.; Kapoor, S.; Haram, S. K. *Carbon* **2007**, *45*, 2126.
(665) Khanderi, J.; Hoffmann, R. C.; Engstler, J.; Schneider, J. J.; Arras, J.; Claus, P.; Cherkashinin, G. *Chem.—Eur. J.* **2010**, *16*, 2300.
(666) Hu, J.; Shi, J.; Li, S.; Qin, Y.; Guo, Z.-X.; Song, Y.; Zhu, D. *Chem. Phys. Lett.* **2005**, *401*, 352.
(667) Zanella, R.; Basiuk, E. V.; Santiago, P.; Basiuk, V. A.; Mireles, E.; Puente-Lee, I.; Saniger, J. M. *J. Phys. Chem. B* **2005**, *109*, 16290.
(668) Tao, L.; Chen, G.; Mantovani, G.; York, S.; Haddleton, D. M. *Chem. Commun.* **2006**, 4949.
(669) Li, H.; Jo, J. K.; Zhang, L.; Ha, C. S.; Suh, H.; Kim, I. *Adv. Funct. Mater.* **2010**, *20*, 3864.
(670) Zhang, Y.; Dai, H. *Appl. Phys. Lett.* **2000**, 77.
(671) Chin, K. C.; Gohel, A.; Chen, W. Z.; Elim, H. I.; Ji, W.; Chong, G. L.; Sow, C. H.; Wee, A. T. S. *Chem. Phys. Lett.* **2005**, *409*, 85.
(672) Goad, D. G. W.; Moskovits, M. *J. Appl. Phys.* **1978**, *49*, 2929.
(673) Brumlik, C. J.; Martin, C. R. *J. Am. Chem. Soc.* **1991**, *113*, 3174.
(674) Martin, C. R. *Adv. Mater.* **1991**, *3*, 457.
(675) Martin, C. R. *Science* **1994**, *266*, 1961.
(676) Preston, C. K.; Moskovits, M. *J. Phys. Chem.* **1988**, *92*, 2957.
(677) Foss, C. A.; Hornyak, G. L.; Stockert, J. A.; Martin, C. R. *J. Phys. Chem.* **1994**, *98*, 2963.
(678) Hurst, S. J.; Payne, E. K.; Qin, L. D.; Mirkin, C. A. *Angew. Chem., Int. Ed.* **2006**, *45*, 2672.
(679) Martin, C. R. *Acc. Chem. Res.* **1995**, *28*, 61.
(680) Park, S.; Lim, J.-H.; Chung, S.-W.; Mirkin, C. A. *Science* **2004**, *303*, 348.
(681) Ciszek, J. W.; Huang, L.; Wang, Y.; Mirkin, C. A. *Small* **2008**, *4*, 206.
(682) Chen, X.; Li, S.; Xue, C.; Banholzer, M. J.; Schatz, G. C.; Mirkin, C. A. *ACS Nano* **2008**, *3*, 87.
(683) Lim, J. K.; Ciszek, J. W.; Huo, F.; Jang, J.-W.; Hwang, S.; Mirkin, C. A. *Nano Lett.* **2008**, *8*, 4441.
(684) Martin, C. R. *Chem. Mater.* **1996**, *8*, 1739.
(685) Routkevitch, D.; Bigioni, T.; Moskovits, M.; Xu, J. M. *J. Phys. Chem.* **1996**, *100*, 14037.
(686) Sun, L.; Searson, P. C.; Chien, C. L. *Appl. Phys. Lett.* **1999**, *74*, 2803.
(687) Tonucci, R. J.; Justus, B. L.; Campillo, A. J.; Ford, C. E. *Science* **1992**, *258*, 783.
(688) Wu, C. G.; Bein, T. *Science* **1994**, *264*, 1757.
(689) Beck, J. S.; Vartuli, J. C.; Roth, W. J.; Leonowicz, M. E.; Kresge, C. T.; Schmitt, K. D.; Chu, C. T. W.; Olson, D. H.; Sheppard, E. W.; McCullen, S. B.; Higgins, J. B.; Schlenker, J. L. *J. Am. Chem. Soc.* **1992**, *114*, 10834.
(690) Ozin, G. A. *Adv. Mater.* **1992**, *4*, 612.
(691) Thompson, G. E.; Furneaux, R. C.; Wood, G. C.; Richardson, J. A.; Goode, J. S. *Nature* **1978**, *272*, 433.
(692) Furneaux, R. C.; Rigby, W. R.; Davidson, A. P. *Nature* **1989**, *337*, 147.
(693) Lee, W.; Ji, R.; Gosele, U.; Nielsch, K. *Nat. Mater.* **2006**, *5*, 741.
(694) Masuda, H.; Fukuda, K. *Science* **1995**, *268*, 1466.
(695) Thompson, G. E.; Wood, G. C. *Nature* **1981**, *290*, 230.
(696) Masuda, H.; Asoh, H.; Watanabe, M.; Nishio, K.; Nakao, M.; Tamamura, T. *Adv. Mater.* **2001**, *13*, 189.
(697) Asoh, H.; Ono, S.; Hirose, T.; Nakao, M.; Masuda, H. *Electrochim. Acta* **2003**, *48*, 3171.
(698) Smith, J. T.; Hang, Q.; Franklin, A. D.; Janes, D. B.; Sands, T. D. *Appl. Phys. Lett.* **2008**, *93*, 043108.
(699) Wirtz, M.; Martin, C. R. *Adv. Mater.* **2003**, *15*, 455.
(700) Brumlik, C. J.; Menon, V. P.; Martin, C. R. *J. Mater. Res.* **1994**, *9*, 1174.
(701) Menon, V. P.; Martin, C. R. *Anal. Chem.* **1995**, *67*, 1920.
(702) De Leo, M.; Pereira, F. C.; Moretto, L. M.; Scopece, P.; Polizzi, S.; Ugo, P. *Chem. Mater.* **2007**, *19*, 5955.
(703) Jirage, K. B.; Hulteen, J. C.; Martin, C. R. *Science* **1997**, *278*, 655.
(704) Nishizawa, M.; Menon, V. P.; Martin, C. R. *Science* **1995**, *268*, 700.
(705) Yao, J.; Liu, Z. W.; Liu, Y. M.; Wang, Y.; Sun, C.; Bartal, G.; Stacy, A. M.; Zhang, X. *Science* **2008**, *321*, 930.
(706) Kabashin, A. V.; Evans, P.; Pastkovsky, S.; Hendren, W.; Wurtz, G. A.; Atkinson, R.; Pollard, R.; Podolskiy, V. A.; Zayats, A. V. *Nat. Mater.* **2009**, *8*, 867.
(707) Zong, R. L.; Zhou, J.; Li, Q.; Du, B.; Li, B.; Fu, M.; Qi, X. W.; Li, L. T.; Buddhudu, S. *J. Phys. Chem. B* **2004**, *108*, 16713.
(708) Almawlawi, D.; Liu, C. Z.; Moskovits, M. *J. Mater. Res.* **1994**, *9*, 1014.
(709) Hornyak, G. L.; Patrissi, C. J.; Martin, C. R. *J. Phys. Chem. B* **1997**, *101*, 1548.
(710) Payne, E. K.; Shuford, K. L.; Park, S.; Schatz, G. C.; Mirkin, C. A. *J. Phys. Chem. B* **2006**, *110*, 2150.
(711) Preston, C. K.; Moskovits, M. *J. Phys. Chem.* **1993**, *97*, 8495.
(712) Sandrock, M. L.; Pibel, C. D.; Geiger, F. M.; Foss, C. A. *J. Phys. Chem. B* **1999**, *103*, 2668.
(713) Qin, L.; Banholzer, M. J.; Millstone, J. E.; Mirkin, C. A. *Nano Lett.* **2007**, *7*, 3849.
(714) Nicewarner-Pena, S. R.; Freeman, R. G.; Reiss, B. D.; He, L.; Pena, D. J.; Walton, I. D.; Cromer, R.; Keating, C. D.; Natan, M. J. *Science* **2001**, *294*, 137.
(715) Martin, B. R.; Dermody, D. J.; Reiss, B. D.; Fang, M. M.; Lyon, L. A.; Natan, M. J.; Mallouk, T. E. *Adv. Mater.* **1999**, *11*, 1021.
(716) Keating, C. D.; Natan, M. J. *Adv. Mater.* **2003**, *15*, 451.
(717) Kim, S.; Kim, S. K.; Park, S. *J. Am. Chem. Soc.* **2009**, *131*, 8380.
(718) Sioss, J. A.; Keating, C. D. *Nano Lett.* **2005**, *5*, 1779.
(719) Qin, L. D.; Park, S.; Huang, L.; Mirkin, C. A. *Science* **2005**, *309*, 113.
(720) Osberg, K. D.; Schmucker, A. L.; Senesi, A. J.; Mirkin, C. A. *Nano Lett.* **2011**, *11*, 820.
(721) Qin, L. D.; Zou, S. L.; Xue, C.; Atkinson, A.; Schatz, G. C.; Mirkin, C. A. *Proc. Natl. Acad. Sci. U.S.A.* **2006**, *103*, 13300.
(722) Zheng, G.; Qin, L.; Mirkin, C. A. *Angew. Chem., Int. Ed.* **2008**, *47*, 1938.
(723) Zheng, G.; Chen, X.; Mirkin, C. A. *Small* **2009**, *5*, 2537.
(724) Pedano, M. L.; Li, S. Z.; Schatz, G. C.; Mirkin, C. A. *Angew. Chem., Int. Ed.* **2010**, *49*, 78.
(725) Li, S.; Pedano, M. a. L.; Chang, S.-H.; Mirkin, C. A.; Schatz, G. C. *Nano Lett.* **2010**, *10*, 1722.
(726) Wei, W.; Li, S. Z.; Millstone, J. E.; Banholzer, M. J.; Chen, X. D.; Xu, X. Y.; Schatz, G. C.; Mirkin, C. A. *Angew. Chem., Int. Ed.* **2009**, *48*, 4210.
(727) Wei, W.; Li, S. Z.; Qin, L. D.; Xue, C.; Millstone, J. E.; Xu, X. Y.; Schatz, G. C.; Mirkin, C. A. *Nano Lett.* **2008**, *8*, 3446.

(728) Yoo, S. H.; Park, S. *Adv. Mater.* **2007**, *19*, 1612.
(729) Wu, Y.; Livneh, T.; Zhang, Y. X.; Cheng, G.; Wang, J.; Tang, J.; Moskovits, M.; Stucky, G. D. *Nano Lett.* **2004**, *4*, 2337.
(730) Wu, Y.; Cheng, G.; Katsov, K.; Sides, S. W.; Wang, J.; Tang, J.; Fredrickson, G. H.; Moskovits, M.; Stucky, G. D. *Nat. Mater.* **2004**, *3*, 816.
(731) Gansel, J. K.; Thiel, M.; Rill, M. S.; Decker, M.; Bade, K.; Saile, V.; von Freymann, G.; Linden, S.; Wegener, M. *Science* **2009**, *325*, 1513.
(732) Lee, W.; Scholz, R.; Niesch, K.; Gosele, U. *Angew. Chem., Int. Ed.* **2005**, *44*, 6050.
(733) Huang, C. W.; Hao, Y. W. *Nanotechnology* **2009**, 20.
(734) Tao, F. F.; Guan, M. Y.; Jiang, Y.; Zhu, J. M.; Xu, Z.; Xue, Z. L. *Adv. Mater.* **2006**, *18*, 2161.
(735) Mu, C.; Yn, Y. X.; Wang, R. M.; Wu, K.; Xu, D. S.; Guo, G. L. *Adv. Mater.* **2004**, *16*, 1550.
(736) Fukuoka, A.; Sakamoto, Y.; Guan, S.; Inagaki, S.; Sugimoto, N.; Fukushima, Y.; Hirahara, K.; Iijima, S.; Ichikawa, M. *J. Am. Chem. Soc.* **2001**, *123*, 3373.
(737) Ryoo, R.; Kim, J. M.; Ko, C. H.; Shin, C. H. *J. Phys. Chem.* **1996**, *100*, 17718.
(738) Liu, Z.; Sakamoto, Y.; Ohsuna, T.; Hiraga, K.; Terasaki, O.; Ko, C. H.; Shin, H. J.; Ryoo, R. *Angew. Chem.* **2000**, *112*, 3237.
(739) Kang, H.; Jun, Y.-w.; Park, J.-I.; Lee, K.-B.; Cheon, J. *Chem. Mater.* **2000**, *12*, 3530.
(740) Arbiol, J.; Cabot, A.; Morante, J. R.; Chen, F.; Liu, M. *Appl. Phys. Lett.* **2002**, *81*, 3449.
(741) Shin, H. J.; Ko, C. H.; Ryoo, R. *J. Mater. Chem.* **2001**, *11*, 260.
(742) Joo, S. H.; Choi, S. J.; Oh, I.; Kwak, J.; Liu, Z.; Terasaki, O.; Ryoo, R. *Nature* **2001**, *412*, 169.
(743) Sasaki, M.; Osada, M.; Higashimoto, N.; Yamamoto, T.; Fukuoka, A.; Ichikawa, M. *J. Mol. Catal. A* **1999**, *141*, 223.
(744) Sasaki, M.; Osada, M.; Sugimoto, N.; Inagaki, S.; Fukushima, Y.; Fukuoka, A.; Ichikawa, M. *Microporous Mesoporous Mater.* **1998**, *21*, 597.
(745) Xia, Y.; Yang, P.; Sun, Y.; Wu, Y.; Mayers, B.; Gates, B.; Yin, Y.; Kim, F.; Yan, H. *Adv. Mater.* **2003**, *15*, 353.
(746) Di Renzo, F.; Cambon, H.; Dutartre, R. *Microporous Mater.* **1997**, *10*, 283.
(747) Kresge, C. T.; Leonowicz, M. E.; Roth, W. J.; Vartuli, J. C.; Beck, J. S. *Nature* **1992**, *359*, 710.
(748) Zhao, D. Y.; Feng, J. L.; Huo, Q. S.; Melosh, N.; Fredrickson, G. H.; Chmelka, B. F.; Stucky, G. D. *Science* **1998**, *279*, 548.
(749) Huo, Q. S.; Margolese, D. I.; Ciesla, U.; Feng, P. Y.; Gier, T. E.; Sieger, P.; Leon, R.; Petroff, P. M.; Schuth, F.; Stucky, G. D. *Nature* **1994**, *368*, 317.
(750) Zhao, D. Y.; Huo, Q. S.; Feng, J. L.; Chmelka, B. F.; Stucky, G. D. *J. Am. Chem. Soc.* **1998**, *120*, 6024.
(751) Davis, M. E. *Nature* **2002**, *417*, 813.
(752) Ko, C. H.; Ryoo, R. *Chem. Commun.* **1996**, 2467.
(753) Lee, K. B.; Lee, S. M.; Cheon, J. *Adv. Mater.* **2001**, *13*, 517.
(754) Cai, W.; Zhang, Y.; Jia, J.; Zhang, L. *Appl. Phys. Lett.* **1998**, *73*, 2709.
(755) Plyuto, Y.; Berquier, J. M.; Jacquiod, C.; Ricolleau, C. *Chem. Commun.* **1999**, 1653.
(756) Huang, M. H.; Choudrey, A.; Yang, P. *Chem. Commun.* **2000**, 1063.
(757) Han, Y.-J.; Kim, J. M.; Stucky, G. D. *Chem. Mater.* **2000**, *12*, 2068.
(758) Hong, B. H.; Bae, S. C.; Lee, C.-W.; Jeong, S.; Kim, K. S. *Science* **2001**, *294*, 348.
(759) Zhang, Z.; Dai, S.; Blom, D. A.; Shen, J. *Chem. Mater.* **2002**, *14*, 965.
(760) Asefa, T.; Lennox, R. B. *Chem. Mater.* **2005**, *17*, 2481.
(761) Wang, D.; Zhou, W. L.; McCaughy, B. F.; Hampsey, J. E.; Ji, X.; Jiang, Y. B.; Xu, H.; Tang, J.; Schmehl, R. H.; O'Connor, C.; Brinker, C. J.; Lu, Y. *Adv. Mater.* **2003**, *15*, 130.
(762) Bhattacharyya, S.; Saha, S. K.; Chakravorty, D. *Appl. Phys. Lett.* **2000**, *77*, 3770.
(763) Chen, Z.; Gao, Q.; Wu, C.; Ruan, M.; Shi, J. *Chem. Commun.* **2004**, 1998.
(764) Cai, W.; Hofmeister, H.; Rainer, T. *Physica E* **2001**, *11*, 339.
(765) Cai, W.; Hofmeister, H.; Rainer, T.; Chen, W. *J. Nanopart. Res.* **2001**, *3*, 441.
(766) Guari, Y.; Thieuleux, C.; Mehdi, A.; Reye, C.; Corriu, R. J. P.; Gomez-Gallardo, S.; Philippot, K.; Chaudret, B.; Dutartre, R. *Chem. Commun.* **2001**, 1374.
(767) Bi, H.; Cai, W.; Kan, C.; Zhang, L.; Martin, D.; Trager, F. *J. Appl. Phys.* **2002**, *92*, 7491.
(768) Fukuoka, A.; Araki, H.; Sakamoto, Y.; Sugimoto, N.; Tsukada, H.; Kumai, Y.; Akimoto, Y.; Ichikawa, M. *Nano Lett.* **2002**, *2*, 793.
(769) Fukuoka, A.; Araki, H.; Kimura, J.-i.; Sakamoto, Y.; Higuchi, T.; Sugimoto, N.; Inagaki, S.; Ichikawa, M. *J. Mater. Chem.* **2004**, *14*, 752.
(770) Gu, J. L.; Shi, J. L.; You, G. J.; Xiong, L. M.; Qian, S. X.; Hua, Z. L.; Chen, H. R. *Adv. Mater.* **2005**, *17*, 557.
(771) Perez, M. D.; Otal, E.; Bilmes, S. A.; Soler-Illia, G.; Crepaldi, E. L.; Grosso, D.; Sanchez, C. *Langmuir* **2004**, *20*, 6879.
(772) Andersson, M.; Birkedal, H.; Franklin, N. R.; Ostomel, T.; Boettcher, S.; Palmqvist, A. E. C.; Stucky, G. D. *Chem. Mater.* **2005**, *17*, 1409.
(773) Besson, S.; Gacoin, T.; Ricolleau, C.; Boilot, J.-P. *Chem. Commun.* **2003**, 360.
(774) Calvo, A.; Fuertes, M. C.; Yameen, B.; Williams, F. J.; Azzaroni, O.; Soler-Illia, G. J. A. A. *Langmuir* **2010**, *26*, 5559.
(775) Linden, S.; Enkrich, C.; Wegener, M.; Zhou, J.; Koschny, T.; Soukoulis, C. M. *Science* **2004**, *306*, 1351.
(776) Maier, S. A.; Kik, P. G.; Atwater, H. A.; Meltzer, S.; Harel, E.; Koel, B. E.; Requicha, A. A. G. *Nat. Mater.* **2003**, *2*, 229.
(777) Gunnarsson, L.; Bjerneld, E. J.; Xu, H.; Petronis, S.; Kasemo, B.; Kall, M. *Appl. Phys. Lett.* **2001**, *78*, 802.
(778) Deckman, H. W.; Dunsmuir, J. H. *Appl. Phys. Lett.* **1982**, *41*, 377.
(779) Hulteen, J. C.; Van Duyne, R. P. *J. Vac. Sci. Technol., A* **1995**, *13*, 1553.
(780) Hulteen, J. C.; Treichel, D. A.; Smith, M. T.; Duval, M. L.; Jensen, T. R.; Van Duyne, R. P. *J. Phys. Chem. B* **1999**, *103*, 3854.
(781) Haynes, C. L.; Van Duyne, R. P. *J. Phys. Chem. B* **2001**, *105*, 5599.
(782) Haes, A. J.; Zou, S. L.; Schatz, G. C.; Van Duyne, R. P. *J. Phys. Chem. B* **2004**, *108*, 109.
(783) Chan, G. H.; Zhao, J.; Hicks, E. M.; Schatz, G. C.; Van Duyne, R. P. *Nano Lett.* **2007**, *7*, 1947.
(784) Chan, G. H.; Zhao, J.; Schatz, G. C.; Duyne, R. P. V. *J. Phys. Chem. C* **2008**, *112*, 13958.
(785) Jensen, T. R.; Malinsky, M. D.; Haynes, C. L.; Van Duyne, R. P. *J. Phys. Chem. B* **2000**, *104*, 10549.
(786) Jensen, T. R.; Schatz, G. C.; Van Duyne, R. P. *J. Phys. Chem. B* **1999**, *103*, 2394.
(787) Haes, A. J.; Van Duyne, R. P. *J. Am. Chem. Soc.* **2002**, *124*, 10596.
(788) Hall, W. P.; Anker, J. N.; Lin, Y.; Modica, J.; Mrksich, M.; Van Duyne, R. P. *J. Am. Chem. Soc.* **2008**, *130*, 5836.
(789) Haes, A. J.; Chang, L.; Klein, W. L.; Van Duyne, R. P. *J. Am. Chem. Soc.* **2005**, *127*, 2264.
(790) Haes, A. J.; Hall, W. P.; Chang, L.; Klein, W. L.; Van Duyne, R. P. *Nano Lett.* **2004**, *4*, 1029.
(791) McFarland, A. D.; Young, M. A.; Dieringer, J. A.; Van Duyne, R. P. *J. Phys. Chem. B* **2005**, *109*, 11279.
(792) Haynes, C. L.; McFarland, A. D.; Smith, M. T.; Hulteen, J. C.; Van Duyne, R. P. *J. Phys. Chem. B* **2002**, *106*, 1898.
(793) Haynes, C. L.; Van Duyne, R. P. *Nano Lett.* **2003**, *3*, 939.
(794) Kosiorek, A.; Kandulski, W.; Chudzinski, P.; Kempa, K.; Giersig, M. *Nano Lett.* **2004**, *4*, 1359.
(795) Kosiorek, A.; Kandulski, W.; Glaczynska, H.; Giersig, M. *Small* **2005**, *1*, 439.
(796) Hanarp, P.; Sutherland, D. S.; Gold, J.; Kasemo, B. *Colloids Surf., A* **2003**, *214*, 23.

(797) Hanarp, P.; Kall, M.; Sutherland, D. S. *J. Phys. Chem. B* **2003**, *107*, 5768.
(798) Aizpurua, J.; Hanarp, P.; Sutherland, D. S.; Kall, M.; Bryant, G. W.; de Abajo, F. J. G. *Phys. Rev. Lett.* **2003**, 90.
(799) Larsson, E. M.; Alegret, J.; Kall, M.; Sutherland, D. S. *Nano Lett.* **2007**, *7*, 1256.
(800) Larsson, E. M.; Hao, F.; Eurenius, L.; Olsson, E.; Nordlander, P.; Sutherland, D. S. *Small* **2008**, *4*, 1630.
(801) Hao, F.; Larsson, E. M.; Ali, T. A.; Sutherland, D. S.; Nordlander, P. *Chem. Phys. Lett.* **2008**, *458*, 262.
(802) Shumaker-Parry, J. S.; Rochholz, H.; Kreiter, M. *Adv. Mater.* **2005**, *17*, 2131.
(803) Lu, Y.; Liu, G. L.; Kim, J.; Mejia, Y. X.; Lee, L. P. *Nano Lett.* **2005**, *5*, 119.
(804) Bukasov, R.; Shumaker-Parry, J. S. *Nano Lett.* **2007**, *7*, 1113.
(805) Liu, G. L.; Lu, Y.; Kim, J.; Doll, J. C.; Lee, L. P. *Adv. Mater.* **2005**, *17*, 2683.
(806) Fredriksson, H.; Alaverdyan, Y.; Dmitriev, A.; Langhammer, C.; Sutherland, D. S.; Zaech, M.; Kasemo, B. *Adv. Mater.* **2007**, *19*, 4297.
(807) Langhammer, C.; Schwind, M.; Kasemo, B.; Zoric, I. *Nano Lett.* **2008**, *8*, 1461.
(808) Langhammer, C.; Yuan, Z.; Zoric, I.; Kasemo, B. *Nano Lett.* **2006**, *6*, 833.
(809) Dmitriev, A.; Pakizeh, T.; Kall, M.; Sutherland, D. S. *Small* **2007**, *3*, 294.
(810) Correa-Duarte, M. A.; Salgueiriño-Maceira, V.; Rodríguez-González, B.; Liz-Marzán, L. M.; Kosiorek, A.; Kandulski, W.; Giersig, M. *Adv. Mater.* **2005**, *17*, 2014.
(811) Bao, Z.; Chen, L.; Weldon, M.; Chandross, E.; Cherniavskaya, O.; Dai, Y.; Tok, J. B. H. *Chem. Mater.* **2001**, *14*, 24.
(812) Lu, Y.; Xiong, H.; Jiang, X.; Xia, Y.; Prentiss, M.; Whitesides, G. M. *J. Am. Chem. Soc.* **2003**, *125*, 12724.
(813) Love, J. C.; Gates, B. D.; Wolfe, D. B.; Paul, K. E.; Whitesides, G. M. *Nano Lett.* **2002**, *2*, 891.
(814) Hicks, E. M.; Zhang, X.; Zou, S.; Lyandres, O.; Spears, K. G.; Schatz, G. C.; Van Duyne, R. P. *J. Phys. Chem. B* **2005**, *109*, 22351.
(815) Dick, L. A.; McFarland, A. D.; Haynes, C. L.; Van Duyne, R. P. *J. Phys. Chem. B* **2002**, *106*, 853.
(816) Camden, J. P.; Dieringer, J. A.; Zhao, J.; Van Duyne, R. P. *Acc. Chem. Res.* **2008**, *41*, 1653.
(817) Stuart, D. A.; Yuen, J. M.; Shah, N.; Lyandres, O.; Yonzon, C. R.; Glucksberg, M. R.; Walsh, J. T.; Van Duyne, R. P. *Anal. Chem.* **2006**, *78*, 7211.
(818) Zhang, X. Y.; Young, M. A.; Lyandres, O.; Van Duyne, R. P. *J. Am. Chem. Soc.* **2005**, *127*, 4484.
(819) Rindzevicius, T.; Alaverdyan, Y.; Dahlin, A.; Hook, F.; Sutherland, D. S.; Kall, M. *Nano Lett.* **2005**, *5*, 2335.
(820) Rindzevicius, T.; Alaverdyan, Y.; Sepulveda, B.; Pakizeh, T.; Kall, M.; Hillenbrand, R.; Aizpurua, J.; de Abajo, F. J. G. *J. Phys. Chem. C* **2007**, *111*, 1207.
(821) Lee, S. H.; Bantz, K. C.; Lindquist, N. C.; Oh, S.-H.; Haynes, C. L. *Langmuir* **2009**, *25*, 13685.
(822) Xu, L.; Zhou, W. L.; Frommen, C.; Baughman, R. H.; Zakhidov, A. A.; Malkinski, L.; Wang, J.-Q.; Wiley, J. B. *Chem. Commun.* **2000**, 997.
(823) Bartlett, P. N.; Birkin, P. R.; Ghanem, M. A. *Chem. Commun.* **2000**, 1671.
(824) Szamocki, R.; Reculusa, S.; Ravaine, S.; Bartlett, P. N.; Kuhn, A.; Hempelmann, R. *Angew. Chem., Int. Ed.* **2006**, *45*, 1317.
(825) Braun, P. V.; Wiltzius, P. *Adv. Mater.* **2001**, *13*, 482.
(826) Stein, A.; Schroden, R. C. *Curr. Opin. Solid State Mater. Sci.* **2001**, *5*, 553.
(827) Bartlett, P. N.; Baumberg, J. J.; Birkin, P. R.; Ghanem, M. A.; Netti, M. C. *Chem. Mater.* **2002**, *14*, 2199.
(828) Netti, M. C.; Coyle, S.; Baumberg, J. J.; Ghanem, M. A.; Birkin, P. R.; Bartlett, P. N.; Whittaker, D. M. *Adv. Mater.* **2001**, *13*, 1368.
(829) Kelf, T. A.; Sugawara, Y.; Cole, R. M.; Baumberg, J. J.; Abdelsalam, M. E.; Cintra, S.; Mahajan, S.; Russell, A. E.; Bartlett, P. N. *Phys. Rev. B* **2006**, *74*, 245415.
(830) Baumberg, J. J.; Kelf, T. A.; Sugawara, Y.; Cintra, S.; Abdelsalam, M. E.; Bartlett, P. N.; Russell, A. E. *Nano Lett.* **2005**, *5*, 2262.
(831) Abdelsalam, M. E.; Mahajan, S.; Bartlett, P. N.; Baumberg, J. J.; Russell, A. E. *J. Am. Chem. Soc.* **2007**, *129*, 7399.
(832) Mahajan, S.; Richardson, J.; Brown, T.; Bartlett, P. N. *J. Am. Chem. Soc.* **2008**, *130*, 15589.
(833) Kelf, T. A.; Sugawara, Y.; Baumberg, J. J.; Abdelsalam, M.; Bartlett, P. N. *Phys. Rev. Lett.* **2005**, 95.
(834) Yan, H.; Blanford, C. F.; Holland, B. T.; Parent, M.; Smyrl, W. H.; Stein, A. *Adv. Mater.* **1999**, *11*, 1003.
(835) Egan, G. L.; Yu, J. S.; Kim, C. H.; Lee, S. J.; Schaak, R. E.; Mallouk, T. E. *Adv. Mater.* **2000**, *12*, 1040.
(836) Jiang, P.; Bertone, J. F.; Colvin, V. L. *Science* **2001**, *291*, 453.
(837) Kuroda, Y.; Kuroda, K. *Angew. Chem., Int. Ed.* **2010**, *49*, 6993.
(838) Kuroda, Y.; Yamauchi, Y.; Kuroda, K. *Chem. Commun.* **2010**, *46*, 1827.
(839) Ebbesen, T. W.; Lezec, H. J.; Ghaemi, H. F.; Thio, T.; Wolff, P. A. *Nature* **1998**, *391*, 667.
(840) Xia, Y.; Whitesides, G. M. *Annu. Rev. Mater. Sci.* **1998**, *28*, 153.
(841) Kwak, E.-S.; Henzie, J.; Chang, S.-H.; Gray, S. K.; Schatz, G. C.; Odom, T. W. *Nano Lett.* **2005**, *5*, 1963.
(842) Henzie, J.; Barton, J. E.; Stender, C. L.; Odom, T. W. *Acc. Chem. Res.* **2006**, *39*, 249.
(843) Gao, H.; Henzie, J.; Odom, T. W. *Nano Lett.* **2006**, *6*, 2104.
(844) Henzie, J.; Lee, M. H.; Odom, T. W. *Nat. Nanotechnol.* **2007**, *2*, 549.
(845) Lee, M. H.; Gao, H.; Henzie, J.; Odom, T. W. *Small* **2007**, *3*, 2029.
(846) Lee, M. H.; Gao, H.; Odom, T. W. *Nano Lett.* **2009**, *9*, 2584.
(847) Yang, J.-C.; Gao, H.; Suh, J. Y.; Zhou, W.; Lee, M. H.; Odom, T. W. *Nano Lett.* **2010**, *10*, 3173.
(848) Lee, M. H.; Lin, J. Y.; Odom, T. W. *Angew. Chem., Int. Ed.* **2010**, *49*, 3057.
(849) Malyarchuk, V.; Hua, F.; Mack, N.; Velasquez, V.; White, J.; Nuzzo, R.; Rogers, J. *Opt. Express* **2005**, *13*, 5669.
(850) Malyarchuk, V.; Stewart, M. E.; Nuzzo, R. G.; Rogers, J. A. *Appl. Phys. Lett.* **2007**, *90*, 203113.
(851) Truong, T. T.; Maria, J.; Yao, J.; Stewart, M. E.; Lee, T.-W.; Gray, S. K.; Nuzzo, R. G.; Rogers, J. A. *Nanotechnology* **2009**, *20*, 434011.
(852) Henzie, J.; Lee, J.; Lee, M. H.; Hasan, W.; Odom, T. W. *Annu. Rev. Phys. Chem.* **2009**, *60*, 147.
(853) Henzie, J.; Kwak, E.-S.; Odom, T. W. *Nano Lett.* **2005**, *5*, 1199.
(854) Henzie, J.; Shuford, K. L.; Kwak, E.-S.; Schatz, G. C.; Odom, T. W. *J. Phys. Chem. B* **2006**, *110*, 14028.
(855) Lee, J.; Hasan, W.; Lee, M. H.; Odom, T. W. *Adv. Mater.* **2007**, *19*, 4387.
(856) Lee, J.; Hasan, W.; Stender, C. L.; Odom, T. W. *Acc. Chem. Res.* **2008**, *41*, 1762.
(857) Gao, H.; Henzie, J.; Lee, M. H.; Odom, T. W. *Proc. Natl. Acad. Sci. U.S.A.* **2008**, *105*, 20146.
(858) Gao, H.; Yang, J.-C.; Lin, J. Y.; Stuparu, A. D.; Lee, M. H.; Mrksich, M.; Odom, T. W. *Nano Lett.* **2010**, *10*, 2549.
(859) Park, M.; Chaikin, P. M.; Register, R. A.; Adamson, D. H. *Appl. Phys. Lett.* **2001**, *79*, 257.
(860) Shin, K.; Leach, K. A.; Goldbach, J. T.; Kim, D. H.; Jho, J. Y.; Tuominen, M.; Hawker, C. J.; Russell, T. P. *Nano Lett.* **2002**, *2*, 933.
(861) Ansari, I. A.; Hamley, I. W. *J. Mater. Chem.* **2003**, *13*, 2412.
(862) Lu, J.; Chamberlin, D.; Rider, D. A.; Liu, M. Z.; Manners, I.; Russell, T. P. *Nanotechnology* **2006**, *17*, 5792.
(863) Park, S.; Wang, J. Y.; Kim, B.; Russell, T. P. *Nano Lett.* **2008**, *8*, 1667.
(864) Zschech, D.; Kim, D. H.; Milenin, A. P.; Hopfe, S.; Scholz, R.; Goring, P.; Hillebrand, R.; Senz, S.; Hawker, C. J.; Russell, T. P.; Steinhart, M.; Gosele, U. *Nanotechnology* **2006**, *17*, 2122.
(865) Masuda, H.; Satoh, M. *Jpn. J. Appl. Phys., Part 2* **1996**, *35*, L126.

(866) Masuda, H.; Yasui, K.; Nishio, K. *Adv. Mater.* **2000**, *12*, 1031.
(867) Nakayama, K.; Tanabe, K.; Atwater, H. A. *Appl. Phys. Lett.* **2008**, *93*, 121904.
(868) Sander, M. S.; Tan, L. S. *Adv. Funct. Mater.* **2003**, *13*, 393.
(869) Dickey, M. D.; Weiss, E. A.; Smythe, E. J.; Chiechi, R. C.; Capasso, F.; Whitesides, G. M. *ACS Nano* **2008**, *2*, 800.
(870) Renard, C.; Ricolleau, C.; Fort, E.; Besson, S.; Gacoin, T.; Boilot, J.-P. *Appl. Phys. Lett.* **2002**, *80*, 300.
(871) Li, Y.; Su, H.; Wong, K. S.; Li, X.-Y. *J. Phys. Chem. C* **2010**, *114*, 10463.
(872) Choi, D.; Choi, Y.; Hong, S.; Kang, T.; Lee, L. P. *Small* **2010**, *6*, 1741.
(873) Gu, G. H.; Suh, J. S. *J. Phys. Chem. C* **2010**, *114*, 7258.
(874) Becker, M.; Stelzner, T.; Steinbrück, A.; Berger, A.; Liu, J.; Lerose, D.; Gösele, U.; Christiansen, S. *ChemPhysChem* **2009**, *10*, 1219.
(875) Qiu, T.; Wu, X. L.; Shen, J. C.; Ha, P. C. T.; Chu, P. K. *Nanotechnology* **2006**, *17*, 5769.
(876) Li, X.; Chen, G.; Yang, L.; Jin, Z.; Liu, J. *Adv. Funct. Mater.* **2010**, *20*, 2815.
(877) Leng, W.; Yasseri, A. A.; Sharma, S.; Li, Z.; Woo, H. Y.; Vak, D.; Bazan, G. C.; Kelley, A. M. *Anal. Chem.* **2006**, *78*, 6279.
(878) Galopin, E.; Barbillat, J.; Coffinier, Y.; Szunerits, S.; Patriarche, G.; Boukherroub, R. *ACS Appl. Mater. Interfaces* **2009**, *1*, 1396.
(879) Zhang, B.; Wang, H.; Lu, L.; Ai, K.; Zhang, G.; Cheng, X. *Adv. Funct. Mater.* **2008**, *18*, 2348.
(880) Fan, J. G.; Zhao, Y. P. *Langmuir* **2008**, *24*, 14172.
(881) Chen, L.; Luo, L.; Chen, Z.; Zhang, M.; Zapien, J. A.; Lee, C. S.; Lee, S. T. *J. Phys. Chem. C* **2009**, *114*, 93.
(882) Fritzsche, W.; Bohm, K. J.; Unger, E.; Kohler, J. M. *Appl. Phys. Lett.* **1999**, *75*, 2854.
(883) Winningham, T. A.; Whipple, S. G.; Douglas, K. *J. Vac. Sci. Technol., B* **2001**, *19*, 1796.
(884) Becerril, H. A.; Woolley, A. T. *Small* **2007**, *3*, 1534.
(885) Deng, Z.; Mao, C. *Angew. Chem., Int. Ed.* **2004**, *43*, 4068.
(886) Losic, D.; Mitchell, J. G.; Voelcker, N. H. *New J. Chem.* **2006**, *30*, 908.
(887) Ueno, T. *J. Mater. Chem.* **2008**, *18*, 3741.
(888) Douglas, T.; Young, M. *Science* **2006**, *312*, 873.
(889) Aniagyei, S. E.; DuFort, C.; Kao, C. C.; Dragnea, B. *J. Mater. Chem.* **2008**, *18*, 3763.
(890) Strable, E.; Finn, M. G. *Viruses Nanotechnol.* **2009**, *327*, 1.
(891) Mann, S.; Shenton, W.; Li, M.; Connolly, S.; Fitzmaurice, D. *Adv. Mater.* **2000**, *12*, 147.
(892) Alivisatos, A. P.; Johnsson, K. P.; Peng, X. G.; Wilson, T. E.; Loweth, C. J.; Bruchez, M. P.; Schultz, P. G. *Nature* **1996**, *382*, 609.
(893) Loweth, C. J.; Caldwell, W. B.; Peng, X. G.; Alivisatos, A. P.; Schultz, P. G. *Angew. Chem., Int. Ed.* **1999**, *38*, 1808.
(894) Claridge, S. A.; Goh, S. L.; Frechet, J. M. J.; Williams, S. C.; Micheel, C. M.; Alivisatos, A. P. *Chem. Mater.* **2005**, *17*, 1628.
(895) Fu, A.; Micheel, C. M.; Cha, J.; Chang, H.; Yang, H.; Alivisatos, A. P. *J. Am. Chem. Soc.* **2004**, *126*, 10832.
(896) Ackerson, C. J.; Sykes, M. T.; Kornberg, R. D. *Proc. Natl. Acad. Sci. U.S.A.* **2005**, *102*, 13383.
(897) Zanchet, D.; Micheel, C. M.; Parak, W. J.; Gerion, D.; Williams, S. C.; Alivisatos, A. P. *J. Phys. Chem. B* **2002**, *106*, 11758.
(898) Claridge, S. A.; Mastroianni, A. J.; Au, Y. B.; Liang, H. W.; Micheel, C. M.; Frechet, J. M. J.; Alivisatos, A. P. *J. Am. Chem. Soc.* **2008**, *130*, 9598.
(899) Niemeyer, C. M.; Burger, W.; Peplies, J. *Angew. Chem., Int. Ed.* **1998**, *37*, 2265.
(900) Deng, Z.; Tian, Y.; Lee, S.-H.; Ribbe, A. E.; Mao, C. *Angew. Chem., Int. Ed.* **2005**, *44*, 3582.
(901) Weizmann, Y.; Patolsky, F.; Popov, I.; Willner, I. *Nano Lett.* **2004**, *4*, 787.
(902) Bidault, S.; de Abajo, F. J. G.; Polman, A. *J. Am. Chem. Soc.* **2008**, *130*, 2750.
(903) Yao, H.; Yi, C. Q.; Tzang, C. H.; Zhu, J. J.; Yang, M. S. *Nanotechnology* **2007**, *18*, 7.
(904) Mastroianni, A. J.; Claridge, S. A.; Alivisatos, A. P. *J. Am. Chem. Soc.* **2009**, *131*, 8455.
(905) Sonnichsen, C.; Reinhard, B. M.; Liphardt, J.; Alivisatos, A. P. *Nat. Biotechnol.* **2005**, *23*, 741.
(906) Aldaye, F. A.; Sleiman, H. F. *Angew. Chem., Int. Ed.* **2006**, *45*, 2204.
(907) Aldaye, F. A.; Sleiman, H. F. *J. Am. Chem. Soc.* **2007**, *129*, 4130.
(908) Lo, P. K.; Karam, P.; Aldaye, F. A.; McLaughlin, C. K.; Hamblin, G. D.; Cosa, G.; Sleiman, H. F. *Nat. Chem.* **2010**, *2*, 319.
(909) Lo, P. K.; Altvater, F.; Sleiman, H. F. *J. Am. Chem. Soc.* **2010**, *132*, 10212.
(910) Storhoff, J. J.; Lazarides, A. A.; Mucic, R. C.; Mirkin, C. A.; Letsinger, R. L.; Schatz, G. C. *J. Am. Chem. Soc.* **2000**, *122*, 4640.
(911) Jin, R.; Wu, G.; Li, Z.; Mirkin, C. A.; Schatz, G. C. *J. Am. Chem. Soc.* **2003**, *125*, 1643.
(912) Elghanian, R.; Storhoff, J. J.; Mucic, R. C.; Letsinger, R. L.; Mirkin, C. A. *Science* **1997**, *277*, 1078.
(913) Storhoff, J. J.; Elghanian, R.; Mucic, R. C.; Mirkin, C. A.; Letsinger, R. L. *J. Am. Chem. Soc.* **1998**, *120*, 1959.
(914) Taton, T. A.; Mirkin, C. A.; Letsinger, R. L. *Science* **2000**, *289*, 1757.
(915) Cao, Y. C.; Jin, R.; Mirkin, C. A. *Science* **2002**, *297*, 1536.
(916) Cao, Y. C.; Jin, R.; Nam, J.-M.; Thaxton, C. S.; Mirkin, C. A. *J. Am. Chem. Soc.* **2003**, *125*, 14676.
(917) Nam, J.-M.; Park, S.-J.; Mirkin, C. A. *J. Am. Chem. Soc.* **2002**, *124*, 3820.
(918) Nam, J.-M.; Thaxton, C. S.; Mirkin, C. A. *Science* **2003**, *301*, 1884.
(919) Mirkin, C. A.; Letsinger, R. L.; Mucic, R. C.; Storhoff, J. J.; Elghanian, R. Nanoparticles having oligonucleotides attached on surface and use for detecting nucleic acids. WO Patent 9804740, Feb 5, 1998.
(920) Mucic, R. C.; Storhoff, J. J.; Mirkin, C. A.; Letsinger, R. L. *J. Am. Chem. Soc.* **1998**, *120*, 12674.
(921) Sadasivan, S.; Dujardin, E.; Li, M.; Johnson, C. J.; Mann, S. *Small* **2005**, *1*, 103.
(922) Sebba, D. S.; Lazarides, A. A. *J. Phys. Chem. C* **2008**, *112*, 18331.
(923) Sebba, D. S.; Mock, J. J.; Smith, D. R.; LaBean, T. H.; Lazarides, A. A. *Nano Lett.* **2008**, *8*, 1803.
(924) Sebba, D.; LaBean, T.; Lazarides, A. *Appl. Phys. B: Lasers Opt.* **2008**, *93*, 69.
(925) Chen, Y.; Mao, C. *Small* **2008**, *4*, 2191.
(926) Hazarika, P.; Ceyhan, B.; Niemeyer, C. M. *Angew. Chem., Int. Ed.* **2004**, *43*, 6469.
(927) Niemeyer, C. M.; Ceyhan, B. *Angew. Chem., Int. Ed.* **2001**, *40*, 3685.
(928) Li, M.; Mann, S. *J. Mater. Chem.* **2004**, *14*, 2260.
(929) Kanaras, A. G.; Wang, Z.; Brust, M.; Cosstick, R.; Bates, A. D. *Small* **2007**, *3*, 590.
(930) Kanaras, A. G.; Wang, Z.; Hussain, I.; Brust, M.; Cosstick, R.; Bates, A. D. *Small* **2007**, *3*, 67.
(931) Hurst, S. J.; Hill, H. D.; Macfarlane, R. J.; Wu, J.; Dravid, V. P.; Mirkin, C. A. *Small* **2009**, *5*, 2156.
(932) Xu, X.; Rosi, N. L.; Wang, Y.; Huo, F.; Mirkin, C. A. *J. Am. Chem. Soc.* **2006**, *128*, 9286.
(933) Huo, F.; Lytton-Jean, A. K. R.; Mirkin, C. A. *Adv. Mater.* **2006**, *18*, 2304.
(934) Maye, M. M.; Nykypanchuk, D.; Cuisinier, M.; van der Lelie, D.; Gang, O. *Nat. Mater.* **2009**, *8*, 388.
(935) Niemeyer, C. M.; Ceyhan, B.; Hazarika, P. *Angew. Chem., Int. Ed.* **2003**, *42*, 5766.
(936) Dujardin, E.; Mann, S.; Hsin, L.-B.; Wang, C. R. C. *Chem. Commun.* **2001**, 1264.
(937) Kim, J.-Y.; Lee, J.-S. *Nano Lett.* **2009**, *9*, 4564.
(938) Millstone, J. E.; Georganopoulou, D. G.; Xu, X.; Wei, W.; Li, S.; Mirkin, C. A. *Small* **2008**, *4*, 2176.

(939) Kang, T.; Yoo, S. M.; Yoon, I.; Lee, S. Y.; Kim, B. *Nano Lett.* **2010**, *10*, 1189.
(940) Demers, L. M.; Park, S.-J.; Taton, T. A.; Li, Z.; Mirkin, C. A. *Angew. Chem.* **2001**, *113*, 3161.
(941) Park, S.-J.; Lazarides, A. A.; Storhoff, J. J.; Pesce, L.; Mirkin, C. A. *J. Phys. Chem. B* **2004**, *108*, 12375.
(942) Nykypanchuk, D.; Maye, M. M.; van der Lelie, D.; Gang, O. *Nature* **2008**, *451*, 549.
(943) Park, S. Y.; Lytton-Jean, A. K. R.; Lee, B.; Weigand, S.; Schatz, G. C.; Mirkin, C. A. *Nature* **2008**, *451*, 553.
(944) Hill, H. D.; Macfarlane, R. J.; Senesi, A. J.; Lee, B.; Park, S. Y.; Mirkin, C. A. *Nano Lett.* **2008**, *8*, 2341.
(945) Xiong, H.; van der Lelie, D.; Gang, O. *Phys. Rev. Lett.* **2009**, *102*, 015504.
(946) Macfarlane, R. J.; Lee, B.; Hill, H. D.; Senesi, A. J.; Seifert, S.; Mirkin, C. A. *Proc. Natl. Acad. Sci. U.S.A.* **2009**, *106*, 10493.
(947) Maye, M. M.; Kumara, M. T.; Nykypanchuk, D.; Sherman, W. B.; Gang, O. *Nat. Nanotechnol.* **2010**, *5*, 116.
(948) Cheng, W.; Hartman, M. R.; Smilgies, D.-M.; Long, R.; Campolongo, M. J.; Li, R.; Sekar, K.; Hui, C.-Y.; Luo, D. *Angew. Chem., Int. Ed.* **2010**, *49*, 380.
(949) Macfarlane, R. J.; Jones, M. R.; Senesi, A. J.; Young, K. L.; Lee, B.; Wu, J.; Mirkin, C. A. *Angew. Chem., Int. Ed.* **2010**, *49*, 4589.
(950) Jones, M. R.; Macfarlane, R. J.; Lee, B.; Zhang, J.; Young, K. L.; Senesi, A. J.; Mirkin, C. A. *Nat. Mater.* **2010**, *9*, 913.
(951) Maeda, Y.; Tabata, H.; Kawai, T. *Appl. Phys. Lett.* **2001**, *79*, 1181.
(952) Le, J. D.; Pinto, Y.; Seeman, N. C.; Musier-Forsyth, K.; Taton, T. A.; Kiehl, R. A. *Nano Lett.* **2004**, *4*, 2343.
(953) Pinto, Y. Y.; Le, J. D.; Seeman, N. C.; Musier-Forsyth, K.; Taton, T. A.; Kiehl, R. A. *Nano Lett.* **2005**, *5*, 2399.
(954) Zheng, J. W.; Constantinou, P. E.; Micheel, C.; Alivisatos, A. P.; Kiehl, R. A.; Seeman, N. C. *Nano Lett.* **2006**, *6*, 1502.
(955) Sharma, J.; Chhabra, R.; Andersen, C. S.; Gothelf, K. V.; Yan, H.; Liu, Y. *J. Am. Chem. Soc.* **2008**, *130*, 7820.
(956) Ding, B.; Deng, Z.; Yan, H.; Cabrini, S.; Zuckermann, R. N.; Bokor, J. *J. Am. Chem. Soc.* **2010**, *132*, 3248.
(957) Zhang, J. P.; Liu, Y.; Ke, Y. G.; Yan, H. *Nano Lett.* **2006**, *6*, 248.
(958) Xiao, S.; Liu, F.; Rosen, A. E.; Hainfeld, J. F.; Seeman, N. C.; Musier-Forsyth, K.; Kiehl, R. A. *J. Nanopart. Res.* **2002**, *4*, 313.
(959) Ding, B. Q.; Cabrini, S.; Zuckermann, R. N.; Bokor, J. *J. Vac. Sci. Technol., B* **2009**, *27*, 184.
(960) Sharma, J.; Chhabra, R.; Liu, Y.; Ke, Y. G.; Yan, H. *Angew. Chem., Int. Ed.* **2006**, *45*, 730.
(961) Kuzuya, A.; Koshi, N.; Kimura, M.; Numajiri, K.; Yamazaki, T.; Ohnishi, T.; Okada, F.; Komiyama, M. *Small* **2010**, *6*, 2664.
(962) Kumar, A.; Pattarkine, M.; Bhadbhade, M.; Mandale, A. B.; Ganesh, K. N.; Datar, S. S.; Dharmadhikari, C. V.; Sastry, M. *Adv. Mater.* **2001**, *13*, 341.
(963) Gu, H.; Chao, J.; Xiao, S.-J.; Seeman, N. C. *Nature* **2010**, *465*, 202.
(964) Sharma, J.; Chhabra, R.; Cheng, A.; Brownell, J.; Liu, Y.; Yan, H. *Science* **2009**, *323*, 112.
(965) Wang, G.; Zhang, J.; Murray, R. W. *Anal. Chem.* **2002**, *74*, 4320.
(966) Patolsky, F.; Weizmann, Y.; Lioubashevski, O.; Willner, I. *Angew. Chem., Int. Ed.* **2002**, *41*, 2323.
(967) Beyer, S.; Nickels, P.; Simmel, F. C. *Nano Lett.* **2005**, *5*, 719.
(968) Lee, J. H.; Wernette, D. P.; Yigit, M. V.; Liu, J.; Wang, Z.; Lu, Y. *Angew. Chem., Int. Ed.* **2007**, *46*, 9006.
(969) Coomber, D.; Bartczak, D.; Gerrard, S. R.; Tyas, S.; Kanaras, A. G.; Stulz, E. *Langmuir* **2010**, *26*, 13760.
(970) Nakao, H.; Shiigi, H.; Yamamoto, Y.; Tokonami, S.; Nagaoka, T.; Sugiyama, S.; Ohtani, T. *Nano Lett.* **2003**, *3*, 1391.
(971) Wang, G.; Murray, R. W. *Nano Lett.* **2003**, *4*, 95.
(972) Warner, M. G.; Hutchison, J. E. *Nat. Mater.* **2003**, *2*, 272.
(973) Sastry, M.; Kumar, A.; Datar, S.; Dharmadhikari, C. V.; Ganesh, K. N. *Appl. Phys. Lett.* **2001**, *78*, 2943.
(974) Yonezawa, T.; Onoue, S. Y.; Kimizuka, N. *Chem. Lett.* **2002**, 1172.
(975) McMillan, R. A.; Paavola, C. D.; Howard, J.; Chan, S. L.; Zaluzec, N. J.; Trent, J. D. *Nat. Mater.* **2002**, *1*, 247.
(976) Medalsy, I.; Dgany, O.; Sowwan, M.; Cohen, H.; Yukashevska, A.; Wolf, S. G.; Wolf, A.; Koster, A.; Almog, O.; Marton, I.; Pouny, Y.; Altman, A.; Hoseyov, O. S.; Porath, D. *Nano Lett.* **2008**, *8*, 473.
(977) Hu, M. H.; Qian, L. P.; Brinas, R. P.; Lymar, E. S.; Hainfeld, J. F. *Angew. Chem., Int. Ed.* **2007**, *46*, 5111.
(978) Hall, S. R.; Shenton, W.; Engelhardt, H.; Mann, S. *ChemPhysChem* **2001**, *2*, 184.
(979) Bergkvist, M.; Mark, S. S.; Yang, X.; Angert, E. R.; Batt, C. A. *J. Phys. Chem. B* **2004**, *108*, 8241.
(980) Mark, S. S.; Bergkvist, M.; Yang, X.; Teixeira, L. M.; Bhatnagar, P.; Angert, E. R.; Batt, C. A. *Langmuir* **2006**, *22*, 3763.
(981) Mo, X.; Krebs, M. P.; Yu, S. M. *Small* **2006**, *2*, 526.
(982) Lamm, M. S.; Sharma, N.; Rajagopal, K.; Beyer, F. L.; Schneider, J. P.; Pochan, D. J. *Adv. Mater.* **2008**, *20*, 447.
(983) Ryadnov, M. G.; Ceyhan, B.; Niemeyer, C. M.; Woolfson, D. N. *J. Am. Chem. Soc.* **2003**, *125*, 9388.
(984) Ryadnov, M. G.; Woolfson, D. N. *J. Am. Chem. Soc.* **2004**, *126*, 7454.
(985) Stevens, M. M.; Flynn, N. T.; Wang, C.; Tirrell, D. A.; Langer, R. *Adv. Mater.* **2004**, *16*, 915.
(986) Aili, D.; Enander, K.; Rydberg, J.; Lundstrom, I.; Baltzer, L.; Liedberg, B. *J. Am. Chem. Soc.* **2006**, *128*, 2194.
(987) Aili, D.; Enander, K.; Rydberg, J.; Nesterenko, I.; Bjorefors, F.; Baltzer, L.; Liedberg, B. *J. Am. Chem. Soc.* **2008**, *130*, 5780.
(988) Aili, D.; Enander, K.; Baltzer, L.; Liedberg, B. *Nano Lett.* **2008**, *8*, 2473.
(989) Sharma, N.; Top, A.; Kiick, K. L.; Pochan, D. J. *Angew. Chem., Int. Ed.* **2009**, *48*, 7078.
(990) Fu, X. Y.; Wang, Y.; Huang, L. X.; Sha, Y. L.; Gui, L. L.; Lai, L. H.; Tang, Y. Q. *Adv. Mater.* **2003**, *15*, 902.
(991) Matsui, H.; Pan, S.; Douberly, G. E. *J. Phys. Chem. B* **2001**, *105*, 1683.
(992) Banerjee, I. A.; Yu, L.; Matsui, H. *Nano Lett.* **2003**, *3*, 283.
(993) Li, L.-S.; Stupp, S. I. *Angew. Chem., Int. Ed.* **2005**, *44*, 1833.
(994) Wong, M. S.; Cha, J. N.; Choi, K.-S.; Deming, T. J.; Stucky, G. D. *Nano Lett.* **2002**, *2*, 583.
(995) Connolly, S.; Fitzmaurice, D. *Adv. Mater.* **1999**, *11*, 1202.
(996) Caswell, K. K.; Wilson, J. N.; Bunz, U. H. F.; Murphy, C. J. *J. Am. Chem. Soc.* **2003**, *125*, 13914.
(997) Wang, L.; Zhu, Y.; Xu, L.; Chen, W.; Kuang, H.; Liu, L.; Agarwal, A.; Xu, C.; Kotov, N. A. *Angew. Chem., Int. Ed.* **2010**, *49*, 5472.
(998) Shenton, W.; Davis, S. A.; Mann, S. *Adv. Mater.* **1999**, *11*, 449.
(999) Park, S.-J.; Lazarides, A. A.; Mirkin, C. A.; Letsinger, R. L. *Angew. Chem., Int. Ed.* **2001**, *40*, 2909.
(1000) Brown, S. *Nano Lett.* **2001**, *1*, 391.
(1001) Cobbe, S.; Connolly, S.; Ryan, D.; Nagle, L.; Eritja, R.; Fitzmaurice, D. *J. Phys. Chem. B* **2002**, *107*, 470.
(1002) Shindel, M. M.; Mohraz, A.; Mumm, D. R.; Wang, S.-W. *Langmuir* **2008**, *25*, 1038.
(1003) Shindel, M. M.; Mumm, D. R.; Wang, S.-W. *Langmuir* **2010**, *26*, 11103.
(1004) Aslan, K.; Luhrs, C. C.; Pérez-Luna, V. H. *J. Phys. Chem. B* **2004**, *108*, 15631.
(1005) Verma, A.; Srivastava, S.; Rotello, V. M. *Chem. Mater.* **2005**, *17*, 6317.
(1006) Srivastava, S.; Verma, A.; Frankamp, B. L.; Rotello, V. M. *Adv. Mater.* **2005**, *17*, 617.
(1007) Kaur, P.; Maeda, Y.; Mutter, A. C.; Matsunaga, T.; Xu, Y.; Matsui, H. *Angew. Chem., Int. Ed.* **2010**, *49*, 8375.
(1008) Blum, A. S.; Soto, C. M.; Wilson, C. D.; Cole, J. D.; Kim, M.; Gnade, B.; Chatterji, A.; Ochoa, W. F.; Lin, T.; Johnson, J. E.; Ratna, B. R. *Nano Lett.* **2004**, *4*, 867.
(1009) Soto, C. M.; Blum, A. S.; Wilson, C. D.; Lazorcik, J.; Kim, M.; Gnade, B.; Ratna, B. R. *Electrophoresis* **2004**, *25*, 2901.

(1010) Wang, Q.; Lin, T. W.; Tang, L.; Johnson, J. E.; Finn, M. G. *Angew. Chem., Int. Ed.* **2002**, *41*, 459.
(1011) Sun, J.; DuFort, C.; Daniel, M.-C.; Murali, A.; Chen, C.; Gopinath, K.; Stein, B.; De, M.; Rotello, V. M.; Holzenburg, A.; Kao, C. C.; Dragnea, B. *Proc. Natl. Acad. Sci. U.S.A.* **2007**, *104*, 1354.
(1012) Chen, C.; Daniel, M.-C.; Quinkert, Z. T.; De, M.; Stein, B.; Bowman, V. D.; Chipman, P. R.; Rotello, V. M.; Kao, C. C.; Dragnea, B. *Nano Lett.* **2006**, *6*, 611.
(1013) Loo, L.; Guenther, R. H.; Lommel, S. A.; Franzen, S. *J. Am. Chem. Soc.* **2007**, *129*, 11111.
(1014) Daniel, M.-C.; Tsvetkova, I. B.; Quinkert, Z. T.; Murali, A.; De, M.; Rotello, V. M.; Kao, C. C.; Dragnea, B. *ACS Nano* **2010**, *4*, 3853.
(1015) Nam, K. T.; Kim, D.-W.; Yoo, P. J.; Chiang, C.-Y.; Meethong, N.; Hammond, P. T.; Chiang, Y.-M.; Belcher, A. M. *Science* **2006**, *312*, 885.
(1016) Lee, S. W.; Lee, S. K.; Belcher, A. M. *Adv. Mater.* **2003**, *15*, 689.
(1017) Everts, M.; Saini, V.; Leddon, J. L.; Kok, R. J.; Stoff-Khalili, M.; Preuss, M. A.; Millican, C. L.; Perkins, G.; Brown, J. M.; Bagaria, H.; Nikles, D. E.; Johnson, D. T.; Zharov, V. P.; Curiel, D. T. *Nano Lett.* **2006**, *6*, 587.
(1018) Dragnea, B.; Chen, C.; Kwak, E.-S.; Stein, B.; Kao, C. C. *J. Am. Chem. Soc.* **2003**, *125*, 6374.
(1019) Niikura, K.; Nagakawa, K.; Ohtake, N.; Suzuki, T.; Matsuo, Y.; Sawa, H.; Ijiro, K. *Bioconjugate Chem.* **2009**, *20*, 1848.
(1020) Li, Z.; Chung, S.-W.; Nam, J.-M.; Ginger, D. S.; Mirkin, C. A. *Angew. Chem.* **2003**, *115*, 2408.
(1021) Rosi, N. L.; Thaxton, C. S.; Mirkin, C. A. *Angew. Chem.* **2004**, *116*, 5616.
(1022) Mukherjee, P.; Ahmad, A.; Mandal, D.; Senapati, S.; Sainkar, S. R.; Khan, M. I.; Parishcha, R.; Ajaykumar, P. V.; Alam, M.; Kumar, R.; Sastry, M. *Nano Lett.* **2001**, *1*, 515.
(1023) Berry, V.; Rangaswamy, S.; Saraf, R. F. *Nano Lett.* **2004**, *4*, 939.
(1024) Brousseau, L. C.; Novak, J. P.; Marinakos, S. M.; Feldheim, D. L. *Adv. Mater.* **1999**, *11*, 447.
(1025) Fullam, S.; Cottell, D.; Rensmo, H.; Fitzmaurice, D. *Adv. Mater.* **2000**, *12*, 1430.
(1026) Liu, Q.; Cui, Y.; Gardner, D.; Li, X.; He, S.; Smalyukh, I. I. *Nano Lett.* **2010**, *10*, 1347.
(1027) Bockstaller, M. R.; Lapetnikov, Y.; Margel, S.; Thomas, E. L. *J. Am. Chem. Soc.* **2003**, *125*, 5276.
(1028) Brust, M.; Schiffrin, D. J.; Bethell, D.; Kiely, C. J. *Adv. Mater.* **1995**, *7*, 795.
(1029) Novak, J. P.; Brousseau, L. C.; Vance, F. W.; Johnson, R. C.; Lemon, B. I.; Hupp, J. T.; Feldheim, D. L. *J. Am. Chem. Soc.* **2000**, *122*, 12029.
(1030) Novak, J. P.; Feldheim, D. L. *J. Am. Chem. Soc.* **2000**, *122*, 3979.
(1031) McConnell, W. P.; Novak, J. P.; Brousseau, L. C.; Fuierer, R. R.; Tenent, R. C.; Feldheim, D. L. *J. Phys. Chem. B* **2000**, *104*, 8925.
(1032) Kaminker, R.; Lahav, M.; Motiei, L.; Vartanian, M.; Popovitz-Biro, R.; Iron, M. A.; van der Boom, M. E. *Angew. Chem., Int. Ed.* **2010**, *49*, 1218.
(1033) Park, H.-S.; Agarwal, A.; Kotov, N. A.; Lavrentovich, O. D. *Langmuir* **2008**, *24*, 13833.
(1034) DeVries, G. A.; Brunnbauer, M.; Hu, Y.; Jackson, A. M.; Long, B.; Neltner, B. T.; Uzun, O.; Wunsch, B. H.; Stellacci, F. *Science* **2007**, *315*, 358.
(1035) Lin, S.; Li, M.; Dujardin, E.; Girard, C.; Mann, S. *Adv. Mater.* **2005**, *17*, 2553.
(1036) Olson, M. A.; Coskun, A.; Klajn, R.; Fang, L.; Dey, S. K.; Browne, K. P.; Grzybowski, B. A.; Stoddart, J. F. *Nano Lett.* **2009**, *9*, 3185.
(1037) Ciesa, F.; Plech, A.; Mattioli, C.; Pescatori, L.; Arduini, A.; Pochini, A.; Rossi, F.; Secchi, A. *J. Phys. Chem. C* **2010**, *114*, 13601.
(1038) Puigmartí-Luis, J.; Pérez del Pino, Á.; Laukhina, E.; Esquena, J.; Laukhin, V.; Rovira, C.; Vidal-Gancedo, J.; Kanaras, A. G.; Nichols, R. J.; Brust, M.; Amabilino, D. B. *Angew. Chem., Int. Ed.* **2008**, *47*, 1861.
(1039) Rance, G. A.; Marsh, D. H.; Bourne, S. J.; Reade, T. J.; Khlobystov, A. N. *ACS Nano* **2010**, *4*, 4920.
(1040) Correa-Duarte, M. A.; Pérez-Juste, J.; Sánchez-Iglesias, A.; Giersig, M.; Liz-Marzán, L. M. *Angew. Chem., Int. Ed.* **2005**, *44*, 4375.
(1041) Correa-Duarte, M. A.; Sobal, N.; Liz-Marzán, L. M.; Giersig, M. *Adv. Mater.* **2004**, *16*, 2179.
(1042) Kim, B.; Sigmund, W. M. *Langmuir* **2004**, *20*, 8239.
(1043) Kim, S. N.; Slocik, J. M.; Naik, R. R. *Small* **2010**, *6*, 1992.
(1044) Moghaddam, M. J.; Taylor, S.; Gao, M.; Huang, S.; Dai, L.; McCall, M. J. *Nano Lett.* **2003**, *4*, 89.
(1045) Fási, A.; Pálinkó, I.; Seo, J. W.; Kónya, Z.; Hernadi, K.; Kiricsi, I. *Chem. Phys. Lett.* **2003**, *372*, 848.
(1046) Jiang, K.; Eitan, A.; Schadler, L. S.; Ajayan, P. M.; Siegel, R. W.; Grobert, N.; Mayne, M.; Reyes-Reyes, M.; Terrones, H.; Terrones, M. *Nano Lett.* **2003**, *3*, 275.
(1047) Weizmann, Y.; Lim, J.; Chenoweth, D. M.; Swager, T. M. *Nano Lett.* **2010**, *10*, 2466.
(1048) Biju, V.; Itoh, T.; Makita, Y.; Ishikawa, M. *J. Photochem. Photobiol., A* **2006**, *183*, 315.
(1049) Ou, Y.-Y.; Huang, M. H. *J. Phys. Chem. B* **2006**, *110*, 2031.
(1050) Han, L.; Wu, W.; Kirk, F. L.; Luo, J.; Maye, M. M.; Kariuki, N. N.; Lin, Y.; Wang, C.; Zhong, C.-J. *Langmuir* **2004**, *20*, 6019.
(1051) Zhang, M.; Su, L.; Mao, L. *Carbon* **2006**, *44*, 276.
(1052) Ellis, A. V.; Vijayamohanan, K.; Goswami, R.; Chakrapani, N.; Ramanathan, L. S.; Ajayan, P. M.; Ramanath, G. *Nano Lett.* **2003**, *3*, 279.
(1053) Sainsbury, T.; Fitzmaurice, D. *Chem. Mater.* **2004**, *16*, 2174.
(1054) Yang, B.; Kamiya, S.; Shimizu, Y.; Koshizaki, N.; Shimizu, T. *Chem. Mater.* **2004**, *16*, 2826.
(1055) Lvov, Y. M.; Price, R. R.; Selinger, J. V.; Singh, A.; Spector, M. S.; Schnur, J. M. *Langmuir* **2000**, *16*, 5932.
(1056) Rasch, M. R.; Rossinyol, E.; Hueso, J. L.; Goodfellow, B. W.; Arbiol, J.; Korgel, B. A. *Nano Lett.* **2010**, *10*, 3733.
(1057) Hegmann, T.; Qi, H.; Marx, V. M. *J. Inorg. Organomet. Polym. Mater.* **2007**, *17*, 483.
(1058) Kossyrev, P. A.; Yin, A.; Cloutier, S. G.; Cardimona, D. A.; Huang, D.; Alsing, P. M.; Xu, J. M. *Nano Lett.* **2005**, *5*, 1978.
(1059) Muller, J.; Sonnichsen, C.; von Poschinger, H.; von Plessen, G.; Klar, T. A.; Feldmann, J. *Appl. Phys. Lett.* **2002**, *81*, 171.
(1060) Murali, S.; Xu, T.; Marshall, B. D.; Kayatin, M. J.; Pizarro, K.; Radhakrishnan, V. K.; Nepal, D.; Davis, V. A. *Langmuir* **2010**, *26*, 11176.
(1061) Qi, H.; Hegmann, T. *J. Mater. Chem.* **2006**, *16*, 4197.
(1062) Qi, H.; Lepp, A.; Heiney, P. A.; Hegmann, T. *J. Mater. Chem.* **2007**, *17*, 2139.
(1063) Kanayama, N.; Tsutsumi, O.; Kanazawa, A.; Ikeda, T. *Chem. Commun.* **2001**, 2640.
(1064) In, I.; Jun, Y.-W.; Kim, Y. J.; Kim, S. Y. *Chem. Commun.* **2005**, 800.
(1065) Fong, W.-K.; Hanley, T. L.; Thierry, B.; Kirby, N.; Boyd, B. J. *Langmuir* **2010**, *26*, 6136.
(1066) Boal, A. K.; Ilhan, F.; DeRouchey, J. E.; Thurn-Albrecht, T.; Russell, T. P.; Rotello, V. M. *Nature* **2000**, *404*, 746.
(1067) Srivastava, S.; Frankamp, B. L.; Rotello, V. M. *Chem. Mater.* **2005**, *17*, 487.
(1068) Li, B.; Li, C. Y. *J. Am. Chem. Soc.* **2007**, *129*, 12.
(1069) Li, B.; Wang, B. B.; Ferrier, R. C. M.; Li, C. Y. *Macromolecules* **2009**, *42*, 9394.
(1070) Ojha, S.; Beppler, B.; Dong, H.; Matyjaszewski, K.; Garoff, S.; Bockstaller, M. R. *Langmuir* **2010**, *26*, 13210.
(1071) Oh, H. S.; Liu, S.; Jee, H.; Baev, A.; Swihart, M. T.; Prasad, P. N. *J. Am. Chem. Soc.* **2010**, *132*, 17346.
(1072) Khanal, B. P.; Zubarev, E. R. *Angew. Chem., Int. Ed.* **2007**, *46*, 2195.
(1073) Akamatsu, K.; Shimada, M.; Tsuruoka, T.; Nawafune, H.; Fujii, S.; Nakamura, Y. *Langmuir* **2010**, *26*, 1254.

(1074) Gupta, S.; Agrawal, M.; Uhlmann, P.; Simon, F.; Oertel, U.; Stamm, M. *Macromolecules* **2008**, *41*, 8152.
(1075) Bang, J.; Jeong, U.; Ryu, D. Y.; Russell, T. P.; Hawker, C. J. *Adv. Mater.* **2009**, *21*, 4769.
(1076) Bockstaller, M. R.; Mickiewicz, R. A.; Thomas, E. L. *Adv. Mater.* **2005**, *17*, 1331.
(1077) Haryono, A.; Binder, W. H. *Small* **2006**, *2*, 600.
(1078) Moon, J. H.; Yang, S. *Chem. Rev.* **2010**, *110*, 547.
(1079) Paquet, C.; Kumacheva, E. *Mater. Today* **2008**, *11*, 48.
(1080) Rozenberg, B. A.; Tenne, R. *Prog. Polym. Sci.* **2008**, *33*, 40.
(1081) Shenhar, R.; Norsten, T. B.; Rotello, V. M. *Adv. Mater.* **2005**, *17*, 657.
(1082) Yoo, S. I.; Kwon, J. H.; Sohn, B. H. *J. Mater. Chem.* **2007**, *17*, 2969.
(1083) Tsuchiya, K.; Nagayasu, S.; Okamoto, S.; Hayakawa, T.; Hihara, T.; Yamamoto, K.; Takumi, I.; Hara, S.; Hasegawa, H.; Akasaka, S.; Kosikawa, N. *Opt. Express* **2008**, *16*, 5362.
(1084) Kannaiyan, D.; Cha, M. A.; Jang, Y. H.; Sohn, B. H.; Huh, J.; Park, C.; Kim, D. H. *New J. Chem.* **2009**, *33*, 2431.
(1085) Chan, Y. N. C.; Schrock, R. R.; Cohen, R. E. *J. Am. Chem. Soc.* **1992**, *114*, 7295.
(1086) Chan, Y. N. C.; Schrock, R. R.; Cohen, R. E. *Chem. Mater.* **1992**, *4*, 24.
(1087) Chan, Y. N. C.; Craig, G. S. W.; Schrock, R. R.; Cohen, R. E. *Chem. Mater.* **1992**, *4*, 885.
(1088) Saito, R.; Okamura, S.; Ishizu, K. *Polymer* **1992**, *33*, 1099.
(1089) Spatz, J. P.; Roescher, A.; Möller, M. *Adv. Mater.* **1996**, *8*, 337.
(1090) Zehner, R. W.; Lopes, W. A.; Morkved, T. L.; Jaeger, H.; Sita, L. R. *Langmuir* **1998**, *14*, 241.
(1091) Acharya, H.; Sung, J.; Sohn, B. H.; Kim, D. H.; Tamada, K.; Park, C. *Chem. Mater.* **2009**, *21*, 4248.
(1092) Zubarev, E. R.; Xu, J.; Sayyad, A.; Gibson, J. D. *J. Am. Chem. Soc.* **2006**, *128*, 15098.
(1093) Lopes, W. A.; Jaeger, H. M. *Nature* **2001**, *414*, 735.
(1094) Sohn, B. H.; Seo, B. H. *Chem. Mater.* **2001**, *13*, 1752.
(1095) Spatz, J. P.; Mossmer, S.; Hartmann, C.; Moller, M.; Herzog, T.; Krieger, M.; Boyen, H. G.; Ziemann, P.; Kabius, B. *Langmuir* **2000**, *16*, 407.
(1096) Thompson, R. B.; Ginzburg, V. V.; Matsen, M. W.; Balazs, A. C. *Macromolecules* **2002**, *35*, 1060.
(1097) Chiu, J. J.; Kim, B. J.; Kramer, E. J.; Pine, D. J. *J. Am. Chem. Soc.* **2005**, *127*, 5036.
(1098) Li, Q. F.; He, J. B.; Glogowski, E.; Li, X. F.; Wang, J.; Emrick, T.; Russell, T. P. *Adv. Mater.* **2008**, *20*, 1462.
(1099) Bockstaller, M.; Kolb, R.; Thomas, E. L. *Adv. Mater.* **2001**, *13*, 1783.
(1100) Bockstaller, M. R.; Thomas, E. L. *J. Phys. Chem. B* **2003**, *107*, 10017.
(1101) Zhao, Y.; Thorkelsson, K.; Mastroianni, A. J.; Schilling, T.; Luther, J. M.; Rancatore, B. J.; Matsunaga, K.; Jinnai, H.; Wu, Y.; Poulsen, D.; Frechet, J. M. J.; Alivisatos, A. P.; Xu, T. *Nat. Mater.* **2009**, *8*, 979.
(1102) Karg, M.; Lu, Y.; Carbo-Argibay, E.; Pastoriza-Santos, I.; Perez-Juste, J.; Liz-Marzán, L. M.; Hellweg, T. *Langmuir* **2009**, *25*, 3163.
(1103) Deshmukh, R. D.; Liu, Y.; Composto, R. J. *Nano Lett.* **2007**, *7*, 3662.
(1104) Mistark, P. A.; Park, S.; Yalcin, S. E.; Lee, D. H.; Yavuzcetin, O.; Tuominen, M. T.; Russell, T. P.; Achermann, M. *ACS Nano* **2009**, *3*, 3987.
(1105) Hanaoka, T.-A.; Heilmann, A.; Kröll, M.; Kormann, H.-P.; Sawitowski, T.; Schmid, G.; Jutzi, P.; Klipp, A.; Kreibig, U.; Neuendorf, R. *Appl. Organomet. Chem.* **1998**, *12*, 367.
(1106) Lahav, M.; Sehayek, T.; Vaskevich, A.; Rubinstein, I. *Angew. Chem., Int. Ed.* **2003**, *42*, 5576.
(1107) Westcott, S. L.; Oldenburg, S. J.; Lee, T. R.; Halas, N. J. *Chem. Phys. Lett.* **1999**, *300*, 651.
(1108) Gittins, D. I.; Susha, A. S.; Schoeler, B.; Caruso, F. *Adv. Mater.* **2002**, *14*, 508.
(1109) Liu, H.; Alivisatos, A. P. *Nano Lett.* **2004**, *4*, 2397.
(1110) Xue, J.; Wang, C.; Ma, Z. *Mater. Chem. Phys.* **2007**, *105*, 419.
(1111) Sadtler, B.; Wei, A. *Chem. Commun.* **2002**, 1604.
(1112) Hiramatsu, H.; Osterloh, F. E. *Langmuir* **2003**, *19*, 7003.
(1113) Caruso, F.; Spasova, M.; Salgueiriño-Maceira, V.; Liz-Marzán, L. M. *Adv. Mater.* **2001**, *13*, 1090.
(1114) Graf, C.; Dembski, S.; Hofmann, A.; Rühl, E. *Langmuir* **2006**, *22*, 5604.
(1115) Liang, Z.; Susha, A. S.; Caruso, F. *Adv. Mater.* **2002**, *14*, 1160.
(1116) Jun, Y.; Yu, D.; George, M. C.; Braun, P. V. *J. Am. Chem. Soc.* **2010**, *132*, 9958.
(1117) Lu, L.; Zhang, H.; Sun, G.; Xi, S.; Wang, H.; Li, X.; Wang, X.; Zhao, B. *Langmuir* **2003**, *19*, 9490.
(1118) Ryan, D.; Nagle, L.; Rensmo, H. k.; Fitzmaurice, D. *J. Phys. Chem. B* **2002**, *106*, 5371.
(1119) Dong, A. G.; Wang, Y. J.; Tang, Y.; Ren, N.; Yang, W. L.; Gao, Z. *Chem. Commun.* **2002**, 350.
(1120) Xiao, M.; Chen, H.; Ming, T.; Shao, L.; Wang, J. *ACS Nano* **2010**, *4*, 6565.
(1121) Guo, S.; Dong, S.; Wang, E. *Chem.—Eur. J.* **2009**, *15*, 2416.
(1122) Caruntu, D.; Cushing, B. L.; Caruntu, G.; O'Connor, C. J. *Chem. Mater.* **2005**, *17*, 3398.
(1123) Spasova, M.; Salgueirino-Maceira, V.; Schlachter, A.; Hilgendorff, M.; Giersig, M.; Liz-Marzán, L. M.; Farle, M. *J. Mater. Chem.* **2005**, *15*, 2095.
(1124) Bao, J.; Chen, W.; Liu, T.; Zhu, Y.; Jin, P.; Wang, L.; Liu, J.; Wei, Y.; Li, Y. *ACS Nano* **2007**, *1*, 293.
(1125) Wang, Y.; Chen, G.; Yang, M.; Silber, G.; Xing, S.; Tan, L. H.; Wang, F.; Feng, Y.; Liu, X.; Li, S.; Chen, H. *Nat. Commun.* **2010**, *1*, 87.
(1126) Wei, Y. H.; Bishop, K. J. M.; Kim, J.; Soh, S.; Grzybowski, B. A. *Angew. Chem., Int. Ed.* **2009**, *48*, 9477.
(1127) Lee, J.; Govorov, A. O.; Dulka, J.; Kotov, N. A. *Nano Lett.* **2004**, *4*, 2323.
(1128) Lee, J.; Hernandez, P.; Lee, J.; Govorov, A. O.; Kotov, N. A. *Nat. Mater.* **2007**, *6*, 291.
(1129) Lee, J.; Javed, T.; Skeini, T.; Govorov, A. O.; Bryant, G. W.; Kotov, N. A. *Angew. Chem., Int. Ed.* **2006**, *45*, 4819.
(1130) Gunawidjaja, R.; Peleshanko, S.; Ko, H.; Tsukruk, V. V. *Adv. Mater.* **2008**, *20*, 1544.
(1131) Hutchison, J. A.; Centeno, S. P.; Odaka, H.; Fukumura, H.; Hofkens, J.; Uji-i, H. *Nano Lett.* **2009**, *9*, 995.
(1132) Lee, S. J.; Baik, J. M.; Moskovits, M. *Nano Lett.* **2008**, *8*, 3244.
(1133) Wei, H.; Hao, F.; Huang, Y.; Wang, W.; Nordlander, P.; Xu, H. *Nano Lett.* **2008**, *8*, 2497.
(1134) Fang, Y.; Wei, H.; Hao, F.; Nordlander, P.; Xu, H. *Nano Lett.* **2009**, *9*, 2049.
(1135) Kang, T.; Yoon, I.; Kim, J.; Hee, H.; Kim, B. *Chem.—Eur. J.* **2010**, *16*, 1351.
(1136) Osterloh, F. E.; Martino, J. S.; Hiramatsu, H.; Hewitt, D. P. *Nano Lett.* **2002**, *3*, 125.
(1137) Wang, C. G.; Chen, J.; Talavage, T.; Irudayaraj, J. *Angew. Chem., Int. Ed.* **2009**, *48*, 2759.
(1138) Salant, A.; Amitay-Sadovsky, E.; Banin, U. *J. Am. Chem. Soc.* **2006**, *128*, 10006.
(1139) Liu, K.; Nie, Z.; Zhao, N.; Li, W.; Rubinstein, M.; Kumacheva, E. *Science* **2010**, *329*, 197.
(1140) Cui, Y.; Björk, M. T.; Liddle, J. A.; Sönnichsen, C.; Boussert, B.; Alivisatos, A. P. *Nano Lett.* **2004**, *4*, 1093.
(1141) Xiong, X.; Makaram, P.; Busnaina, A.; Bakhtari, K.; Somu, S.; McGruer, N.; Park, J. *Appl. Phys. Lett.* **2006**, *89*, 193108.
(1142) Xia, Y.; Yin, Y.; Lu, Y.; McLellan, J. *Adv. Funct. Mater.* **2003**, *13*, 907.
(1143) Grabar, K. C.; Freeman, R. G.; Hommer, M. B.; Natan, M. J. *Anal. Chem.* **1995**, *67*, 735.
(1144) Grabar, K. C.; Smith, P. C.; Musick, M. D.; Davis, J. A.; Walter, D. G.; Jackson, M. A.; Guthrie, A. P.; Natan, M. J. *J. Am. Chem. Soc.* **1996**, *118*, 1148.

(1145) Braunstein, P.; Kormann, H.-P.; Meyer-Zaika, W.; Pugin, R.; Schmid, G. *Chem.—Eur. J.* **2000**, *6*, 4637.
(1146) Sehayek, T.; Lahav, M.; Popovitz-Biro, R.; Vaskevich, A.; Rubinstein, I. *Chem. Mater.* **2005**, *17*, 3743.
(1147) Jani, A. M. M.; Kempson, I. M.; Losic, D.; Voelcker, N. H. *Angew. Chem., Int. Ed.* **2010**, *49*, 7933.
(1148) Dotzauer, D. M.; Dai, J.; Sun, L.; Bruening, M. L. *Nano Lett.* **2006**, *6*, 2268.
(1149) Dotzauer, D. M.; Bhattacharjee, S.; Wen, Y.; Bruening, M. L. *Langmuir* **2009**, *25*, 1865.
(1150) Ko, H.; Tsukruk, V. V. *Small* **2008**, *4*, 1980.
(1151) Ko, H.; Chang, S.; Tsukruk, V. V. *ACS Nano* **2008**, *3*, 181.
(1152) Konya, Z.; Puntes, V. F.; Kiricsi, I.; Zhu, J.; Ager, J. W.; Ko, M. K.; Frei, H.; Alivisatos, P.; Somorjai, G. A. *Chem. Mater.* **2003**, *15*, 1242.
(1153) Fan, H.; Yang, K.; Boye, D. M.; Sigmon, T.; Malloy, K. J.; Xu, H.; López, G. P.; Brinker, C. J. *Science* **2004**, *304*, 567.
(1154) Fan, H.; Wright, A.; Gabaldon, J.; Rodriguez, A.; Brinker, C. J.; Jiang, Y. B. *Adv. Funct. Mater.* **2006**, *16*, 891.
(1155) Fan, H. Y.; Gabaldon, J.; Brinker, C. J.; Jiang, Y. B. *Chem. Commun.* **2006**, 2323.
(1156) Han, Y.; Sukhishvili, S.; Du, H.; Cefaloni, J.; Smolinsko, B. *J. Nanosci. Nanotechnol.* **2008**, *8*, 5791.
(1157) Velev, O. D.; Tessier, P. M.; Lenhoff, A. M.; Kaler, E. W. *Nature* **1999**, *401*, 548.
(1158) Tessier, P. M.; Velev, O. D.; Kalambur, A. T.; Rabolt, J. F.; Lenhoff, A. M.; Kaler, E. W. *J. Am. Chem. Soc.* **2000**, *122*, 9554.
(1159) Velev, O. D.; Kaler, E. W. *Adv. Mater.* **2000**, *12*, 531.
(1160) Kuncicky, D. M.; Prevo, B. G.; Velev, O. D. *J. Mater. Chem.* **2006**, *16*, 1207.
(1161) Yi, D. K.; Lee, J. H.; Rogers, J. A.; Paik, U. *Appl. Phys. Lett.* **2009**, 94.
(1162) Wang, D.; Salgueiriño-Maceira, V.; Liz-Marzán, L. M.; Caruso, F. *Adv. Mater.* **2002**, *14*, 908.
(1163) Dieringer, J. A.; Wustholz, K. L.; Masiello, D. J.; Camden, J. P.; Kleinman, S. L.; Schatz, G. C.; Van Duyne, R. P. *J. Am. Chem. Soc.* **2008**, *131*, 849.
(1164) Banholzer, M. J.; Millstone, J. E.; Qin, L. D.; Mirkin, C. A. *Chem. Soc. Rev.* **2008**, *37*, 885.
(1165) Shafer-Peltier, K. E.; Haynes, C. L.; Glucksberg, M. R.; Van Duyne, R. P. *J. Am. Chem. Soc.* **2003**, *125*, 588.
(1166) Lyandres, O.; Shah, N. C.; Yonzon, C. R.; Walsh, J. T.; Glucksberg, M. R.; Van Duyne, R. P. *Anal. Chem.* **2005**, *77*, 6134.
(1167) Yuen, J. M.; Shah, N. C.; Walsh, J. T.; Glucksberg, M. R.; Van Duyne, R. P. *Anal. Chem.* **2010**, *82*, 8382.
(1168) Banholzer, M. J.; Osberg, K. D.; Li, S.; Mangelson, B. F.; Schatz, G. C.; Mirkin, C. A. *ACS Nano* **2010**, *4*, 5446.
(1169) Dahlin, A.; Zäch, M.; Rindzevicius, T.; Käll, M.; Sutherland, D. S.; Höök, F. *J. Am. Chem. Soc.* **2005**, *127*, 5043.
(1170) Chen, S.; Svedendahl, M.; Käll, M.; Gunnarsson, L.; Dmitriev, A. *Nanotechnology* **2009**, *20*, 434015.
(1171) Langhammer, C.; Zoric, I.; Kasemo, B. *Nano Lett.* **2007**, *7*, 3122.
(1172) Larsson, E. M.; Langhammer, C.; Zoric, I.; Kasemo, B. *Science* **2009**, *326*, 1091.
(1173) Stockman, M. I. *Nature* **2010**, *467*, 541.
(1174) Link, S.; El-Sayed, M. A. *Annu. Rev. Phys. Chem.* **2003**, *54*, 331.
(1175) Link, S.; El-Sayed, M. A. *Int. Rev. Phys. Chem.* **2000**, *19*, 409.